AIIM

Association for Information and Image Management
1100 Wayne Avenue, Suite 1100
Silver Spring, Maryland 20910
301/587-8202

Centimeter

Inches

MANUFACTURED TO AIIM STANDARDS
BY APPLIED IMAGE, INC.

1 of 3

DOE/PC/90310--T14
(DE94017110)
Distribution Category UC-113

COMBUSTION OF DENSE STREAMS OF COAL PARTICLES

A Final Report
(Aug. 29, 1990 - Feb. 28, 1994)

by

Kalyan Annamalai
Chengapalli Gopalakrishnan
Xiangyang Du

Mechanical Engineering
Texas A&M University
College Station, TX 77843-3123

May 1994

Prepared for
U.S. Department of Energy
Pittsburgh Energy Technology Center
P.O.Box 10940,
Pittsburgh, Pa. 15236

Grant # DE-FG22-90PC90310

COMBUSTION OF DENSE STREAMS OF COAL PARTICLES

ABSTRACT

The USA consumes almost 94 quads of energy (1 quad = 10^{15} BTU or 1.05×10^{15} KJ). The utilities account for about 30 quads of fossil energy where coal is predominantly used as energy source. The coal is ground to finer size and fired into the boiler as dense suspension. Under dense conditions, the particles burn at slower rate due to deficient oxygen within the interparticle spacing. Thus interactions exist amongst the particles for dense clouds. While the earlier literature dealt with combustion processes of isolated particles, the recent research focusses upon the interactive combustion. The interactive combustion studies include arrays consisting of a finite number of particles, and streams and clouds of a large number of particles. Particularly stream combustion models assume cylindrical geometry and predict the ignition and combustion characteristics. The models show that the ignition starts homogeneously for dense streams of coal particles and the ignition time show a minimum as the stream denseness is increased, and during combustion, there appears to be an inner flame within the stream and an outer flame outside the stream for a short period of time. The present experimental investigation is an attempt to verify the model predictions.

The set-up consists of a flat flame burner for producing hot vitiated gases, a locally fluidizing feeder system for feeding coal particles, a particle collection probe for collecting particles and an image processing system for analyzing the flame structure. The particles are introduced as a stream into the hot gases and subsequently they ignite and burn. The ash % of fired and collected particles are determined and used to estimate the gasification efficiency or

burnt fraction. The parametric studies include gas temperature, oxygen % in gases, residence time, and A:F ratio of the stream.

In the vicinity of the burner, the gasification efficiency increases with the cloud a:f ratio, reaches a maximum and decreases as the cloud becomes very dilute. The mathematical models support this trend. Further the results are consistent with the experimental findings of minimum in ignition time with the cloud denseness.It is found that the gasification efficiency increases first with A:F ratio of the stream but decreases for large A:F. The models support such a trend in the vicinity of the fuel injector. The gasification efficiency increases with the reaction zone height (residence time) due to increase in residence time. The gasification efficiency increases with the gas temperature and the oxygen concentration.

The image processing system provides results on ignition mechanism of streams and flame structure. The cold coal stream does not seem to diverge like the air jet, thus maintaining its cylindrical geometry. Within the ignition regime, the flame images show a peak in pixel values at the periphery of the dense cloud confirming the homogeneous ignition mode for dense clouds. For the dilute clouds, the peak occurs at the center of the cloud, indicating heterogenous ignition. The flame images of the dense clouds seem to indicate the formation of double flame (inner and outer flames). The inner flame travels towards the center while the outer diffusion flame diverges. However dilute clouds do not reveal such a phenomenon.

TABLE OF CONTENTS

Page #

ABSTRACT ii

TABLE OF CONTENTS iv

LIST OF FIGURES vii

LIST OF TABLES xiii

I INTRODUCTION 1

1.1 Scope of the Present Work 9

II LITERATURE REVIEW 10

2.1 Coal 10
2.2 Coal Vs Droplet Combustion 11
2.3 Isolated Particle Combustion 11
2.3.1 Carbon 11
2.3.2 Coal 13
2.4 Interactive Array Combustion 14
2.5 Stream Combustion 15
2.6 Stream Combustion Models 23
2.7 Optical Techniques in Combustion 26
2.7.1 High Speed Photography 28
2.7.2 Digital Imaging 28

III OBJECTIVES 40

IV DESCRIPTION OF EXPERIMENTAL APPARATUS 41

4.1 Experimental Set Up 41
4.2 Flat Flame Burner 41
4.3 Locally Fluidizing Feeder (LFF) 43
4.4 Particle Collection System 48
4.5 Diagnostics 51
4.5.1 Gas Temperature 51
4.5.2 Gas Composition 51
4.6 Image Processing Equipment 53
4.6.1 C.I.D Camera 55

4.6.2 Frame Grabber 55
4.6.3 Video Monitor 56
4.6.4 EPIX (4MIP) Image Processing Software 56
4.6.5 486 Personal Computer 58

4.7 Particle Preparation Systems 58
4.7.1 Coal Crusher 58
4.7.2 Laboratory Oven 60

V DESCRIPTION OF EXPERIMENTAL PROCEDURE 61

5.1 Experimental Procedure 61
5.2 Stabilization of Flat Methane Flame 62
5.3 Gas Temperature 63

5.4 Oxygen Concentration 69
5.5 Cloud A:F Ratio 69

5.6 Operating Parameters for the Camera 73
5.7 Stream Velocity 74

VI RESULTS AND DISCUSSION 79

6.1 Overview of the Experiments Conducted 79
6.2 Gasification Efficiency 84
6.3 Experimental Data on Gasification Efficiency 84
6.3.1 Effect of Reaction Zone Height (or Residence Time) 84

6.3.2 Effect of A:F Ratio 85
6.3.3 Effect of Oxygen Concentration 89
6.3.4 Effect of Gas Temperature 93
6.3.5 Model Results on Gasification Efficiency 93

6.4 Digital Imaging of Coal Stream 93
6.5 Digital Imaging of Ignition 105
6.5.1 Effect of A:F Ratio on Ignition 107
6.5.2 Effect of Oxygen Concentration over Ignition 110
6.5.3 Effect of Gas Temperature on Ignition 114

6.6 Digital Imaging of Group Combustion 124
6.6.1 Group Flame 124
6.6.2 Double Flame 131
6.6.3 Effect of A:F Ratio on Flame Structure 131

6.6.4 Effect of Reaction Zone Height on Flame Structure 139

6.6.5 Effect of Oxygen Concentration on the Flame Structure 139

6.6.6 Effect of Gas Temperature over Flame Structure . . 144

VII CONCLUSIONS 157

REFERENCES 160B

APPENDIX A. MEASUREMENT OF VELOCITY OF FLOWING PARTICLES 164

APPENDIX B. CALCULATION OF $[O_2]$ CONCENTRATION 167

APPENDIX C. GROUP IGNITION AND COMBUSTION OF COAL PARTICLE STREAMS 168

APPENDIX D. GROUP IGNITION AND COMBUSTION MODEL WITH CLOUD EXPANSION 196

LIST OF FIGURES

FIGURE		Page #
1.1	Energy Consumption Figures in Quads (PETC Review, 1993)	2
1.2	Electricity Generation by Fuel Source (Annual Energy Review, 1991) .	3
1.3	Illustration of Group Combustion for a Cloud of Particles.	6
1.4	Array, Stream and Cloud Combustion of Coal Particles	8
2.1	Single and Double Film Models for Coal Combustion	12
2.2	Schematic of Experimental Apparatus for Continuous Flow (Petarca et al., 1986).	17
2.3	Transparent Wall Reactor (TWR) (Solomon et al., 1988).	19
2.4	Photographs of Different Coal Flames from TWR (Solomon et al., 1988).	20
2.5	Apparatus Set Up for Reaction Rate Measurements (Field, 1970).	21
2.6	Comparison of Experimental and Theoretical Burning Away Curves (Leesley et al., 1972)	24
2.7	A Laminar Flow Reactor Set Up (LFR) (Annamalai et al., 1993). . . .	25
2.8	Group Combustion Model for a Cylindrical Cloud of Particles (Annamalai et al., 1991)	27
2.9	Combustion of Single Spray Burning Under Large DI Engine Conditions (Scott, 1969)	29
2.10	Intermittent Combustion Sequence for High Volatile Coal (Kharbat, 1992)	32
2.11	Formation of Common Flame for Two Interacting Particles (Kharbat, 1992)	33
2.12	Series of Flame Images for Filter Paper Burning in 18% Oxygen (Weiland, 1993)	34
2.13	Flame Position Vs Time From Ignition, for Filter Paper and Laboratory Wiper Samples (Weiland, 1993)	35
2.14	Two Dimensional Light Scattering Experimental Set Up Showing a Thin Sheet of Laser Light Passing Through the Area of Interest (Lee et al., 1990)	37
2.15	Water Spray From 35mm Camera (Top) and Spray Image (Bottom)	

	(Lee et al., 1990)	38
4.1	Flat Flame Burner	42
4.2	Exploded View of Flat Flame Burner	44
4.3	Schematic for Flat Flame Experimental Set Up	45
4.4	Locally Fluidized Feeder (LFF) (Annamalai et al., 1992)	46
4.5	Coal Feeder Set Up	49
4.6	Particle Collection Probe Set Up	50
4.7	Temperature and Oxygen Concentration Measurement System	52
4.8	Image Processing System Set Up	54
4.9	Coal Crusher Unit	59
5.1	Stable Flat Methane Flame	64
5.2	Gas Temperature Profiles With No Carrier Air	65
5.3	Gas Temperature With Carrier Air at the Center	66
5.4	Gas Temperature With and Without Carrier Air	67
5.5	Gas Temperature for Higher Methane Flow	68
5.6	Oxygen Concentration for Various Oxygen Flows	70
5.7	Variation of Mass Flow Rate	71
5.8	Mass Flow Rate Vs Dilution Flow	72
5.9	Candle Flame Images	75
5.10	Two Successive Frames of Coal Stream	77
5.11	Pixel Contours Along Y Direction at the Center of the Burner	78
6.1	Proximate Analysis for PSOC 1336 Coal	80
6.2	Gasification Efficiency Vs. A:F Ratio and Residence Time at 6.5% Oxygen Conc	86
6.3	Gasification Efficiency Vs. A:F Ratio and Residence Time at 10% Oxygen Conc	87
6.4	Gasification Efficiency Vs. A:F Ratio and Residence Time at 12.5% Oxygen Conc	88
6.5	Gasification Efficiency Vs. A:F Ratio and Oxygen Conc (4 cm Height)	90
6.6	Gasification Efficiency Vs. A:F Ratio and Oxygen Conc (5 cm Height)	91

6.7 Gasification Efficiency Vs. A:F Ratio and Oxygen Conc (6 cm Height) 92

6.8 Effect of Gas Temperature on Gasification Efficiency 94

6.9 Theoretical Results for a Cylindrical Coal Cloud (Du et al., 1993) . . . 95

6.10 Cylindrical Coal Stream 97

6.11 Coal Flame Divergence at 4 cm Reaction Zone Height 98

6.12 Coal Flame Divergence at 6 cm Reaction Zone Height 99

6.13 Air Jet Divergence 101

6.14 Coal Stream Divergence 102

6.15 Coal Stream Flame for 0.3% Oxygen Conc. (Carrier : Air) 103

6.16 Coal Stream Flame for 0.3% Oxygen Conc. (Carrier : Nitrogen) 104

6.17 Pure Pyrolysis of Coal Stream 106

6.18 Jump in Pixel Value Due to Ignition 108

6.19 Pixel Contours for Heterogeneous Ignition Mode 109

6.20 Six Successive Frames of Dilute Coal Cloud Ignition (1200 K, 10% Oxygen Conc., 2.75 A:F Ratio) 111

6.21 Pixel Contours for Homogeneous Ignition Mode 112

6.22 Six Successive Frames of Dense Coal Cloud Ignition (1200 K, 10% Oxygen Conc., 0.85 A:F Ratio) 113

6.23 Pixel Contours for Homogeneous Model (12.5% Oxygen Conc.) 115

6.24 Six Successive Frames of Dense Cloud Ignition (1200 K, 12.5% Oxygen Conc., 0.594 A:F Ratio) 116

6.25 Pixel Contours for Heterogeneous Ignition Mode (12.5% Oxygen Conc.) 117

6.26 Six Successive Frames of Heterogeneous Ignition (1200 K, 12.5% Oxygen Conc., 2.2 A:F Ratio) 118

6.27 Pixel Contours for a Dilute Cloud at High Temperature 1400 K 120

6.28 Six Successive Frames of Ignition of Dilute Coal Cloud (1400 K, 10% Oxygen Conc., 4 A:F Ratio) 121

6.29 Pixel Contours for Homogeneous Ignition of Dense Clouds at 1400 K and 10% Oxygen Conc 122

6.30 Six Successive Frames of Homogeneous Ignition for Dense Cloud (1400 K, 10% Oxygen Conc., 0.79 A:F Ratio) 123

6.31 Homogeneous Ignition for Dense Cloud (A:F Ratio 0.85) 125

6.32 Heterogeneous Ignition for Dilute Cloud (A:F Ratio 2.75) 126

6.33 Homogeneous Ignition for Dense Cloud (A:F Ratio 0.594) 127

6.34 Heterogeneous Ignition for Dilute Cloud (A:F Ratio 2.2) 128

6.35 Homogeneous Ignition for Dense Cloud (A:F Ratio 0.9) 129

6.36 Ignition of Dilute Cloud (A:F Ratio 4.0) 130

6.37 Six Successive Frames of a Dense Cloud Combustion (1200 K, 6.5% Oxygen Conc., 0.8 A:F Ratio) 133

6.38 Flame Boundaries for the Six Successive Frames of Dense Cloud Combustion (1200 K, 6.5% Oxygen Conc., 0.8 A:F Ratio) 134

6.39 Six Successive Frames of Dilute Cloud Combustion (1200 K, 6.5% Oxygen Conc., 2.42 A:F Ratio) 135

6.40 Flame Boundaries for the Six Successive Frames of Dilute Cloud Combustion (1200 K, 6.5% Oxygen Conc., 2.42 A:F Ratio) 136

6.41 Six Successive Frames of Cloud Combustion (1200 K, 6.5% Oxygen Conc., 1.347 A:F Ratio) 137

6.42 Flame Boundaries for the Six Successive Frames of Cloud Combustion (1200 K, 6.5% Oxygen Conc., 1.347 A:F Ratio) 138

6.43 Six Successive Frames of Dense Cloud Combustion (1200 K, 6.5% Oxygen Conc., 0.776 A:F Ratio) 140

6.44 Flame Boundaries for the Six Successive Frames of Dense Cloud Combustion (1200 K, 6.5% Oxygen Conc., 0.776 A:F Ratio) 141

6.45 Six Successive Frames of Cloud Combustion (1200 K, 6.5% Oxygen Conc., 1.44 A:F Ratio) 142

6.46 Flame Boundaries for the Six Successive Frames of Cloud Combustion (1200 K, 6.5% Oxygen Conc., 1.44 A:F Ratio) 143

6.47 Six Successive Frames of Dense Cloud Combustion (1200 K, 12.5% Oxygen Conc., 0.8 A:F Ratio) 145

6.48 Flame Boundaries for the Six Successive Frames of Dense Cloud Combustion (1200 K, 12.5% Oxygen Conc., 0.8 A:F Ratio) 146

6.49 Six Successive Frames of Dilute Cloud Combustion (1200 K, 12.5% Oxygen Conc., 2.0 A:F Ratio) 147

6.50 Flame Boundaries for the Six Successive Frames of Dilute Cloud Combustion (1200 K, 12.5% Oxygen Conc., 2.0 A:F Ratio) 148

6.51 Six Successive Frames of Dense Cloud Combustion (1400 K, 12.5% Oxygen Conc., 0.96 A:F Ratio) 149

6.52 Flame Boundaries for the Six Successive Frames of Dense Cloud Combustion (1400 K, 12.5% Oxygen Conc., 0.96 A:F Ratio) 150

6.53 Six Successive Frames of Cloud Combustion (1400 K, 12.5% Oxygen Conc., 1.2 A:F Ratio) 151

6.54 Six Successive Frames of Dilute Cloud Combustion (1400 K, 12.5% Oxygen Conc., 3.0 A:F Ratio) 152

6.55 Double Flame Formation at the Cloud Periphery 154

6.56 Dense Stream Combustion at High Oxygen Concentration 155

6.57 Stream Combustion of Dense Cloud (Reaction Zone Height 4 cm) . . . 156

APPENDIX C

Fig. 1a Cylindrical model 187

Fig. 1b Temperature Profile 187

Fig. 2 Ignition time versus coal number density (R_c=0.225 cm, d_p=64 μm, Y_{O2}=0.23, $T_{g,0}$=300 K, $T_{p,0}$ = 300 K) 188

Fig. 3 Comparison between the predicted and measured ignition time (R_c=0.225 cm, T_∞= 1100 K, d_p=64 μm) 189

Fig 4 Flame profile at different time (R_c=0.225 cm, T_∞=1500, d_p=64 μm, Y_{O2}=0.23, $T_{g,0}$=300 K,$T_{p,0}$=300 K) 190

Fig. 5 Effect of cloud denseness (coal/air=0.5, R_c=0.225 cm, T_∞=1500 K, d_p=64 μm, Y_{O2}=0.23) 191

Fig. 6 Effect of cloud denseness (coal/air=1, R_c=0.225 cm, T_∞=1500 K, d_p=64 μm, Y_{O2}=0.23) 192

Fig. 7 Effect of cloud denseness (coal/air=2, R_c=0.225 cm, T_∞=1500 K, d_p=64 μm, Y_{O2} = 0.23) 193

Fig.8 Flat flame burner set up 194

Fig.9 Coal stream flame (reaction zone height 6 cm) (coal type-PSOC1336, d_p=64 μm, $Y_{O2,\infty}$ = 0.063, A:F = 0.42, mass flow rate of coal-0.0718 g/sec) 195

APPENDIX D

Fig. 1	Gas velocity and particle velocity at cloud boundary and boundary movement (T_∞=1100 K, R_c=0.225 cm, d_p=64 μm, n=50.9 E+07 particles/m^3, Ignition time = 48.07)	203
Fig. 2	Particle velocity distribution at different time (T_∞=1100 K, R_c=0.225 cm, d_p=64 μm, n=50.9 E+07 particles/m^3, Ignition time = 48.07)	204
Fig. 3	Number density distribution with cloud radius (T_∞=1100 K, R_c=0.225 cm, d_p=64 μm, n=50.9 E+07 particles/m^3, Ignition time = 48.07)	205
Fig. 4	Flame at t=53.9 ms (with cloud expansion) (T_∞=1100 K, R_c=0.225 cm, d_p=64 μm, n=50.9 E+07 particles/m^3, Ignition time=48.07)	206

LIST OF TABLES

TABLE **Page #**

6.1 Ultimate Analysis of PSOC 1336 Coal (as Received) 81

6.2 Proximate Analysis of PSOC 1336 Coal (Dry Basis) 82

6.3 Operating Parameters 83

APPENDIX C

1. Base Case Data 185

CHAPTER I

INTRODUCTION

The USA consumes almost 94 quads (1 quad = 10^{15} BTU = 1.05×10^{15} KJ) of energy every year (Fig. 1.1). The primary energy sources of North America are fossil fuels, hydroelectric power plants and nuclear reactors. The electric utilities account for 30 quads of energy. Of all the fossil fuels used in electric utility and industrial power plants today, coal is the most important (Fig. 1.2). Coal is the most dominant and abundant solid fossil fuel and USA is known to comprise about 75% of world coal reserves. Coal is economically competitive to other gaseous and liquid fuels. Lignite costs $1/ MMBTU while gas costs $2/MMBTU.

The primary air carries the pulverized fuel (pf) as dense suspension into the boiler. The A:F ratio at the fuel nozzle is of the order of 2:1. The remaining air called secondary air, is imparted a tangential motion with the swirl vanes mounted on the fuel nozzle. The tangential motion results in the creation of hot recirculation zone (RZ). The pf on contact with RZ gases ignites and burns downstream. The ignition and combustion near the burner occurs essentially in the dense mode. The combustion research on fossil fuel is essential for the following reasons.

1) To improve the combustion efficiency, reduce fuel consumption and hence minimize CO_2 release to atmosphere.

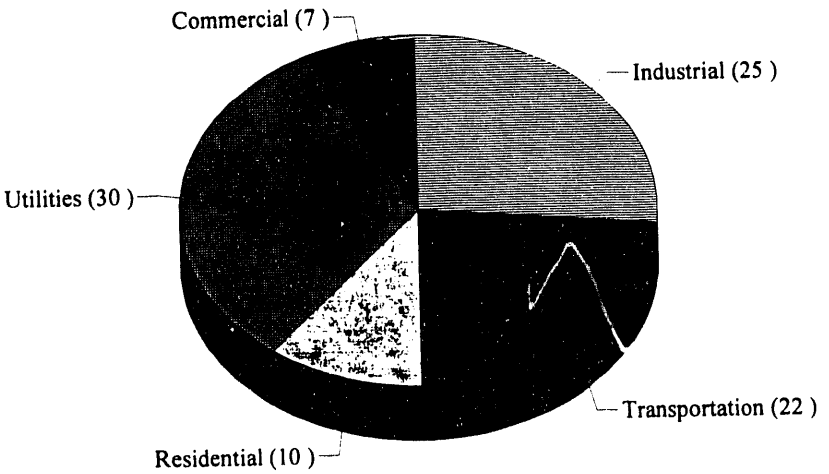

Fig. 1.1 Energy Consumption Figures in Quads (PETC Review, 1993).

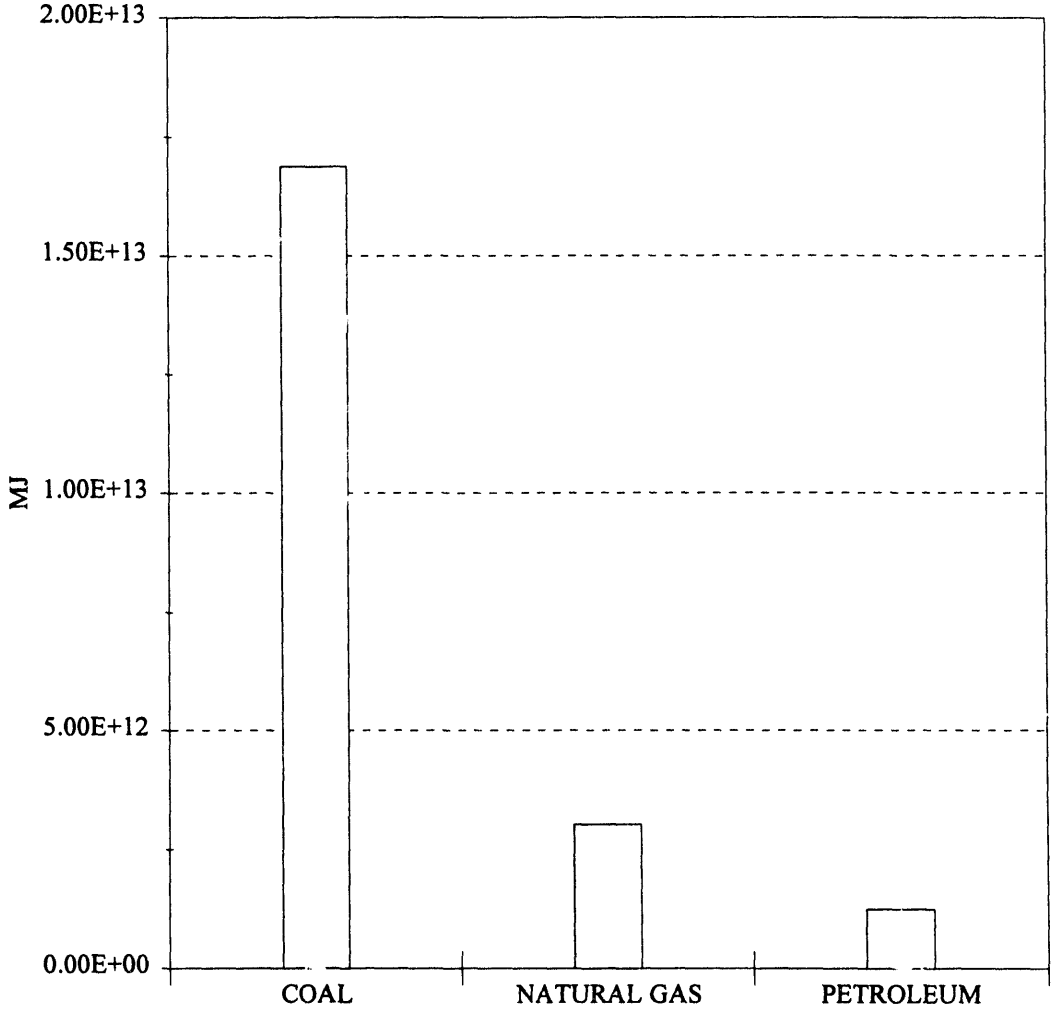

Fig. 1.2 Electricity Generation by Fuel Source (Annual Energy Review, 1991)

2) To reduce the emission of pollutants which include NOx, SOx and particulates.

3) To reduce the ash slagging and fouling problems.

4) To improve the combustor design.

In order to predict the performance of the burner, one must understand the basic processes governing the combustion of pf suspension.

Extensive work has been done to study pyrolysis, ignition and combustion of isolated particles on the belief that the suspension behavior closely follows the combustion process of an isolated particle. However the particles are closely spaced near the burner and hence interactive effects are important. Prior to the discussion on effects of interaction, combustion process will be briefly described. Coal typically consists of 40% volatile matter (VM) or combustible gases and 60% fixed carbon (FC). One possible scenario of combustion process is as follows: When a coal particle is placed in a hot furnace, it undergoes pyrolysis and gases like CO, CO_2, CH_4, C_2H_2 etc are released. The volatiles diffuse into the hot ambience where they react with oxygen to establish a flame in the gas phase outside the particle. Such a process is called homogeneous ignition. After the volatiles are exhausted, the gaseous flame is extinguished and now oxygen diffuses to the carbon surface and forms a surface flame. The CO_2 and CO formed as a result of oxidation reactions diffuse out to the ambience. The other possible scenario is as follows. If VM is low or coal is of low heating value, the surface flame may be established first. Such a process is called heterogeneous

ignition. The VM if any burns along with FC. The results of the isolated particle analysis are used for making simple calculations of ignition mechanism: heterogeneous vs homogeneous and burning time. However when there are too many particles in a cloud, the results are different. The pyrolysis and burning rates are reduced due to the presence of other particles because of competition for heat and oxygen. Hence the assumption of isolated particle behavior for a particle in the cloud is not justified unless the cloud is dilute. Thus interactive effects must be accounted for.

Consider a cloud of radius Rc (Fig. 1.3). If the cloud is dilute, the oxygen mass fraction in the interparticle space will be same as the ambient mass fraction. In this case, the particle is said to be burning in isolated particle combustion(ISOC) mode without any interactive influence from the neighboring particles (Fig. 1.3). The total burning rate of the cloud is just the sum of isolated particle burning rates. If the number of particles is increased in the cloud of same radius Rc, then the oxygen mass fraction decreases toward the center of cloud. Combustion under these conditions is called as group combustion (GC). If the number density of the cloud is increased further, severe interaction sets in, the oxygen mass fraction at the cloud surface is negligible and the burning rate is controlled by the mass transfer of the oxygen molecules to the cloud surface rather than to individual particles. Here the combustion is said to occur under sheath mode (SC). Figure 1.3 shows the effect of O_2 interactions only.

Recently literature is emerging on interactive combustion involving a few

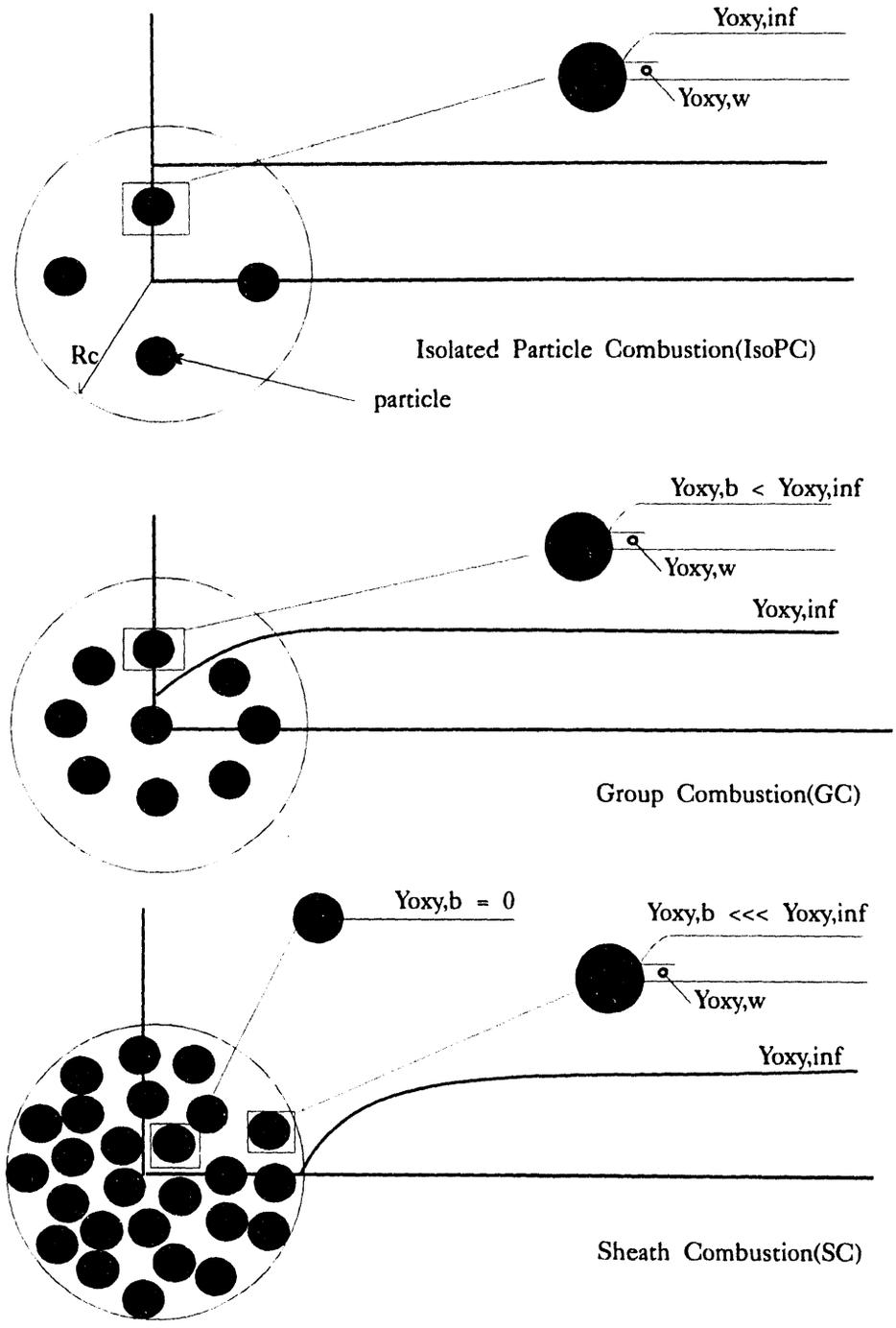

Fig. 1.3 Illustration of Group Combustion for a Cloud of Particles.

particles called array combustion, a stream of large number of particles called stream combustion and finally a cloud of large number of particles called cloud combustion (Fig. 1.4). Array combustion studies involving two particles were carried out in the past (Kharbat, 1992; Gieras et al., 1986). However a practical system involves a large number of interacting particles. The group combustion studies normally involve a cloud containing a large number of particles. Group combustion studies on droplets show that if the interdrop separation is about 7000 times the radius of the drop, individual flame for each droplets can be viewed. Typically, in small scale droplet experiments, a particle density of 10^9 particles/m^3 is used which is far above 200 drops per m^3 required for ISOC. Almost all the practical systems use denser clouds and in order to improve their efficiency, cloud studies are important. While group combustion studies have been carried out for droplet clouds, only recently, mathematical models are reported for different coal cloud configurations. The group combustion models (Ryan et al., 1991; Du et al., 1993) for spherical and cylindrical clouds reveal homogeneous ignition and flame outside the cloud for a dense cloud and heterogeneous ignition for a dilute cloud. Further the burn rate is reduced with increased denseness of the cloud. The results of the theoretical models could not be verified for a spherical cloud since it is difficult to create the cloud under normal gravity. However cylindrical geometry may be easily created. Hence stream experiments are carried out using laminar flow reactors (LFR). Typically in a LFR, a stream of particles are injected downward into a hot vitiated ambience produced by a propane burner (Ruiz et al., 1990). The ignition

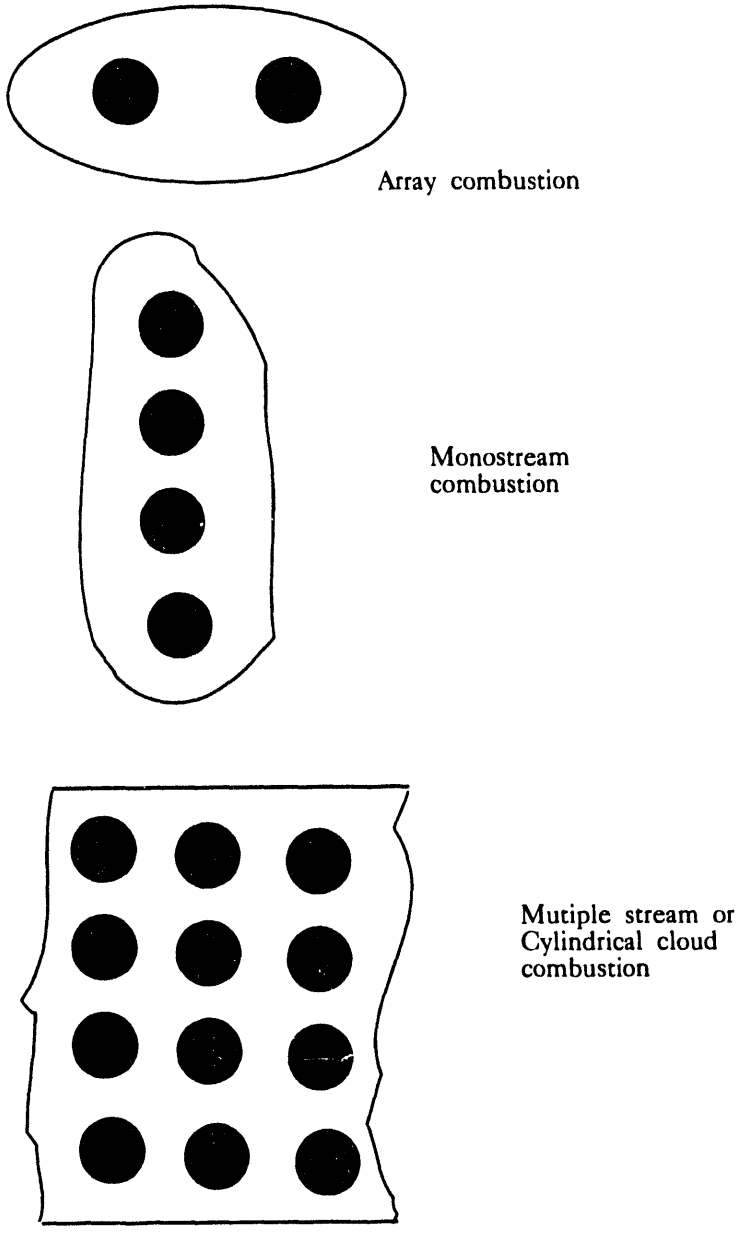

Fig 1.4 Array, Stream and Cloud Combustion of Coal Particles

and combustion behavior of the stream are observed through quartz windows. However, the visualization of coal flames is hindered due to deposition of coal particles on windows. Further it is difficult to distinguish between the central cold coal stream and outer flames due to the brighter flame from photography.

1.1 Scope of the Present Work

The present work uses an unconfined flat flame burner which produces hot vitiated gases. A dense stream of coal particles is injected upward against gravity. The ignition and combustion processes are then captured by a digital camera and stored in the computer for imaging analysis. The analysis of burnt particles and the images captured by digital camera are subsequently used to obtain data on ignition mechanisms and burnt fraction. A non-steady group combustion is developed for a cylindrical stream of particles and the predictions are qualitatively compared with experiments.

CHAPTER II

LITERATURE REVIEW

This chapter presents an overall review of the work in the area of stream combustion. Review is carried out in the following order: isolated particle, array combustion and stream combustion and optical methods employed in the various combustion experiments. Droplet behavior is also reviewed in order to compare the results from droplet and particle combustion studies. The combustion research using image processing is finally also reviewed.

2.1 Coal

Coal is an inhomogeneous organic fuel, formed largely from partially decomposed plant materials. Coals vary greatly in their composition. When a coal particle is placed in a hot furnace, it heats up, releases volatile matter (VM) and the skeletal matter is called fixed carbon (FC). The coal is characterized by proximate and ultimate analysis. The proximate analysis yields VM, FC, moisture and ash. The ultimate analysis yields the elemental composition. Typical coal composition include 65-95% carbon, 2 -7% hydrogen, up to 25% oxygen, 10% sulphur and 1-2% nitrogen. Inorganic mineral matter (ash) as high as 50% has been observed but 5-15% is more typical. Moisture levels commonly vary from 2% - 20%, but values as high as 70% has been observed (Smoot, 1985). The coal rank increases with the period of aging which results in loss of volatile matter.

2.2 Coal Vs Droplet Combustion

It is important to realize the differences in the combustion process of combustion of oil drops and coal particles. Considering a single oil drop placed in a hot furnace, the heat wave propagates to the drop surface and heats up the oil drop. Vapors mix with surrounding oxygen and establish a diffusion flame well outside the droplet surface. This flame is fed by the vapor from the drop and oxygen coming from the ambience. In the case of coal, it pyrolyses, produces volatiles which diffuse into the ambience, react with oxygen and establish a flame. As the volatiles in coal are depleted, the flame moves toward the particle, finally a surface flame is formed with a reaction dominated by carbon oxidation. When flame is farther away from the particle surface during homogeneous combustion of volatiles the flame attains a larger surface area which results in increased burn rate.. But in char combustion, the oxygens must be transported to the particle surface where the reaction surface area is less leading to slower combustion rate for char as compared to the combustion of volatiles.

2.3 Isolated Particle Combustion

2.3.1 Carbon

The major fraction of heat released from coal is due to combustion of carbon. Oxygen reacts with carbon and produces CO or CO_2. The CO and CO_2 produced at the particle surface diffuse through the film zone into the ambience where CO is oxidized to CO_2 (Fig 2.1). The four important heterogeneous reactions are:

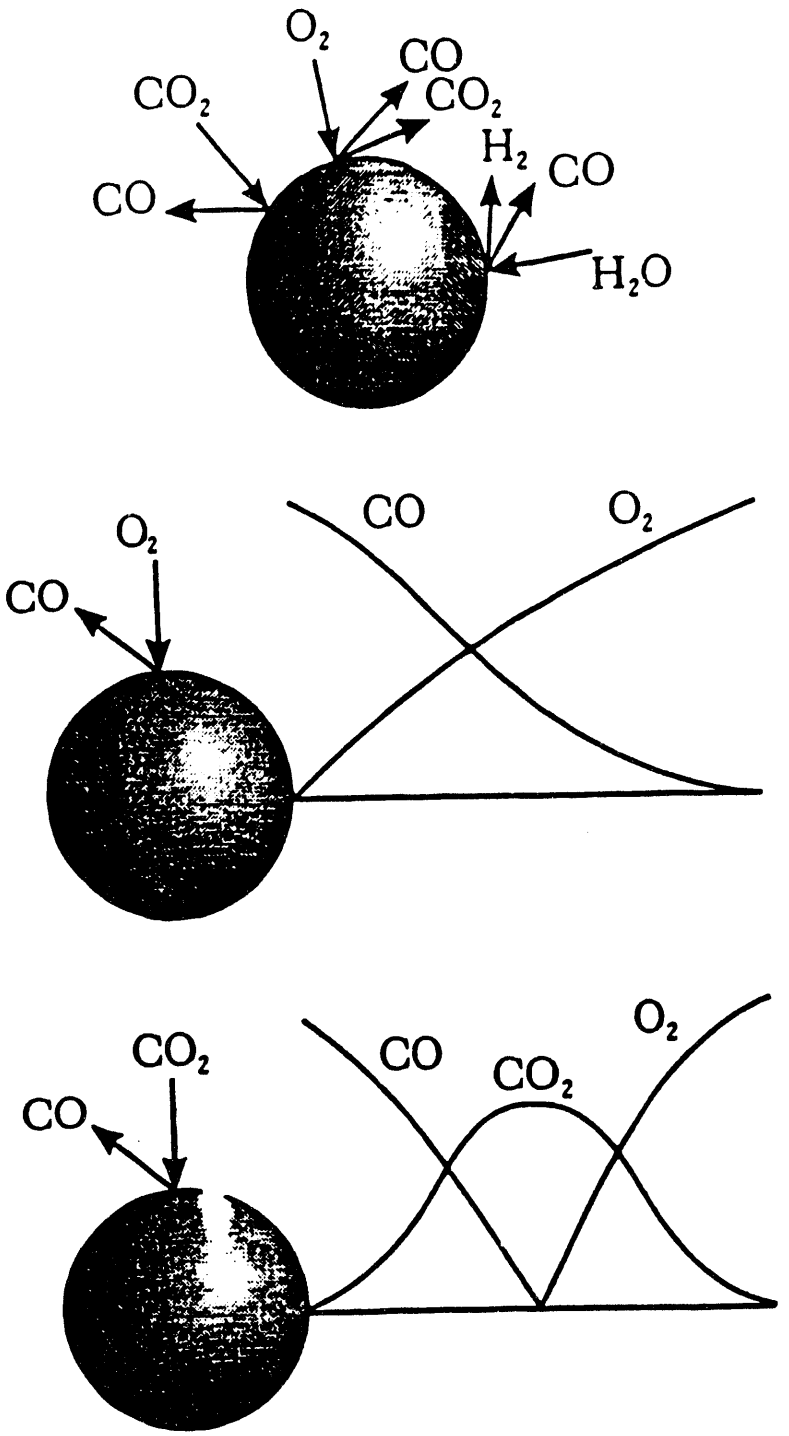

Fig 2.1 Single and Double Film Models for Coal Combustion

$$C(s) + \frac{1}{2}O_2 \rightarrow CO \quad (1)$$

$$C(s) + O_2 \rightarrow CO_2 \quad (2)$$

$$C(s) + CO_2 \rightarrow 2CO \quad (3)$$

$$C(s) + H_2O(g) \rightarrow CO + H_2 \quad (4)$$

The CO produced from the surface reacts with O_2 in the gas phase to produce CO_2 by the following reaction.

$$CO + \frac{1}{2}O_2 \rightarrow CO_2 \quad (5)$$

As the carbon is heated, the temperature increases. Subsequently the reaction becomes rapid resulting in rapid increase in temperature or ignition. Since oxygen consumption is fast and the O_2 must diffuse through the film, the combustion is essentially controlled by diffusion of oxygen. As the particle size decreases, the mass transfer rate increases and hence combustion may become kinetics controlled (Annamalai et al., 1993). The ignition of carbon/char is called heterogeneous ignition.

2.3.2 Coal

Coal is a partially pyrolyzing solid. The volatiles released from coal can either ignite in the gas phase or the carbon can react with oxygen resulting in heterogeneous ignition. Thus for coal, the ignition can be in either heterogeneous (carbon oxidation) or homogeneous mode depending upon its volatile content. Larger the particle size,

more the quantity of volatiles released and homogeneous ignition mechanism is more likely. On the other hand, for smaller particle sizes, flammable mixture cannot be produced due to very little volatiles released. Thus the carbon in the coal reacts with the oxygen adjacent to the particle resulting in heterogeneous ignition. Extensive research studies have been done on ignition of coal particles (Howard and Essenhigh, 1967; Annamalai and Durbetaki, 1977; Bandyopadhayay et al., 1972; Karcz et al., 1980). These studies reveal an increase in ignition temperature and tendency to ignite heterogeneously as the particle size decreases.

2.4 Interactive Array Combustion

Suppose two coal particles are suddenly placed far apart in a quiescent and hot environment. Each particle releases volatiles and establishes a flame around each particle. If particles are placed at closer interparticle spacing, the particles form a common flame called group flame due to deficient O_2 within interparticle spacing. The interactions result in reduced interstitial temperature, lowered heating rate and temperature of the particles and increased volatile concentration or fuel rich regime. Most importantly, the mass burning rate of each particle is less as compared to isolated particle mass burning rate. The correction factor to isolated particle mass burning rate is defined as

$$\eta = \frac{\dot{m}_{s,c}}{\dot{m}_{iso}}$$

in analogy to the droplet literature. Similarly, the volatile yield is also affected by

interactions. One can define a Q factor for the reduced volatile yield.

$$Q = \frac{VM_{iso}}{VM_{ASTM}}$$

where VM_{ASTM} corresponds to ASTM volatile yield obtained by placing a cloud of particles in a crucible. It should be noted that Q factor is approximately the inverse of correction factor. Gieras et al., (1986) conducted experimental and theoretical investigations on ignition and combustion of coal particles arranged in a row under zero and normal gravity conditions. The effects of particle size, coal type and oxygen concentration in the hot ambience on the ignition process were investigated. The burn rate is apparently unaffected by gravity.

2.5 Stream Combustion

The particle ignition and combustion have been studied experimentally using a stream or cloud of particles. Bradley et al., (1984) seeded small amounts of graphite in the laminar,flat,low pressure fuel-lean methane-air flat flame to study the oxidation rates. The velocity profiles of the particles through the flames were measured by laser Doppler anemometry. Gas temperature was measured by two color method. The particle size distribution were measured from the visibility of the scattered Doppler signal. An appreciable increase in the oxidation rate was observed in the flame reaction zone attributable to the transient species or radicals in the reaction zone.

Midkiff et al., (1986) determined the extent of heterogeneous combustion in the

rapid-devolatilization regime by using 40 cm^2 burner with coal fed by a pressurized, fluidized-bed-type feeder. Gas and particle temperatures were measured using a pyrometer. Gas samples were extracted at various heights along the burner's vertical centerline using a water-cooled suction probe. The solid samples were extracted in separate experiments from the same flame positions using a water cooled probe. The proximate analyses of the partially burned solids were used to determine the mass fraction of the initial or unburned, dry, ash free coal remaining as ASTM fixed carbon and volatile matter at various residence times by using ash as a tracer. Because the ash vaporization is expected to be kinetically limited and because it is only the early,rapid-devolatilization phase that is of interest here,errors due to the alteration of ash content should be minimum. The experimental results show that heterogeneous combustion can be quite important in the rapid-devolatilization phase of pulverized coal flames and necessitate that heterogeneous processes be included in the models of pollutant formation during the rapid combustion period of coal flames.

Petarca et al., (1986) fed a known quantity of coal from a dryer by a N_2/O_2 stream into a small reactor. The experimental set up is shown in Fig. 2.2. The reaction was started by feeding air, preheated to the reactor temperature. Samples of the product gas were analyzed every 8-10 min during the first 2 or 3 hrs and at longer intervals thereafter. The effect of temperature, oxygen partial pressure, particle size, and gas flow rate were evaluated. The rate of oxidation decreased with increasing time of oxidation, the lower the temperature, the faster the rate decreased.

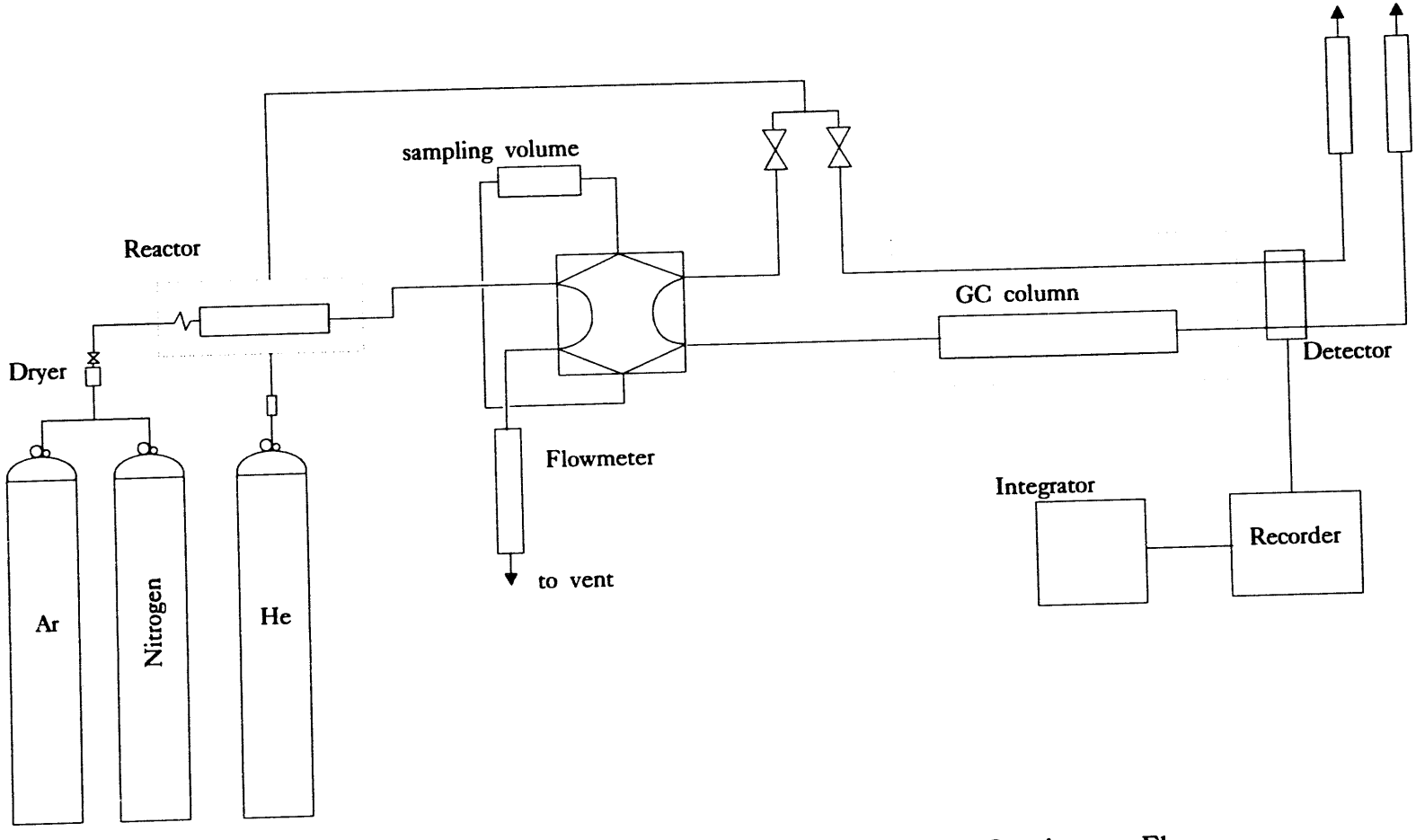

Fig. 2.2 Schematic of Experimental Apparatus for Continuous Flow (Petarca et al., 1986).

Solomon et al., (1988) applied Fourier Transform Infrared (FT-IR) Emission and Transmission (E/T) technique to study coal flames produced in a transparent wall reactor. The transparent wall reactor (TWR) used consists of an electrically heated furnace and a heat exchanger. Dry air heated through heat exchanger enters the reactor at a temperature of 850 deg C and at a velocity of 2.8 m/s. Coal entrained in a cold carrier gas (dry air) is injected through a coaxial 4 mm diameter tube. The arrangement is shown in Fig. 2.3. Short exposure photographs show particle tracks which indicate that coal particles are moving with a velocity of 2.5 m/s near the injector and 4.8 m/s in the flame. The particles gain velocity from the hot gas by momentum transfer. Photographs are presented in Fig. 2.4. A comparison of the ignition of several samples suggests that ignition of chars is heterogeneous, ignition of high rank coals (high quality VM) is homogeneous but low rank coals (low quality VM) exhibit both homogeneous and heterogeneous contributions to ignition.

Field (1970) fed dry char particles into the preheated gas stream through alumina feeder tube purged with nitrogen. The transit time of the particles in the reaction zone is controlled by the mainstream gas velocity and not by the rate of fall under gravity. The apparatus is shown in Fig. 2.5. The gas and the reactor wall temperatures were adjusted to be equal to each other. The transit time calculated from the measurements of gas velocity was 27 ms for a transit distance of 120 mm at the total gas flow rate 80 L/m(cold). The transit time of the particles in the reaction zone is controlled by the mainstream gas velocity and is inversely proportional to the gas

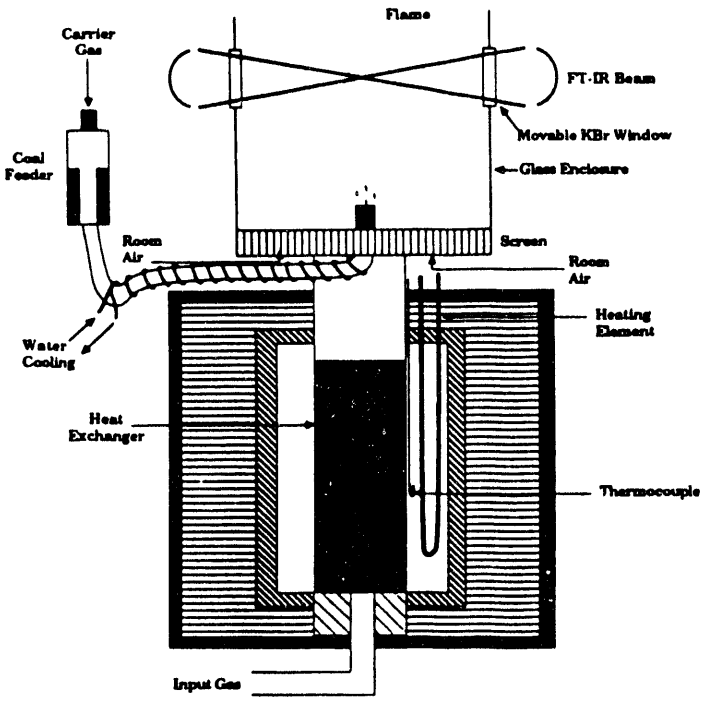

Fig. 2.3 Transparent Wall Reactor (TWR)
(Solomon et al., 1988).

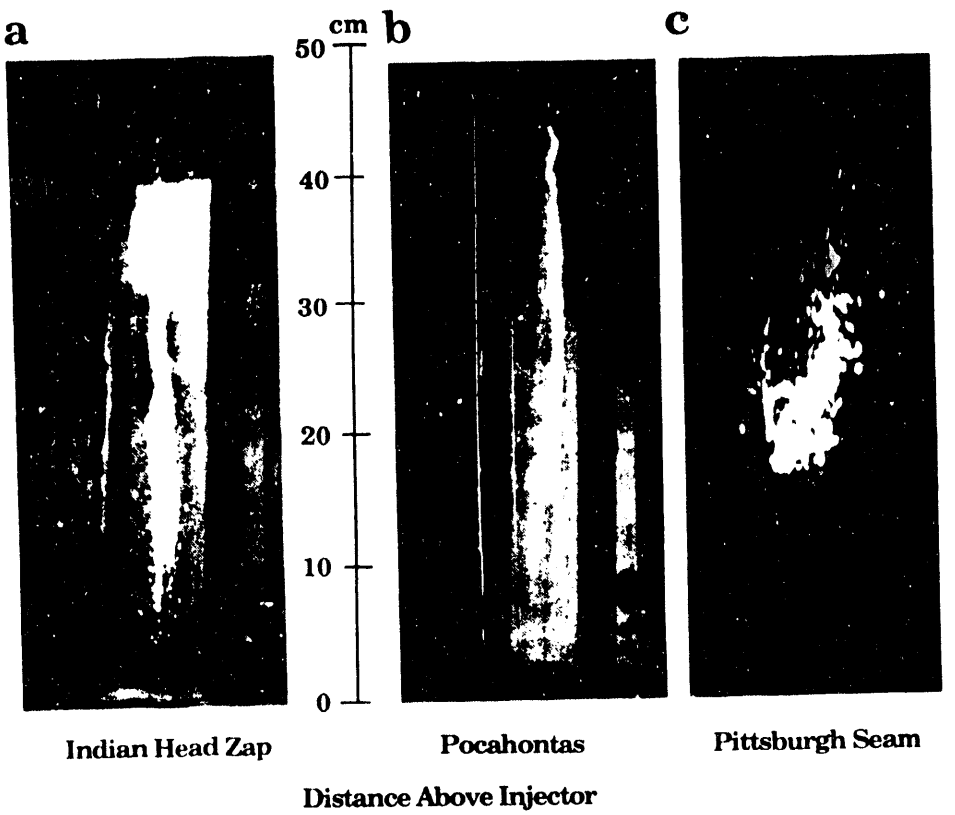

Fig. 2.4 Photographs of Different Coal Flames from TWR (Solomon et al., 1988).

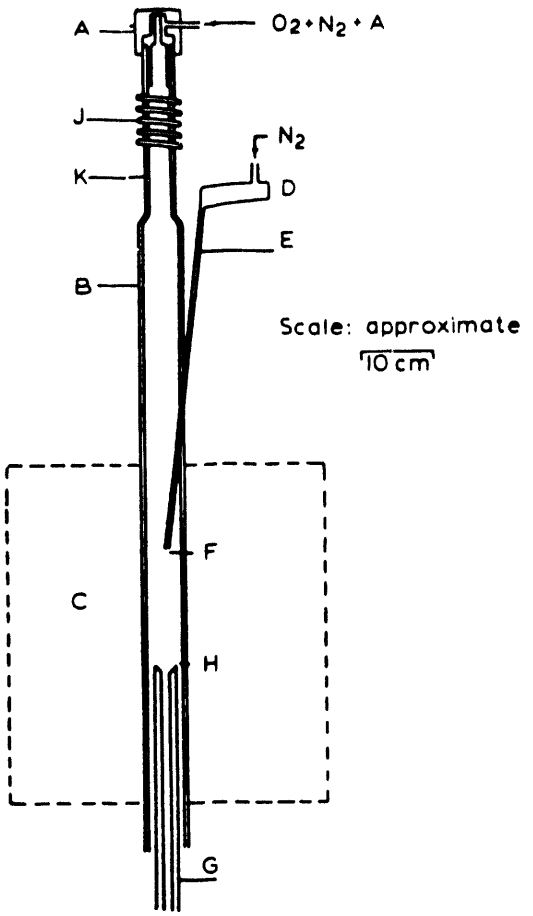

Fig. 2.5 Apparatus Set Up for Reaction Rate Measurements (Field, 1970).

temperature. Eleven coals were tested to cover the range from anthracite to low rank coal. It was reported that the surface reaction rate coefficient is strongly dependent on coal type and increases linearly with surface temperature, the rate of increase depending on the coal.

Wall et al., (1988) used electrically heated LFR with coal stream fed through a water cooled injector for the coal ignition experiments. Particle heating rates are estimated at 10^3-10^4 C/s and the coal residence time as about 900-1100 ms for 63-93 micron particles. As the furnace is slowly heated at 10 deg C/min, an early consumption of oxygen is measured, the initial flashing is observed by using photo multiplier with no associated change in the extent of combustion followed by rapid combustion. Flashing is shown to be an extremely rare event with only a single flash observed for several thousand coal particles fed.

Absolute rates of combustion of four types of carbon particles were determined by Mulcahy (1971) using LFR. The particles within a narrow size range were injected continuously into a stream of preheated gas containing oxygen. The progressive combustion of the carbon was measured by determining the CO_2 and O_2 contents of samples of gas taken from the reactor. By using species balance, the carbon burn rates are calculated and these are then related to the temperature of particles at each position. The gas velocity measurements were the least satisfactory and were used only in an indirect way. Experimental results show the measured rates are less than the limiting diffusion rates over the whole temperature range and the difference increases as the

particle size decreases indicating kinetic control. For larger particles, the measured rate approaches the diffusion rate at the highest temperature.

Leesley et al., (1972) used a 1 D furnace with coal feeding at the rate of 40 g/m. The fraction of unburnt coal remaining at any point in the flame was calculated from the amount of CO_2 present at that point. The time for the flame to travel between the two sampling ports was calculated from the volumetric furnace gas flow rate, the average temperature between the two points and the cross sectional area of the furnace. Both theoretical and experimental burning results have high correlations as shown in Fig. 2.6

A detailed review on group ignition and combustion of coal particles was undertaken by Annamalai et al. (1993). In these experiments a LFR was used with coal particles injected as a cylindrical stream in order to verify the theoretical results (Fig. 2.7). The location of the flame was observed and photographed through a pair of 38 cm long, 19 mm wide quartz windows located diametrically opposite of each other in the walls of the reactor unit. From the knowledge of ignition distance and velocity of particles, (assumed to be same as main carrier velocity) ignition times were estimated. Ignition times show a minimum as the mass flow rate was gradually increased from dilute to dense condition. These findings qualitatively confirm the results from the group ignition theory.

2.6 Stream Combustion Models

Theoretical research in group combustion in the area of liquid drop clouds was

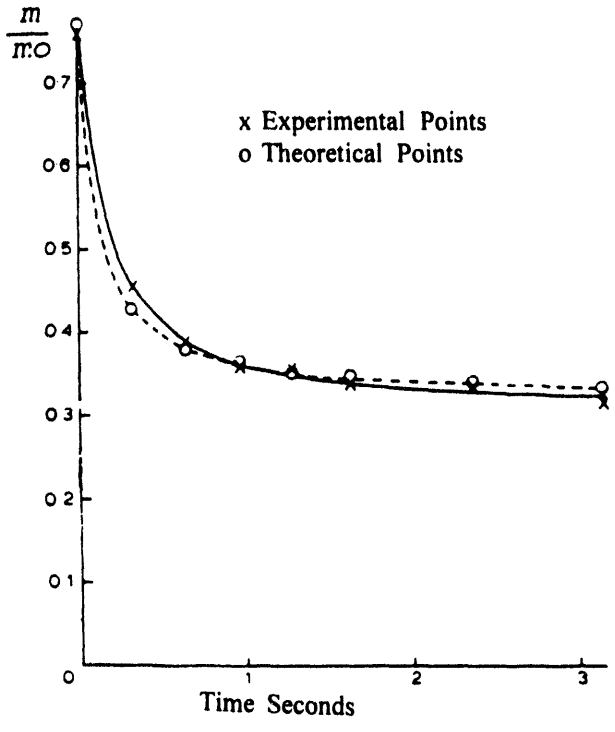

Fig. 2.6 Comparison of Experimental and Theoretical Burning Away Curves (Leesley et al., 1972).

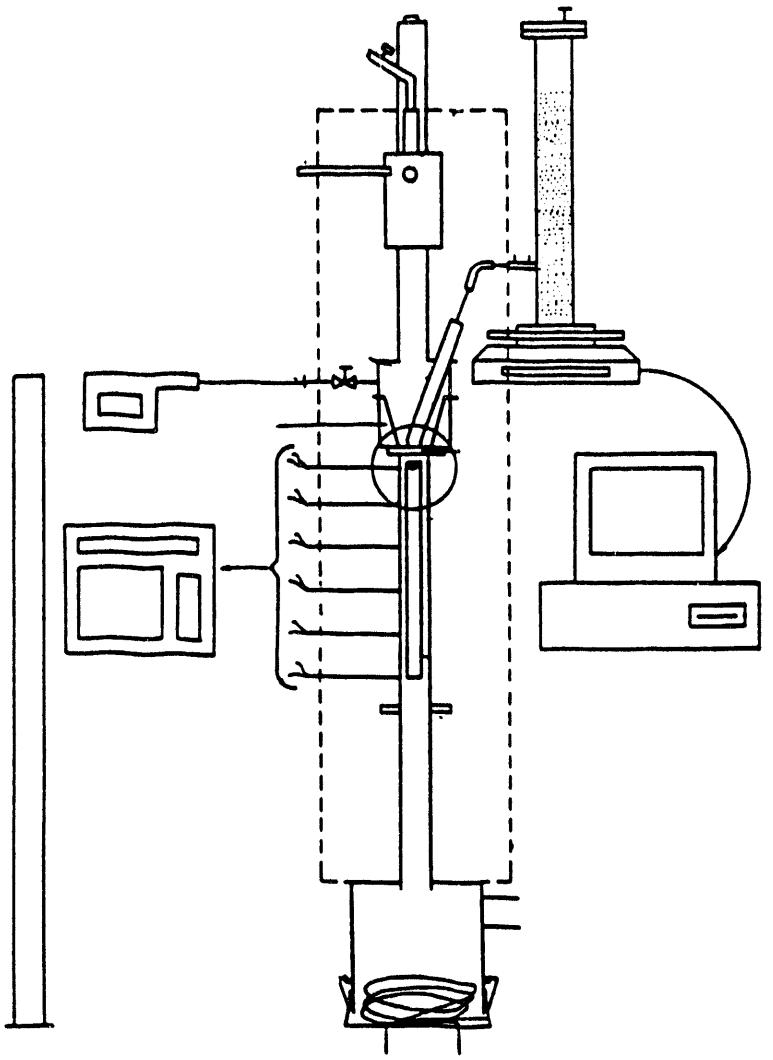

Fig. 2.7 A Laminar Flow Reactor Set Up (LFR)
(Annamalai et al., 1993).

carried out in 70's and 80's. Recently, the model was extended to coal particles by Ryan et al. (1991). The spherical and stream models (Fig. 2.8) indicate i) homogeneous ignition for dense clouds and the heterogeneous ignition for dilute clouds ii) reduction in ignition time as the cloud denseness is increased but increases again beyond certain cloud denseness (A:F 2:1 in the cloud) iii) formation of a diffusion flame outside the cloud and premixed flame inside the cloud (called double flame) in the initial periods of combustion of volatiles iv) reduced burn rate per particle as the cloud denseness is increased under diffusion controlled combustion condition and v) reduction in NOx production with increased cloud denseness.

2.7 Optical Techniques in Combustion

Practically, all combustion systems use solid and liquid fuels which are introduced into the combustion chamber as sprays. These include stationary combustion devices such as furnaces as well as mobiles systems such as internal combustion engines, turbines and rocket engines. Over the past decade, emphasis on pollution control and improved performance has led to better understanding of the fundamental combustion processes like droplet vaporization, particle pyrolysis, droplet and particle combustion, interactive effects in a spray and spray combustion. Real time studies in combustion will be of greater value in this respect. Spray formation and combustion mostly involve highly turbulent flow field conditions. Therefore instantaneous spatially resolved information is also important in order to under to understand the characteristics of the spray or soot formation processes in turbulent flows. This interest

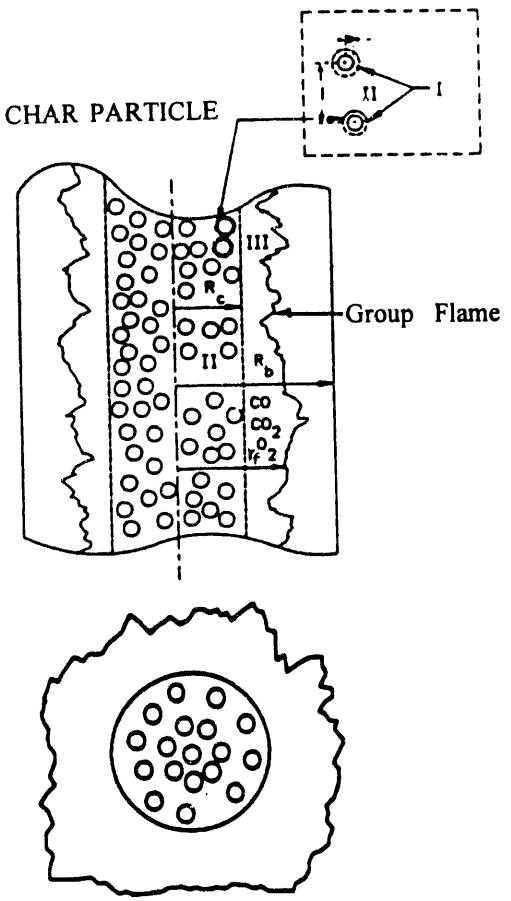

Fig. 2.8 Group Combustion Model for a Cylindrical Cloud of Particles (Annamalai et al., 1991).

insitu techniques has led to significant developments in the area of digital optical techniques for providing non-intrusive measurements.

2.7.1 High Speed Photography

High Speed photography at several thousand frames per second was used extensively by Scott (1969) for studying spray combustion behavior in diesel engines. A few of their studies have been carried out in combustion chambers simulated to resemble those used in practice under normal engine conditions. Sequence of individual frames provide valuable information on the nature of the combustion process in combustion engines. Figure 2.9 shows the combustion sequence in a swirl chamber indirect injection (IDI) engine of the Ricardo Comet V design. Magnified color photographs of the flame around a single fuel spray provide additional insight into the compression ignition and flame development processes.

2.7.2 Digital Imaging

Each photograph of frame sequence in a high speed photography is a hard copy and localized analysis of a particular photograph is impossible. If each frame can be stored as a file in the computer, then the contents of that file can be processed for the investigation. Such a procedure is possible with digital images. Digital images are reproductions derived from the dissection of an object or the image in a photographic negative or positive into electronically encoded picture elements (pixels) by focussing the image onto a Charge-Coupled Device (CCD) or Charge Injection Device (CID). Such a sensor consists of a large number of photosensitive elements. During the

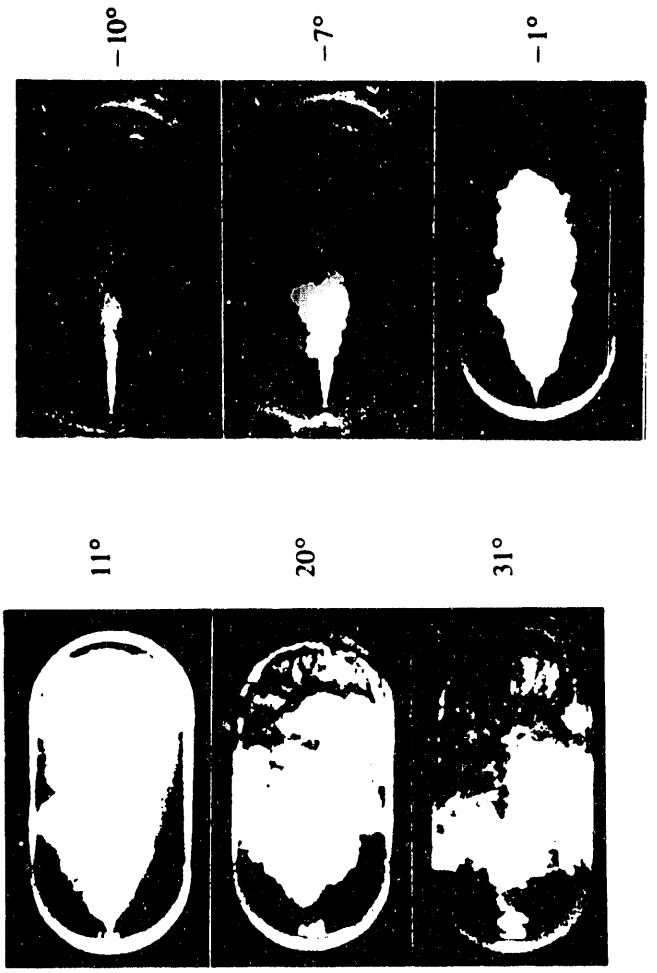

Fig. 2.9 Combustion of Single Spray Burning Under Large DI Engine Conditions (Scott, 1969).

accumulation phase, each element collects electrical charges, which are generated by absorbed photons. Thus the collected charge is proportional to the illumination. In the read out phase, these charges are sequentially transported across the chip from sensor to sensor and finally converted to an electric voltage. This information is immediately converted to binary numbers (digits). In the digital form, the data can be recorded, stored, processed for image enhancement and transmitted at very high speeds over long distances.

Images contain huge amounts of data. Each point on the image can be stored as a byte. Each image frame would occupy memory depending upon its number of data points (pixels). Applications which analyze time varying processes like spray studies can not be analyzed with a single frame but require the analysis of image sequences. The storage requirements then increase tremendously. Also enormous computer power is required to handle these huge image files. Hence, for a complete image processing set up, one requires a sensor (CCD/CID), frame grabber (interface between the camera and the computer) and a powerful computer with large storage capacity. These requirements are now made available because of advancement in semiconductor technology.

Digital Image processing technique has been employed to determine isolated particle behavior and interactive effects between the particles by Kharbat (1992). The time between the successive frames is as low as 33 ms. With digital image processing, one observed a phenomenon called intermittent combustion for a few high volatile coal

particles. The coal flame was formed at 540 ms, vanished at 600 ms, formed again at 630 ms, vanished at 720 ms and eventually formed again at 750 ms. All these images are presented in Fig. 2.10. The interaction between particles in a binary array can be visualized from the Fig. 2.11. A common flame is formed around two particles when the interparticle distance is narrowed down.

Karen J. Weiland (1993) used an intensified array camera to capture very weak (low luminosity) flames of thin paper samples in low gravity experiments at NASA Lewis Research Center. The sample is either an ashless filter paper or a laboratory wiper which burns inside a sealed chamber which is filled with 21%,18% or 15% O_2 in N_2 at 1 atm. The camera views the edge of the paper and its output is recorded on videotape. The flame images are analyzed using a commercial visual data analysis software package. The edge of the flame is specified to occur at a gray pixel level of say 60 out of 255. The gray level is fixed for each flame so that it is the same from frame to frame. The software package allows the user to measure the pixel position of the specified gray level in a single frame. The flame positions are measured at every 0.1 sec to calculate the flame spread rate. This feature of the image processing software aids in the motion analysis using a sequence of flame images. A series of flame images for ashless filter paper burning in 18% oxygen is shown in Fig. 2.12. Flame positions versus time from ignition for ashless filter paper and laboratory wiper samples are plotted in Fig. 2.13.

As stated above, an image is a matrix of data points with the value of each data

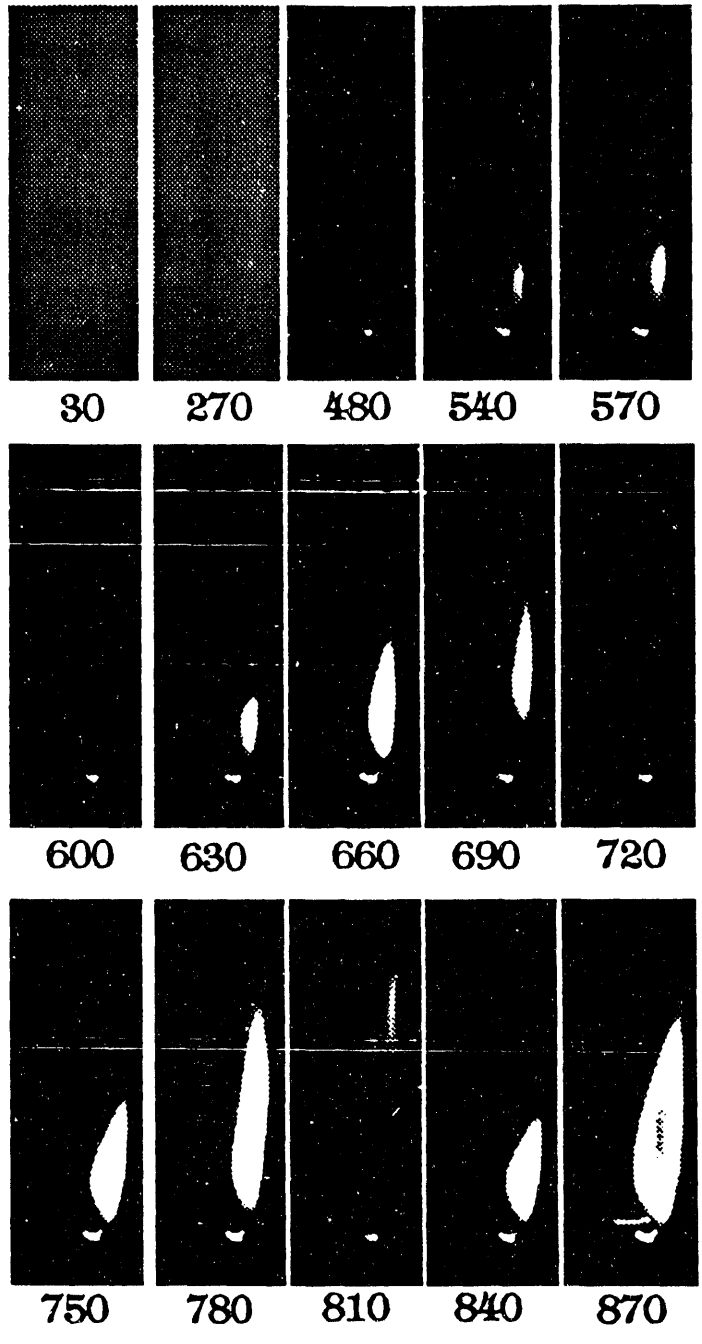

Fig. 2.10 Intermittant Combustion Sequence for High Volatile Coal (Kharbat, 1992).

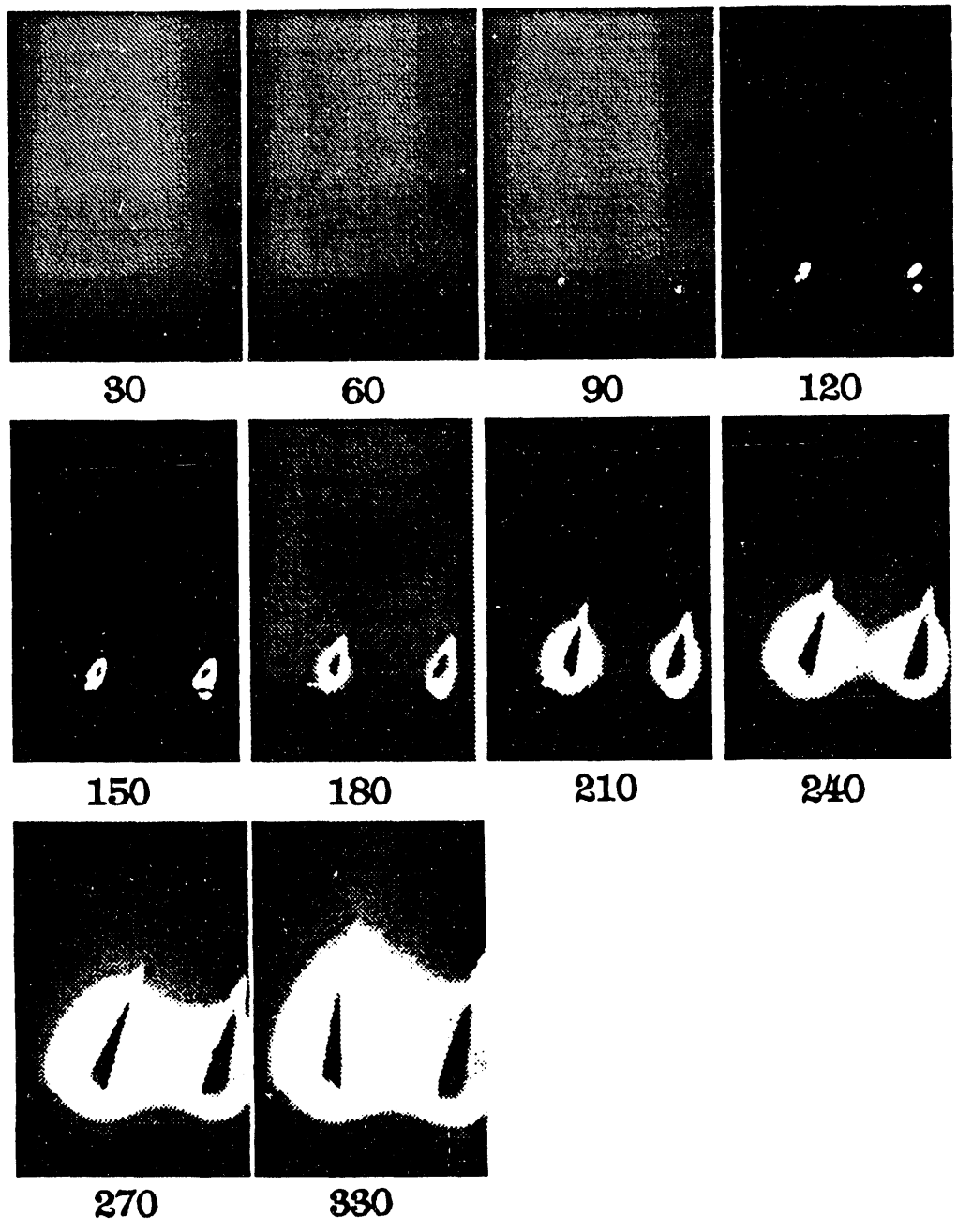

Fig. 2.11 Formation of Common Flame for Two Interacting Particles (Kharbat, 1992).

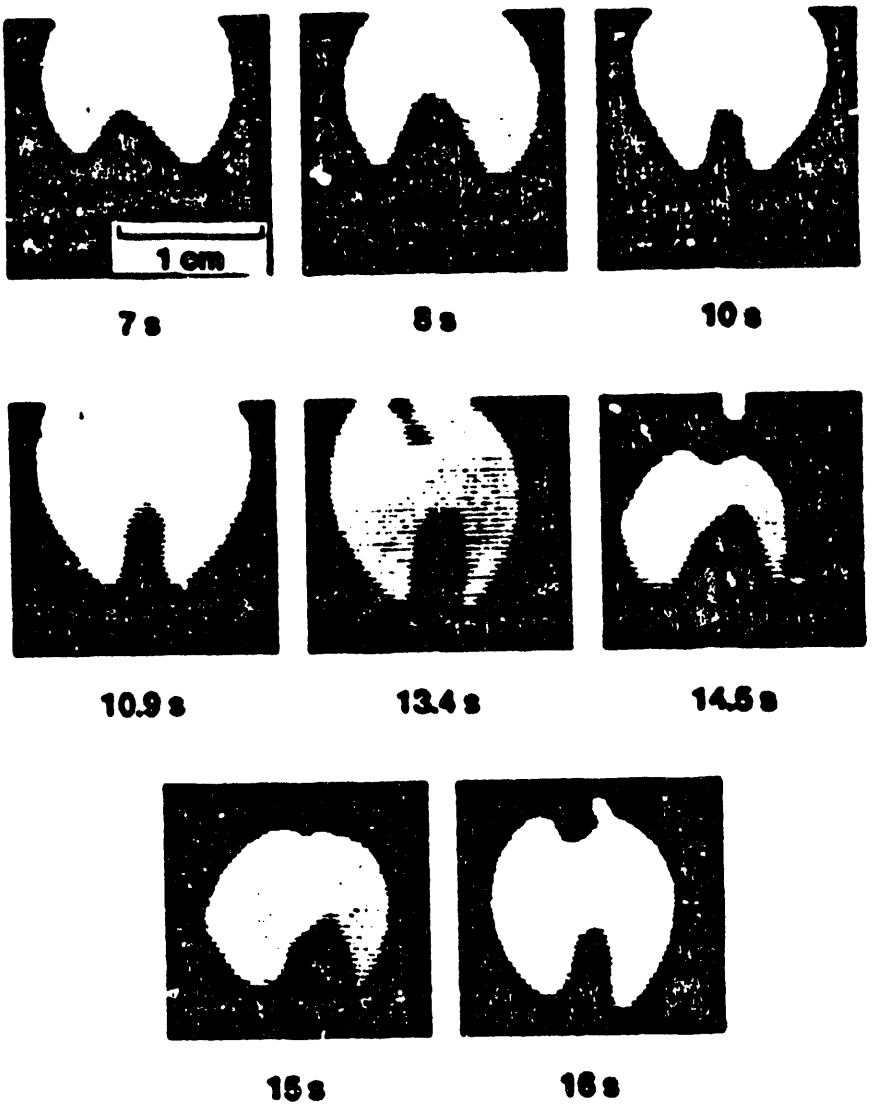

Fig. 2.12 Series of Flame Images for Filter Paper Burning in 18% Oxygen (Weiland, 1993).

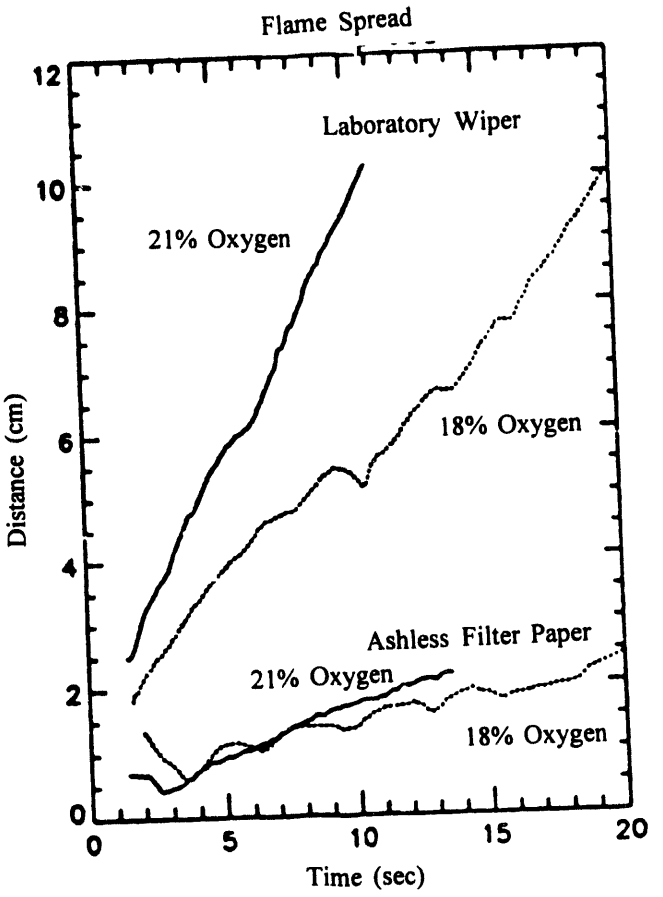

Fig. 2.13 Flame Position Vs Time From Ignition, for Filter Paper and Laboratory Wiper Samples (Weiland, 1993).

point being dependent on the light intensity at a spatial location. Hence, the light source used plays a significant role in image processing applications. In combustion studies, the flames are the light sources. In non-reacting flow studies, an external light source is required to have a detailed images. A laser imaging approach was used by W. Lee et al., (1990) to discriminate the soot particles and droplets in a spray. A thin sheet of laser light was made to pass through the spray. The experimental set up which makes use of 2D light scattering techniques is shown in Fig. 2.14. A pair of simultaneous images were taken using vertically and horizontally polarized scattered light obtained with a beam splitter and two 35 mm cameras. The images on the negative films were digitized using a CID solid state camera with a resolution of 512 by 512 pixels and a frame grabber. The digitized images were analyzed using a personal computer. Figure 2.15 shows water spray obtained by both 35 mm camera and using the image study. The experiment done with the ethylene diffusion flame tracks the soot particles. For highly transient combustion phenomena, such as Diesel and rocket engine combustion, the present planar laser scattering approach may yield new information.

Image processing applications were limited thus far only to combustion of particle, array of particles, papers and for non reacting sprays. It was shown that this relatively new technique provides an excellent tool for transient combustion analysis and flame spread calculations. In the present research, the application is extended to coal particle spray combustion to observe group flame, flame structure and the tracking

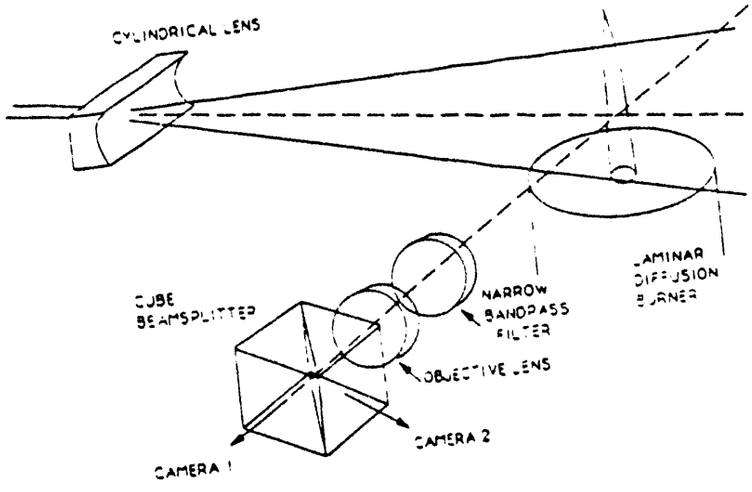

Fig. 2.14 Two Dimensional Light Scattering Experimental Set Up Showing a Thin Sheet of Laser Light Passing Through the Area of Interest (Lee et al., 1990).

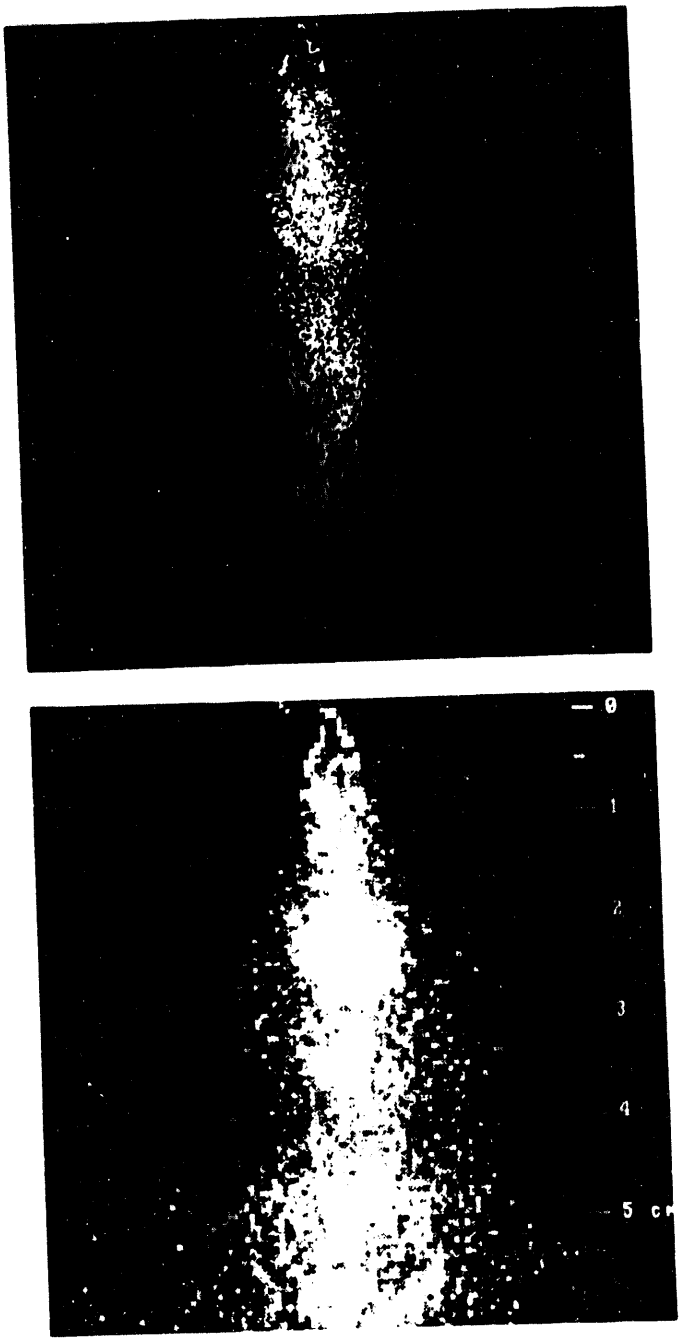

Fig. 2.15 Water Spray From 35mm Camera (Top) and Spray Image (Bottom) (Lee et al., 1990).

of coal stream.

CHAPTER III

OBJECTIVES

The primary objectives of the current research work are to investigate the ignition and combustion behavior of dense streams of coal particles using a flat flame burner facility and digital imaging system and to develop and verify the model results. In order to achieve the stated objectives, the following tasks must be performed.

1. Design, and build an experimental set up suitable for coal stream experiments.
2. Conduct experiments on coal particles with different operating parameters viz gas temperature, oxygen concentration, residence time and analyze the gasification efficiency results.
3. Use an existing image processing systems to capture the ignition and combustion behavior of coal streams.
4. Analyze the captured coal stream flame images for homogeneous and heterogenous ignition modes and flame structure under the different operating parameters.
5. Develop a model on group ignition and combustion of cylindrical cloud of coal particles and compare the data qualitatively with the model results

CHAPTER IV

DESCRIPTION OF EXPERIMENTAL APPARATUS

This chapter describes the experimental set up including various components and their functions. Experimental apparatus includes three main units, *viz.*, i) a flat flame burner, and ii) video imaging system, and iii) particle collection system.

4.1 Experimental Set Up

The experimental set up consists of i) a flat flame burner for generation of hot gases, ii) a locally fluidizing feeder for feeding of coal particles iii) burnt particle collection system for collecting the burnt particles for later analysis iv) diagnostics set up for gas sampling and temperature measurements v) video imaging system for capturing the flame images and vi) particle preparation facilities for grinding the particles, drying and sieving to various sizes. Each of these components is explained in detail in the following sections.

4.2 Flat Flame Burner

The experimental facility centers around the flat flame burner. The burner used is a Holthius flat flame burner manufactured by McKenna Products. A schematic of the burner is presented in Fig. 4.1. The burner is of cylindrical construction with a 6 cm diameter flame area. The flame produced is stabilized above a 6 cm diameter sintered stainless steel disk with cooling coils embedded within the disk. Water is used as the active cooling medium to facilitate rapid flame stabilization. Any surges which exist in the reactant stream at this point are settled in the cavity located below the

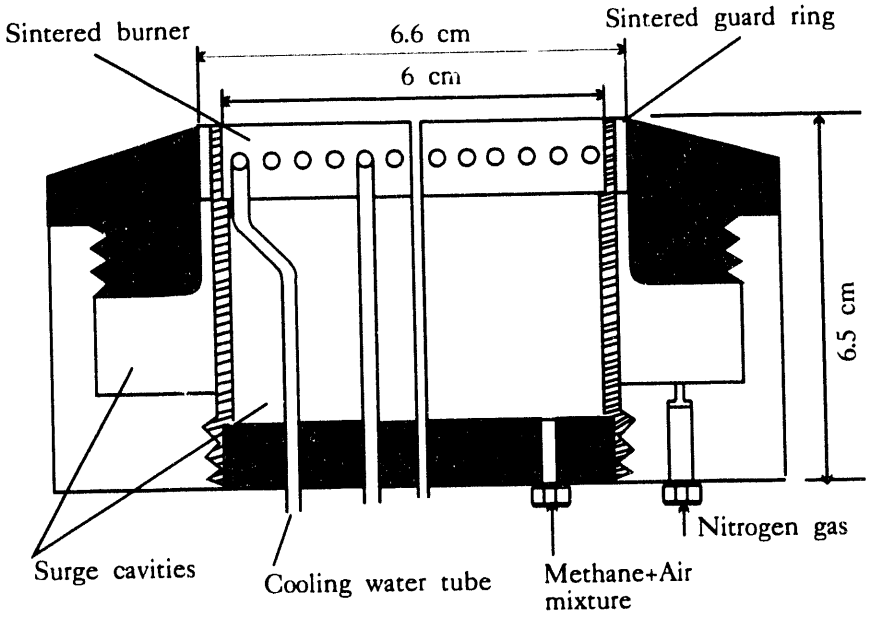

Fig. 4.1 Flat Flame Burner.

sintered disk. The flames produced are shielded from the entrainment effects by passing N_2 (inert) around the flame holder through a bronze porous plug of 6.6 cm diameter. The inert gas is introduced to the bottom of the burner into a cavity so that any surges present are damped out. This burner has a hollow stainless steel tube of internal dia 2.03 mm fixed at its center serving as a coal particle injector. The major components of the flat flame burner are shown in the exploded view (Fig. 4.2). The burner is fixed onto a vertically traversing table which is located on a mobile table. This set up enables the vertical translation of the flat flame burner.

A mixture of methane and air is used as a flammable mixture for establishing the flat flame. Flow meter 0 to 5 SCFH and 0 to 100 SCFH are used for methane and air flows respectively. The air to fuel ratio is controlled by adjusting the flows in the control panel. Nitrogen serves as the inert gas flowing through the annular porous ring. Methane and nitrogen are supplied from two separate cylinders while shop supply is used for air. Water flow to the burner is also metered through the flowmeter. Figure 4.3 shows the schematic of the flat flame burner facility.

4.3 Locally Fluidizing Feeder (LFF)

The LFF system shown in Fig. 4.4 is described in detain elsewhere (Annamalai et al., 1992) consists of the coal container (1), the feeder lid (2), and the locally fluidized off take system (3). The coal container is 3.81 cm (1.5") diameter made of Plexiglass with a flange at the top and closed by the removable lid to allow the replenishment of the feeder. A gasket (4) is used in between the flange and the lid to

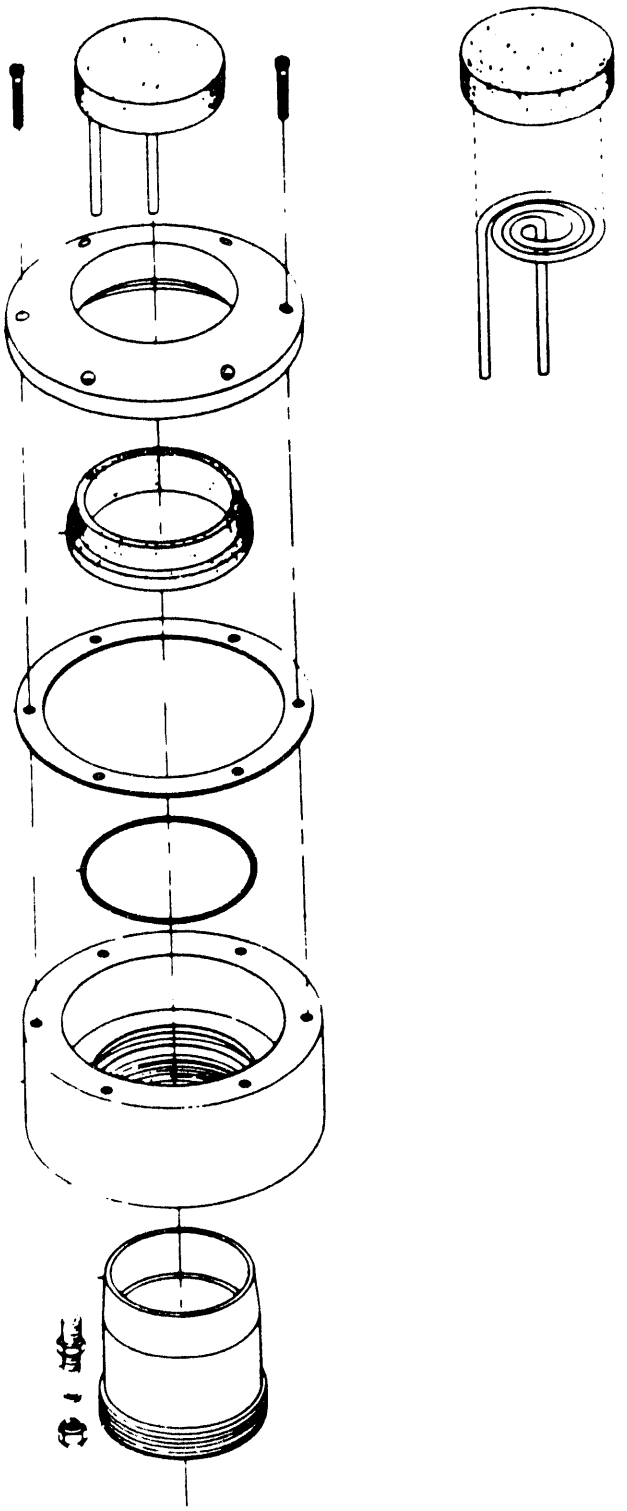

Fig. 4.2 Exploded View of Flat Flame Burner.

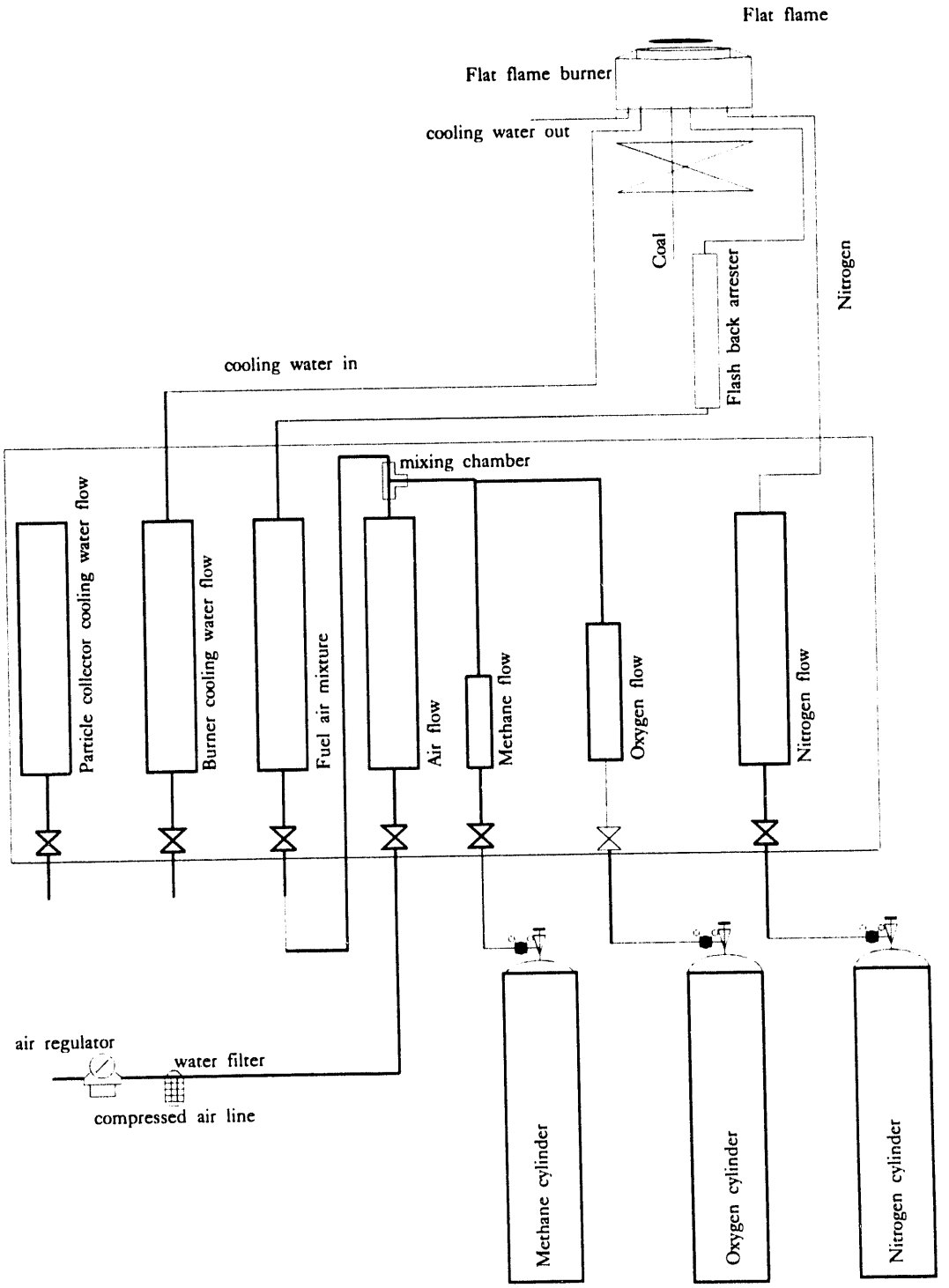

Fig. 4.3 Schematic for Flat Flame Burner Experimental Set Up.

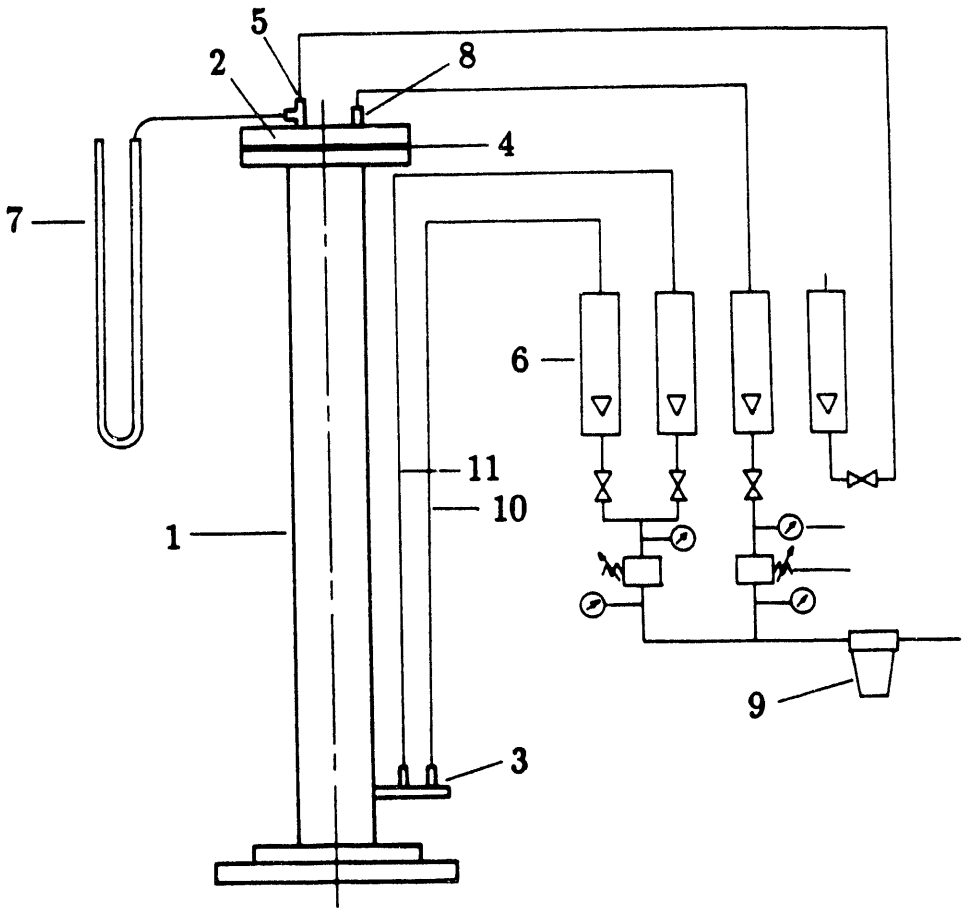

1. Coal Container
2. Lid
3. Off-take System
4. Cork Gasket
5. Pressurizing Air
6. Rotameter
7. Manometer
8. Exhaust Air Port
9. Water Separator
10. Dilution Air Line
11. Fluidization Air Line

Fig. 4.4 Locally Fluidized Feeder (LFF) (Annamalai et al., 1992).

arrest the air leak. The lid is a Plexiglass disk in which two threaded holes have been drilled. Brass fittings are fastened onto these holes (5 and 8) and connected by hoses one of which is for manometer (7) to measure the bed pressure and other is for the exhaust air to flow through a flow meter (8). A female threaded brass adapter is glued to the container at a height of 25.4 mm (1") from its bottom end. This adapter helps fixing the locally fluidizing off-take system onto the container and entering the coal bed. The dilution air enters through (10) while the fluidizing air enters through (11). Compressed air via a pressure regulator (9) was used for the experiments.

The central part of the feeder is the off-take system. The off take system consists of a transport tube (1), the dilution air jacket (2) and the fluidization air jacket (3). The transport tube is a 20 mm long, 1.5 mm id stainless steel tube. At 14 cm from the off take point, there are 1.0 mm dia holes (6) drilled radially through the tube wall. This portion of the transfer tube is covered by dilution air jacket. The transport tube is surrounded by the fluidization air stainless steel jacket (3) of 6.7 mm length and 6.5 mm id which provides 2 mm annular gap between the transport tube and the annular jacket. An annular plastic filter is mounted between the fluidizing air jacket and the transport tube at the off take point. The filter serves as the air distributer to the bed for the local fluidization around the off take point. The dilution air (9) enters the transport tube through four dilution holes. The dilution air creates a positive pressure in the transport tube thereby affecting the pressure differential between the hopper and the point at which dilution air enters the tube and hence coal flow is controlled by dilution

air. The transfer tube is then connected to the flat flame burner coal injector tube through a stainless steel tube and a short PVC hose.

The feeder is placed on a highly sensitive digital balance to register the instantaneous weight reading of the feeder. The balance is connected to a 286 personal computer to store the digital values with time for calculating coal mass flow rate. The feeder is supplied with fluidizing and pressuring air as explained before and these flows are metered with the flow meters on the control panel. These flowmeter readings along with coal mass flow rates determine the A:F ratio of the coal flow. The positive fluidized bed pressure is necessary for overcoming the frictional resistance through the small injector tube. The entire set up of the feeder is shown in the Fig. 4.5.

4.4 Particle Collection System

The schematic of the particle collection system is shown in Fig. 4.6. The sampling probe is designed as a separate component which can be fixed at any location above the burner. The particle collection tube is of 1/4" dia OD and 3/16" ID and is made of copper. This tube is housed in a water jacket made of copper near its inlet end. The outside diameter of the jacket is limited to 7/8" to avoid blocking the coal flame. It is made of conical shape to avoid eddies in the wake of the flow. The water jacket has one inlet tube which provides efficient cooling at the tip. The cooling is used to arrest any coal reaction once the particles enter the probe. The probe is connected to a vacuum pump via a collection beaker made of pyrex glass. The collection beaker has an outlet for measuring the suction pressure. The distance

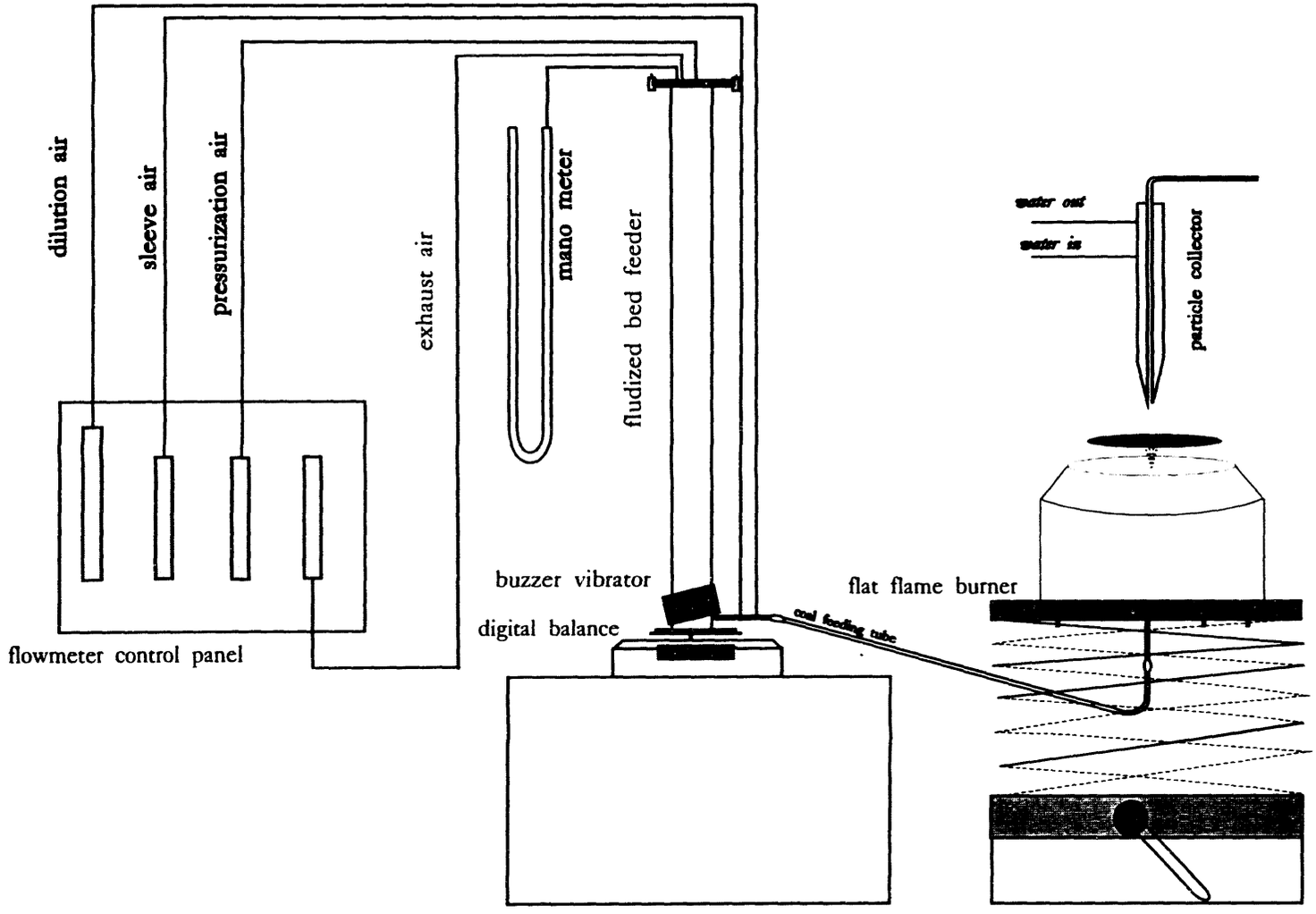

Fig. 4.5 Coal Feeder Set Up.

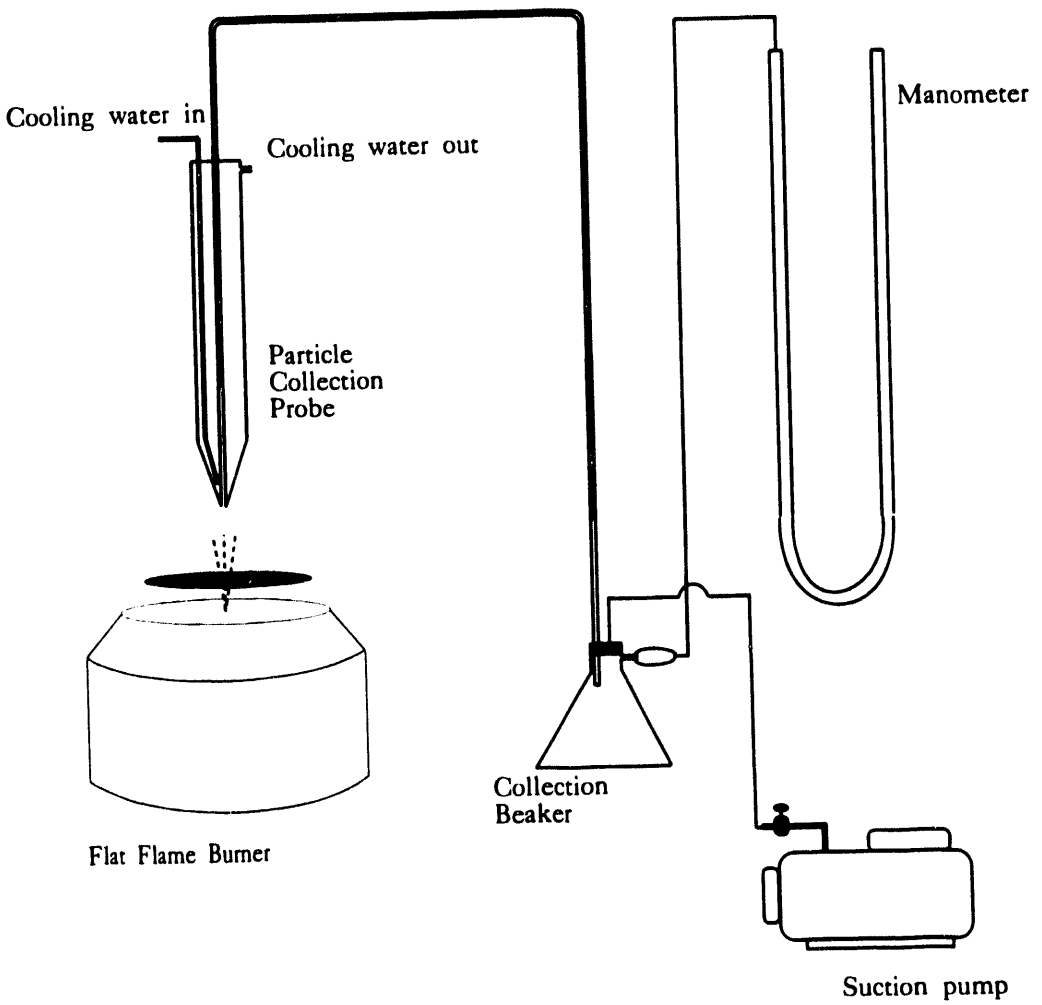

Fig. 4.6 Particle Collection Probe Set Up.

between the flat flame burner and probe tip can be varied to have different residence times for the coal stream.

The water vapor from the methane combustion condenses when they contact the cold surface of the collection probe. Sometimes these water droplets enter the suction probe, wet the coal which blocks the flow of coal. Further the suction pressure is affected. In order to avoid condensation, warm water is supplied to the cooling system.

4.5 Diagnostics

The two important governing parameters in the combustion of coal stream are gas temperature and the oxygen concentration in the vitiated gases generated by the flat flame burner. The arrangement is shown in Fig. 4.7.

4.5.1 Gas Temperature

The temperature is measured by a 0.010" Pt-Rh thermocouple connected to a data acquisition system and then to a 286 personal computer. Generally, the gas temperature is measured at different heights starting from 1 cm height to 5 cm for all the gas flows. Both fuel (methane) and air flows are adjusted to get the required temperature above the burner.

4.5.2 Gas Composition

The oxygen concentration in the products is measured by a Lancom 6500 portable analyzer which measures CO, O_2, SOx, NO_2, NO and HC etc and calculates the efficiency and excess air values for six different gases. The aluminum framed

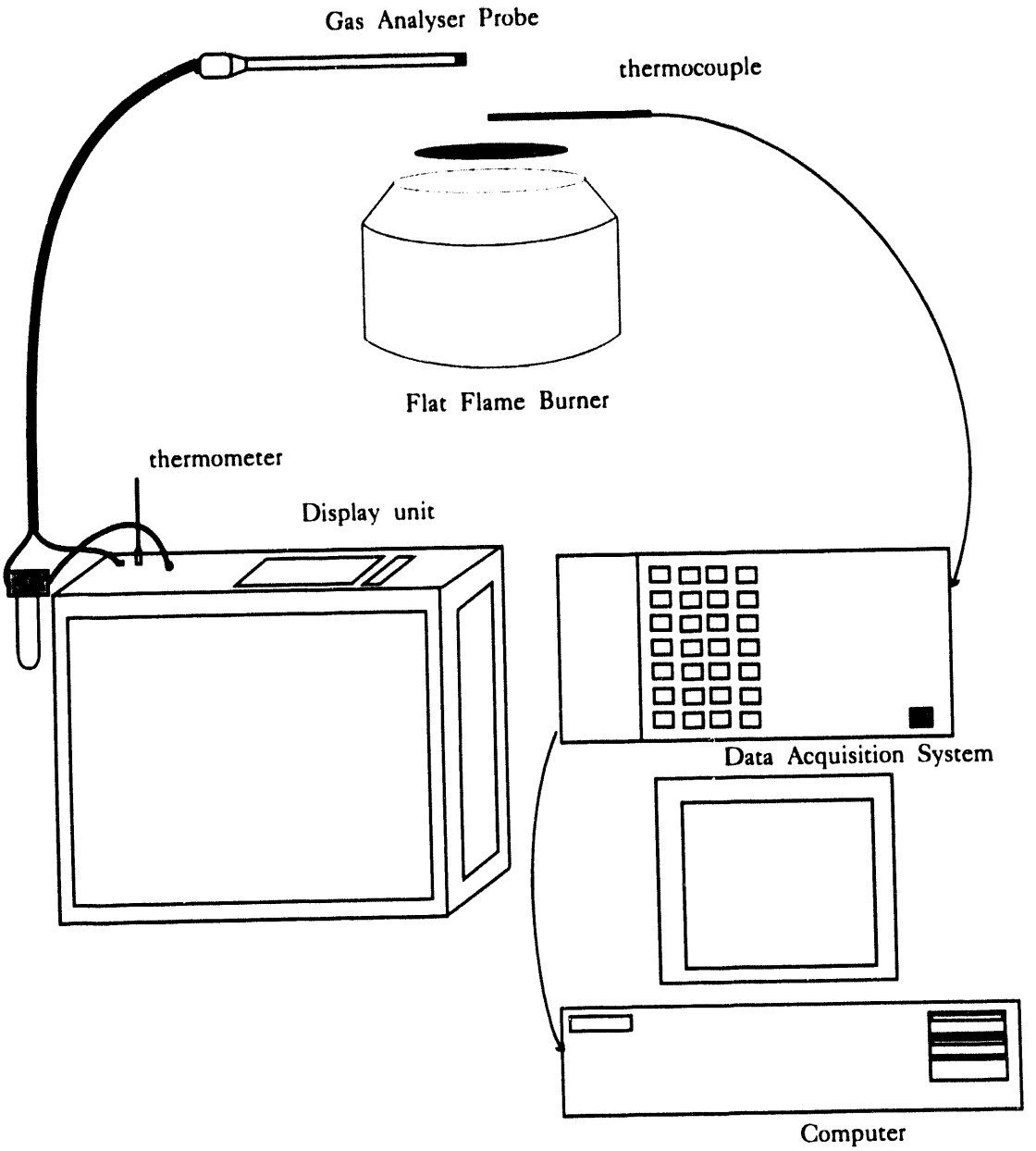

Fig. 4.7 Temperature and Oxygen Concentration Measurement System.

wooden case has a separating hinged lid that holds the probe, water catch pot and accessories. The lead acid battery will maintain the operation of the full instrument for a full working day when fully charged. Operational procedure is carried out by following the user friendly menu on the liquid crystal display and using the keyboard on the same front panel. Simultaneous display of all measured and calculated values gives a complete overview of the combustion situation. Automatic air purging of the sensors occurs every time the instrument is switched off after operations are completed. This ensures accuracy of readings and conserves the sensor life.

The probe is placed in the product gas stream 4 cm away from the flame. The probe tip becomes red hot if placed near the flame. The probe has three filters. The first one is a stainless steel sintered filter and is fitted to the tip of the pistol grip probe. The filter serves to prevent particulate entering the analyzer. The second filter is attached to the water catch pot, housed in a plastic case, which removes 99.9% of all particles over 0.9 microns in size. The third filter is situated in the gas module. This is a disposable filter that filters the SO_2 and NOx in order to reduce the cross interference with the CO measurements.

4.6 Image Processing Equipment

The flame ignition and combustion behavior are captured using an image processing equipment. A brief explanation of the digital image processing system is given here in this section. the details are given elsewhere (Kharbat 1992). The major components of the system are: i) CID camera ii) frame grabber iii) video monitor iv)

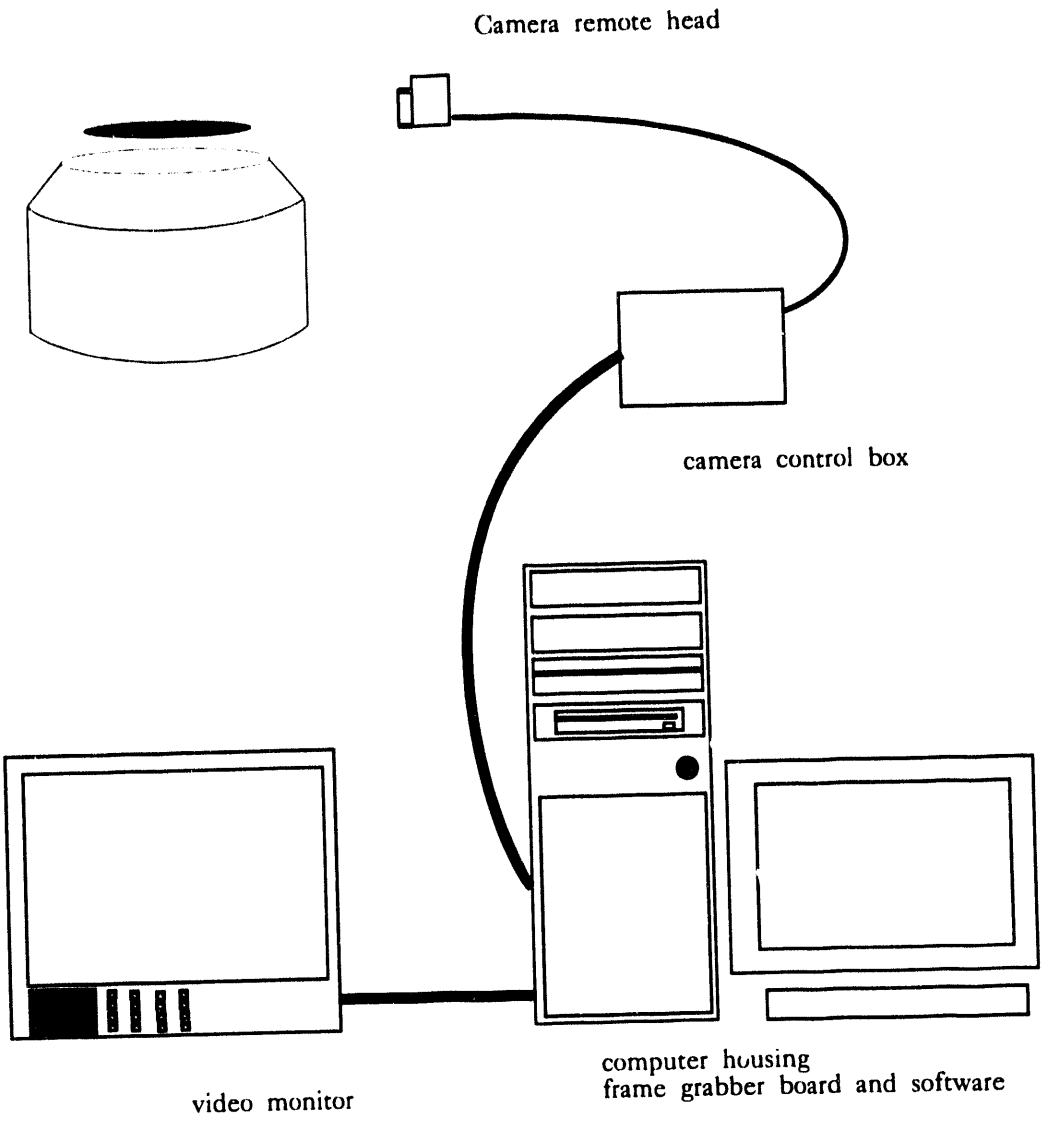

Fig. 4.8 Image Processing System Set Up.

image processing software and v) 486 personal computer. Assembly of all these units is shown in Fig. 4.8

4.6.1 C. I. D Camera

This Charged Injection Device camera has an array of 635*532 pixels. Of this 123 pixels in each line and 20 in each column are blanked making 512*512 active pixel array. The image is captured using wide open shutter from left to right and top to bottom, starting from top left corner of the image and proceeds to the first horizontal line and the second horizontal line until the whole image is scanned. The element rate clock which is pixel reading rate is set at 10 MHz (100 ns). Hence for an array of 635*532 ie 337820 pixels or a frame, it takes 337820*100 ns = 33.8 ms. In one second, this digital camera can take 30 frames. The image will display only 512*512 pixel array while the other pixels are blanked zero. The quality of the image depends on focussing sharply on the array. A lens of 25 mm focal length is used. The distance between the lens and the array is adjusted using the threaded rings and distance pieces.

4.6.2 Frame Grabber

The image processing board is an image acquisition and processing device. It offers unparalleled flexibility in video acquisition and display.

Each point on the frame is stored in a byte. Each frame can at maximum be represented by 512 * 512 pixels (picture elements), i.e. it will be of size 262144 bytes. When a sequence of event is captured, it will need multi frames. The maximum number of frames that can be captured depends entirely on the memory of this frame

grabber. The one used is of 4 MB capacity. This allows to store 16 frames of 512*512 size to be stored at a time. This number can be increased if the image is reduced from 512 * 512 size. Most of the time, only a small window of the whole 512*512 will be of interest, and thereby, more frames of the same sequence can be stored. Though number of frames are increased, the time between two frames cannot be decreased from 33 ms in the present system.

4.6.3 Video Monitor

A high resolution color monitor (Sony PVM-1342Q) is integrated with the image processing system to provide a tool for visual observation of both the digitizing and displaying processes. While digitizing, the combustion process is observed and the camera is focussed and its position is adjusted, simply by visual observation of the monitor's displayed image. The image processing software can perform various operations to improve understanding the images. The instantaneous results of these operations can be visualized in the monitor. Since it is a color monitor, the grey scale image from the camera can be false color manipulated and viewed in the monitor to distinguish between the coal and methane flat flame.

4.6.4 EPIX (4MIP) Image Processing Software

The 4MIP is an interactive, menu driven program which operates the 4MEG Video frame grabber to perform image acquisition, display and processing. This is the master controlling the camera and as well the frame grabber. In image sequence capturing, two different modes are available. One is to capture images from the

beginning till the memory (4MB in this case) is full. Another is capturing and releasing unless that sequence is selected. When selected, the last 16 frames (depending upon the size of each image) will be stored. This is preferred over the first mode as it is more convenient for selecting a sequence. Once frozen, it is to be stored as multi buffer file before beginning the digitizing process again. A single frame can also digitized and stored. Each frame of the multi buffer file can be saved as a single file for manipulating them using other desktop software.

The software offers various edge detecting operators, and boundary operators which are very useful in detecting coal stream from the flames. Images can be zoomed for indepth study of a localized area. Each row and column of a image can be written as a data file for spread sheet applications. Various copying, resizing and rotating of images are available. Two image operations like addition, subtraction, comparing two images for difference, addition of two images are helpful for the stream progress study. Apart from these operations, text can added to each frame. The image measurements allow calibrating image rulers in arbitrary units, moving and rotating the rulers to measure image object distances and angles.

Since each image frame is a two dimensional array of data, it can be manipulated as any other data file using other software also. Various colors can assigned to the different pixel locations based on pixel value (0 to 255). For example, pixel locations having values above 225 can be given red color while locations with 200 to 224 pixel values can be assigned yellow color.

4.6.5 486 Personal Computer

The most important and controlling component of image processing system is the 486 personal computer. A tape drive is added for increased storing facility. The tape drive can handle 150/250 MB data cartridges.

4.7 Particle Preparation Systems

Coal is received from the Penn state coal and organic petrology laboratories in the form of 5 cm dia particles. These coal chunks need to be crushed to the laboratory size which is in microns. The micronized particles when stored tend to absorb moisture from the atmosphere. Hence the particles need to be dried before loading them in coal feeder. A coal crusher and a laboratory furnace are used in the sample preparation. The following section presents a brief description the units.

4.7.1 Coal Crusher

The overall assembly of the unit manufactured by M/S Sweco is shown in Fig. 4.9. This Vibro Energy Grinding Mill uses small amounts of energy with high frequency vibration to break down the material. Basically the Vibro-Energy Grinding Mill consists of a grinding chamber and vibratory mechanism. The vibrating mechanism is a vertical shaft motor with eccentric weights at each end. The grinding chamber is in the form of a vertical cylinder or annulus which is filled with very hard grinding media, like alumina cylinders. The cylinders are available in different sizes to be selected depending upon the final size of the material being ground. The material is introduced into the voids between the grinding media. The vibrating mechanism is

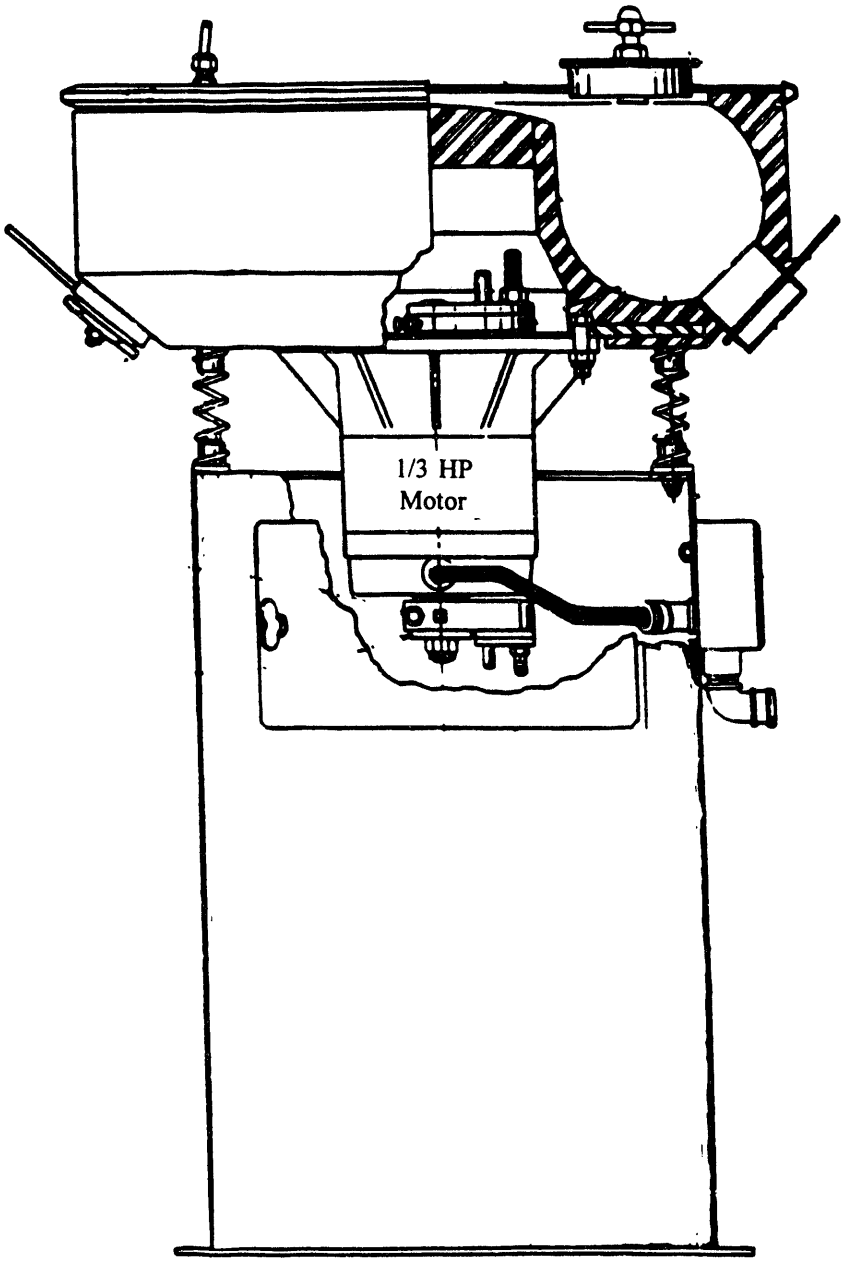

Fig. 4.9 Coal Crusher Unit.

attached to the lower part of the grinding chamber. The grinding chamber is suspended above the base on the high tensile steel springs. All energy from the motor is imparted directly to the grinding media without intermediate gear drives or clutches which creates a continuous spiralling mass of product and media traveling around the center column.

Generally, it takes 10 to 15 hours of continuous running to break the size from 5 cm dia to 100 microns. It needs to be operated for longer hours when the size required is even smaller.

4.7.2 Laboratory Oven

The oven is a small size electric oven capable of heating upto 200 deg C. The heating elements are located at the bottom. Two trays are provided above those elements for placing the samples. One of the top three vent holes serves as a thermometer holder. The oven temperature is controlled by a thermostat marked with reference numbers. Few trial setting of the thermostat will help find the correct thermostat mark to get the needed temperature in the oven. The air circulation damper is kept open to allow the moisture to escape and be replaced by room air. For drying purposes, better temperature uniformity is obtained with this damper open. A temperature of 70 deg C is used for coal particle drying kept for an hour. The dried samples are now ready for experiments.

CHAPTER V

DESCRIPTION OF EXPERIMENTAL PROCEDURE

An operating procedure for the experiments is presented in this chapter. It also deals with the tests conducted to set the operating parameters of the experiments. The operating parameters include the A:F ratio of the stream, gas temperature, and O_2 concentration. The operating characteristics of the flat flame burner under different fuel flow conditions are also investigated.

5.1 Experimental Procedure

A low swelling coal PSOC 1336 was selected for the experiments due to its easy grindability and flowability. It is crushed, sieved to the required size and dried in the laboratory oven. The coal feeder is then filled with the particles to half of its height. The particles in the feeder is loosened to avoid caking by shaking the feeder before placing on the digital balance. The output from the digital balance is checked for the proper display of the weight reading. The particle collection setup is cleaned after every experiment to eliminate any samples left by the previous experiment. The probe is fixed to pre-determined height above the burner and is aligned to the coal injector center line. The digital camera is then focussed on to the particle collection probe with a white background. The 486 computer controls the camera and all the images are displayed continuously over the SONY color monitor using a 4MIP software. The captured flame images are then stored in the computer for later detailed investigations.

A predetermined methane air mixture flow is used to achieve a steady flat flame anchored to the burner. The gas temperature and the O_2 concentration for any given flow rate is already known. Experiment is started by switching on the vibrator buzzer strapped on to the feeder and by starting the dilution flow to the feeder. Introducing the fluidization and pressurization air initiates the coal flow into the vitiated environment formed by the methane flame. The burnt coal particles enters the particle collection system after passing through the high temperature zone. These particles are then collected and sent for analyses.

5.2 Stabilization of Flat Methane Flame

First, the burner cooling water is allowed to flow. The water flow is set at 0.5 gpm. Methane flow is then started at 2.7 scfh, air flow is set 26 scfh and ignited. Then the air flow is increased in steps. The flame is yellowish in color to start with and changes its color to blue as the air flow rate is increased. Initially carbon of methane cracks and results in soot burning which gives the characteristic yellow color. Then the air flow is adjusted to get a flat blue flame anchored to the burner. Stabilizing the flat flame at the water cooled burner is difficult. The cooling water flow is reduced in the beginning to get the flame at the burner and later on the flow is allowed to be normal.

When the air flow is increased beyond 55 scfh at methane flow of 2.0 scfh, the flame attains a wavy shape. It presents a very unfavorable temperature zone for the experiments. Different flow rates were attempted to achieve a steady flat flame in order to obtain required gas temperature and O_2 concentrations. The different flame shapes

are presented in Fig. 5.1.

5.3 Gas Temperature

In order to combust coal at given gas temperature, a constant temperature zone must be achieved for a certain vertical distance above the burner. The temperature was measured at different locations above the burner. The maximum temperature is at the center and is at a height of 1 cm for a methane flow of 1.5 SCFH with 100% excess air. The uncorrected temperature values measured at different locations are plotted in Fig. 5.2. It is seen that radial profiles are flat near the burner. However the profiles have peaks at the centers for heights ranging from 2 to 6 cm. These temperature readings may not represent the actual experiment since the coal carrier air may reduce the temperature. Hence the same experiment is repeated with a typical carrier air flow of 7 SCFH flowing at the center of the burner. The temperature values for the second condition are given in Fig. 5.3. The temperatures at the center of the burner with and without carrier air are compared in Fig. 5.4. This figure shows that the mixing appears to be completed at a height of 4 cm above the burner. The mixing time is 2.3 ms with the air velocity(cold) as 17.5 m/s. Figure 5.2 indicates that the temperature variation is within 60 K within a height of 3 cm. A fuel flow rate of 5.2 scfh with 68 scfh of air gives a constant temperature zone of 1400 K. The axial temperature profiles are given in Fig. 5.5. It is seen that the gas temperature is constant almost over a height of 5 cm.

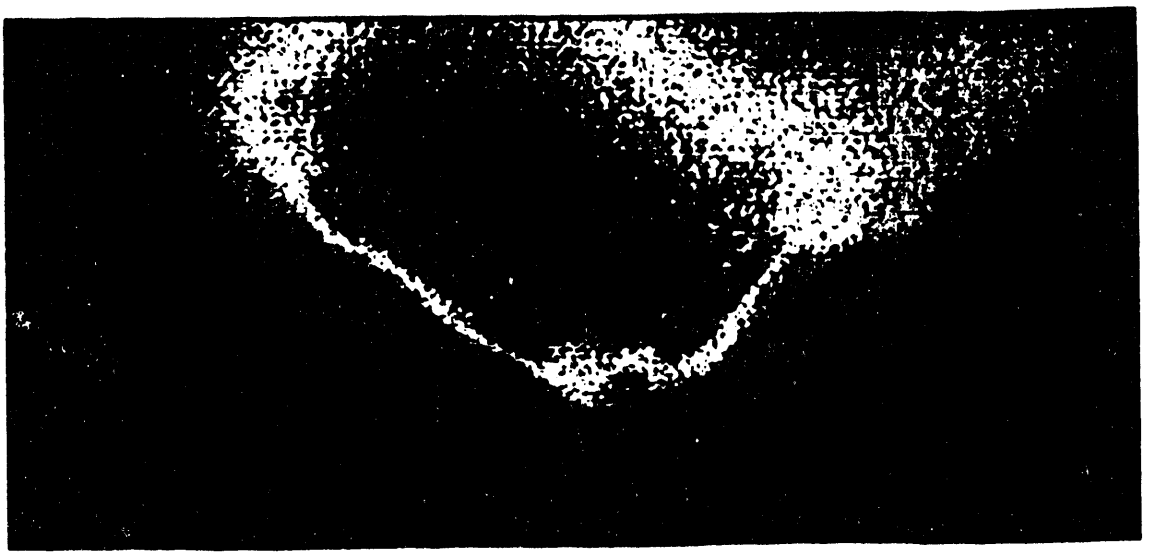

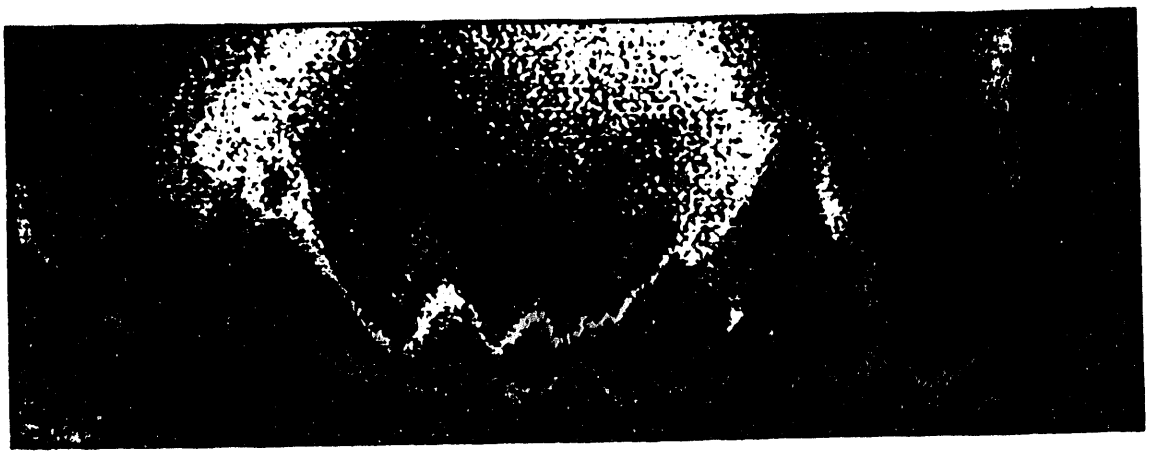

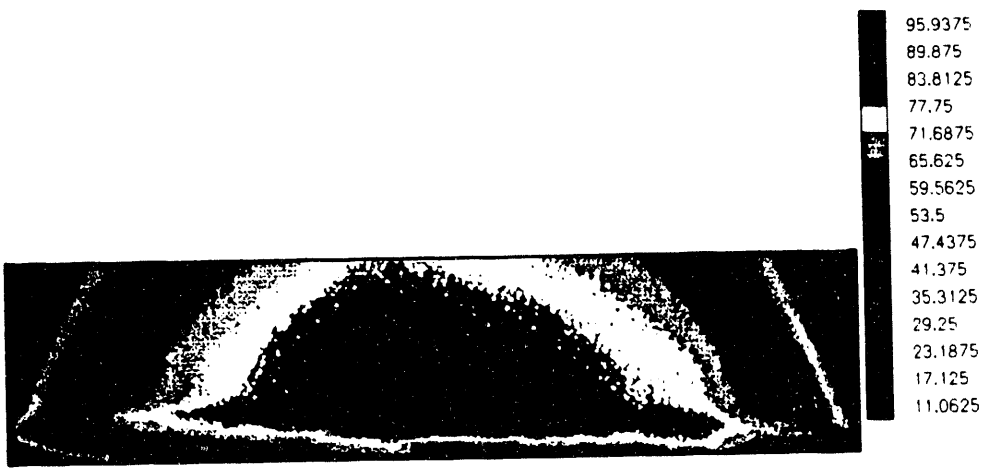

Fig 5.1 Stable Flat Methane Flame

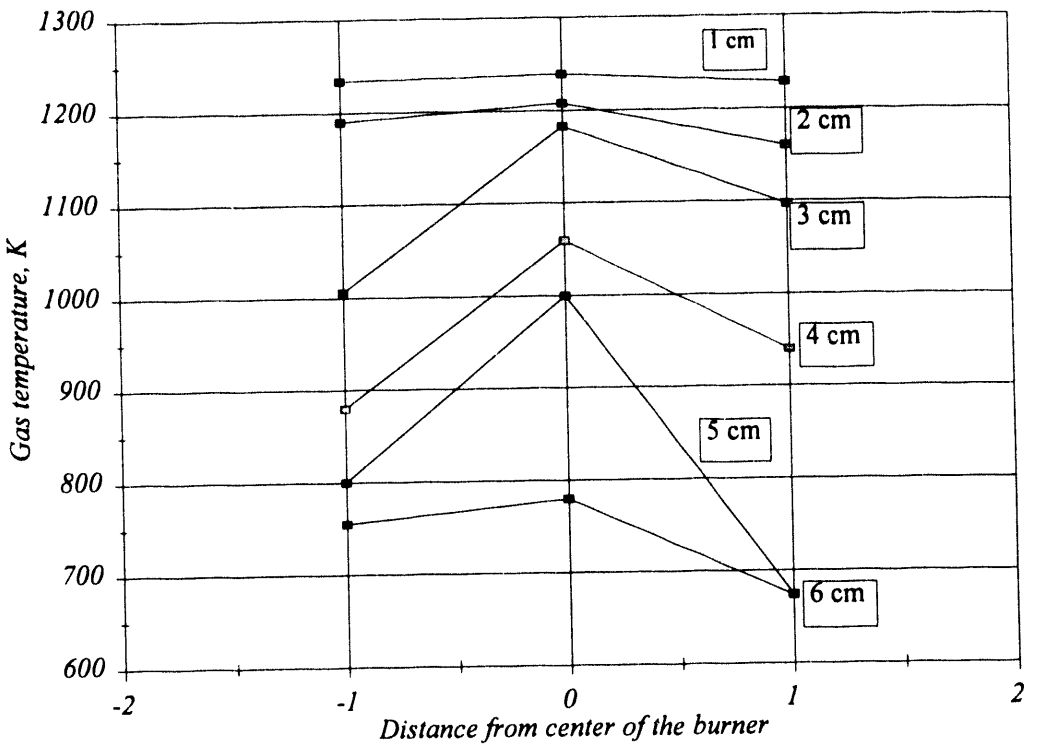

Fig. 5.2 Gas Temperature Profiles With No Carrier Air.

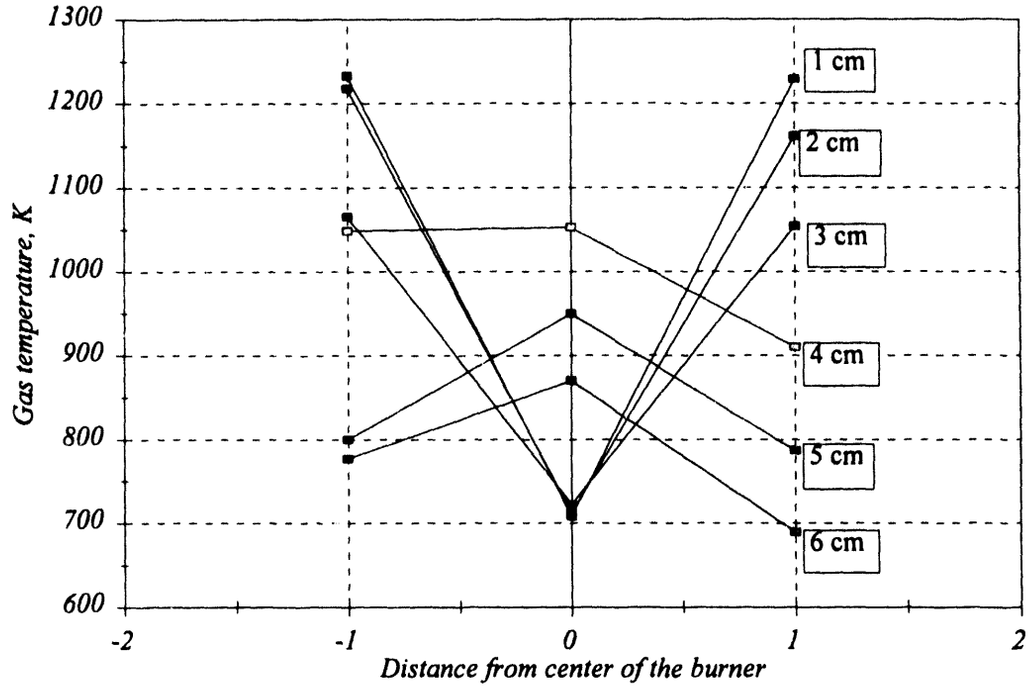

Fig. 5.3 Gas Temperature With Carrier Air at the Center.

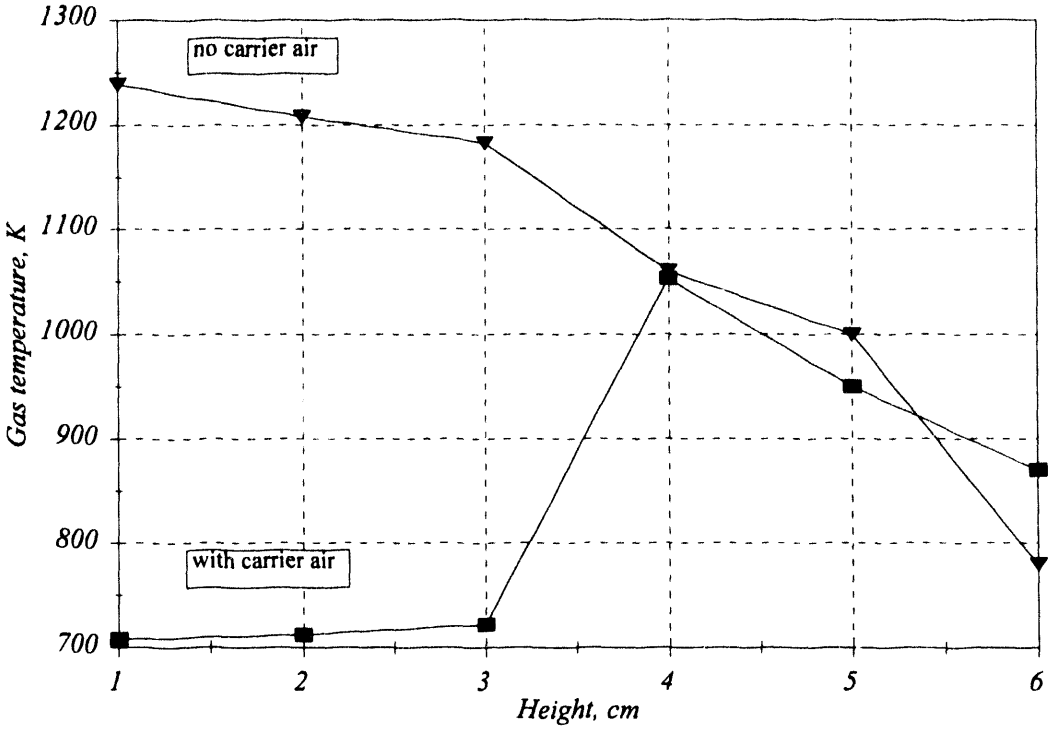

Fig. 5.4 Gas Temperature With and Without Carrier Air.

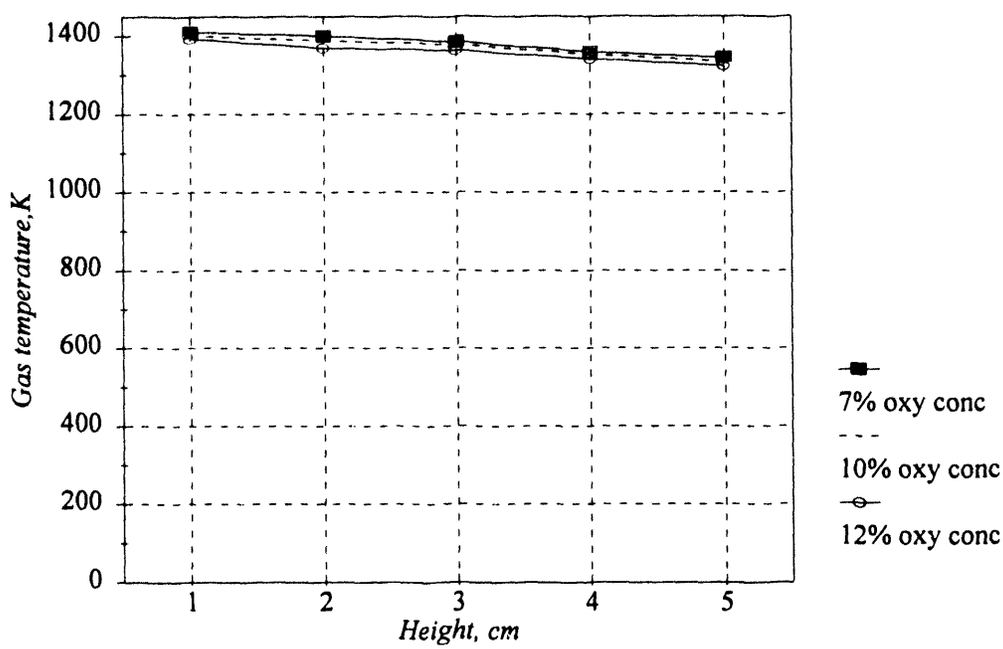

Fig. 5.5 Gas Temperature for Higher Methane Flow.

5.4 Oxygen Concentration

The oxygen concentrations are measured at the standard height of 4 cm above the burner. For a specific methane flow, 100% excess air is expected to have 10% oxygen concentration in the products if complete combustion is assumed. It was necessary to increase the flow beyond 100% excess air to obtain 12.5% O_2 concentration. As explained earlier, it was difficult to get a stable flat flame with increased air flow rates. In order to minimize the stability problem, oxygen from a separate cylinder was introduced into the air fuel mixture. As expected, the increase in O_2 flow increases the O_2 concentration in the products (Fig. 5.6). The oxygen concentration measurements reflect the same trend. The detailed calculations are presented in Appendix B.

5.5 Cloud A:F Ratio

The cloud A:F ratio is estimated using the instantaneous digital balance reading and the carrier air flow rates. The feeder weight reading is registered every 15 sec in the computer. The coal flow is generally allowed for 2 - 3 min. Though the air flow can be maintained constant, coal flow does fluctuate due to non uniform packing density, friction in the tubes and bends in the feeding system. Hence A:F ratio fluctuates during the experiment and the results presented will have an error bar for A:F ratio. A typical mass flow rate is presented in Fig. 5.7. The coal mass flow rate can be altered by adjusting the dilution flow at the feeder. As the dilution rate is increased, mass flow rate decreases as shown in Fig. 5.8.

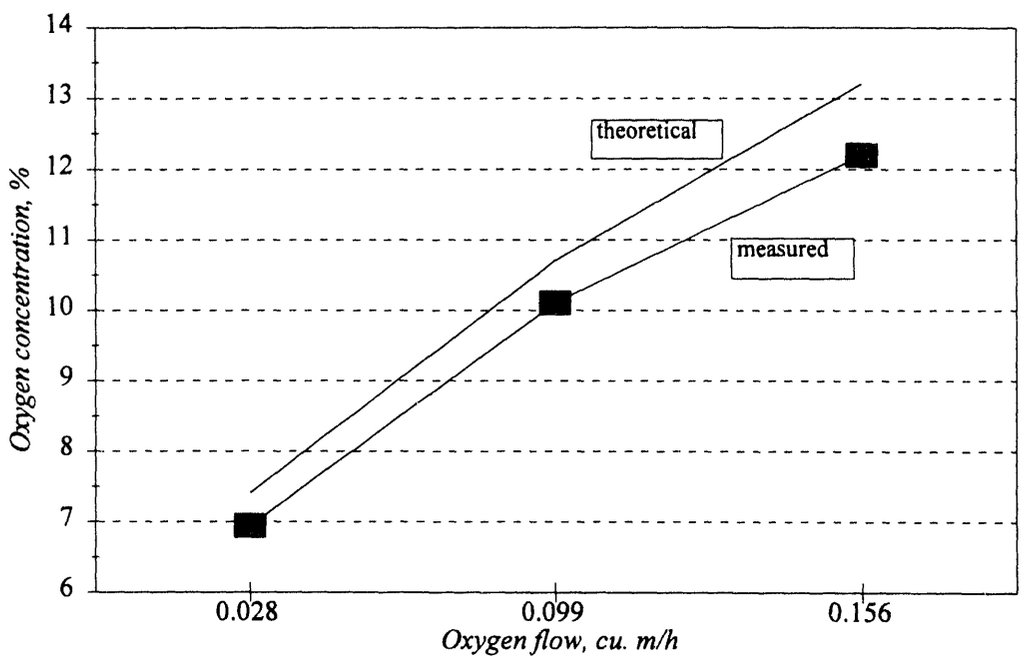

Fig. 5.6 Oxygen Concentration for Various Oxygen Flows.

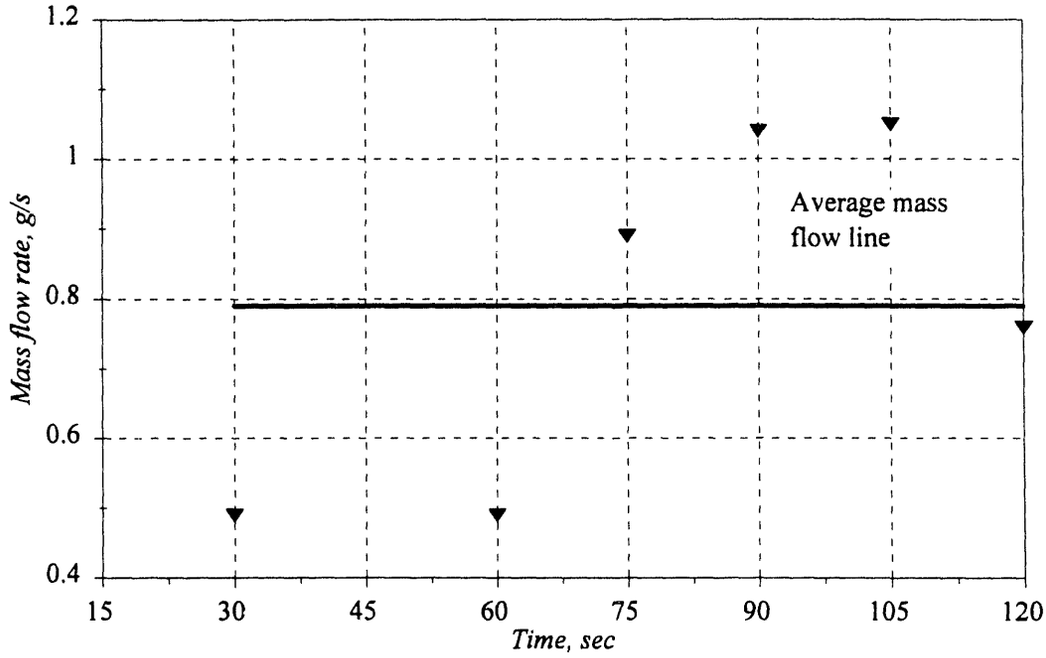

Fig. 5.7 Variation of Mass Flow Rate.

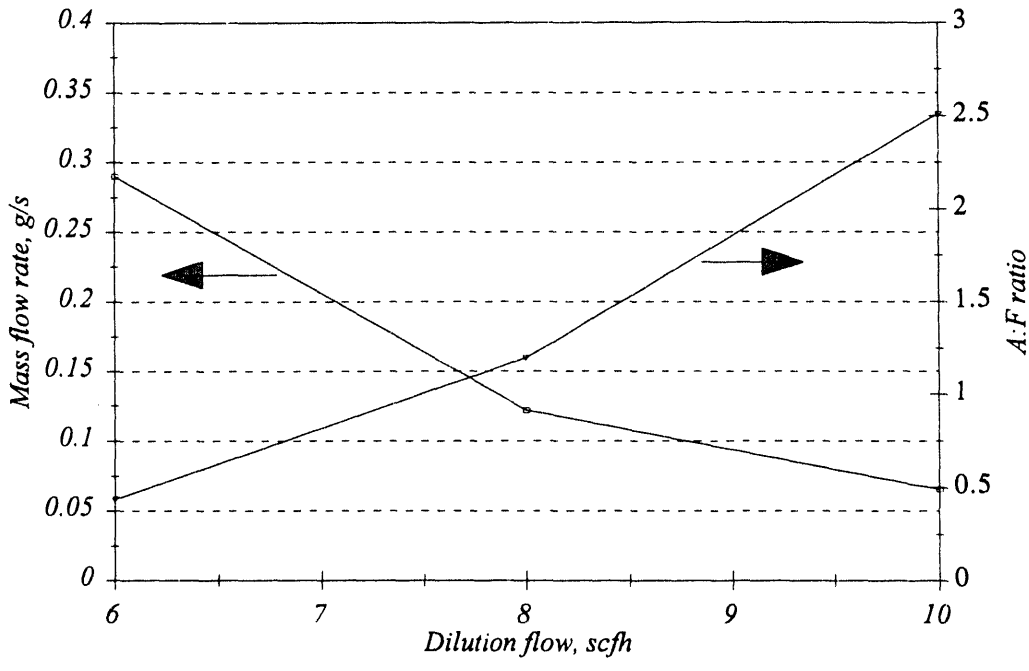

Fig. 5.8 Mass Flow Rate Vs Dilution Flow.

5.6 Operating Parameters for the Camera

The operating parameters for the CIDTEC 2250A camera are i) F-stop ii) object distance and iii) object height. The focal length(f) of the lens used is 25 mm. The F stop which is the unit measure of the ratio of focal length to entrance pupil diameter can be varied from 1.4 to 16. The larger the pupil diameter, the larger the amount of light the system passes and the lower the F stop number. For all applications, F stop of 1.4 is used. since the object is a high temperature flame, for the safety of the camera, the object distance is kept at a minimum of 12 inches. This distance is then increased by trial and error to get a focussed picture. Generally the scene dimensions(mm) are kept at 130 mm width * 96 mm height for all experiments to cover all the reaction zone heights.

The depth of field is the range of distance from the lens that will be in focus at a given F-stop. The larger the F-stop (smaller the aperture) or pupil diameter of a particular system, the greater the depth of field. The depth of field can be calculated using the following formula:

$$\Delta D = \frac{2\ D\ F\ \Delta H}{F\left[\left(\frac{f}{F}\right)^2 + \Delta H^2\right]}$$

where	f = focal length	= 25 mm	= 0.984"
	D = Object distance	= 96 mm	= 3.78"
	F = F stop		= 1.4
	ΔH= resolution	= 3.78/512	= 0.0074"

The depth of field for this application is calculated to be 0.113" which is 2.9 mm. The depth of field is almost same as the cloud diameter (injector diameter 2.03 mm). The pixel values obtained are an average over a distance of 2.9 mm.

The imaging environment has a strong implication on the captured images. The digital camera used for imaging has a high sensitivity of full output at 0.7 foot-candles (7 lux) face plate illumination. The brightness of the scene is merely the product of illumination and reflectance. For example, a piece of white paper might have a reflectance of 0.85 and when it is illuminated by a 10 fc lighting, its brightness would be 8.5 foot-lambert which is enough to give full camera output. Hence, careful consideration is to be given for the selection of the scene background. Figure 5.9 presents a candle flame with white and dark background. It is apparent that the dark background provides a better contrast to the flame images.

5.7 Stream Velocity

The velocity of the coal particles in the stream is generally an unknown factor in all the experiments. Direct flow rate calculations using cold flow of air give very high stream velocity whereas the stream particles are expected to lose their momentum due to the slow moving surrounding gases. An attempt was made for in situ average velocity measurements using photo diodes in which the coal stream is allowed to pass through a pair of diodes which are fixed at a known distance. This method was not effective as the stream was not dense enough to block the light beams falling on the

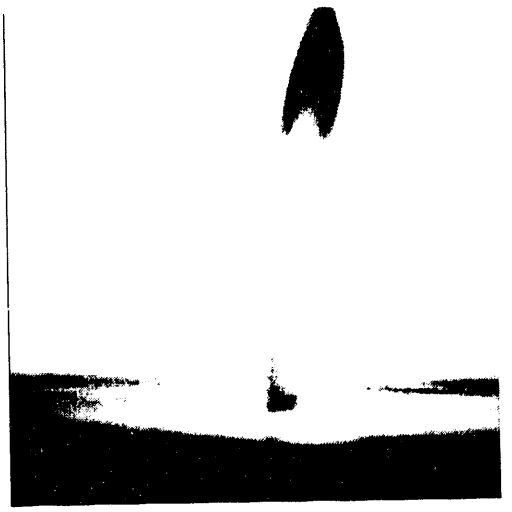

White background

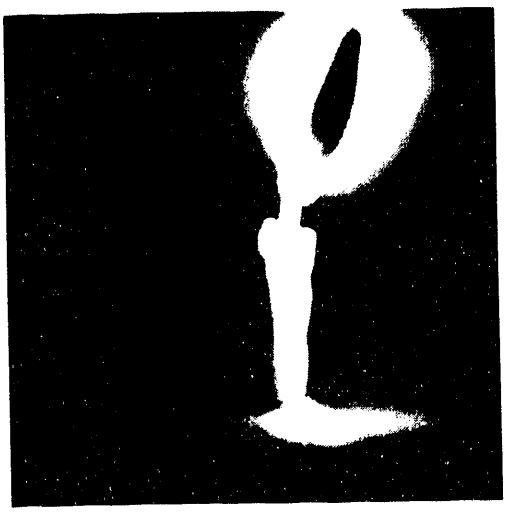

Black background

Fig. 5.9 Candle Flame Images.

diodes. The details of this set up is presented in Appendix A. A more reliable method is later used to find the velocity using digital image processing. It captures images of any transient events at a rate of 30 frames per second. If stream development is captured using a digital camera, two successive frames with a known time gap will give the velocity. The two successive frame images are presented in Fig. 5.10. The pixel contours at the injector centerline are given in Fig. 5.11. The pixel locations for end of stream in the first and the second frame are noted. The real distance between these two is calculated using image scale provided by the software. The pixel clock rate of 100 ns (10 MHz) is used to calculate the time gap between the those pixels. The stream velocity is calculated using both the time gap and distance. The velocity for this case is calculated to be 6.18 m/s with a time of 10.35 ms. The direct flow measurement gives a high value of 35 m/s.

Fig. 5.10 Two Successive Frames of Coal Stream.

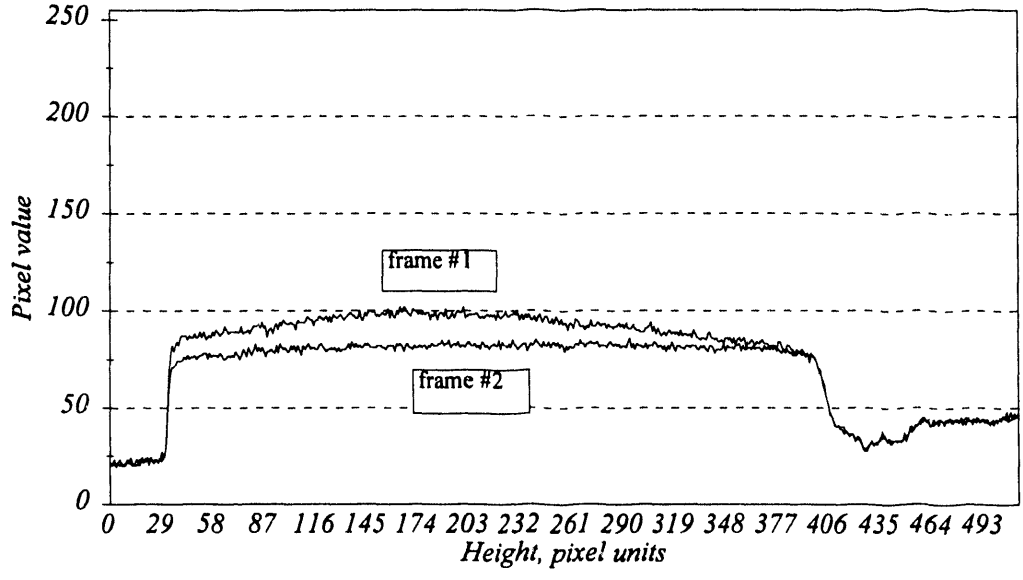

Fig. 5.11 Pixel Contours Along Y Direction at the Center of the Burner.

CHAPTER VI

RESULTS AND DISCUSSION

This chapter analyses the results obtained for different operating parameters. This chapter is divided into two major sections: gasification efficiency and image analysis. In the first part, the effects of particle size, gas temperature, oxygen concentration and residence time on the gasification efficiency are presented while the second part provides results on the flame structure obtained using the image analysis.

6.1 Overview of the Experiments Conducted

A high volatile coal, PSOC 1336 is used for most of the experiments. The proximate analysis on as received basis is given in Fig. 6.1. The ultimate analysis of the coal on as received basis is presented in Table 6.1. The proximate analyses of the coal on dry basis are given in Table 6.2. The following parametric studies were conducted O_2%:6.5-12.5% (10%), T_{gas}:1200-1400K (1200K). The quantities in parentheses represent the base case. Different residence times are obtained by positioning the particle collection system at various distances (4-6 cm) from the burner. The air fuel ratio between the coal particles and the carrier air is varied between 0.5 and 2.0 which is generally the case in pf (pulverized fuel) fired plants. In all the cases, the burnt sample is collected over a set period of time which is typically 2-3 min after the coal flow started. The burnt samples are subsequently analyzed for ash content. Ash percentage difference in the raw coal and burnt coal provides a quantitative measure of the extent of gasification of the particles. Table 6.3 provides the listing of various

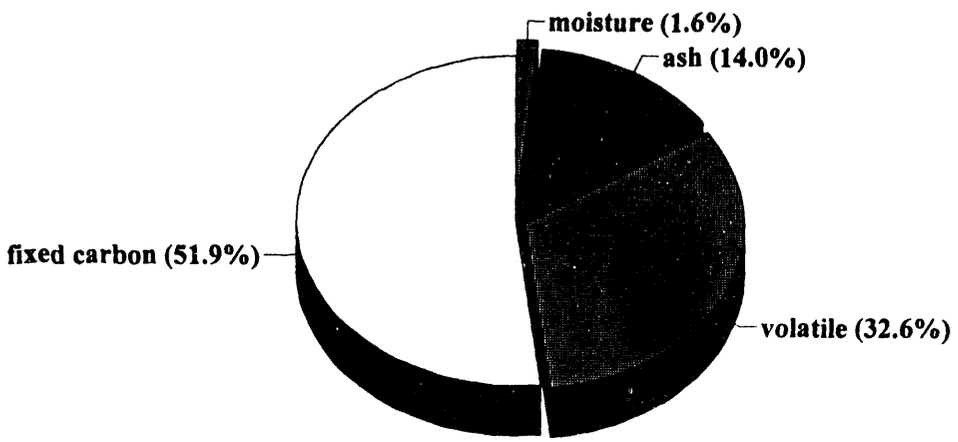

Fig. 6.1 Proximate Analysis for PSOC 1336 Coal.

Table 6.1 Ultimate Analysis of PSOC 1336 Coal (as Received).

% ASH	14.01
% CARBON	71.74
% HYDROGEN	4.58
% NITROGEN	1.34
% TOTAL SULFUR	2.04
% OXYGEN	4.75

Table 6.2 Proximate Analyses of PSOC 1336 Coal (Dry Basis).

	Penn state coal data base	Huffman lab analysis
% ASH	14.23	13.80
% VOLATILE	33.09	29.71
% FIXED CARBON	52.68	56.49

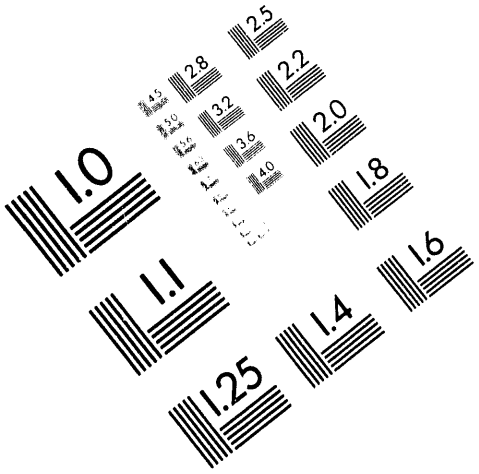

Association for Information and Image Management

1100 Wayne Avenue, Suite 1100
Silver Spring, Maryland 20910

301/587-8202

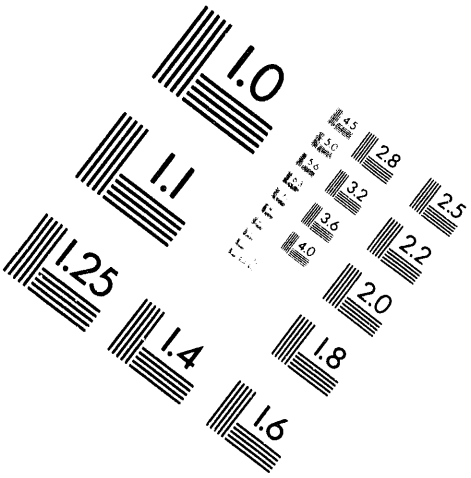

Centimeter

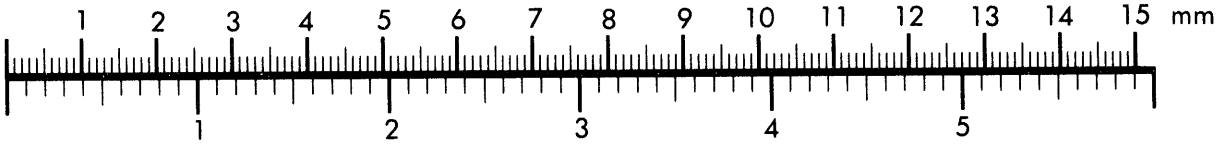

Inches

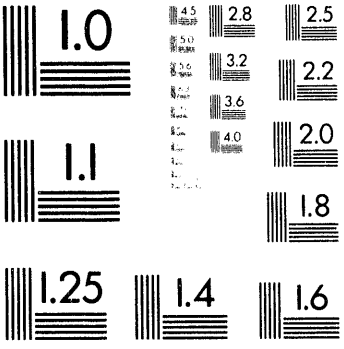

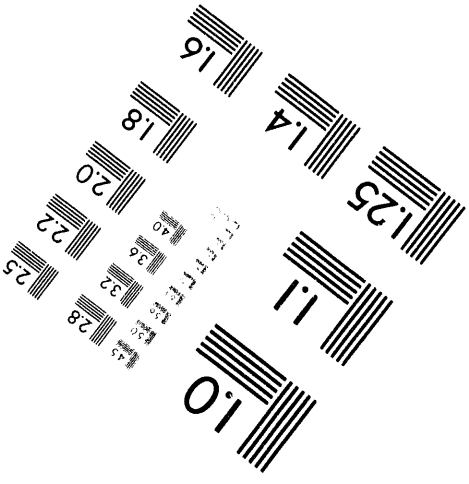

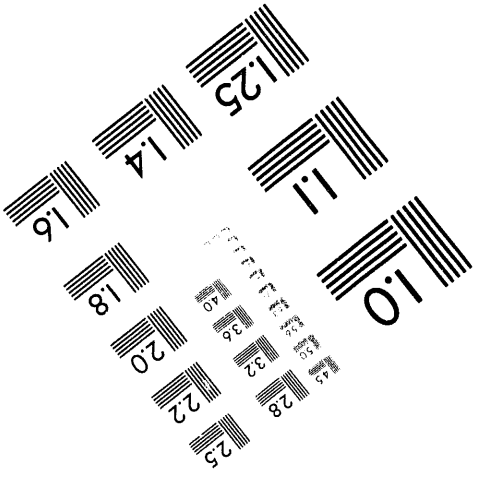

MANUFACTURED TO AIIM STANDARDS
BY APPLIED IMAGE, INC.

2 of 3

Table 6.3. Operating Parameters.

Coal	Gas Temperature (K)	$[O_2]$, %	Cloud A:F Ratio	Reaction zone height (cm)
PSOC 1336	1200	6.5	< 1	4
	1400	10	~ 1	5
		12.5	> 1	6

operating parameters.

6.2 Gasification Efficiency

One may calculate the gasification efficiency based on the ash tracer method. The ash percentage of the coal sample is determined using proximate analysis before and after the experiments. If the coal is completely gasified, only ash will remain resulting in 100% ash in the burnt sample and 100% gasification. Generally, the coal gasifies partially, leading to an ash percentage less than 100. The gasification efficiency is given by the following formula:

$$\eta_g = \frac{100\ (A - A_o)}{A\ (100 - A_o)}$$

where A_o is the ash percentage on dry basis for the unburnt sample while A is the ash percentage on dry basis for the burnt sample. The ash percentage in a sample is determined as per the ASTM standards at the Agricultural Laboratory of Texas A&M University. The complete proximate analyses of burnt and unburnt coal samples are done at Huffman laboratories, Colorado. It should be noted that gasification represents the mass of coal gasified, but not necessarily the gases released are burnt completely in the gas phase. However for the present experimental conditions which involve high temperatures, the gasification efficiency is same as burnt fraction.

6.3 Experimental Data on Gasification Efficiency

6.3.1 Effect of Reaction Zone Height (or Residence Time)

High volatile coal of 64 micron was used for different reaction zone height

starting from 4 to 6 cm. Results are shown in Figs 6.2 to 6.4. The particles heat up as they are injected into the vitiated gases of the methane flame. They pyrolyze, ignite and then combust and the burnt particles are collected at the water cooled particle collection system. If the particle collection system is placed very close to the coal injector, it will result in very low gasification efficiency irrespective of the gas temperature and the oxygen concentration due to insufficient residence time. On the other hand, if the stream is provided with a long residence time, then one may achieve 100% gasification. As shown in Fig. 6.2 for 6.5% [O_2], the gasification efficiency jumped from 0.02 to 0.2 when the reaction zone height is increased from 5 cm to 6 cm for a constant A:F ratio of 2.5. Same trend is observed for A:F ratio of 1 when zone height is increased from 4 to 6 cm. The gasification efficiency values at 4 cm zone height always is lower as compared to values at 5 and 6 cm heights(Figs. 6.3 and 6.4).

6.3.2 Effect of A:F Ratio

When the stream is very dilute, due to the higher quantity of air, more time is required to heat up air which in turn delays the heating rate of the particles. Since there are few particles burnt and large mass of air, the gas temperature surrounding the particles remain low. On the other hand when the stream is very dense, the quantity of air is less but the dense cloud of the particles may require more time to heat up and few particles burn at slower rate due to deficient O_2. It may be argued that higher gasification should result for dilute stream due to increased inter particle spacing and less competition for heat and oxygen provided there is no mixing limitation.

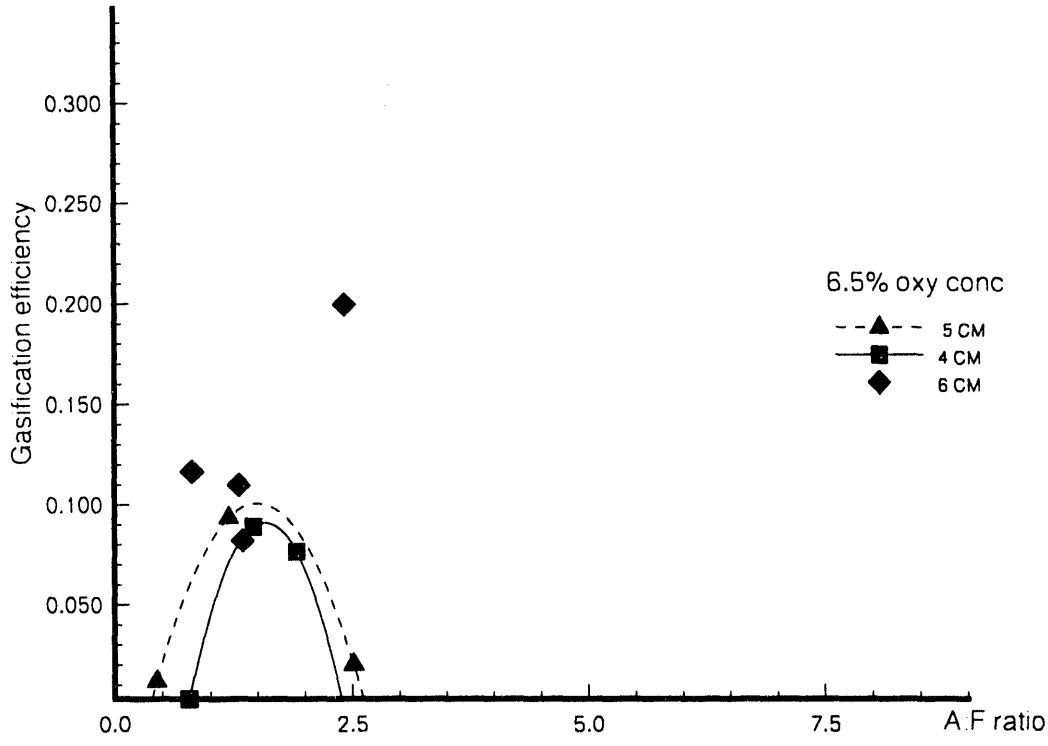

Fig. 6.2 Gasification Efficiency Vs. A:F Ratio and Residence Time at 6.5% Oxygen Conc.

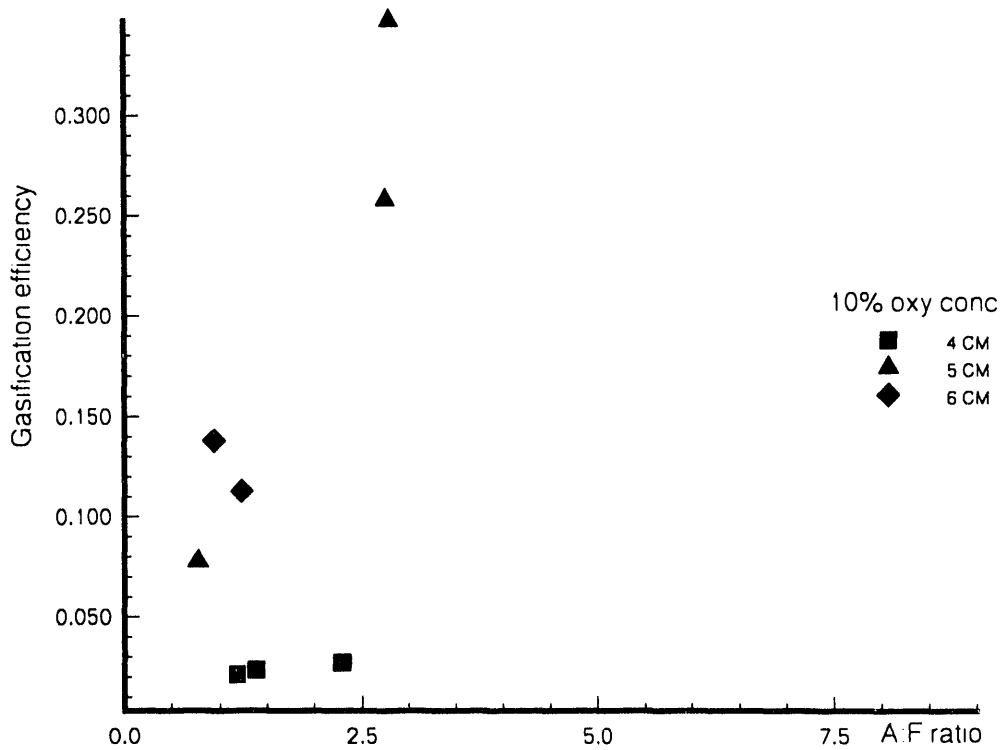

Fig. 6.3 Gasification Efficiency Vs. A:F Ratio and Residence Time at 10% Oxygen Conc.

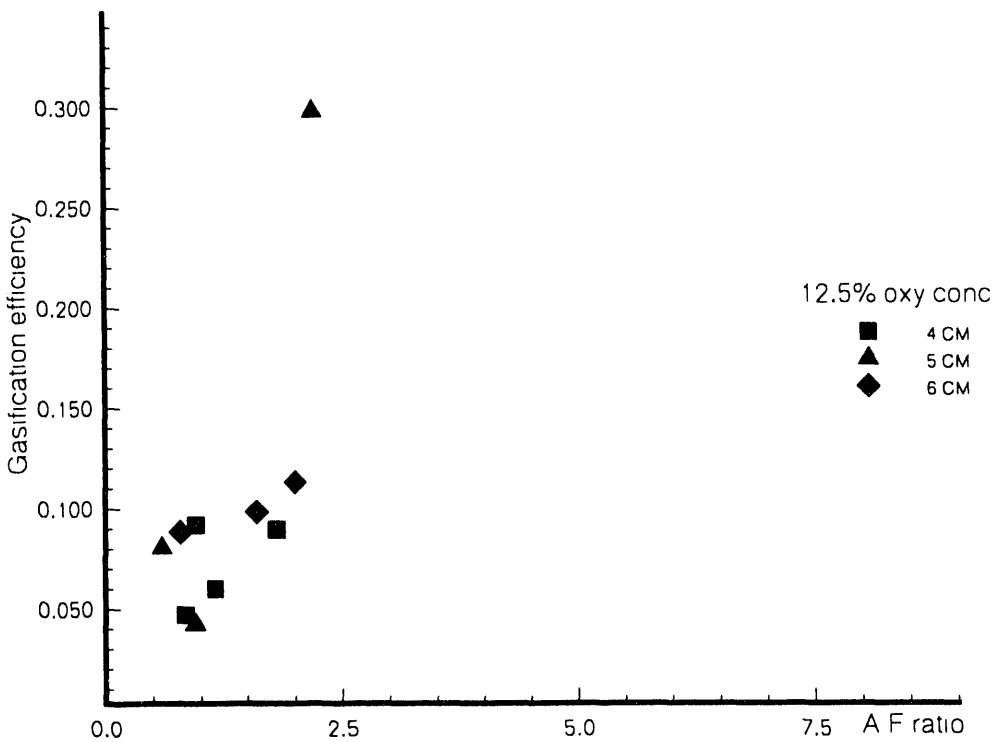

Fig 6.4 Gasification Efficiency Vs. A F Ratio and Residence Time at 12.5% Oxygen Conc.

Experiment is expected to decide which effect is dominant over the other. Hence, experiments were repeated for different air:fuel ratios keeping the same reaction zone height and oxygen concentration. At the reaction zone height of 4 cm, as the A:F ratio increased, the gasification efficiency increases in the beginning, reaches a maximum and starts to decrease. The same trend is shown when the oxygen concentration is increased from 6.5% to 12.5% as shown in Fig. 6.5. But at the reaction zone height of 6 cm, an opposite trend is observed. Due to increased residence time because of higher reaction zone height, second argument seems to be valid for the dilute cloud. Higher gasification efficiency resulted at higher A:F ratio at all the three oxygen concentrations. A mixed trend is observed at the reaction zone height of 5 cm.

6.3.3 Effect of Oxygen Concentration

All combustion processes are oxidation reactions. If there is sufficient oxygen available (i.e. stoichiometric oxygen quantity) for the fuel to react, it will result in complete fuel conversion. Excess oxygen does not aid in the increased gasification, but it can reduce the gasification efficiency indirectly due to reduction in the gas temperature. Fig. 6.6 shows increasing trend in the gasification efficiency due to increase in oxygen concentration from 10% to 12.5%. At the zone height of 6 cm, the effect of oxygen concentration does not seem to have any effect on the gasification efficiency due to higher residence time. All the data points are clustered around 12% gasification as shown in Fig. 6.7.

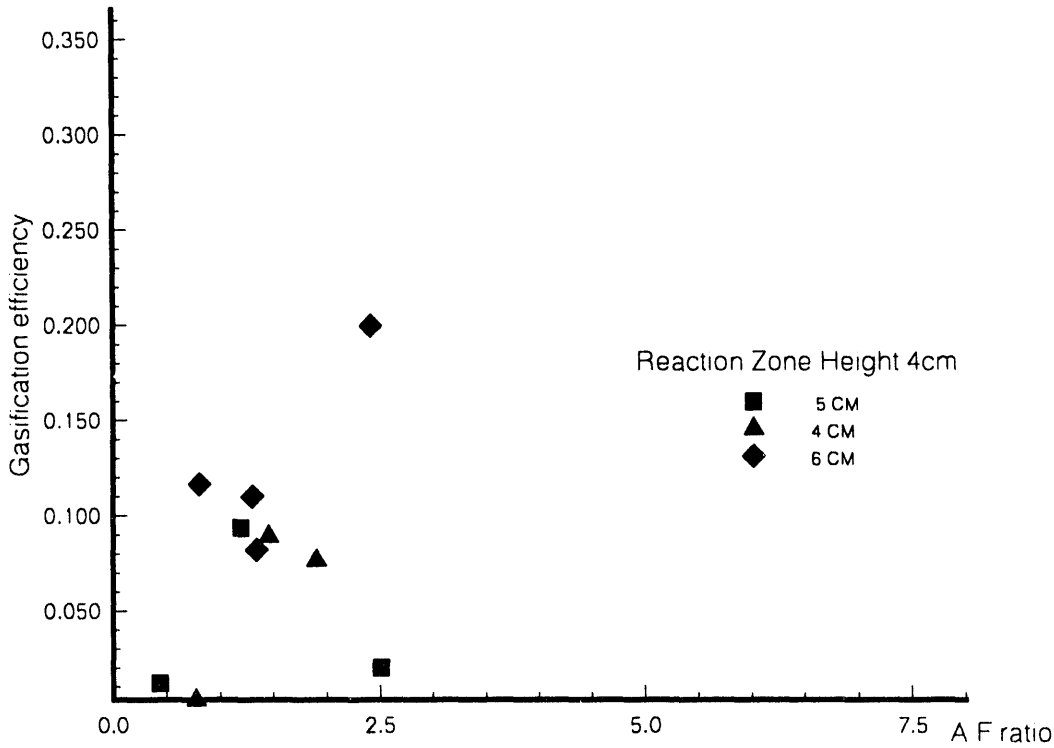

Fig. 6.5 Gasification Efficiency Vs. A:F Ratio and Oxygen Conc. (4 cm Height).

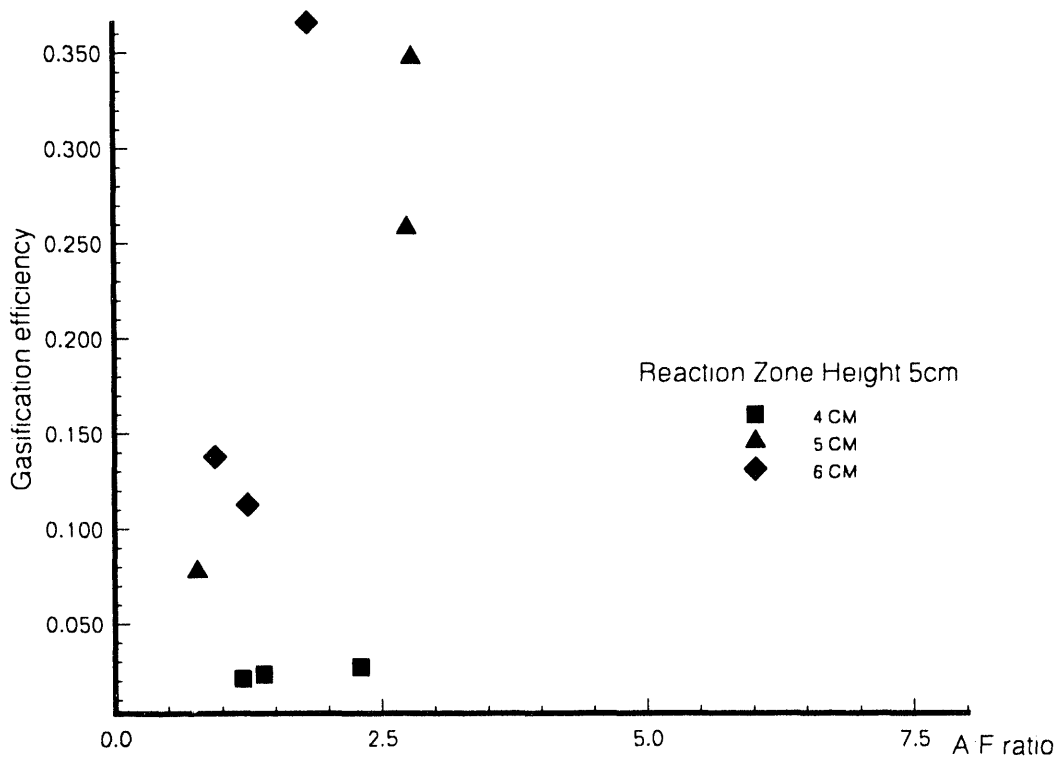

Fig. 6.6 Gasification Efficiency Vs. A:F Ratio and Oxygen Conc. (5 cm Height).

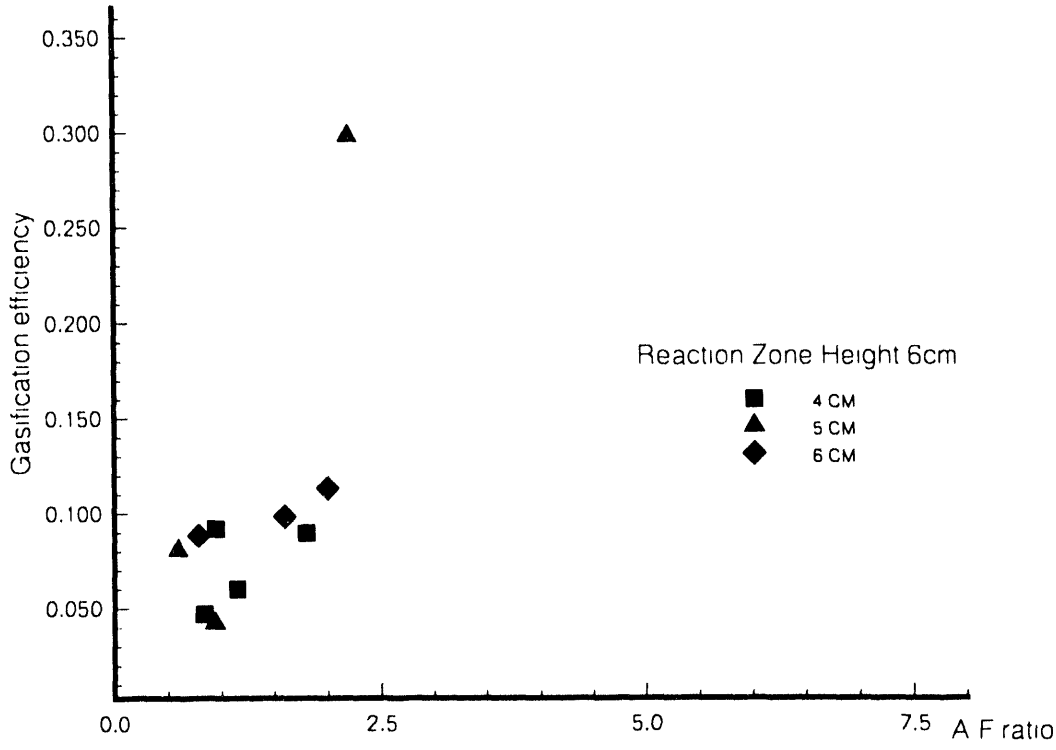

Fig. 6.7 Gasification Efficiency Vs. A:F Ratio and Oxygen Conc. (6 cm Height).

6.3.4 Effect of Gas Temperature

The gas temperature is increased from 1200 K to 1400 K at 10% oxygen concentration. The reaction zone height is maintained at 6 cm. The gasification efficiencies for both these cases are plotted in Fig. 6.8. The increase in gas temperature generally resulted in higher gasification efficiency as expected.

6.3.5 Model Results on Gasification Efficiency

The gasification efficiency results are predicted for a cylindrical cloud model by Du et al., (1993) with and without radiation effects (See Appendixes C and D). As the A:F is increased, the gasification efficiency increases in the beginning, reaches a maximum and starts to decrease (Fig. 6.9). This trend qualitatively conforms to the experimental data shown in Fig. 6.2. for smaller residence time. For higher air:fuel ratio, the stream is dilute and the heat generated by the oxidation of volatiles may not be high enough to heat up the particle resulting in lower gasification efficiency. As the air fuel ratio is decreased, more heat is released due to large quantities of volatiles released and the gasification efficiency increases. If the stream is made denser, more heat is needed to heat the particle due to increased heat sink effect. The competing effects show a peak in gasification efficiency with respect to cloud A:F ratio.

6.4 Digital Imaging of Coal Stream

The coal injector is of 2.03 mm dia. If the relative velocity between the stream and the hot gas is of negligible value, then the coal stream is expected to provide a cylindrical cloud of coal particles with the cloud diameter being 2.03 mm. On the other

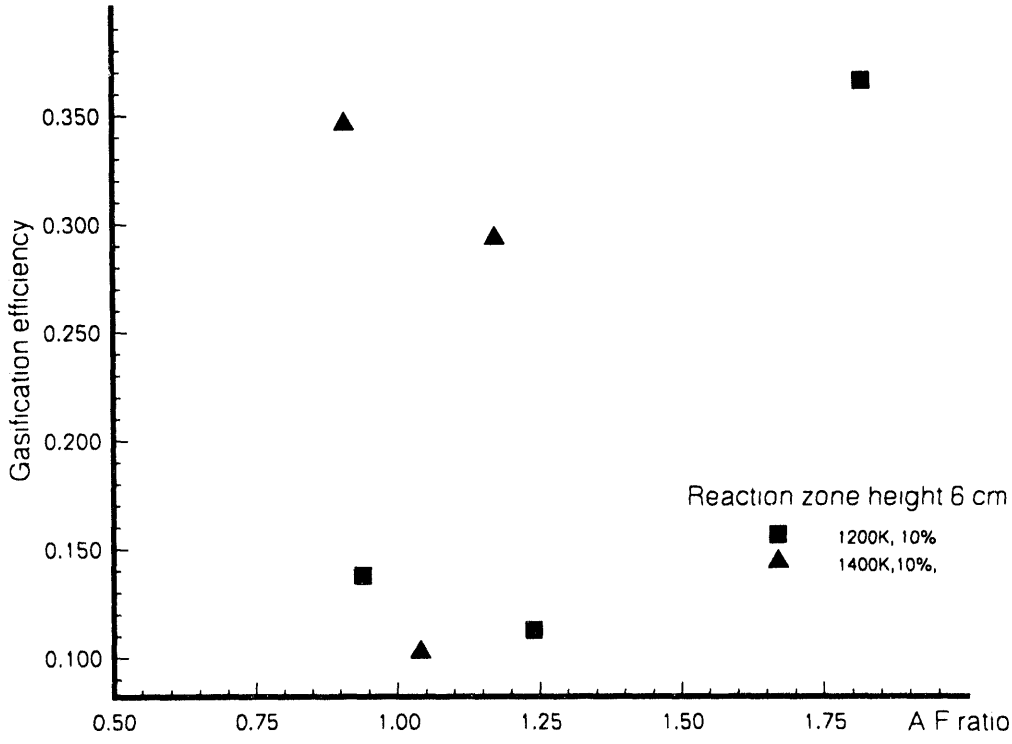

Fig. 6.8 Effect of Gas Temperature on Gasification Efficiency.

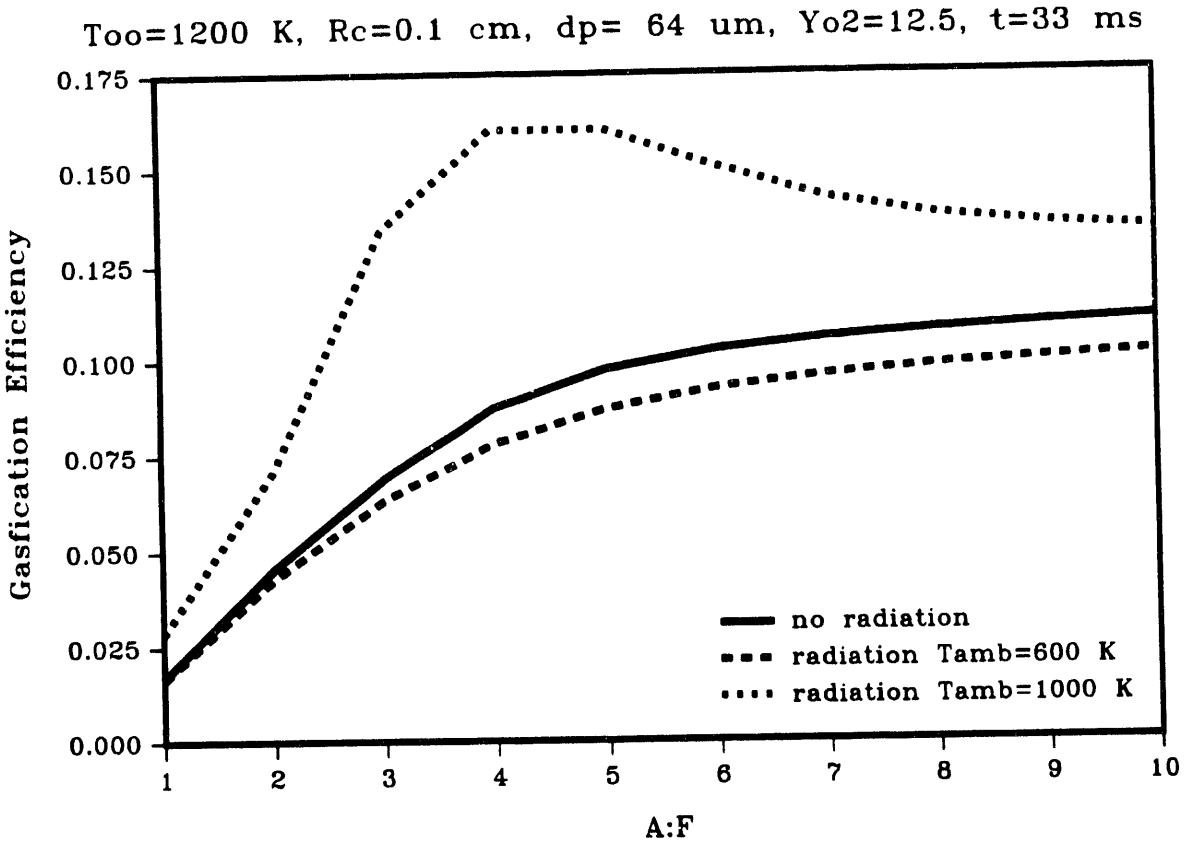

Fig. 6.9 Theoretical Results for a Cylindrical Coal Cloud (Du et al., 1993).

extreme, the cloud is of cylindrical shape of dia. 2.03 mm at very high velocity due to insufficient time for mixing (Fig. 6.10). Typically, the coal particles because of higher carrier air flow travels with a higher velocity than the surrounding gas velocity. The flow calculation gives a cold coal velocity some times as high as 33 m/s while the velocity of the hot gases surrounding the jet is approximately 0.60 m/s. The coal stream transfers its momentum to the surrounding gases and if sufficient time is provided, the coal velocity will asymptotically reach the gas velocity. It is noted that while the estimate of coal velocity is as high as 33 m/s, the measured velocity using digital images is only of the order of 10 m/s. During the process of momentum transfer, the stream entrains the surrounding gases and starts to diverge. Hence it is difficult to obtain the cylindrical cloud throughout the combustion period. Since the gas flow is through a centered porous plug in the flat flame burner, the gas velocity is of the order of 0.6 m/s under hot conditions. Higher gas velocity to match with velocity of fuel jet cannot be achieved since the flat flame will be lifted up. Due to the particle terminal velocity(0.06 m/s) considerations, the stream velocity cannot be brought down below predetermined velocity. Hence the stream divergence is unavoidable. Hence experiments were performed to measure the degree of divergence of the stream. Figure 6.11 shows the stream divergence. It should be noted that the stream diverges partly due to the presence of the particle collection system when placed close to the burner. This effect can be seen from the Fig. 6.12 as the reaction zone height is increased from 4 cm to 6 cm, the divergence angle decreases. To complicate the matter further, the

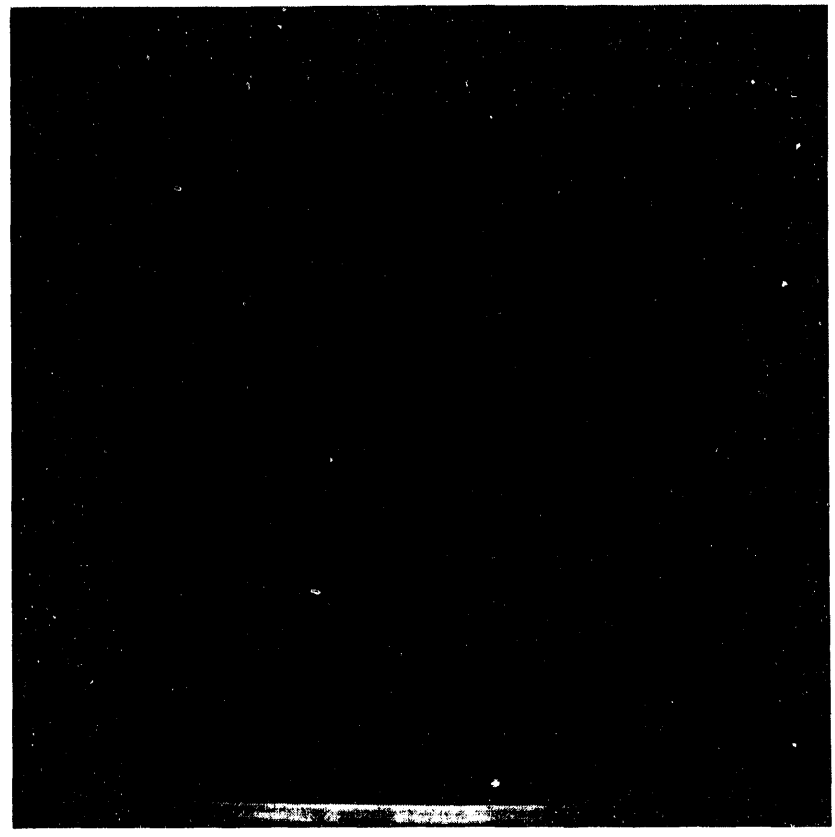

Fig. 6.10 Cylindrical Coal Stream.

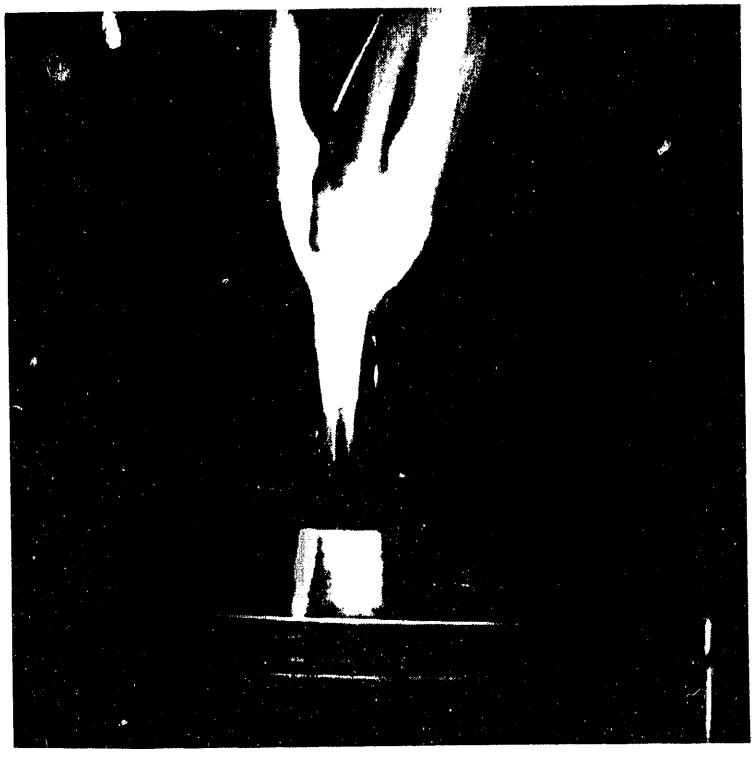

Fig. 6.11 Coal Flame Divergence at 4 cm Reaction Zone Height.

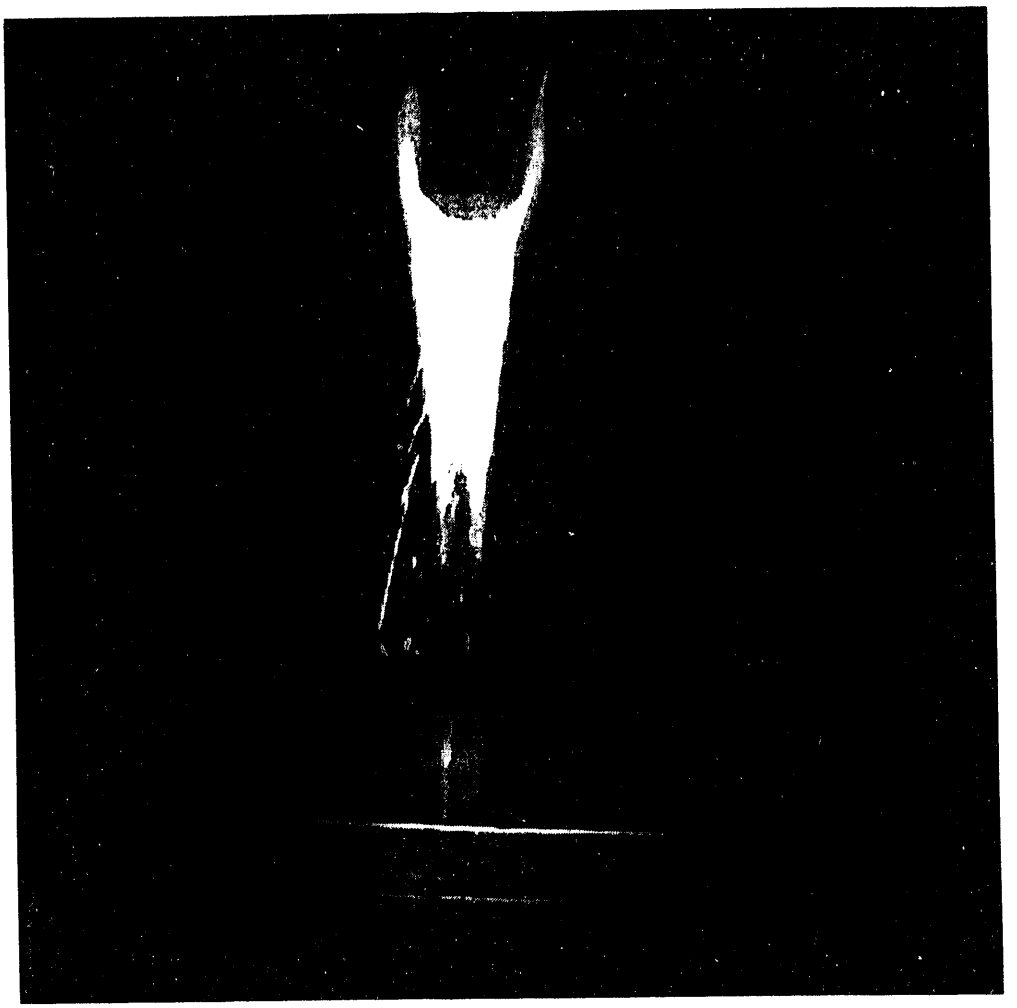

Fig. 6.12 Coal Flame Divergence at 6 cm Reaction Zone Height.

flame divergence may be due to the coal stream divergence or due to the volatiles burning outside the cloud.

A series of experiments with coal stream were conducted in order to ascertain the divergence phenomenon. To start with, just cold air was sent through the coal injector (V_{inj} =29.2 m/s, V_{gas}=0.32 m/s). In order to get the visual image of the jet, trace amount of particles were added by tapping coal feeder. The image is presented in Fig. 6.13 (A:F ratio 6.0). The jet diameter increases to 6 times its original diameter at 6 cm height. Next, coal feed rate is increased to get an air fuel ratio of 6. In both cases, the surrounding flow conditions were kept the same and the shape of the stream is captured using the digital camera. Same behavior as in Fig. 6.13 is obtained but the central coal stream does not diverge as much as the air stream (Fig. 6.14). Stream maintains its cylindrical shape due to the inertia of the solid particles. When such a stream is introduced into a hot ambience, a diverging flame observed more than what is seen under cold flow conditions. The high volatile coal releases volatiles and the flame follows volatiles and results in a diverging jet shape. Another probable reason is that coal air is heated in a hot environment which results in gradual expansion of the jet. Digital images shown later appear to confirm former hypothesis than the latter.

In order to study the stream expansion alone, stream was introduced into the hot ambience with 0.6% oxygen concentration. The stream is just expected to pyrolyze, but due to the O_2 in the carrier air, it resulted in a flame (Fig. 6.15). Subsequently, nitrogen was used as a carrier for coal. It still resulted in a flame (Fig. 6.16). In the last

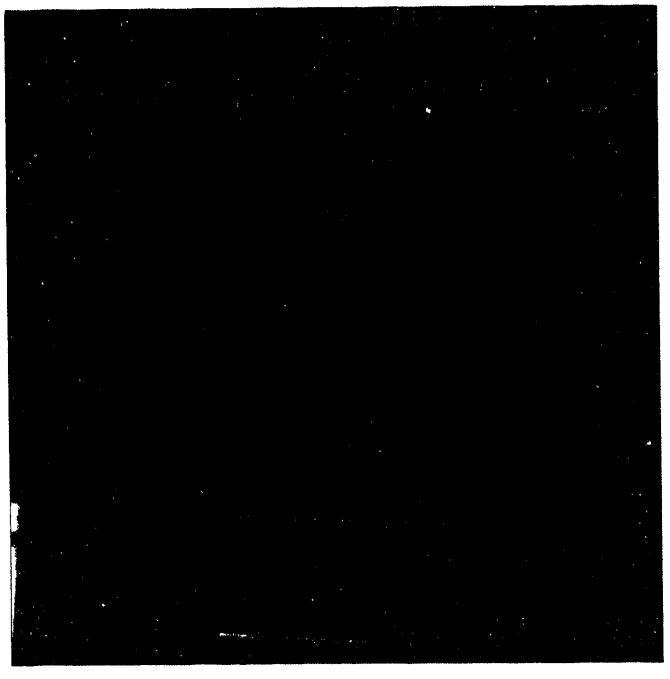

Fig. 6.13 Air Jet Divergence.

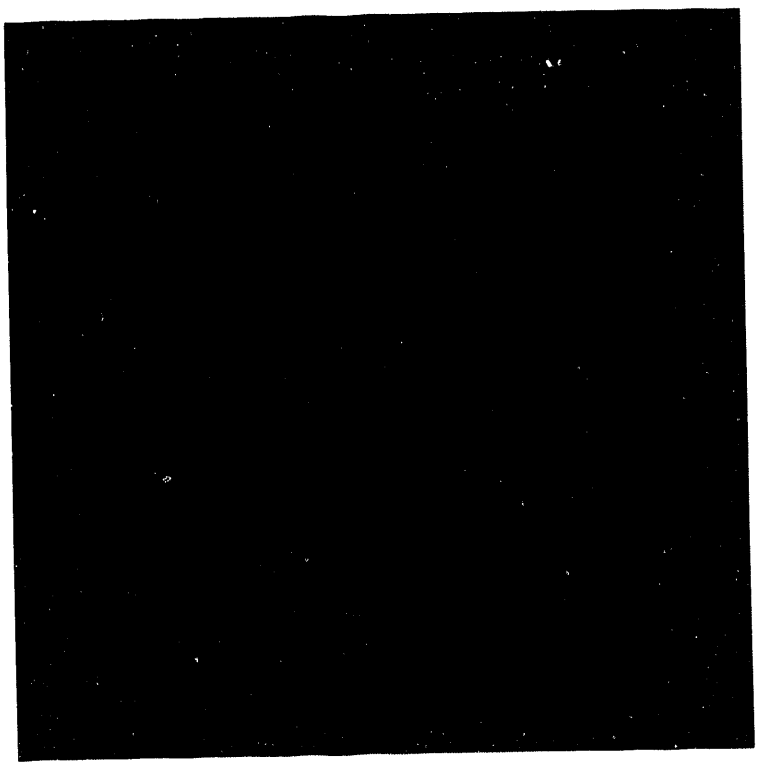

Fig. 6.14 Coal Stream Divergence.

Fig. 6.15 Coal Stream Flame for 0.3% Oxygen Conc. (Carrier : Air).

Fig. 6.16 Coal Stream Flame for 0.3 % Oxygen Conc. (Carrier : Nitrogen).

experiment, the particle collection system placed in the way of the stream is removed. When the coal stream is injected, it combusts with the traces of oxygen available and when all oxygens are consumed, the stream just pyrolyses without flame (Fig. 6.17). Hence it is concluded that coal stream maintains its cylindrical shape without much expansion and the diverging flame as seen in Fig. 6.12 probably follows the volatiles. However the physical presence of the particle collection system may also result in divergence of the flame.

6.5 Digital Imaging of Ignition

The image processing set up captures the flame images every 33 ms. When the coal stream is flowing into the vitiated environment with a constant coal flow, it establishes a steady flame. Except for the initial periods, all the flame images should be the same. These steady flame images will then reveal the ignition characteristics of coal streams. In an actual experiment, the flow fluctuates leading to fluctuating cloud A:F ratios for the same experiment. As the combustion process is very sensitive to A:F ratio, the resulting flame image has to be carefully analyzed.

Each frame image is a pictorial representation of 512*512 array numerical values each varying from 0 to 255. Further, the pixel value is the average brightness value over a depth of 2.07 mm. A darkest point like center of coal stream will have a value of say 60 while a high temperature flame point is represented by a pixel value of 255. Since a burning coal stream has particles under different burning conditions, its pixel value varies from 0 to 255.

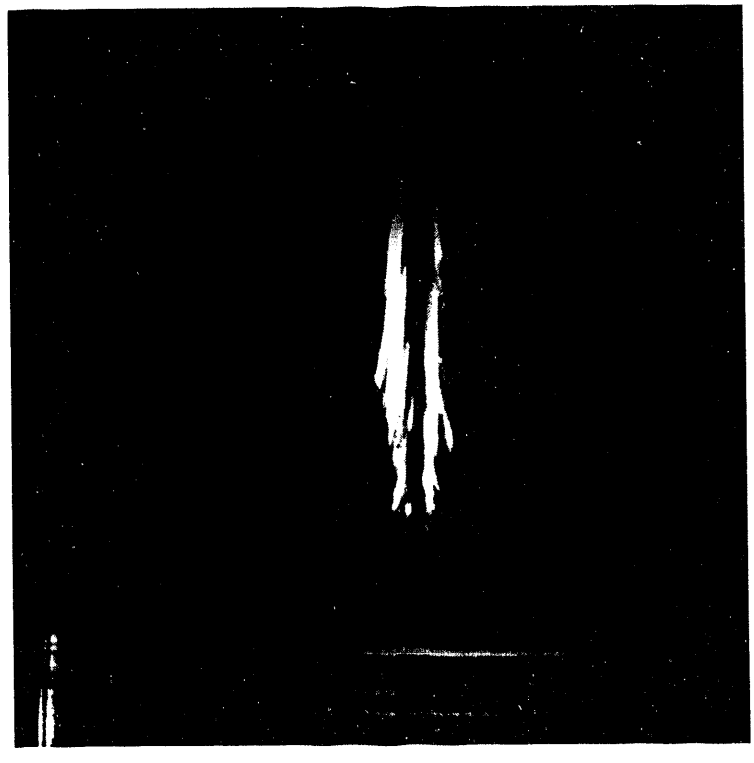

Fig. 6.17 Pure Pyrolysis of Coal Stream.

When the coal stream enters a high temperature zone, the stream heats up, pyrolyses (releases volatiles), then ignites. The ignition process may begin due to homogeneous oxidation of volatiles or due to heterogeneous oxidation at the particle surface. If a particular pixel location in the coal stream jumps in its brightness value then it can be safely concluded as the ignition point because the pixel values are directly proportional to incident light brightness and to the temperature Figure 6.18 shows the pixel trace. It is seen at about 1 cm height, there is a jump in pixel value. The pixel values are tracked axially along the center line of the injector (Y direction). When the coal stream develops in the Y direction, if this sudden jump is observed within the stream diameter, then probably the ignition has occurred heterogeneously. If the pixel location is outside the stream diameter, volatiles ignited first leading to homogeneous ignition.

6.5.1 Effect of A:F Ratio on Ignition

Theoretical models (Ryan et al., 1991; Du et al., 1993) predict a homogeneous ignition (ignition of volatiles) for a dense cloud and heterogeneous ignition (ignition of carbon) for a dilute cloud. Experiments are conducted with varying A:F ratio starting from 0.5 (dense) to 2.0 to study the effect of cloud denseness over the ignition mode. At the gas temperature of 1200 K and at constant oxygen concentration of 10%, A:F ratio is increased from 0.85 to 2.75. The pixel contours near the injector region are plotted for both these cases. Figure 6.19 demonstrates the heterogeneous ignition for the stream of A:F ratio 2.75 since the peak in pixel value occurs an the center of

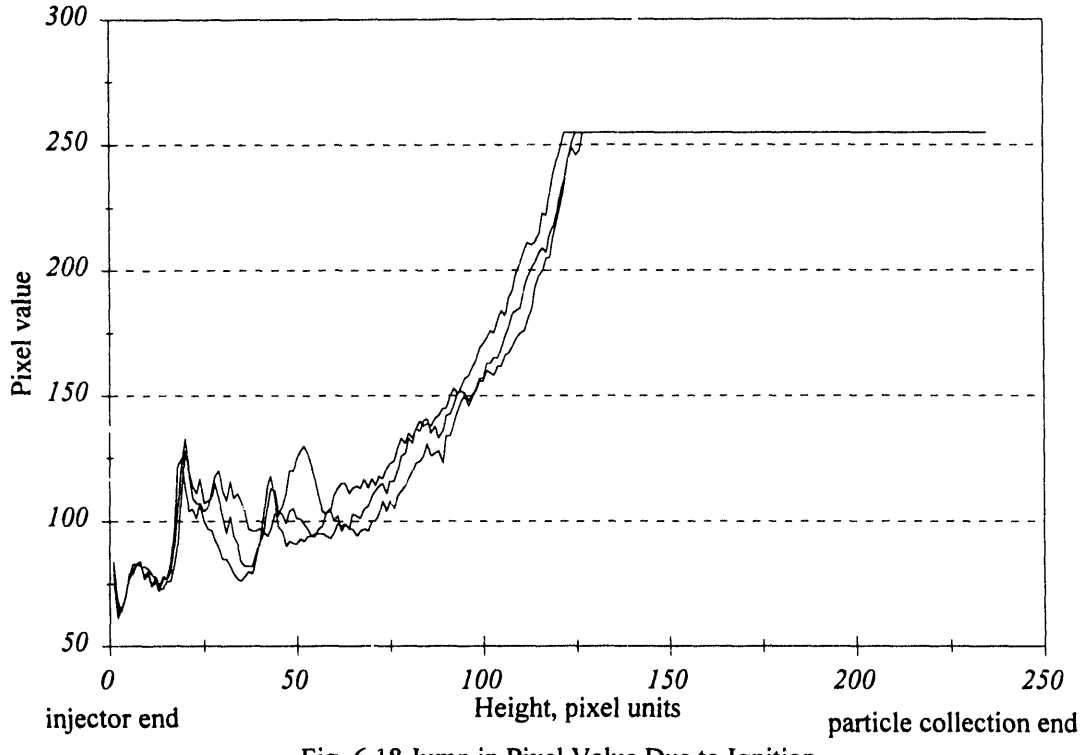

Fig. 6.18 Jump in Pixel Value Due to Ignition.

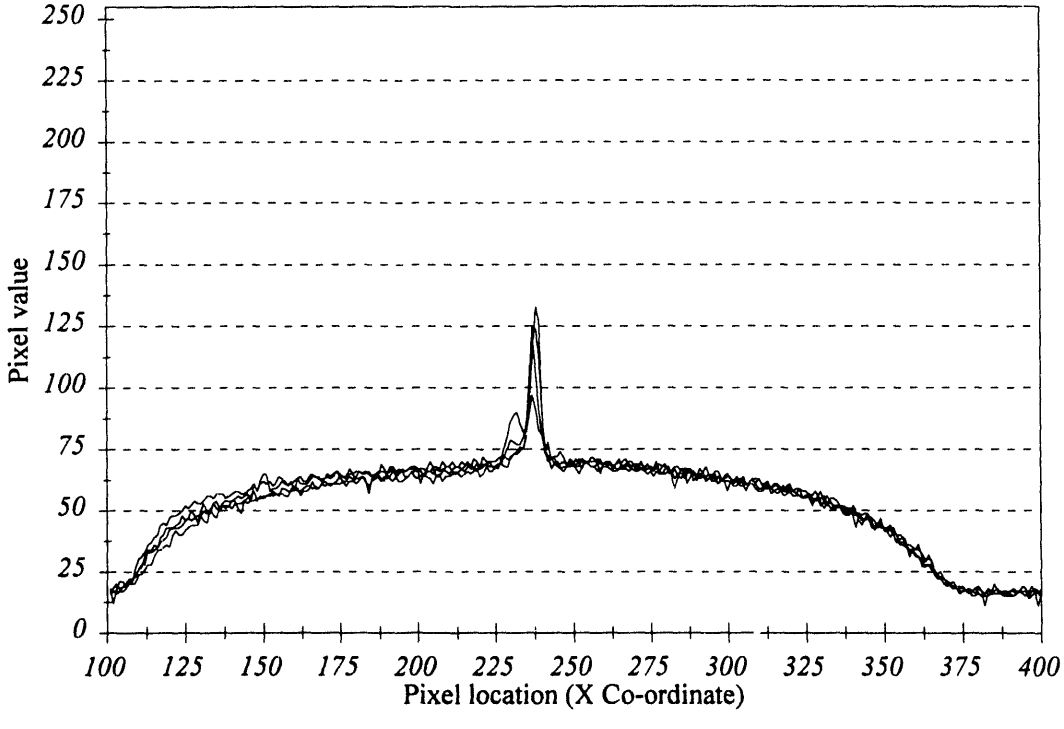

Fig. 6.19 Pixel Contours for Heterogeneous Ignition Mode.

the isolated particles may not form a flammable mixture. As the successive flame images in the Fig. 6.20 shows individual brightness spots in the beginning of the stream. These isolated spots corresponds to the individual particles in the dilute cloud. This is a strong evidence for heterogeneous ignition for the dilute cloud.

On the other hand, if the A:F ratio is decreased to the denser side say 0.85, the mode of ignition switches to pure gaseous side. More the number of particle (number density), more the quantity of volatiles released. These volatiles travel outside the stream and form a flammable mixture with surrounding oxygen/air near the outer edge of the stream. The flammable mixture ignites leading to homogeneous ignition. When the pixel values are tracked horizontally just above the burner, two peaks in pixel values occur near the stream as indicated by the Fig. 6.21. Pixel contours at 6 different levels in close proximity reveal the same pixel contour pattern. Also, Fig. 6.22 shows the increase in pixel brightness outside the stream in all its successive flame images. Pixel brightness is directly proportional to temperature and the temperature increase outside the cloud is evident from the images which leads to the conclusion of homogeneous ignition for dense clouds.

6.5.2 Effect of Oxygen Concentration over Ignition

The oxygen concentration is increased from 10% to 12.5% by allowing pure oxygen to flow with methane air mixture. Experiments are conducted with two different cloud air fuel ratios. Since ignition in the homogeneous mode is mostly in

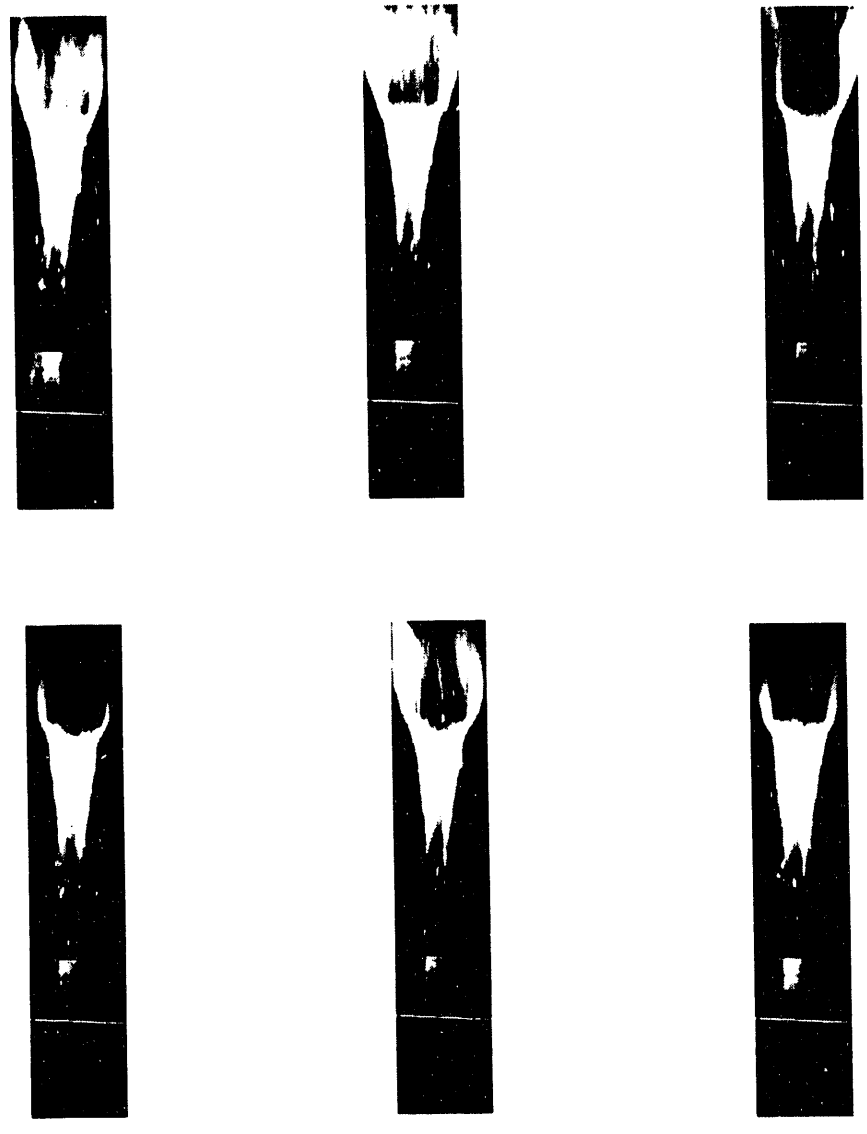

Fig. 6.20 Six Successive Frames of Dilute Coal Cloud Ignition (1200 K, 10% Oxygen Conc., 2.75 A:F Ratio).

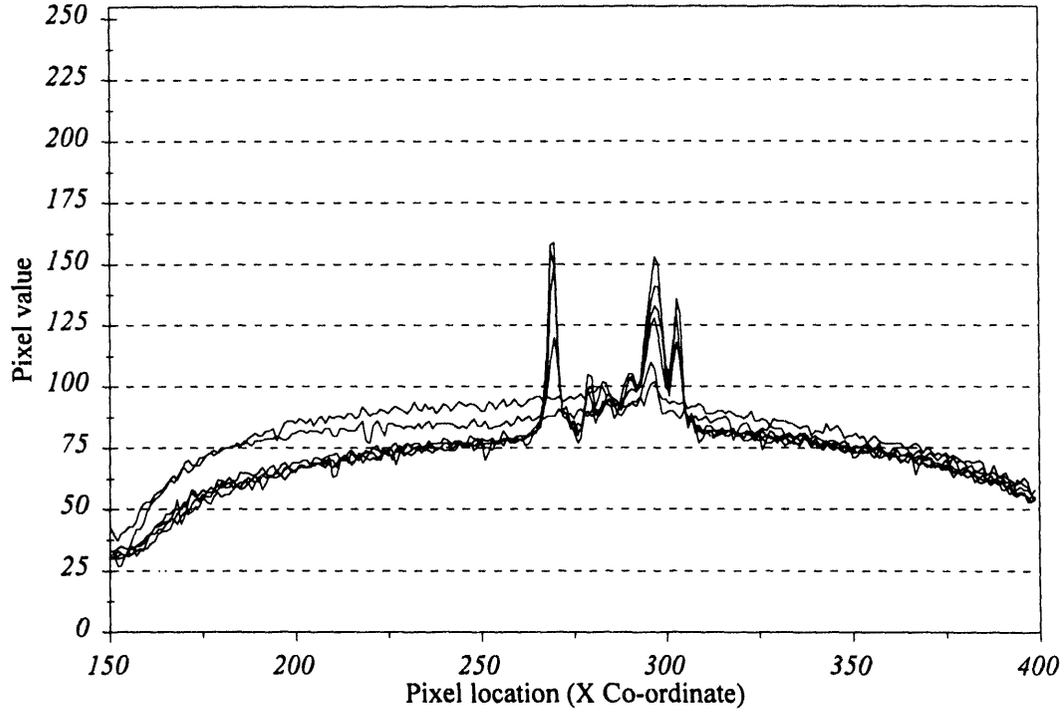

Fig. 6.21 Pixel Contours for Homogeneous Ignition Mode.

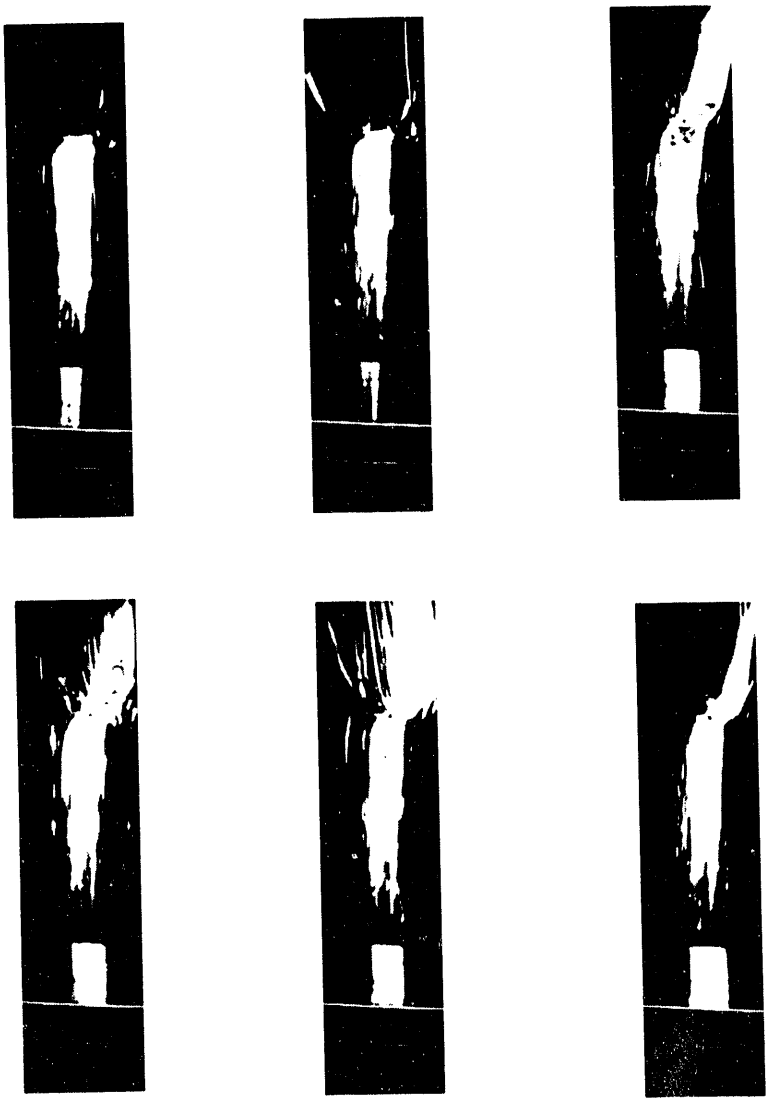

Fig. 6.22 Six Successive Frames of Dense Coal Cloud Ignition (1200 K, 10% Oxygen Conc., 0.85 A:F Ratio).

the ambience, the increase in oxygen concentration will have no effect on the mode of homogeneous ignition. However, increased O_2 results in more transport of O_2 to particle surface and heterogeneous ignition is more likely. Further, the increase in oxygen concentration will have an impact on ignition times.

Figure 6.23 shows the pixel contours near the injector for the dense cloud (A:F ratio 0.594). The peaks in the cloud periphery exhibits homogeneous ignition for this dense cloud at 12.5% oxygen concentration. The observation is similar to Fig. 6.19. The consecutive flame images indicate homogeneous ignition (Fig. 6.24). For the second case, i.e. with dilute cloud (A:F ratio 2.2), the pixel contours peaked at the center of the injector (Fig. 6.25), a characteristic of heterogeneous ignition. Figure 6.26 shows the images of this heterogeneous ignition with high pixel values all over the thin coal stream indicating simultaneous ignition of all the particles in the stream leading to the flat pixel profile (Fig. 6.25) at the center of the stream in stead of just one peak. The effect of oxygen concentration on ignition time cannot visualized due to the unknown coal stream velocity while burning.

6.5.3 Effect of Gas Temperature on Ignition

Ryan et al., (1991) predicted that the size of the heterogeneous regime extends to higher G numbers with increasing gas temperature i.e. even denser cloud may ignite heterogeneously at higher gas temperature. For example, if T_{gas} =1900K with G=5, the ignition is heterogeneous; however if T_{gas} = 1100 K with G = 5, ignition is homogeneous. As the gas temperature is increased, the thermal penetration depth may

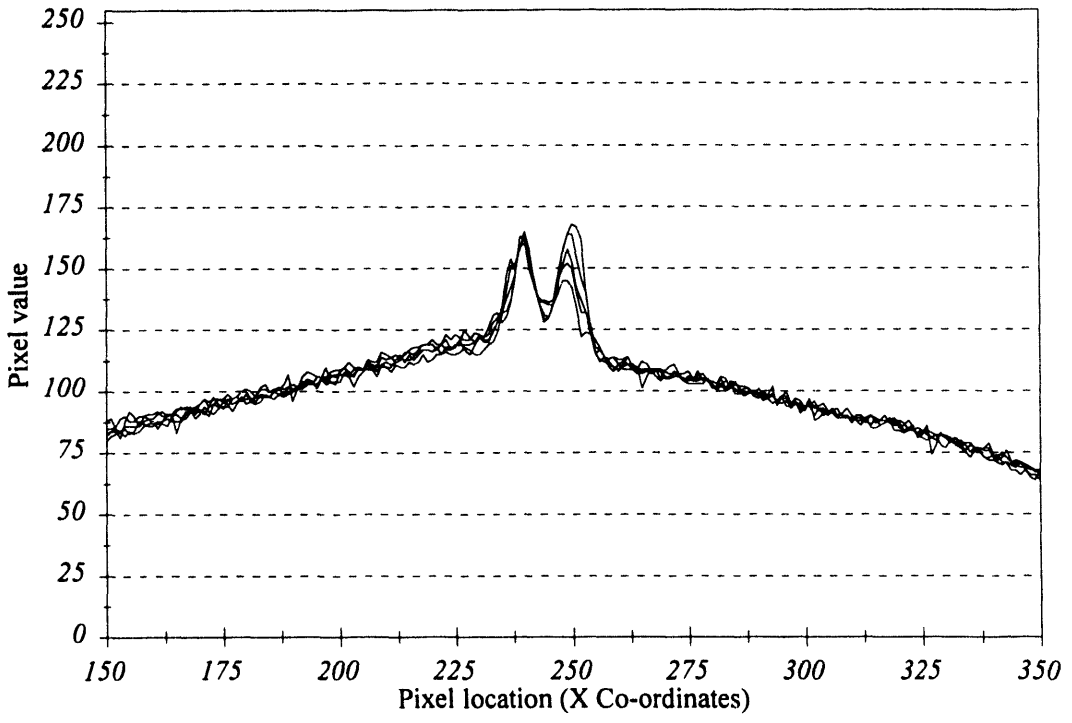

Fig. 6.23 Pixel Contours for Homogeneous Mode (12.5% Oxygen Conc.).

Fig. 6.24 Six Successive Frames of Dense Cloud Ignition (1200 K, 12.5% Oxygen Conc., 0.594 A:F Ratio).

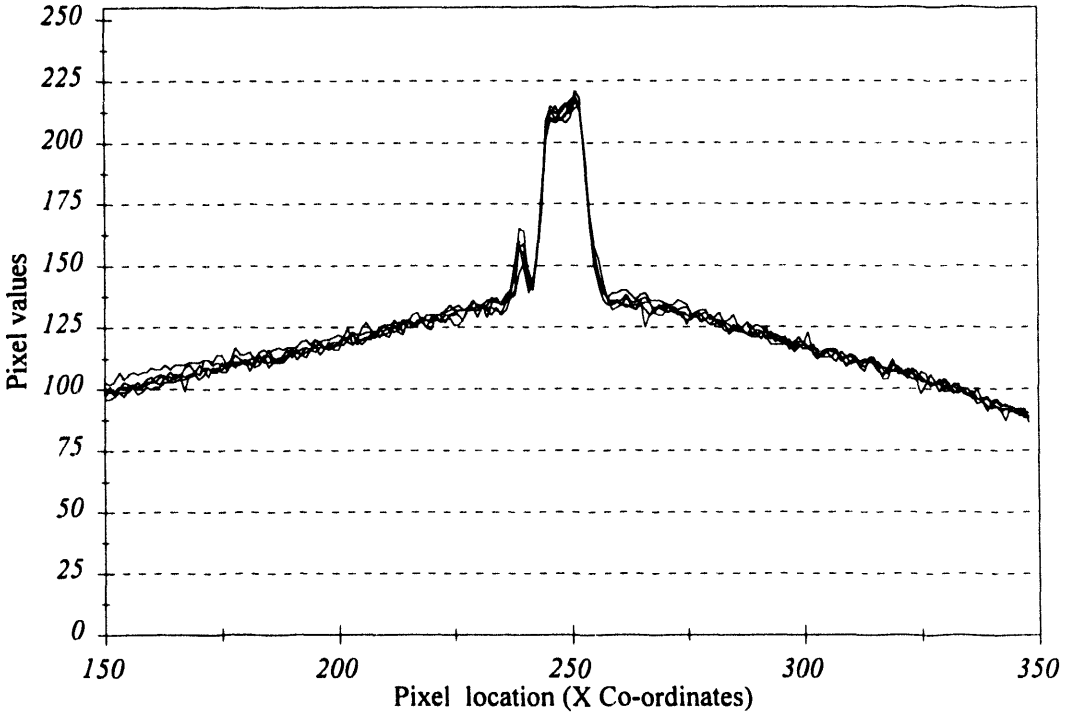

Fig. 6.25 Pixel Contours for Heterogeneous Ignition Mode (12.5% Oxygen Conc.).

Fig. 6.26 Six Successive Frames of Heterogeneous Ignition (1200 K, 12.5% Oxygen Conc., 2.2 A:F Ratio).

char oxidation(heterogeneous ignition). Note that these discussions pertain to dilute clouds only.

According to Du et al., (1994), the ignition of an isolated particle may switch from homogeneous to heterogeneous mode as gas temperature is increased. This is in contrast to the results obtained by Ryan and Annamalai (1991) which suggest that the ignition becomes heterogeneous as gas temperature is increased at the same cloud diluteness. The group models use average concentration for the volatiles in the inter particle spacing which seems to suppress homogeneous ignition.

Experiments were conducted for both 1200 K and 1400 K gas temperatures with dilute and dense coal clouds. The oxygen concentration is kept at 10%. For thc coal cloud with A:F ratio 4:1, ignition mode is not very clear. The pixel contours near the injector show both peaks at the cloud periphery and relatively high pixel values in the cloud (Fig. 6.27). The high ambient temperature leads to sudden heating up of the particle, leading to rapid volatile yield and homogeneous ignition. Other particles which are not at close proximity will result in heterogeneous ignition as expected for a dilute cloud (Fig. 6.28). Figure 6.29 indicates a very clear two peak pixel contour, an attribute of homogeneous combustion. All the images presented in Fig. 6.30 also reflect the same. The models predict that homogeneous ignition (dense cloud) time is less

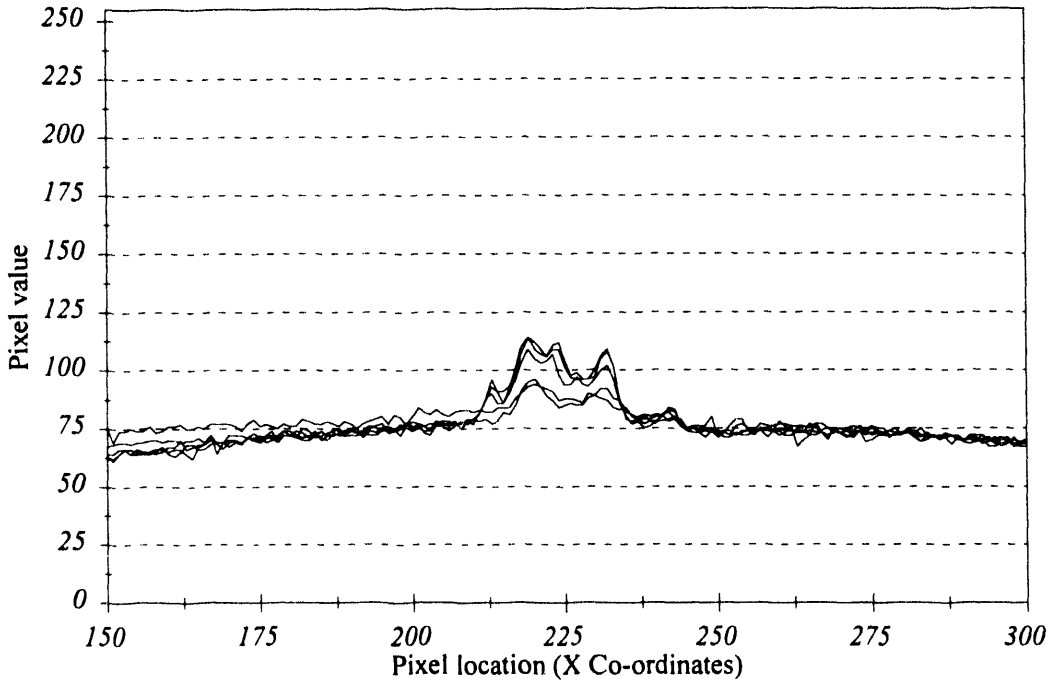

Fig. 6.27 Pixel Contours for a Dilute Cloud at High Temperature 1400 K.

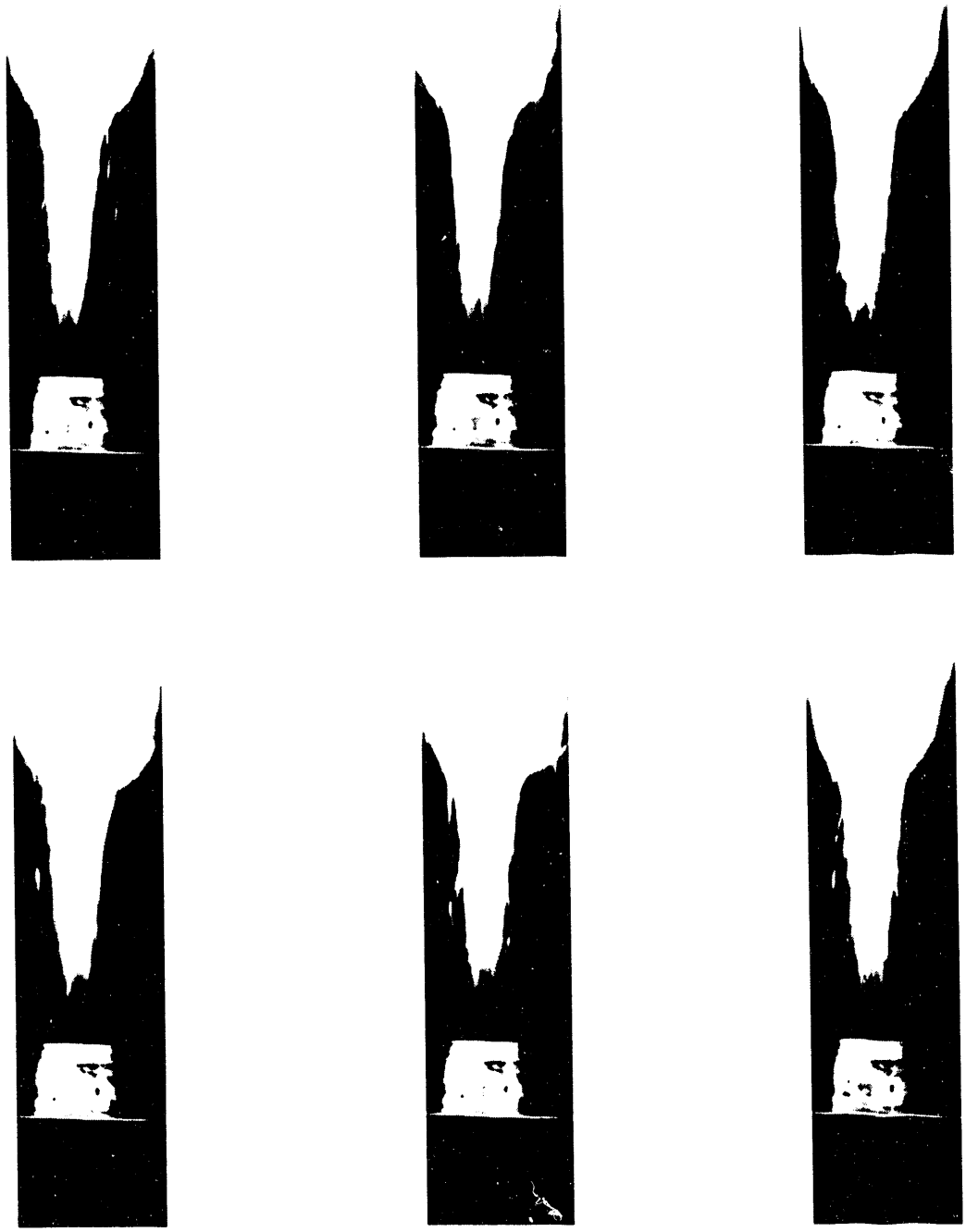

Fig. 6.28 Six Successive Frames of Ignition of Dilute Coal Cloud (1400 K, 10% Oxygen Conc., 4 A:F Ratio).

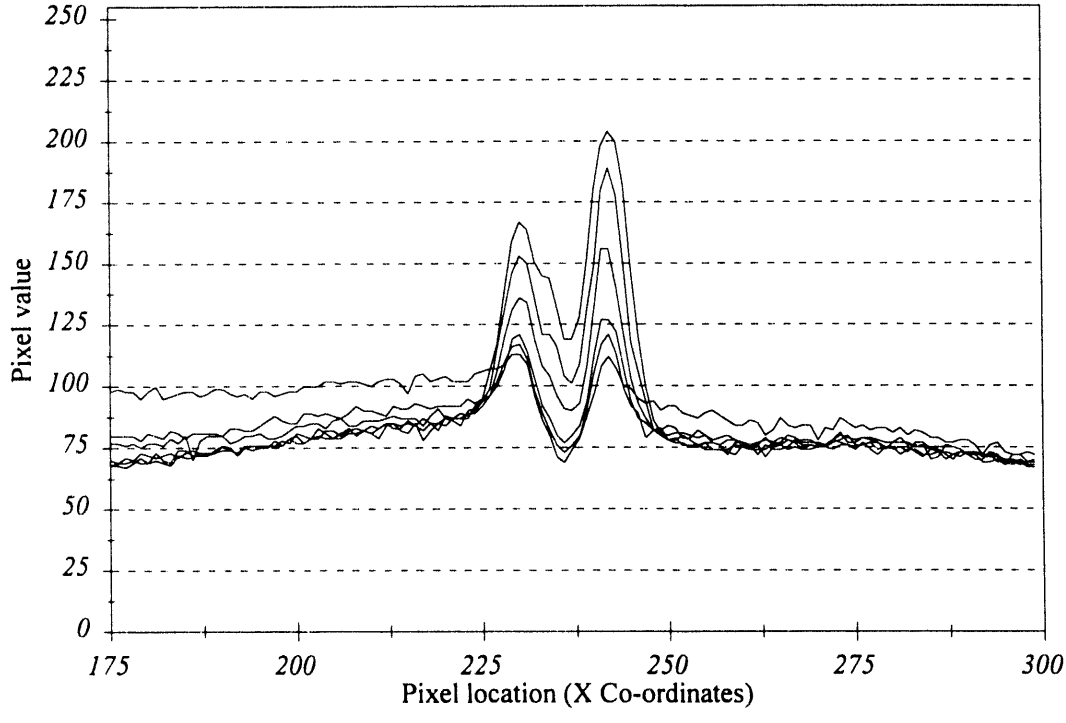

Fig. 6.29 Pixel Contours for Homogeneous Ignition of Dense Cloud at 1400 K and 10% Oxygen Conc.

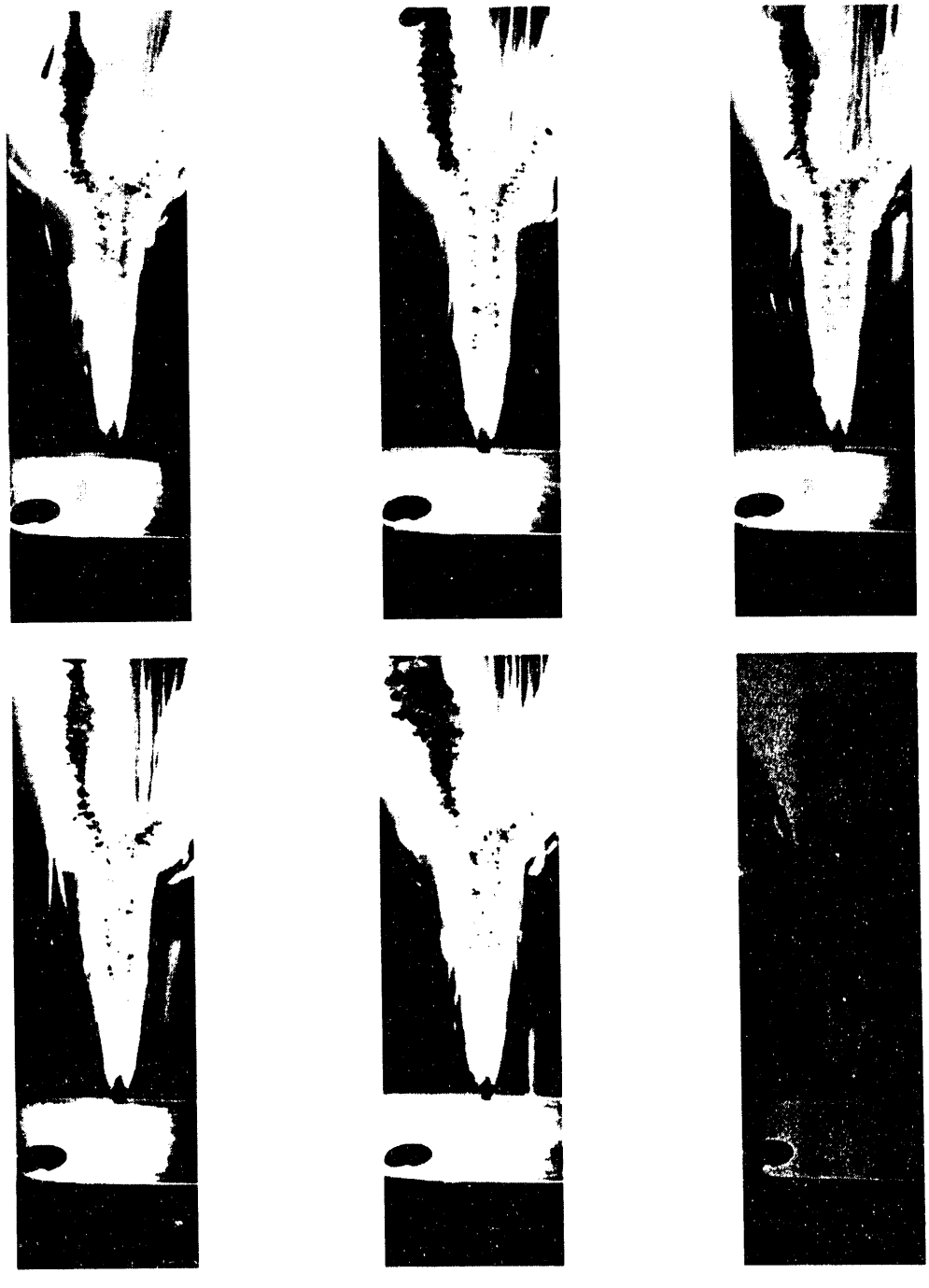

Fig. 6.30 Six Successive Frames of Homogeneous Ignition for Dense Cloud (1400 K, 10% Oxygen Conc., 0.79 A:F Ratio).

compared to heterogeneous ignition (dilute cloud) time. The false color images of the flames at different operating conditions are presented in Figs. 6.31 to 6.36.

6.6 Digital Imaging of Group Combustion

When a single particle burns in the isolated mode, an envelope flame is formed but when a cluster of particles burn, they form a single group flame enveloping all the particles together instead of individual flames around each particle in the cloud due to interactions amongst them. One of the objectives for the image processing system is to visualize the group flame for the dense cloud.

6.6.1 Group Flame

The digital camera captures a two dimensional image of the three dimensional coal stream flame. The camera has a depth of field equal to the stream diameter. The brightness value of a particular pixel location is proportional to the average luminosity across the depth of field. The pixel values for the particles in the outer stream will have very high brightness value as compared to the center of the stream which contains non burning coal particles in the core of the stream. Thus the brightness value at the center of the stream is less due to dark central core. A group flame for a stream will be of a 'W' shape with the outer legs extended farther. If the coal cloud is extremely dilute, then one may not expect group flame. Experiments are done in order to study the effects of A:F ratio, gas temperature, oxygen concentration and the reaction zone height over the flame shape. The image boundary will give the appropriate flame contour.

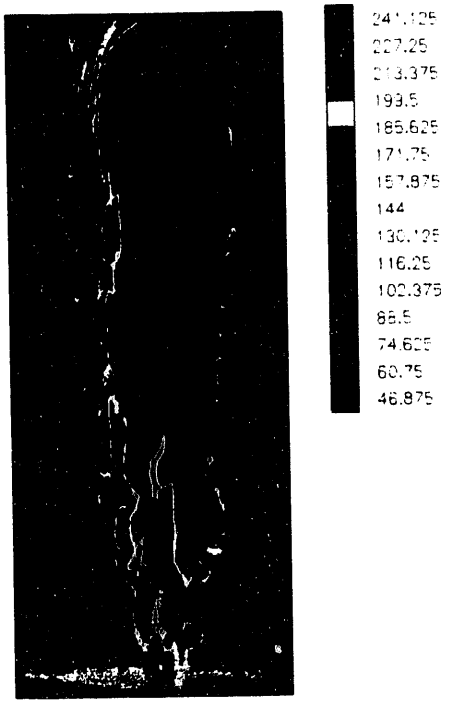

Fig. 6.31 Homogeneous Ignition for Dense Cloud (A F Ratio 0.85).

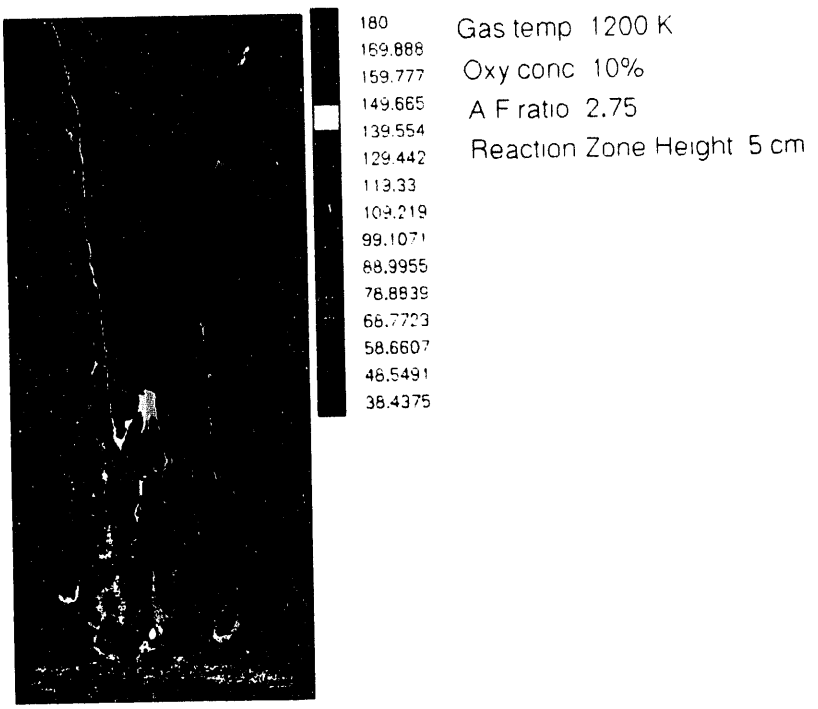

Fig. 6.32 Heterogeneous Ignition for Dilute Cloud (A F Ratio 2.75).

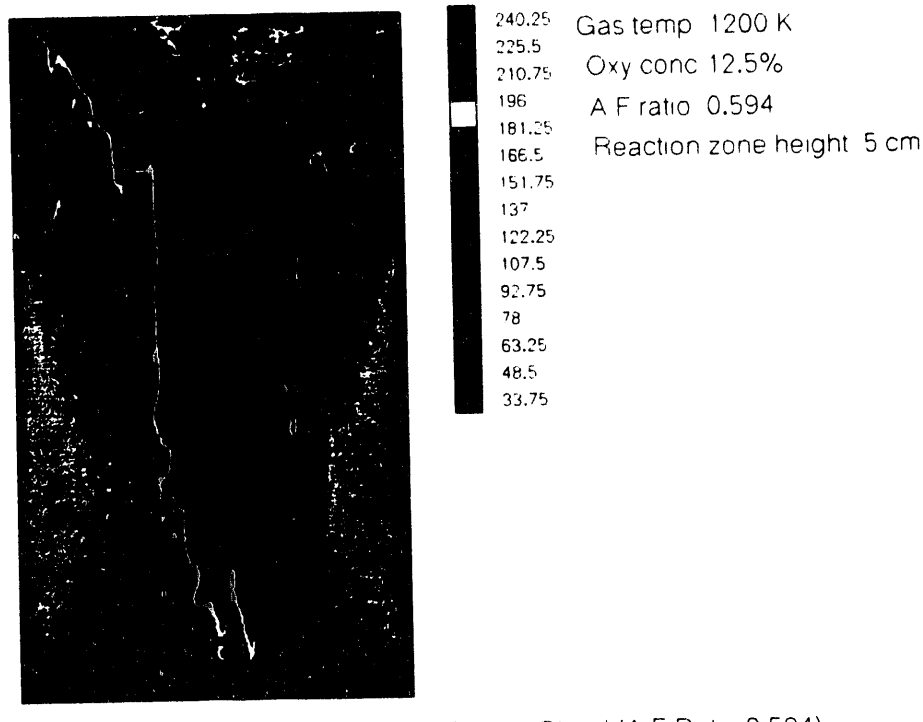

Fig. 6.33 Homogeneous Ignition for Dense Cloud (A F Ratio 0.594).

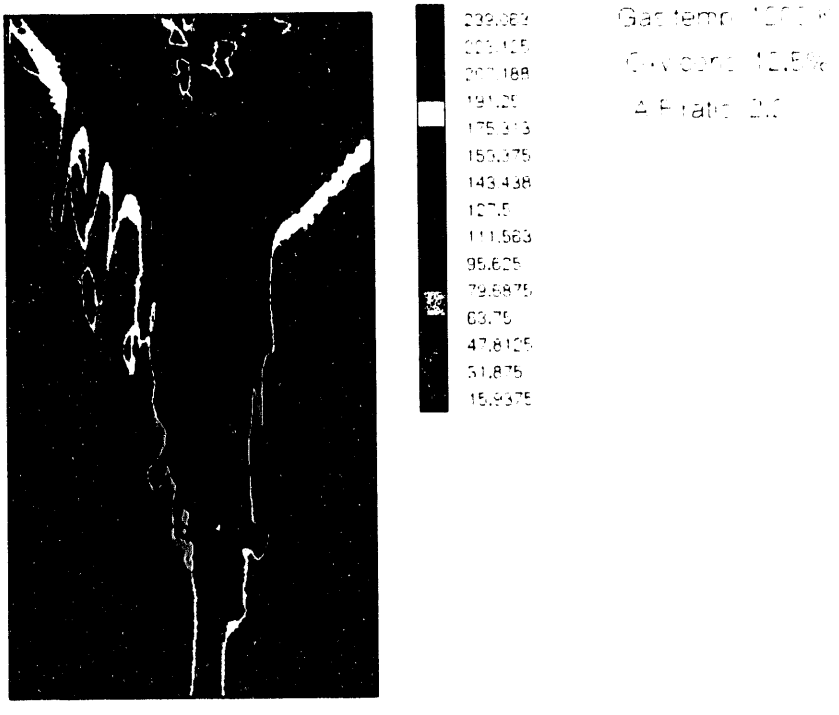

Fig 6.34 Heterogeneous ignition for dilute cloud

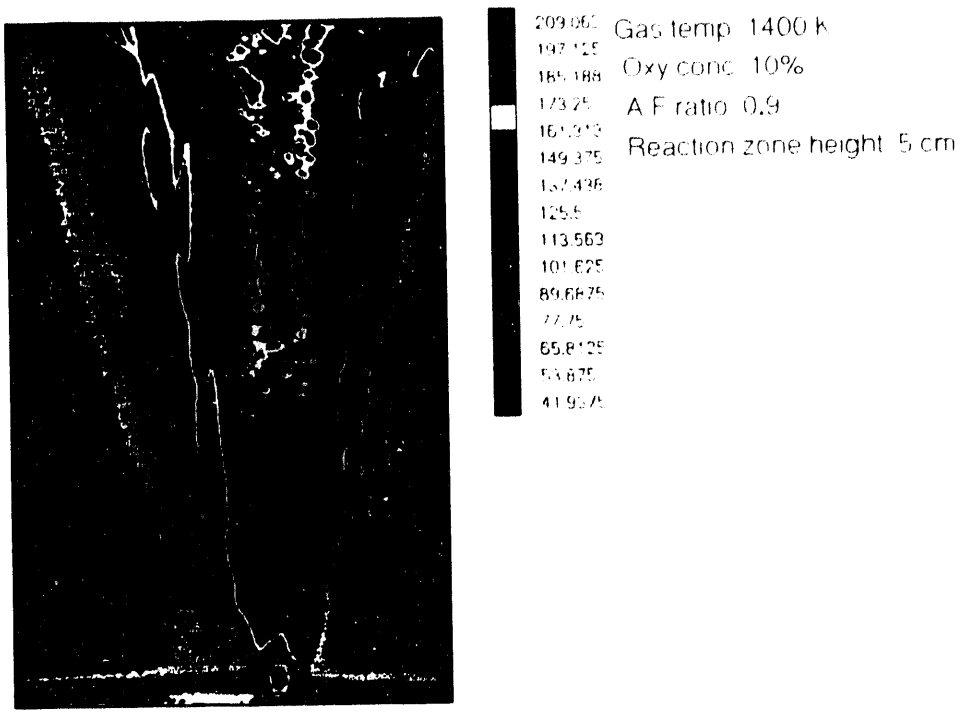

Fig. 6.35 Homogeneous Ignition for Dense Cloud (A F Ratio 0.9).

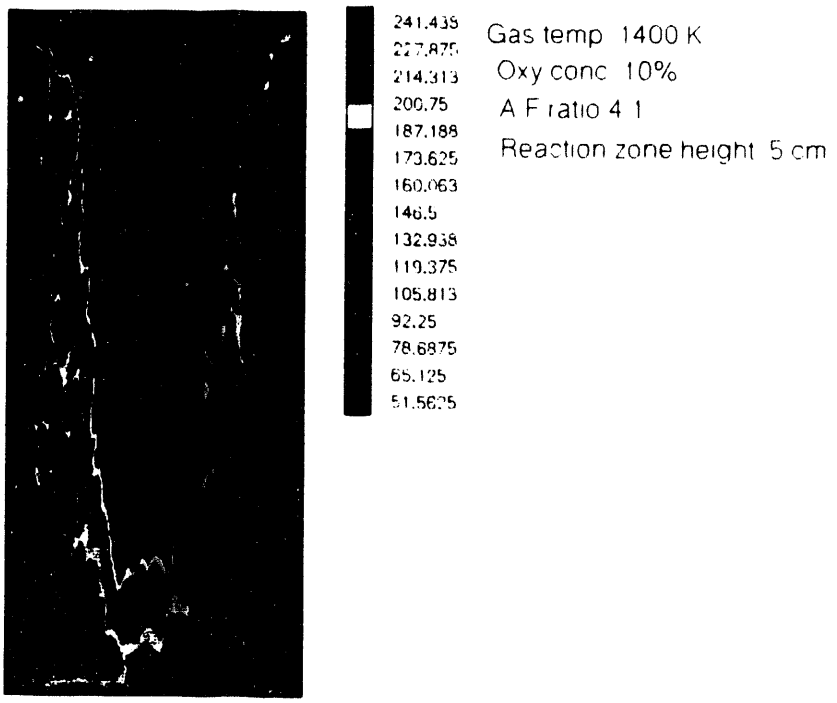

Fig. 6.36 Ignition of Dilute Cloud (A F Ratio 4.1).

6.6.2 Double Flame

The theoretical model proposed by Du et al., (1993) predicts a strange phenomenon in dense cloud combustion. When a dense cylindrical coal stream enters a hot ambience, upon reaching the pyrolysis temperature, the particles release volatiles which diffuse out of the cloud into the high temperature environment. Homogeneous ignition occurs outside the cloud. Since the reaction rate is faster than the volatile production rate from the stream, the flame propagates towards the cloud in search of volatiles. When the flame reaches the cloud surface, the particles heat up rapidly resulting in higher volatile yield. At this point, the stream cloud surface is almost devoid of O_2 while the core contains premixed volatiles and O_2. On the other hand, the zone outside the stream contains no volatiles. Hence two flames emerge with one travelling into the cloud (pre mixed zone) termed as 'inner flame' with the second flame moving away from the stream called 'outer flame' (diffusion flame). The inner flame will disappear once all the volatiles within the stream are consumed. The double flame occurs only for the restricted range of parameters. The model assumes a perfect cylindrical stream whereas, in experiments, it will be very difficult to attain a perfect cylindrical geometry. The stream always diverges due to the particle collection system placed in the center line of the stream as explained earlier.

6.6.3 Effect of A:F Ratio on Flame Structure

The coal stream experiments with cloud A:F ratio ranging from 0.8124 to 2.42 at constant gas temperature of 1200 K, oxygen concentration of 6.5% were conducted.

The reaction zone height is maintained as 6 cm. The six consecutive images for the dense cloud with A:F ratio of 0.8124 are shown in Fig. 6.37. The flame boundaries for these images using edge detection software are given in Fig. 6.38. As anticipated, the ignition always start homogeneously for this dense cloud. The coal stream flame seems to travel in two opposite directions, one towards the ambience and other towards the core of the stream. The divergence in the flame shape follows the contour of the particle collection probe. As the burnt particle flow up, sometimes they get attached to the probe and starts building up. The dark spots in the flame images are due to the deposition of unburnt particles, soot and ash. The deposition occurs particularly for the dense cloud experiments. The images and the flame boundary pictures also show the stray particles flowing out of stream periphery. They ignite heterogeneously.

When the air fuel ratio is increased to 2.42 (dilute cloud), the images obtained from the camera indicates heterogeneous ignition. It was not very clear about the double flame phenomenon as there is no distinction of two flames forming at the cloud radius. Double flame is not expected. The 'V' shapes at the periphery generally is the indication of inner and outer flame formation. The flame image pictures and boundary pictures (Figs. 6.39 and 6.40) does not provide strong evidence for this. When the cloud air fuel ratio is maintained at 1.347 which is not very dilute or dense, the ignition point is farther from the injector at one edge than the other edge. This may be due to the loose particles. Figures 6.41 and 6.42 show heterogeneous ignition with flat ignition profile at the stream. The various flame contours from the successive

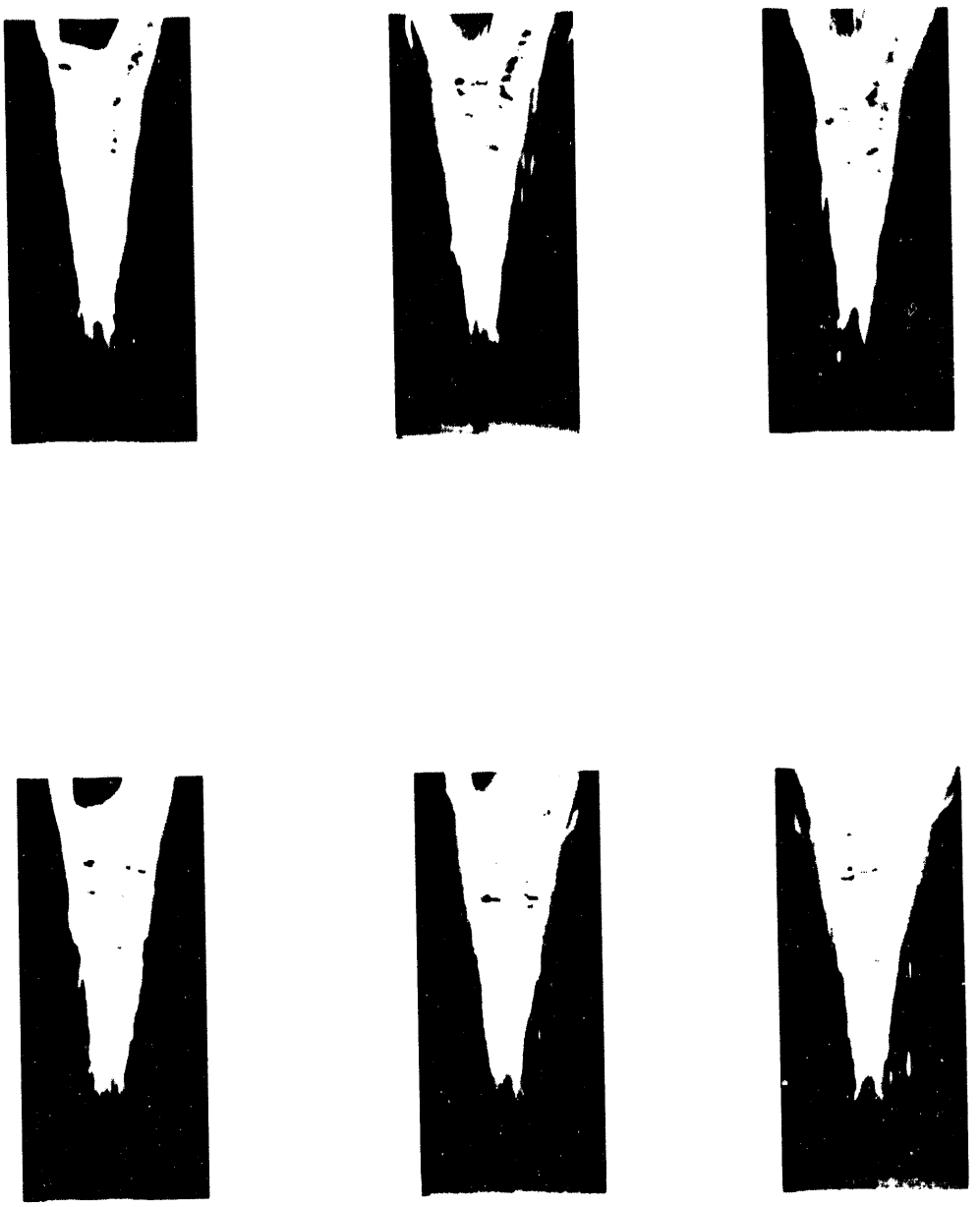

Fig. 6.37 Six Successive Frames of a Dense Cloud Combustion (1200 K, 6.5% Oxygen Conc., 0.8 A:F Ratio).

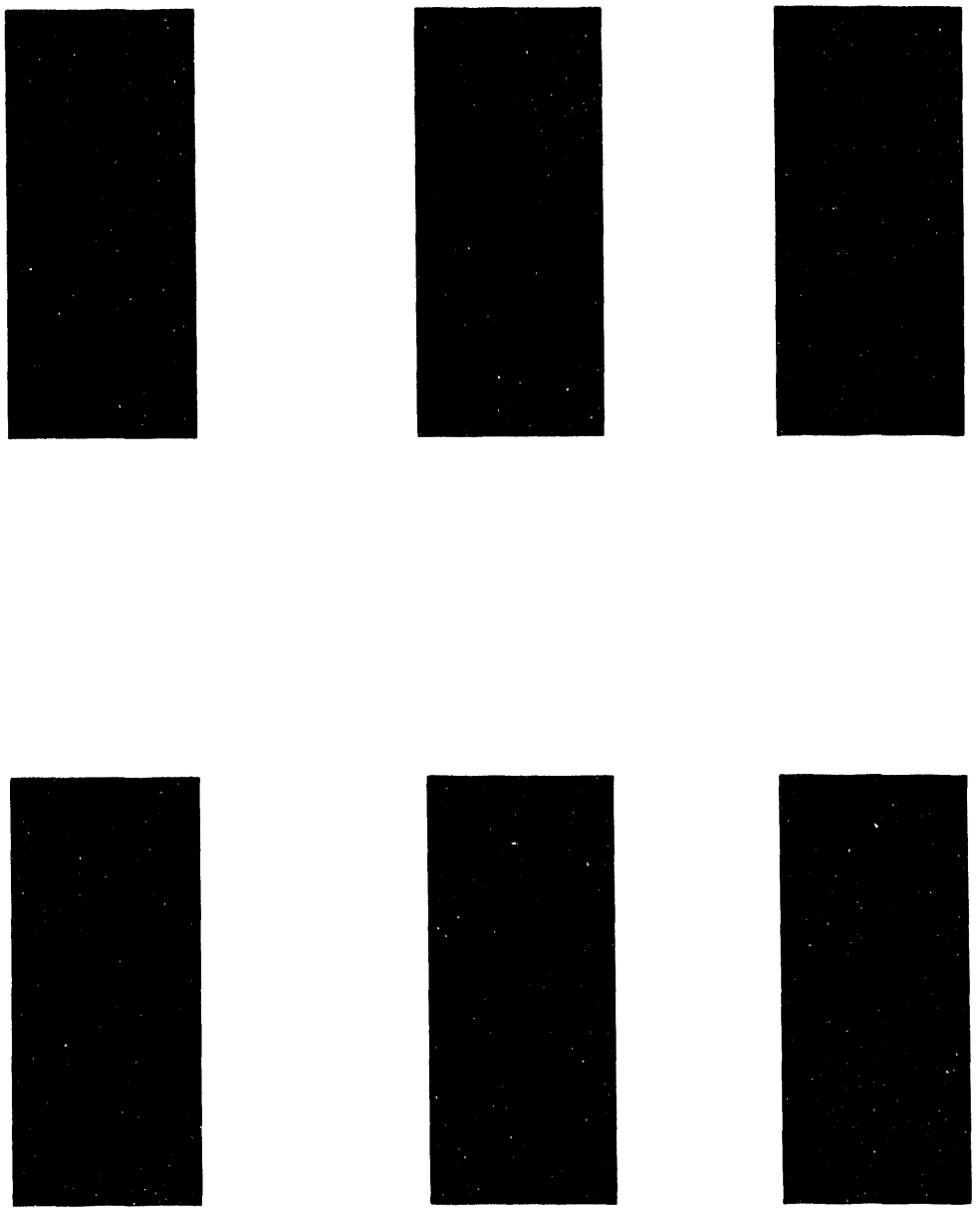

Fig. 6.38 Flame Boundaries for the Six Successive Frames of Dense Cloud Combustion (1200 K, 6.5% Oxygen Conc., 0.8 A:F Ratio).

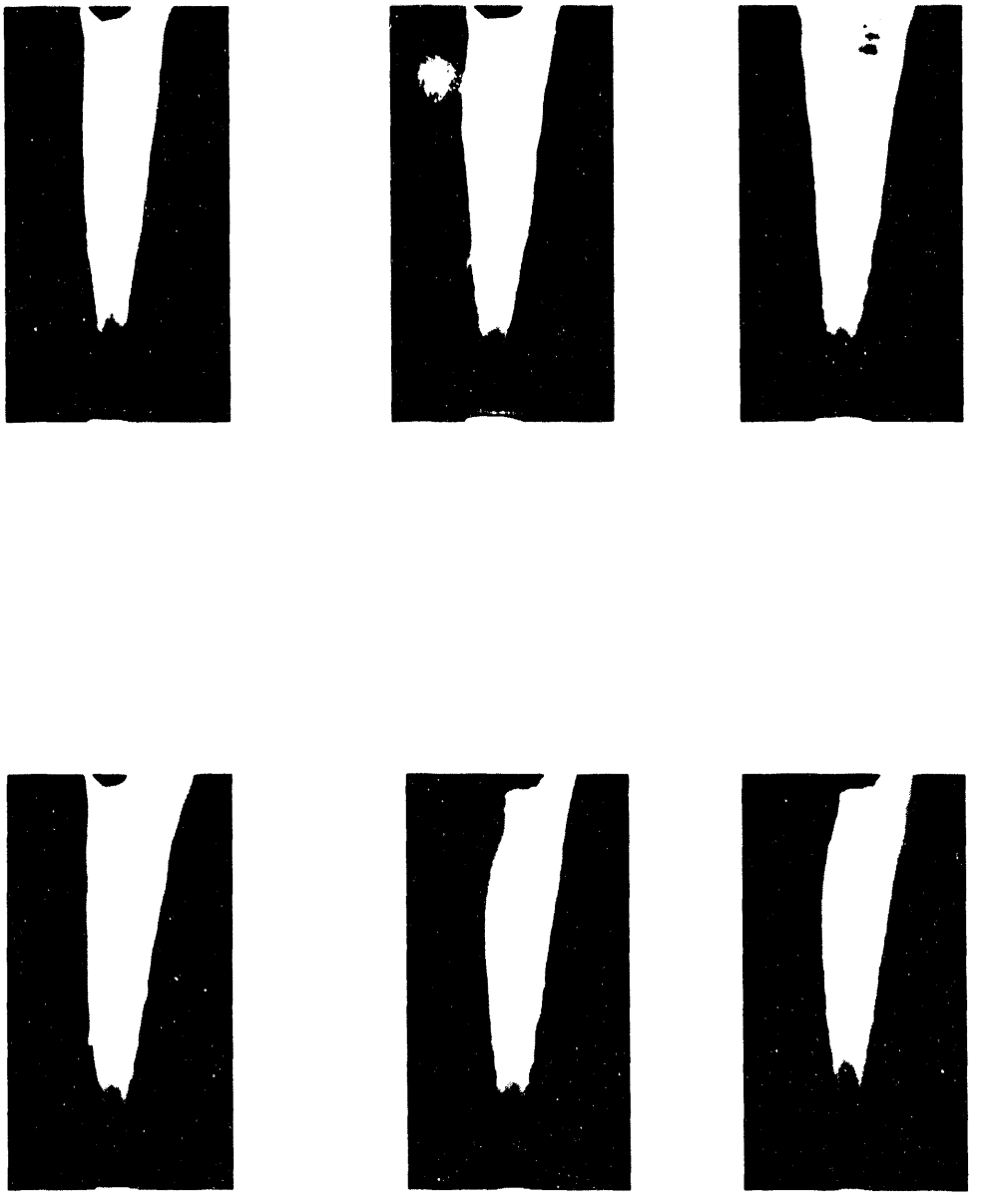

Fig. 6.39 Six Successive Frames of Dilute Cloud Combustion (1200 K, 6.5% Oxygen Conc., 2.42 A:F Ratio).

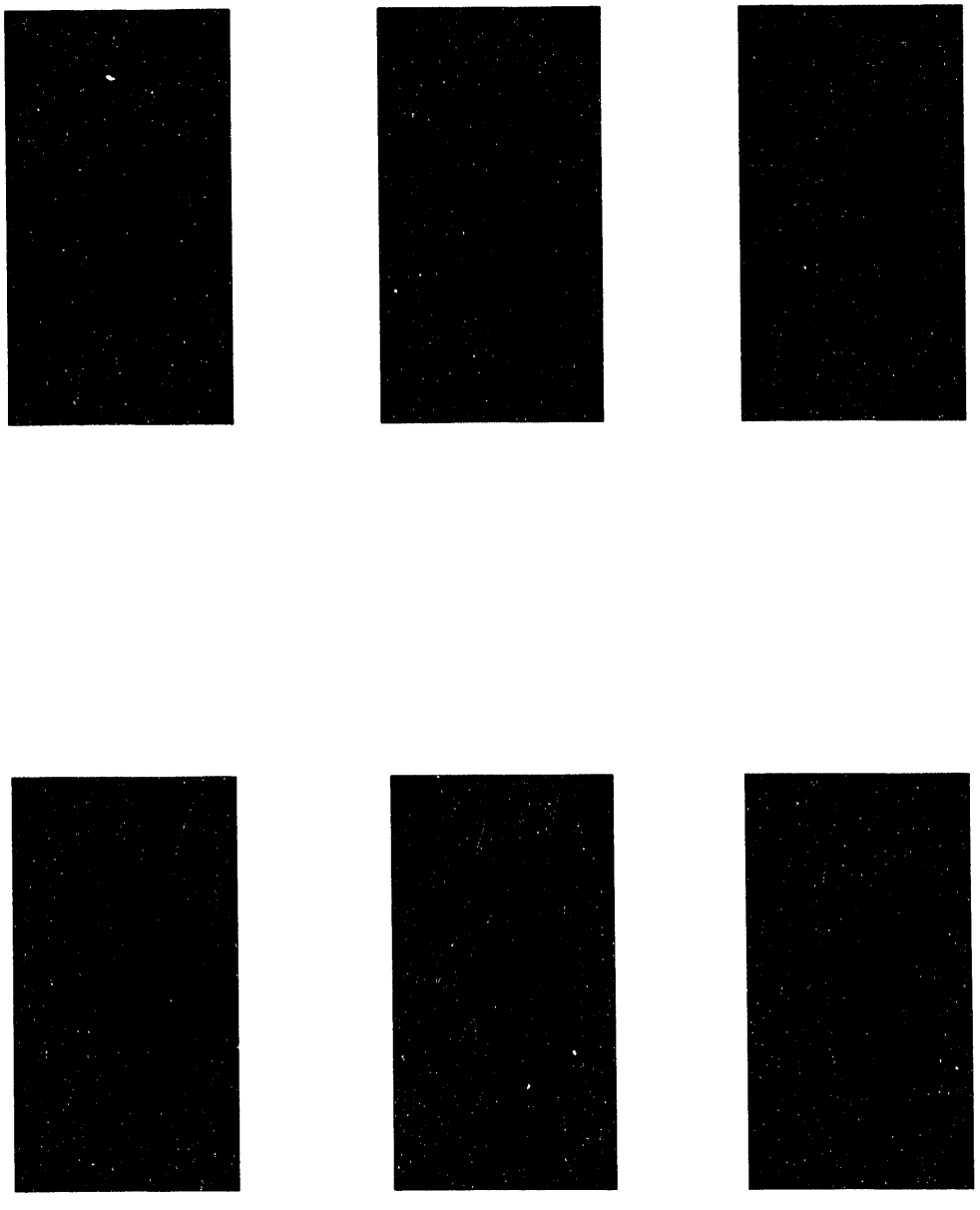

Fig. 6.40 Flame Boundaries for the Six Successive Frames of Dilute Cloud Combustion (1200 K, 6.5% Oxygen Conc., 2.42 A:F Ratio).

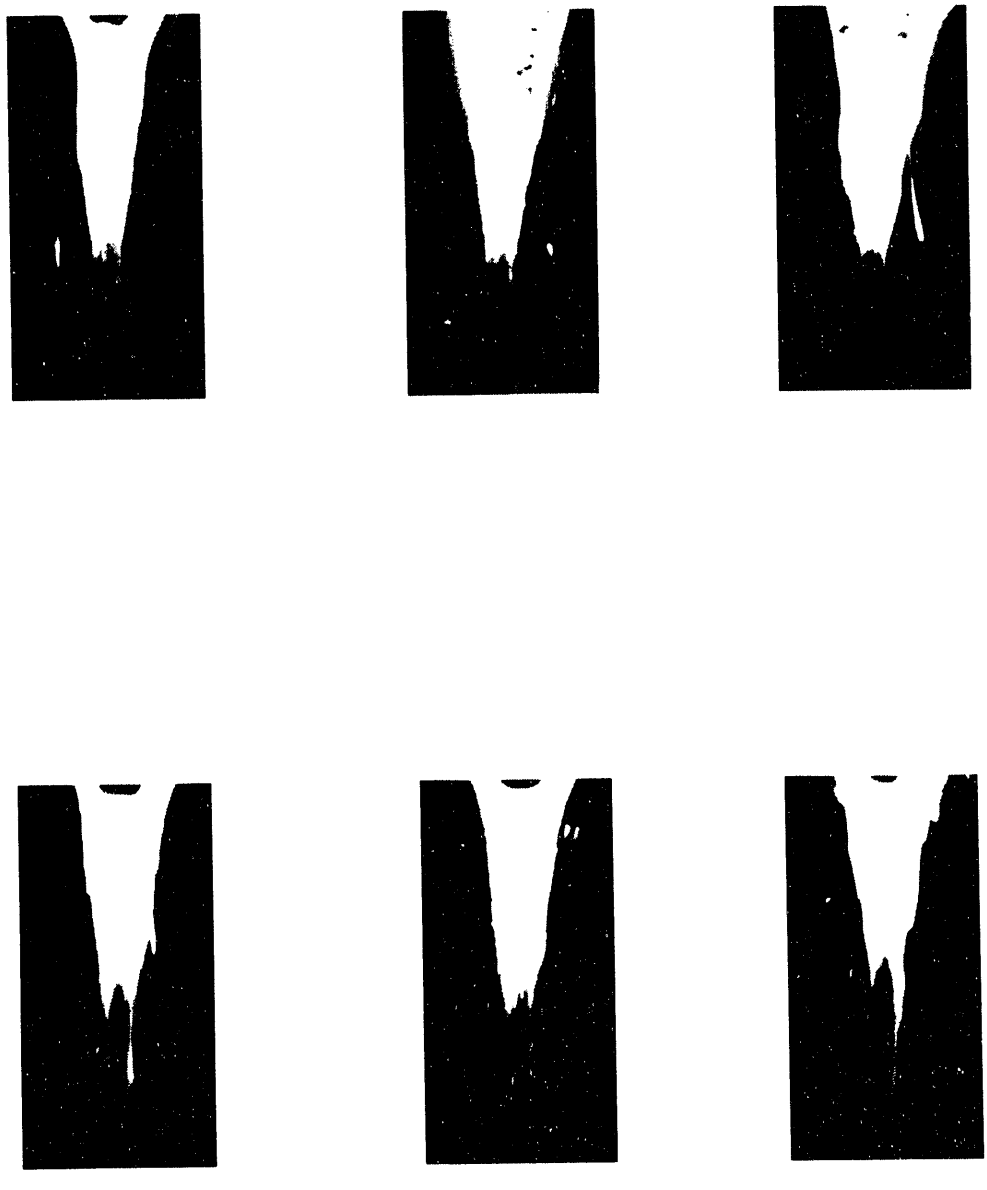

Fig. 6.41 Six Successive Frames of Cloud Combustion (1200 K, 6.5% Oxygen Conc., 1.347 A:F Ratio).

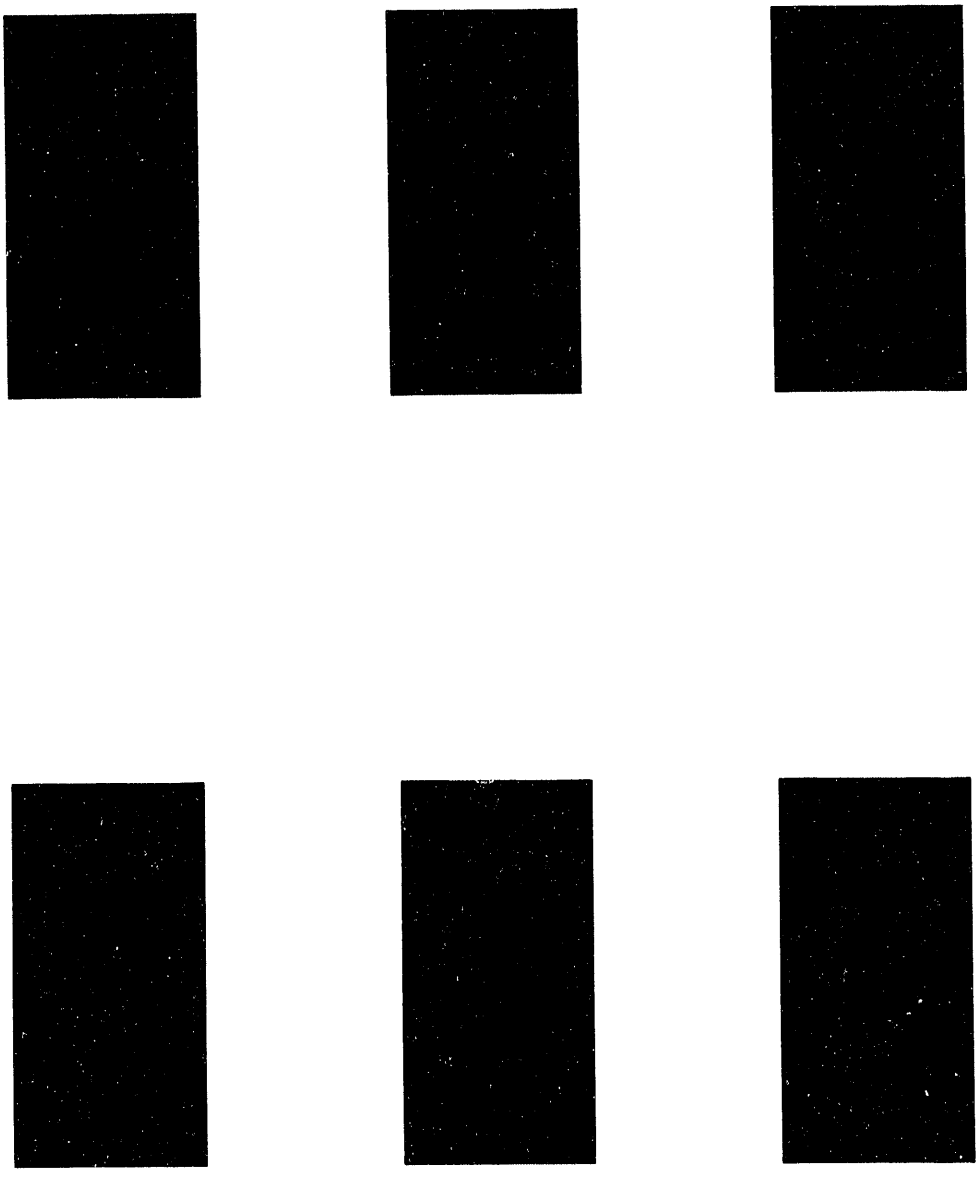

Fig. 6.42 Flame Boundaries for the Six Successive Frames of Cloud Combustion (1200 K, 6.5% Oxygen Conc., 1.347 A:F Ratio).

phenomenon is not visualized in these images and flame boundaries.

6.6.4 Effect of Reaction Zone Height on Flame Structure

The reaction zone height influences the flame structure to a larger extent. When the reaction zone height is reduced from 6 cm to 4 cm or when the collection probe is moved closer to the flat flame burner, the flame diverges very much at the collection point while the stream maintains the cylindrical geometry. For a dense cloud of air fuel ratio 0.776, the ignition point is near the collection point (Fig. 6.43). Though the theoretical models indicates double flame phenomenon strongly for a dense cloud, the image boundaries in Fig 6.44 does not show any of this feature. The close proximity of the particle collection system to the injector affects the flame formation since it results in detaching the particles away from the stream. Both ignition and combustion starts farther away from the burner. For the same reaction zone height, when the air fuel ratio in the cloud is increased to 1.44, relatively better flame contours are obtained.(Fig. 6.45 and 6.46). The heterogenous ignition, a feature of dilute cloud, is also observed. The flame contours do not show the double flame profile. The widening of the flame contour is due to the presence of the collection system. When compared to the flame images captured for 6 cm reaction zone height, the spread of the flame is more.

6.6.5 Effect of Oxygen Concentration on the Flame Structure

When the oxygen concentration is high, the flame does not have to travel very

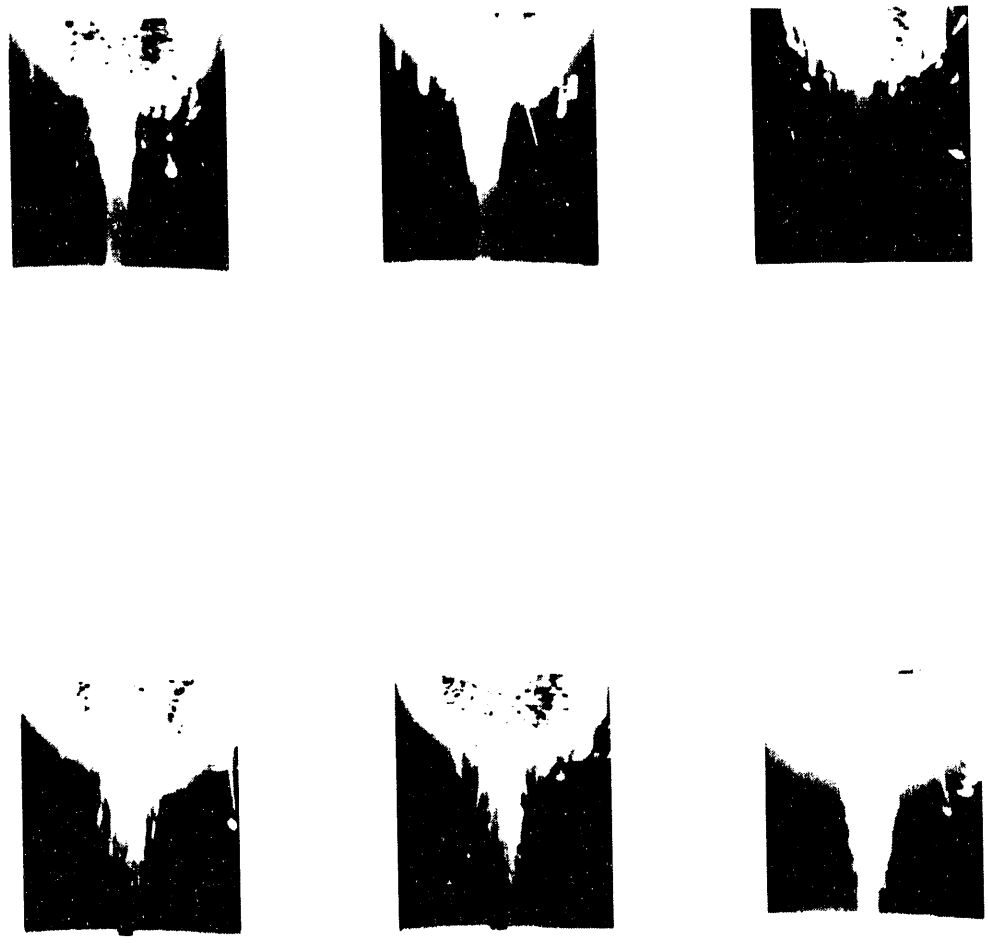

Fig. 6.43 Six Successive Frames of Dense Cloud Combustion (1200 K, 6.5% Oxygen Conc., 0.776 A:F Ratio).

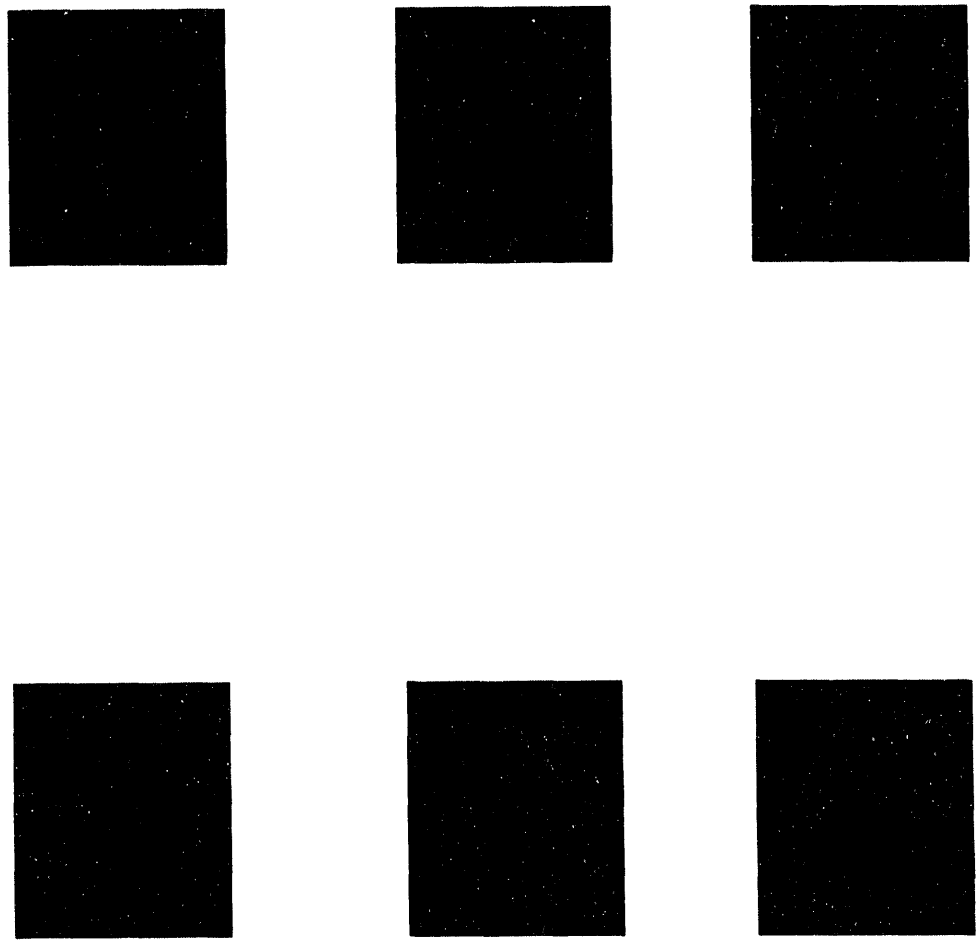

Fig. 6.44 Flame Boundaries for the Six Successive Frames of Dense Cloud Combustion (1200 K, 6.5% Oxygen Conc., 0.776 A:F Ratio).

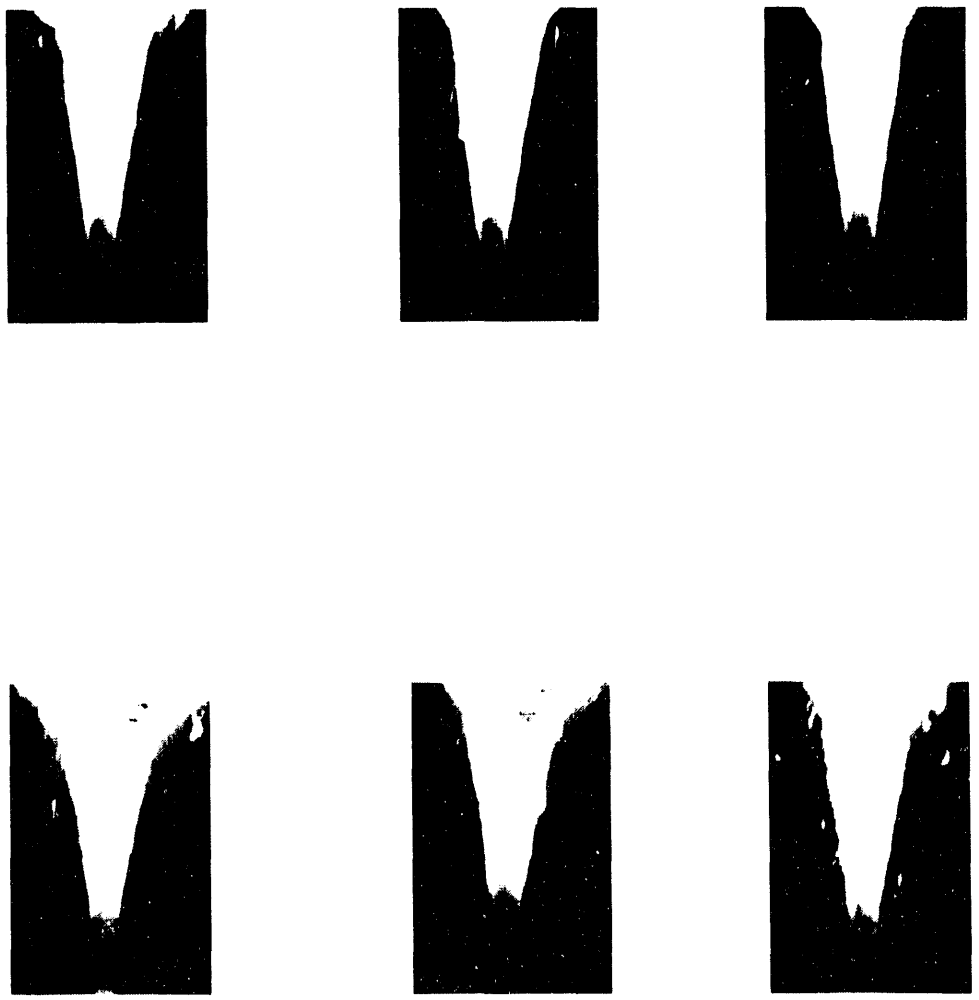

Fig. 6.45 Six Successive Frames of Cloud Combustion
(1200 K, 6.5% Oxygen Conc., 1.44 A:F Ratio).

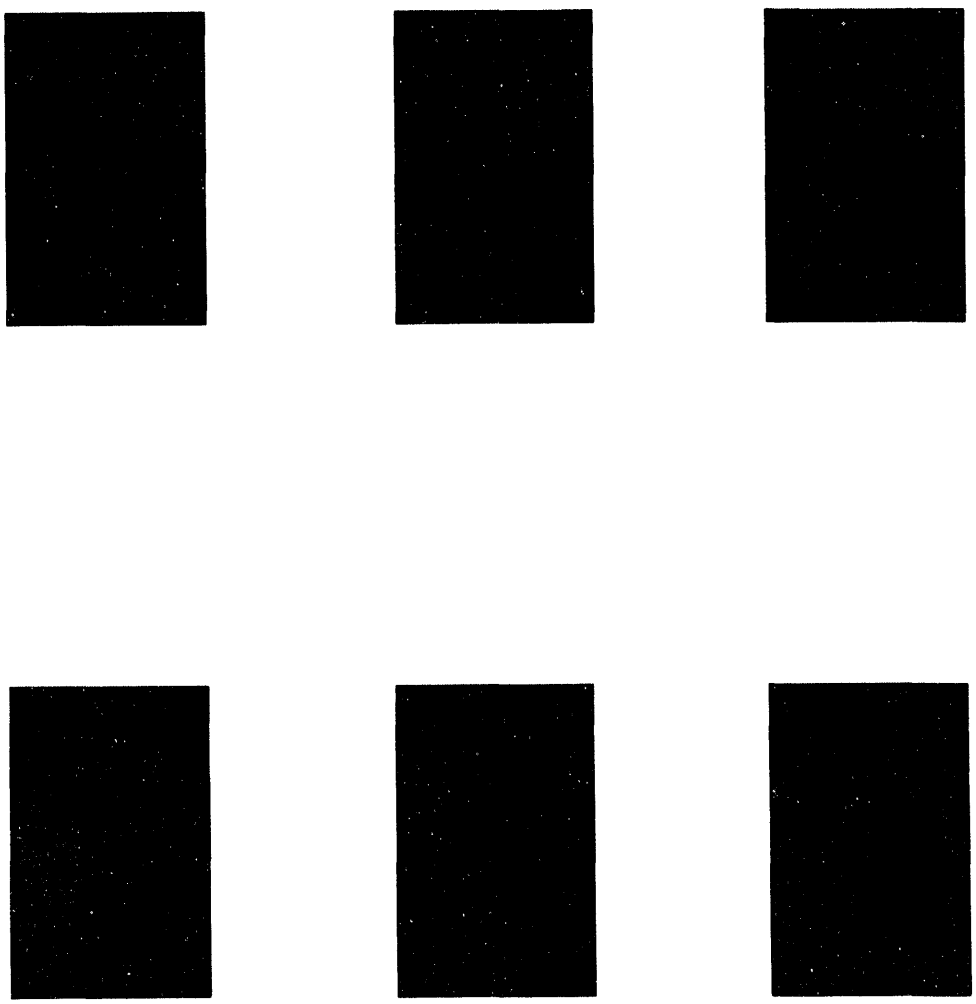

Fig. 6.46 Flame Boundaries for the Six Successive Frames of Cloud Combustion (1200 K, 6.5% Oxygen Conc., 1.44 A:F Ratio).

far in search of oxygen. Hence, the divergence can be expected to get reduced with increase in oxygen concentration resulting in a narrower flame. As the flame images shown in the Fig. 6.47 and flame boundaries in Fig. 6.48 present thinner flames when compared with the flame images obtained with 6.5% oxygen concentration (Fig. 6.37 and 6.38). Ignition always starts homogeneously for this dense cloud (A:F ratio 0.8). The double flame formed but the flame does not spread very much due to the high oxygen concentration in the ambience. When the air fuel ratio is increased to 2.0 for the same condition, the stream diverges to an extent with the carrier air as compared to previous case due to momentum of jet. Distinctive homogeneous or heterogeneous ignition pattern is not observed. The flame images and flame boundaries in Figs. 6.49 and 6.50 also do not show double flame formation as the cloud is dilute.

6.6.6 Effect of Gas Temperature over Flame Structure

The digital camera is very sensitive to the brightness of the object. When gas temperature is increased, ignition occurs close to the burner. Hence the high temperature zone of the flat methane flame interferes with bright coal flame and the coal flame boundaries are not distinctively seen in the images presented in Figs. 6.51 to 6.54. The coal stream at higher gas temperature presents a glowing stream due to higher reaction rate as soon as it enters flat flame as shown in Figs 6.51 to 6.54. Even though cloud A:F ratio varies from 0.96 to 3.0, the effect on the flame structure at high gas temperature is negligible. Also there is no evidence of double flame. The black spots at top of the picture are due to carbon accumulated on the particle collection probe.

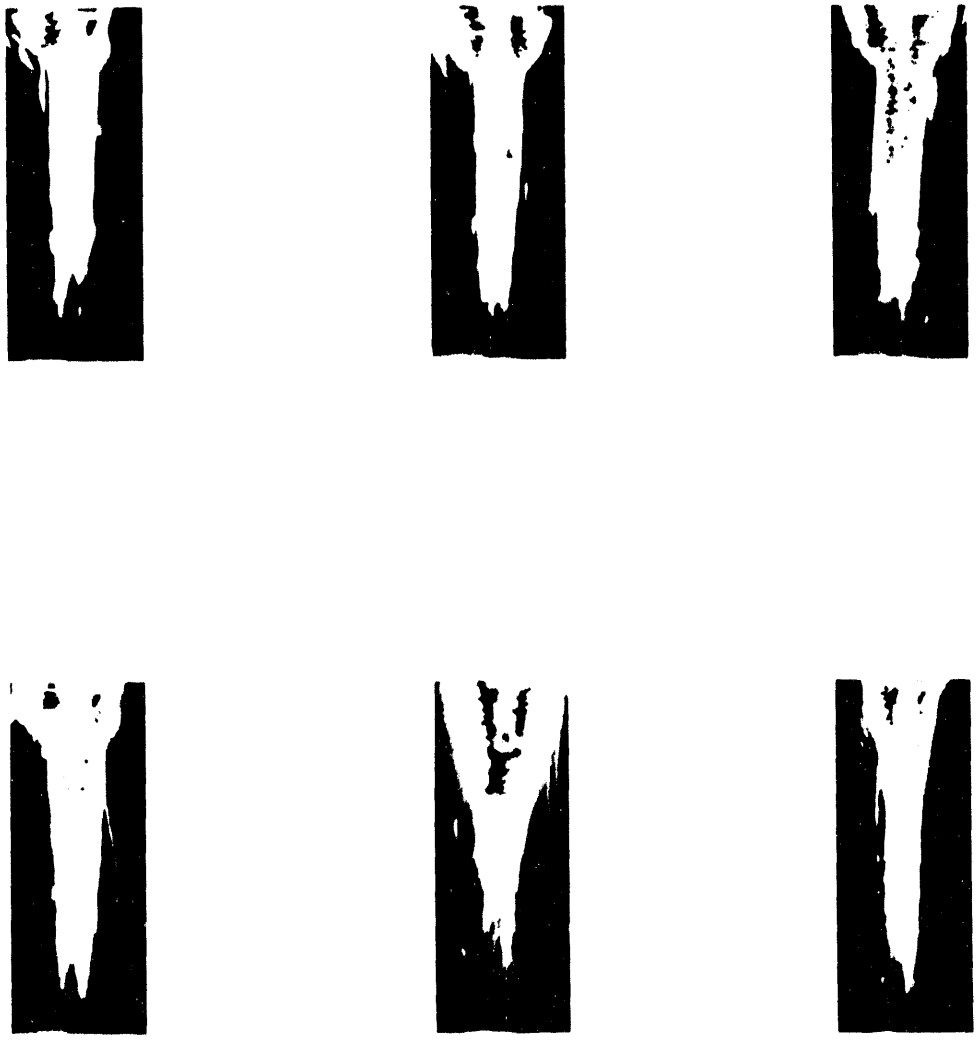

Fig. 6.47 Six Successive Frames of Dense Cloud Combustion (1200 K, 12.5% Oxygen Conc., 0.8 A:F Ratio).

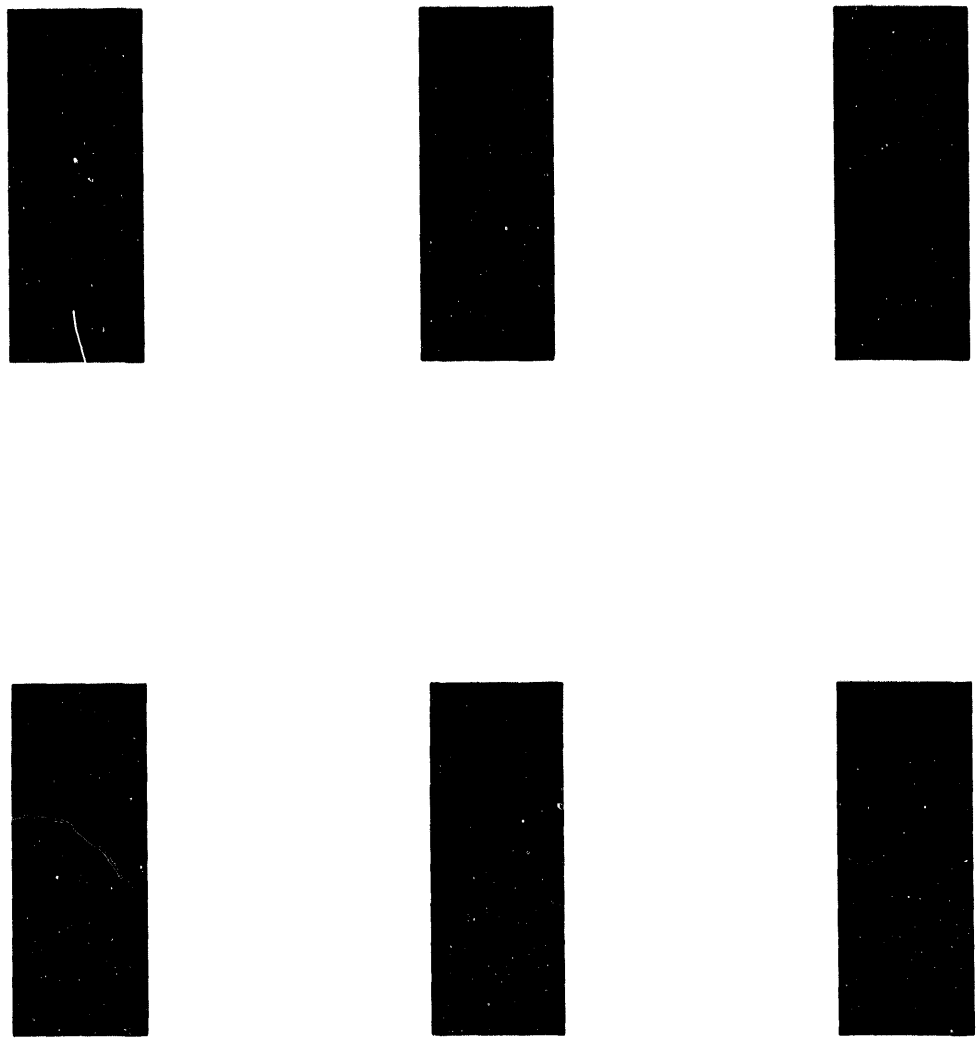

Fig. 6.48 Flame Boundaries for the Six Successive Frames of Dense Cloud Combustion (1200 K, 12.5% Oxygen Conc., 0.8 A:F Ratio).

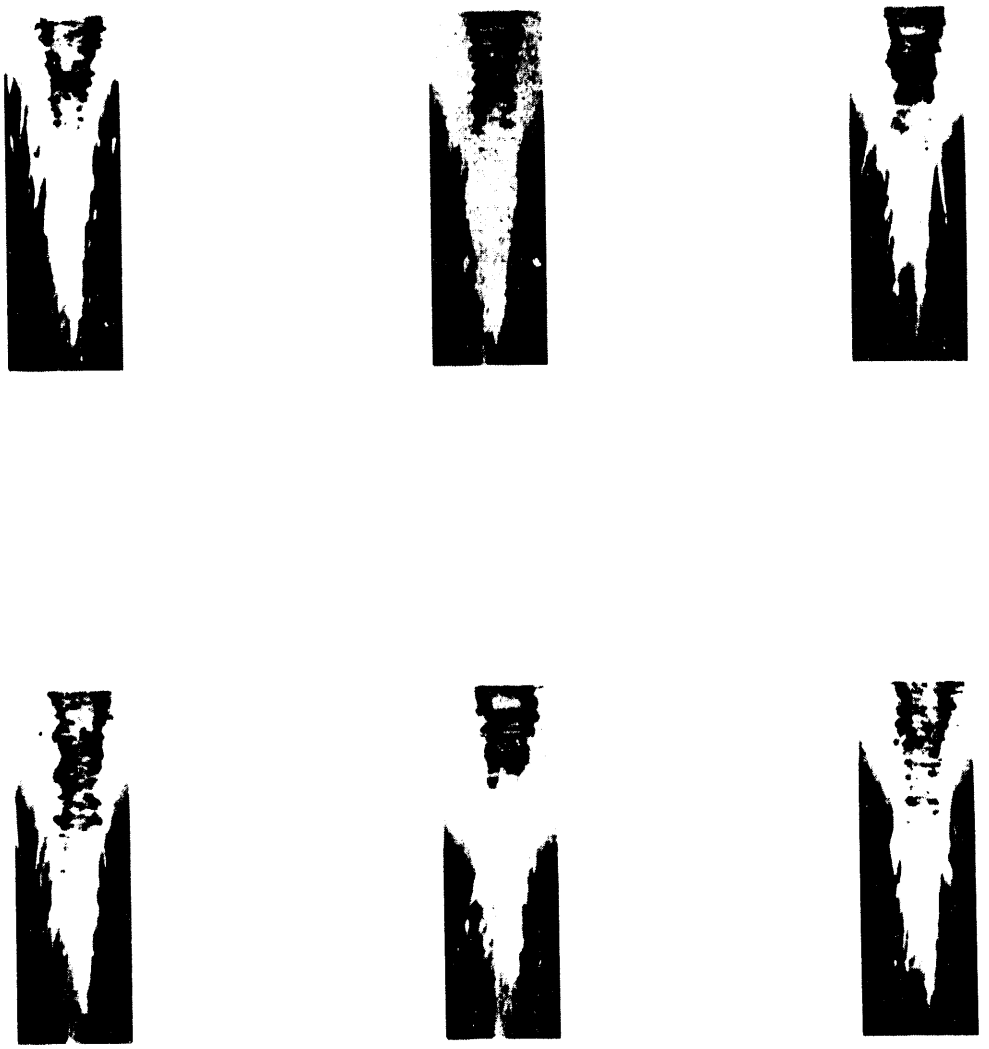

Fig. 6.49 Six Successive Frames of Dilute Cloud Combustion (1200 K, 12.5% Oxygen Conc., 2.0 A:F Ratio).

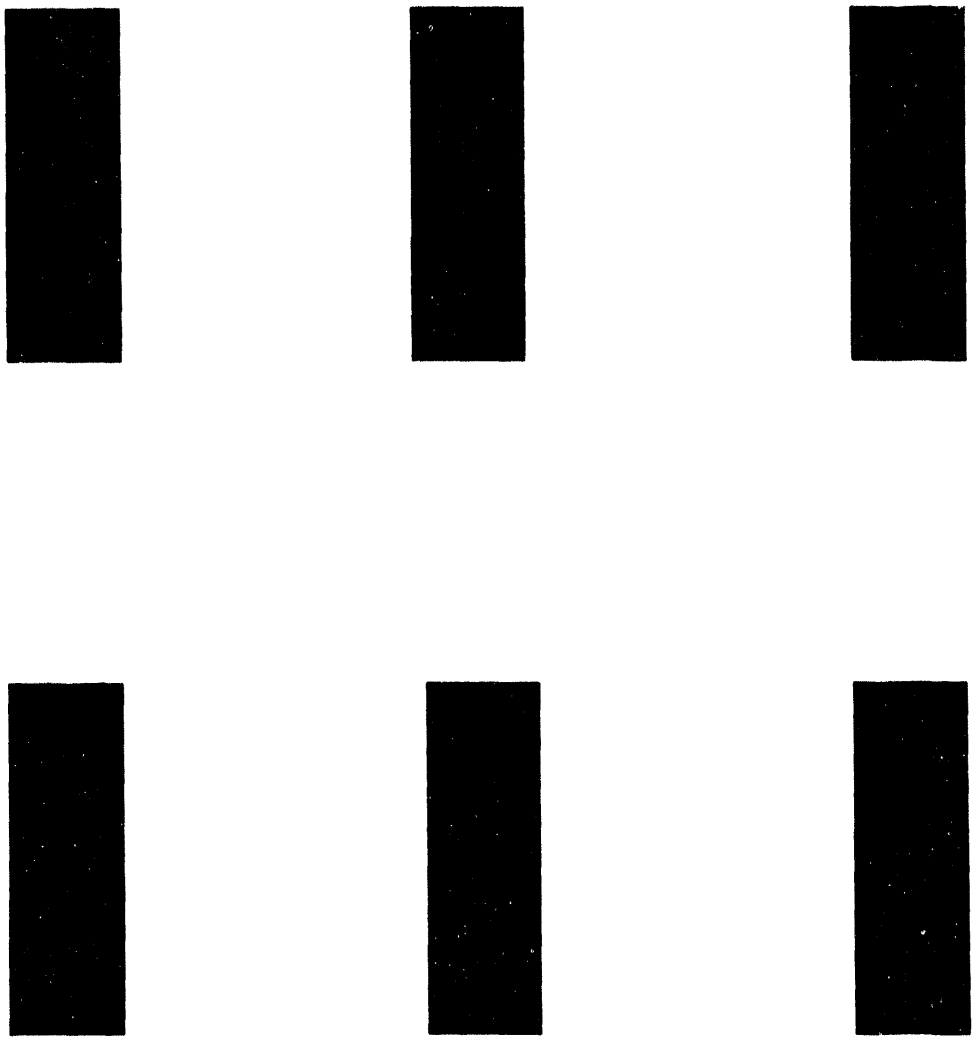

Fig. 6.50 Flame Boundaries for the Six Successive Frames of Dilute Cloud Combustion (1200 K, 12.5% Oxygen Conc., 2.0 A:F Ratio).

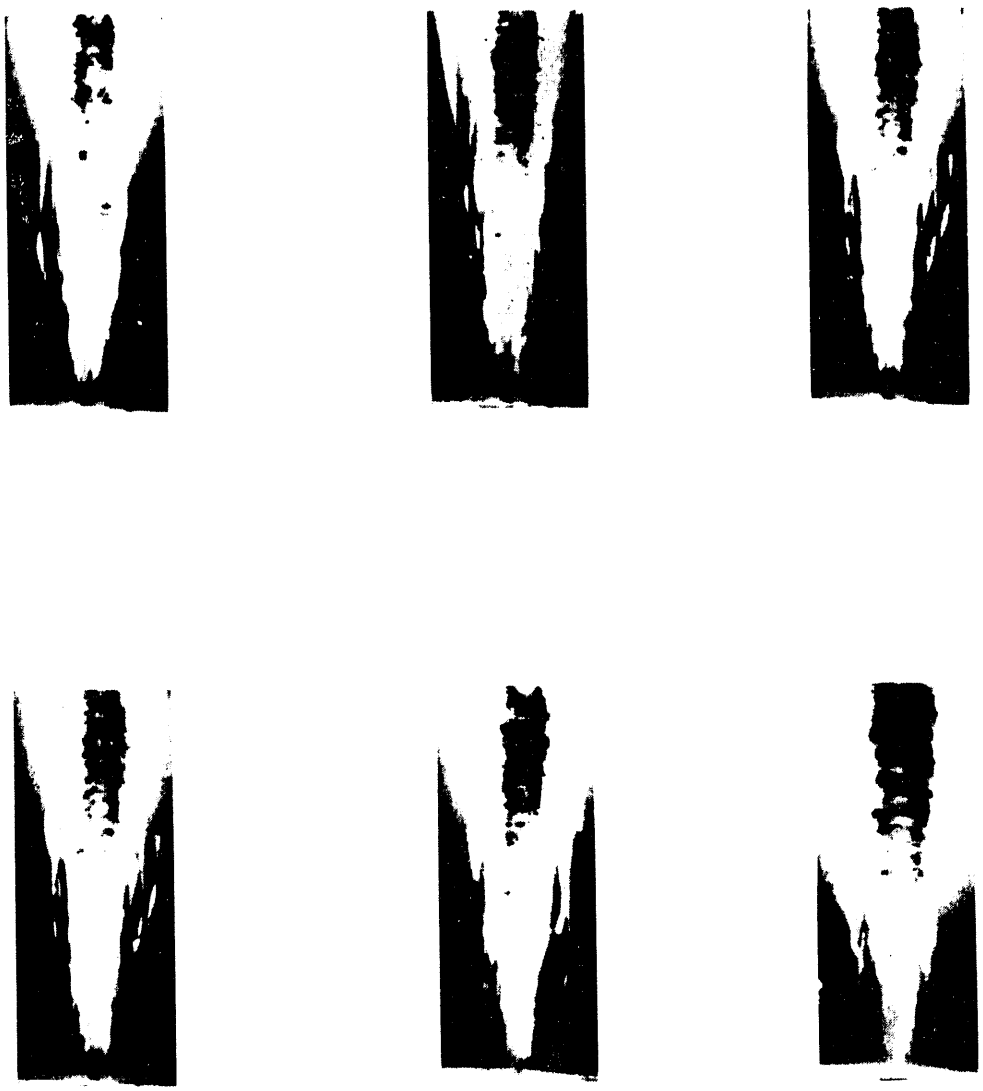

Fig. 6.51 Six Successive Frames of Dense Cloud Combustion (1400 K, 12.5% Oxygen Conc., 0.96 A:F Ratio).

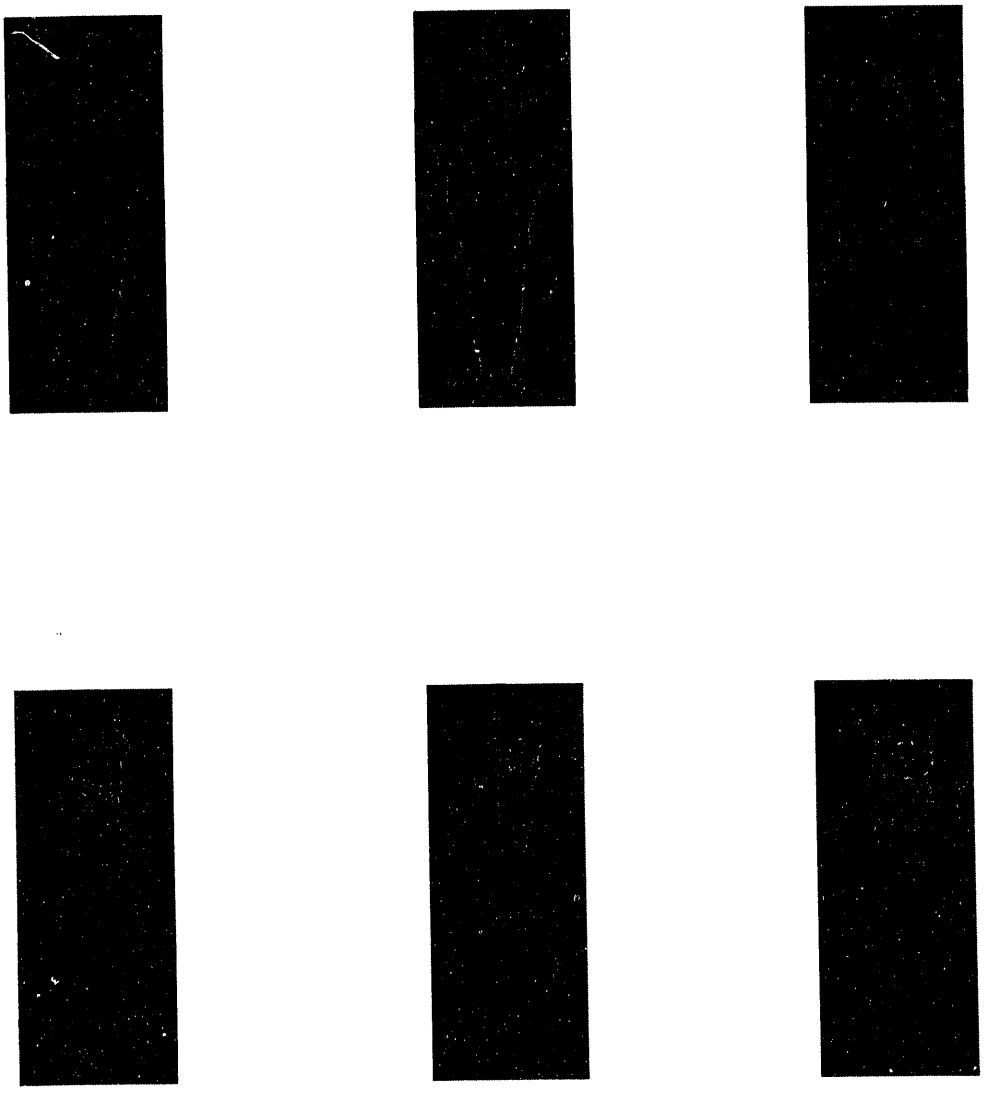

Fig. 6.52 Flame Boundaries for the Six Successive Dense Cloud Combustion (1400 K, 12.5% Oxygen Conc., 0.96 A:F Ratio).

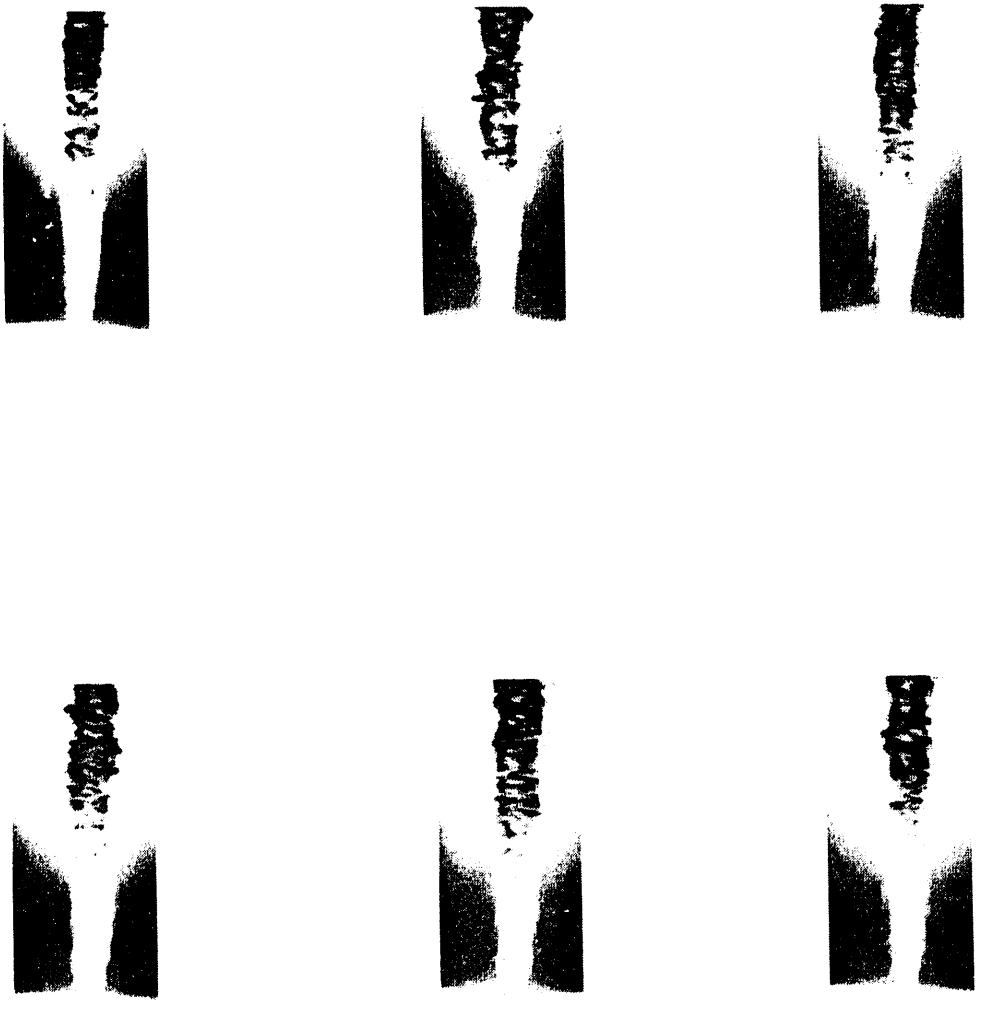

Fig. 6.53 Six Successive Frames of Cloud Combustion
(1400 K, 12.5% Oxygen Conc., 1.2 A:F Ratio).

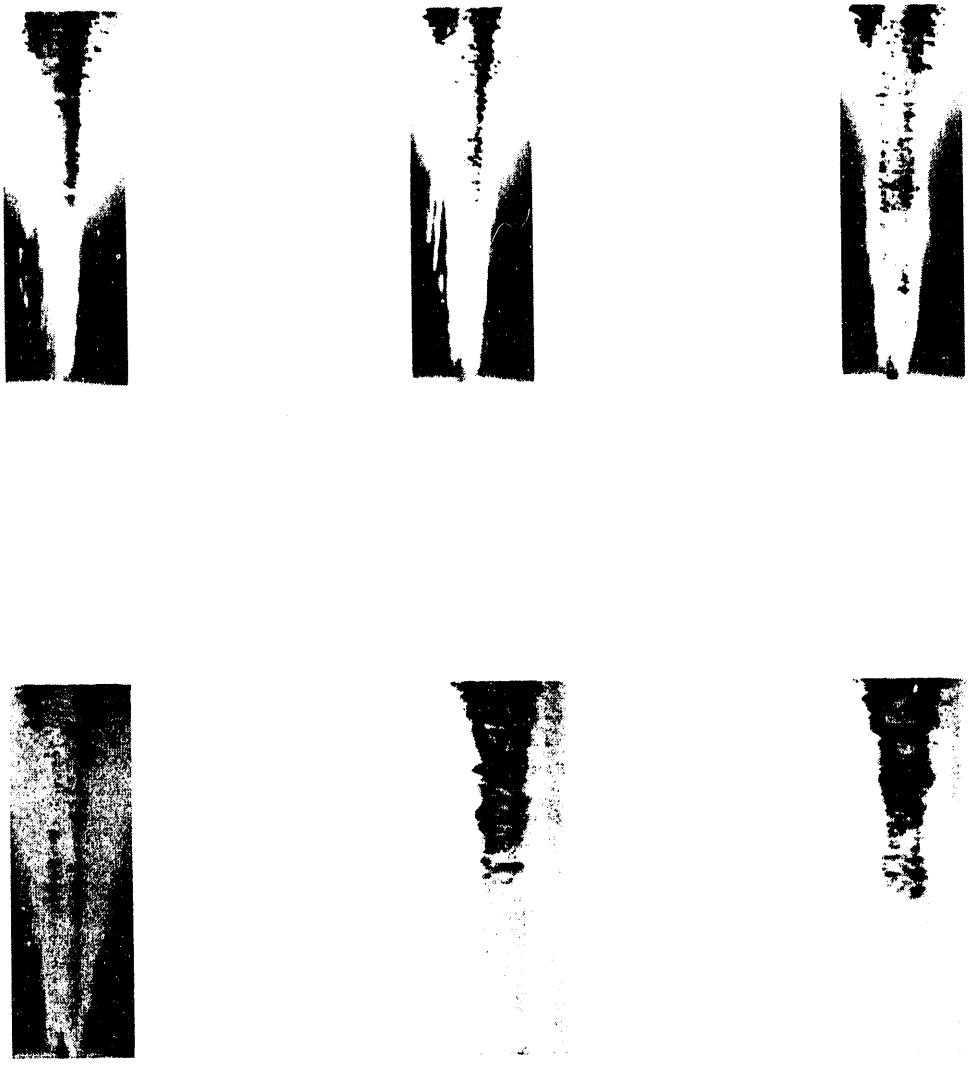

Fig. 6.54 Six Successive Frames of Dilute Cloud Combustion (1400 K, 12.5% Oxygen Conc., 3.0 A:F Ratio).

The false color images of stream flames are presented in Figs. 6.55 to 6.57. The formation of double flame can be observed very clearly for the dense stream.

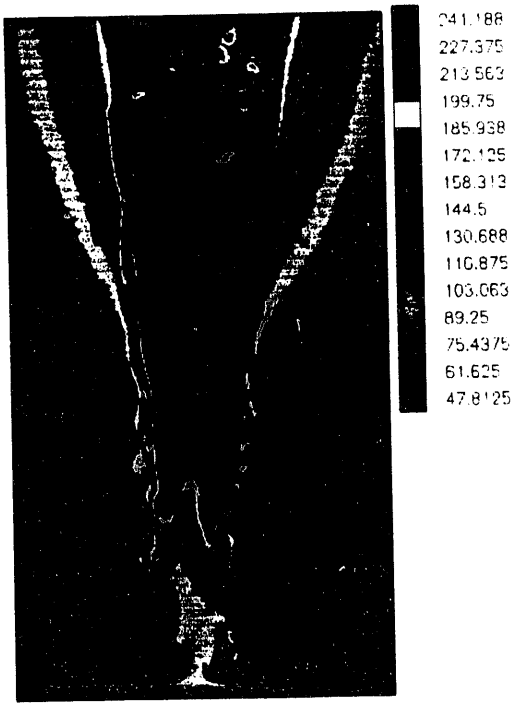

Gas temperature 1200 K
Air Fuel ratio 0.8124
Oxygen concentration 6.5%
Reaction zone height 6 cm

Fig. 6.55 Double Flame Formation at the Cloud Periphery.

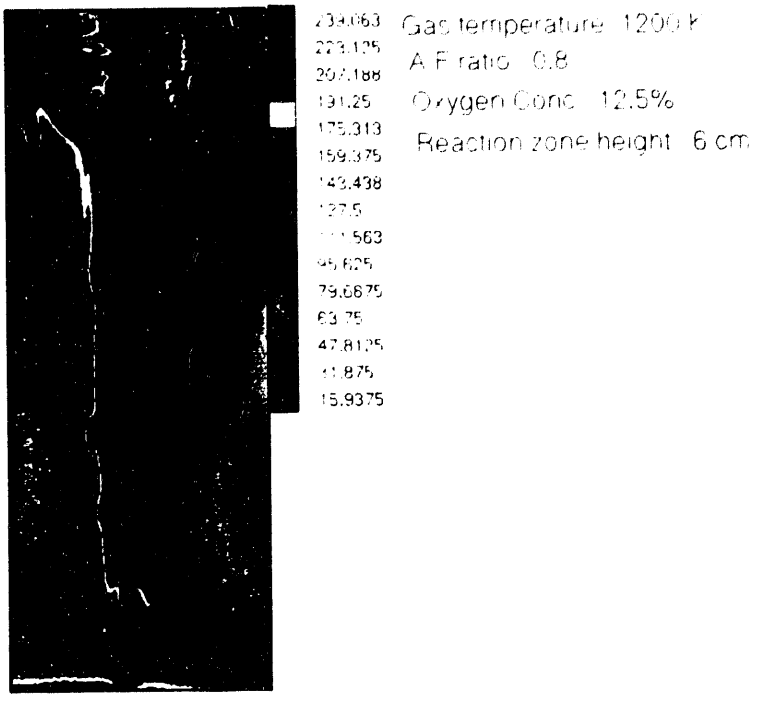

Fig. 6.56 Dense Stream Combustion at High Oxygen Concentration

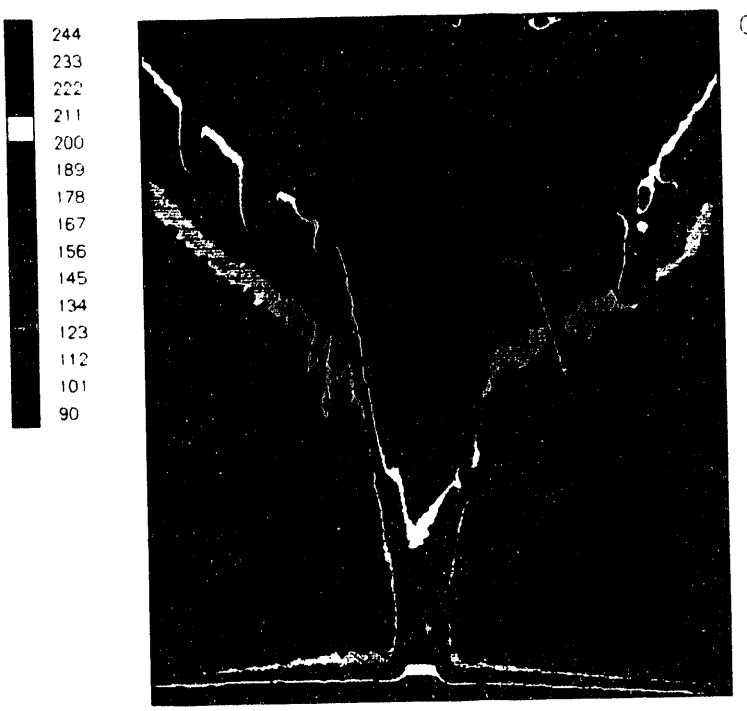

Gas temperature 1200K
A F ratio 0.776
Oxygen concentration 6.5%
Reaction zone height 4 cm

Fig. 6.57 Stream Combustion of Dense Cloud (Reaction Zone Height 4 cm).

CONCLUSIONS

The conclusions are based on the theoretical and experimental data.

I. Theoretical Results

A model for group combustion of a cylindrical stream of coal particles is presented with and without cloud expansion due to heating, ignition and combustion. Detailed results are obtained for transient ignition and combustion behavior for a cloud without considering expansion while limited results are obtained for a cloud with expansion.

i) It is found that homogeneous ignition (ignition of volatiles) occurs for a dense cloud while heterogeneous ignition (ignition of carbon) occurs for a dilute cloud.

ii) Once ignited, the combustion ensues. For short residence times, the plot of gasification efficiency vs cloud A:F ratio results in a maximum.

iii) The group flame moves toward the cloud, reaches the cloud surface and then bifurcates into two flames called inner and outer flames. This new phenomenon is called double flame. The inner flame propagates into unburnt volatile/air mixture in the cloud while the outer diffusion flame moves away from the cloud. The inner flame propagates at the laminar burning velocity and rapidly heats the particles resulting in increased volatile yield. The outer flame is a diffusion flame. The flame moves toward the cloud as the volatiles are depleted. It should be noted that the double flames exist only for dense clouds.

iv) Once the volatiles are exhausted in the core of the cloud, the inner flame disappears.

v) When the volatiles are exhausted, the particles in the cloud starved of oxygen, burn slowly controlled by diffusion rate into the cloud rather than to each particle in the cloud.

vi) Preliminary results are obtained for the model with cloud expansion. The heating of the cloud results in increased cloud radius and reduced ignition times since expansion results in increasing diluteness of cloud. Further the outer flame is at farther distance due to expansion effect. The peaks in temperatures are more pronounced.

The limitation of the model is the assumption of combustion of particles under zero relative velocity.

II. Experimental Results

An experimental set up was designed and constructed for conducting coal stream experiments under different operating parameters *viz* gas temperature, oxygen concentration and residence time. The burnt coal samples were analyzed to determine the extent of gasification. The effects of operating parameters over gasification efficiency were studied. An existing image processing facility was used to capture the coal flame images during experiments using a digital camera. These images were then analyzed for ignition characteristics and flame structures.

The primary results on gasification efficiency are as follows.

i). In the vicinity of the burner, the gasification efficiency increases with the cloud A:F ratio, reaches a maximum and decreases as the cloud becomes very dilute. The mathematical models support this trend. Further the results are consistent with the experimental findings of minimum in ignition time with the cloud denseness.

ii). The gasification efficiency increases with the reaction zone height due to increase in residence time.

iii). The gasification efficiency increases with the gas temperature and the oxygen concentration.

iv). At higher gas temperatures ($T \approx 1400$ K), the ignition is almost instantaneous and more sooting tendency was observed.

The digital image analysis yields the following results.

v). The cold coal stream does not seem to diverge like the air jet, thus maintaining its cylindrical geometry.

vi). Within the ignition regime, the flame images show a peak in pixel values at the periphery of the dense cloud confirming the homogeneous ignition mode for dense clouds. For the dilute clouds, the peak occurs at the center of the cloud, indicating heterogenous ignition.

vii). The flame images of the dense clouds seem to indicate the formation of two flames at the periphery of the cloud. Inner flame then travels towards the center while the outer flame is the diffusion flame. However dilute clouds do not reveal

such a phenomenon.

viii). Qualitative comparisons are given with preliminary experimental data obtained using a digital imaging system.

The primary problems were upward injection of *dense* stream of particles and maintaining the cylindrical geometry. Further the residence time is limited due to difficulties in maintaining uniform ambient temperatures over larger heights over the flat flame burner.

Though not reported in the final report, the technique of digital image analysis was also applied to ignition and combustion of an isolated candle and binary arrays of candles, and an isolated coal particle and binary arrays of coal particles. Results were presented in the DOE topical report submitted in 1992.

REFERENCES

Annamalai, K., and Durbetaki, P., 1977, "A Theory on Transition of Ignition Phase of Coal Particles," *Combustion and Flame,* Vol. 29, pp. 193-208.

Annamalai, K., Ramalingam, S., Dahdah, T., and Chi, D., 1988, "Group Combustion of a Cylindrical Cloud of Char/Carbon Particles," *Journal of Heat Transfer*, ASME, Vol. 110, pp. 190-200.

Annamalai, K., Ruiz, M., Vo, N., and Anand, V., 1992, "Locally Fluidizing Feeder for Powder Transport," *Powder Technology*, Vol. 73, pp. 181-190.

K. Annamalai, and W. Ryan, (1993), " Interactive Processes in Gasification and Combustion - II: Isolated Carbon/coal and Porous Char Particles," *Journal of the Progress in Energy and Combustion Science,* Vol. 19,383-446.

Annual Energy Review, 1991, Energy Information Administration, Office of Energy Markets and End Use, U.S. Department of Energy, Washington D.C.

Bandyopadhyay, S., and Bhaduri, D., 1972, "Predictions of Ignition Temperatures of a Single Coal Particle," *Combustion and Flame,* Vol. 18, pp. 411-415.

Bradley, D., Dixon-Lewis, G., Habik, S., and Mushi, E, M, J., 1984, "The Oxidation of Graphite Powder in Flame Reaction Zone," *20th Symposium (International) on Combustion,* The Combustion Institute, pp. 931-940.

Dixon-Lewis, G., Bradley, D., and Habik, S., 1991, "Oxidation Rates of Carbon Particles in Methane-Air Flames," *Combustion and Flame,* Vol. 86, pp. 12-20.

Du,X., Gopalakrishnan,C. and Annamalai, K., (1994), " Group Ignition and

Combustion of a Cylindrical Stream of Particles," Heat and Mass Transfer 94, Tata-McGraw Hill Publishing Co.,New Delhi, pp:953-959.

Du,X. and Annamalai,K., 1994, " Transient Ignition of Isolated Coal Particle," *Combustion and Flame*, Vol. 97,339-354.

Field, M. A., 1970, "Measurements of the Effect of Rank on Combustion Rates of Pulverized Coal," *Combustion and Flame,* Vol. 14, pp. 237-248.

Gieras, M., Klemens, R., Wolanski, P., and Wojcicki, S., 1986, "Experimental and Theoretical Investigation into the Ignition and Combustion Processes of Single Coal Particles under Zero and Normal Gravity Conditions," *21st Symposium (International) on Combustion,* The Combustion Institute, pp. 315-323.

Howard, J. B., and Essenhigh, R.H., 1967, "Pyrolysis of Coal Particles in Pulverized Fuel Flames," *Industrial Engineering Chemical Process Design and Development,* Vol. 6, pp. 74-84.

Karcz, A., Kordylewski, W., and Rybak, W., 1980, "Evaluation of Kinetic Parameters of Coal Ignition," *Fuel*, Vol. 59, pp. 799-802.

Kharbat, E., 1992, "Digital Image Processing Applications in the Ignition and Combustion of Char/Coal Particles," MS Thesis, Texas A&M University.

Lee, W., Ryan, H.M., Strakey, P. A., and Santoro, R. J., 1990, "The Application of Two-Dimensional Imaging Techniques for Soot and Droplet Studies," ASME Winter Meeting, pp. 117-126.

Leesley, M. E., and Hedley, A. B., 1972, "The Effect of Particle Size Distribution

on the Combustion Rate of a Pulverized Anthracite Dust Cloud," *Journal of the Institute of Fuel*, pp 224-230.

Midkiff, K. C., Altenkirch, R. A., and Peck, R. E., 1986, "Stoichiometry and Coal-Type Effects on Homogeneous Vs Heterogeneous Combustion in Pulverized-Coal Flames," *Combustion and Flame*, Vol. 64, pp. 253-266.

Mulcahy, M. F., and Smith, I. W., 1971, "The Kinetics of Combustion of Pulverized Coke, Anthracite and Coal Chars," *CHEMECA*, Session 2, pp 101-118.

Petarca, L., Tognotti, S., Zanelli, S., and Bertozzi, G., 1986, "An Experimental Study on Oxidation Rates of Coal at Low Temperatures," *21st Symposium (International) on Combustion*. The Combustion Institute, pp. 193-201.

Pittsburgh Energy Technology Center Review, 1993, Spring, pp 30

M.Ruiz, K.Annamalai and T.Dahdah, (1990), "An Experimental Study on Group Ignition of Coal Particle Streams," **Heat Transfer in Fire and Combustion Systems, HTD-Vol 148**, edited by W.L. Grosshandler and H.G. Semerjian, pp. 19-25.

Ryan, W., and Annamalai, K., 1991, "Group Ignition of a Cloud of Coal Particles," *Journal of Heat Transfer*, Vol. 113, pp. 677-687.

Scott, W. M., 1969, "Understanding Diesel Combustion Through the Use of High Speed Moving Pictures in Color," SAE paper 690002, *SAE Trans.*, Vol. 78, 1969.

Smoot, L. D., 1985, *Coal Combustion and Gasification*, Plenum Press, New York, NY.

Solomon, P. R., Chien, P. L., Carangelo, R. M., Best, P. E., and Markham, J. R.,

1988, "Application of FT-IR Emission/Transmission (E/T) Spectroscopy to Study Coal Combustion Phenomena," *22nd Symposium (International) on Combustion,* The Combustion Institute, pp. 211-221.

Wall, T. F., Gururajan, V. S., Phong-Anant, D., Wibberley, L. J., Tata, A., and Lucas, J., 1988, "Indicators of Ignition for Clouds of Pulverized Coal," *Combustion and Flame*, Vol. 72, pp. 111-118.

Weiland, K. J., 1993, "Intensified Array Camera Imaging of Solid Surface Combustion Aboard the NASA Learjet," NASA Lewis Research Center, Ohio.

APPENDIX A

MEASUREMENT OF VELOCITY OF FLOWING PARTICLES

Introduction

Many solid particle combustion experiments are being done using laminar flow reactor. These experiments are also analyzed using mathematical models. The important parameter that influences the results is the velocity of the particles flowing into the reactor. Measuring this velocity is difficult and attempts have been made to measure this velocity using different techniques. Here an optical method is introduced.

Principle

A phototransistor is connected in series with a resistor and is supplied with a 5Volts d.c. This transistor allows current to pass when there is light on it. With lights on, the voltage drop across the transistor is '0'. If the light is disrupted, there will be a voltage drop according to the intensity. The coal particles are injected in between two pairs of light source and the detector placed apart by some known distance. The time difference between the beginning of the voltage drop in the two detectors and the distance between them will give the velocity.

Experimental Set Up

Two photo transistors (NTE 3120) are stuck to the reactor wall with 3 cm gap between them. Light sources (MINI-MAGLITE AAA FLASHLIGHT model M3A016 part no 116-000-139) are placed diametrically opposite to the detectors.. Each of these transistors are connected in series with a resistor 78PR1K trimpot and is given 5v D.C.

voltage. Output is taken across each of the transistors and is sent to input channels of the 2201 digital storage oscilloscope. When there is no light, the voltage across each of the transistor is 5 V. With the lights on, the voltage reduces to '0'.

Experiment

With the d.c. supply and the light sources are on, the voltage curves both channel 1 and 2 of the transistors are flat at 0 V in the oscilloscope. To start with, a coin is dropped in the reactor. This coin falling in the reactor, blocks the light coming from the first and the second sources successively. Hence there is rise in the voltage from 0 to 5 V in both transistor outputs. Since the transistors are placed one below the other by a gap of 3 cm, the voltage rise occur at two different instants. The time difference between the two instances is 31 ms. The velocity of the falling coin is 3cm/31 ms =0.97 m/s. Since the coin blocks the light completely, the voltage rise is full 5 V at the instance.

Since the coal flow may not block the light completely. Polythene paper which is semi transparent is moved across the light sources to set the oscilloscope parameters to capture the voltage waveforms. The voltage per division is reduced to 50 mV from 1V to get any appreciable distortion. The voltage plots are attached.

A thick batch of particles is dropped in the reactor and the wave forms obtained when it is freely falling in the reactor, show a time difference of 32 ms.

Now, a batch of coal particles is injected into the reactor using a jet of air. Since it is a spray of particles, as expected much distorted waveforms with many

are obtained in both the channels. The distortion of the waveforms indicate that there is coal flow. The time lag between the beginning of these wave forms is found to be 4 ms. The velocity is 7.5 m/s.

The oscilloscope can be set to different time and voltage scale. The triggering d.c level can also be adjusted. Depending upon the flow (dense or lean and velocity) conditions, these parameters of the oscilloscope are to be modified to capture the waveforms.

Conclusion

The velocity of the freefalling coin, freefalling batch of particles and coal jet stream were measured using this technique. When measuring the velocity of the coal stream, much difficulty was encountered as it was not dense enough to block the light completely, and hence the fine adjustments of the oscilloscope parameters need to be done to get the voltage plot. Since it is coal stream jet, it will not be possible to get clear "stepped" wave form.

APPENDIX B

CALCULATION OF $[O_2]$ CONCENTRATION

The oxygen concentration in the methane combustion products is calculated for three different oxygen flow rates. The oxygen concentration is one of the operating parameters for the coal stream experiments. Methane and air flow rates are fixed with varying the oxygen flow. The theoretical values are checked with measured values. Measurements are done with the Lancom combustion analyser.

Sample calculation:

Methane	5.3 scfh
Oxygen	3.3 scfh
Air	68 scfh

$$5.3CH_4+14.3(O_2+3.76N_2)+3.3O_2\rightarrow 5.3CO_2+10.6H_2O+7O_2+53.8N_2$$

$$Y_{O_2,dry}=7/(5.3+7+53.8)=10.6\%$$

The measured value for this case is 10.1%

APPENDIX C

Group Ignition and Combustion of Coal Particle Streams

SUMMARY

This paper presents a model for group combustion of a cylindrical stream of coal particles. Results are obtained for transient ignition and combustion behavior. It is found that homogeneous ignition (ignition of volatiles) occurs for a dense cloud while heterogeneous ignition (ignition of carbon) occurs for a dilute cloud. Once ignited, the flame moves toward the cloud, reaches the cloud surface and then bifurcates into two flames called inner and outer flames. The inner flame propagates into unburnt volatile/air mixture in the cloud while the outer diffusion flame moves away from the cloud. The inner flame propagates at the laminar burning velocity and rapidly heats the particles. There is only a diffusion flame outside the cloud after all the oxygen in the cloud is consumed. The flame moves toward the cloud as the volatiles are depleted. The cloud, with the volatiles exhausted and starved of oxygen, burns slowly controlled by diffusion into the cloud rather than to each particle in the cloud. Qualitative comparisons are given with preliminary experimental data obtained using a digital imaging system.

1. INTRODUCTION

Most practical coal combustors use dense sprays/suspensions of drops/particles that result in interactions among the particles. Rather than modeling the ignition and combustion behavior of an isolated coal particle/drop, an isolated combustion model (ISOC), one may consider a cluster of particles/drops, a group combustion model (GC), and study its interactive ignition and combustion behavior. The clusters can be arrays of a few particles, spherical clouds, or streams of many particles [1,2]. Group combustion models have been developed to simulate the group ignition and combustion of a spherical cloud of pulverized coal and char particles. Quasi-steady (QS) and transient results have been obtained for the ignition and combustion of such a cloud. The QS results show that the burning rate of a single particle in the cloud ($\dot{m}_{s,c}$) is lower than the burning rate of the same particle under isolated mode ($\dot{m}_{iso}$). The correction factor, $\eta = \dot{m}_{s,c}/\dot{m}_{iso}$, is found to be smaller for dense clouds than for dilute clouds due to oxygen deficiency [3]. A comprehensive review on the interactive effects in drop and coal suspensions has been recently carried out [1]. The advantages of a spherical cloud model are that the burning rate of a dense cloud of char particles is equal to the combustion rate of a large isolated particle of the same size but with a mass density equal to a cloud mass density and quasi-steady (QS) solution in an infinite ambience can be readily obtained. While the spherical group combustion model is convenient in obtaining simplified results under steady state conditions, it is very difficult to simulate experimentally. However, experiments with a cylindrical stream of coal particles can be done. Thus, a cylindrical group combustion model is more useful in interpreting the experimental data obtained with a monosized stream of particles. Therefore, a group combustion model for a cylindrical cloud is presented. Annamalai et al [4] previously presented QS group combustion analysis for a cylindrical stream of char/carbon particles in a finite ambience but assumed a finite film thickness in the gas phase for heat and mass transfer. The steady state results for spherical and cylindrical clouds are analogous to those of porous char literature for prescribed cloud surface properties. There is no inherently steady state solution for a cylindrical cloud in an infinite ambience. The present paper is the first transient combustion model for a cylindrical cloud of coal particles. Conservation equations are presented for mass, species, and energy. Numerical solutions are presented for the ignition time, group burning rate,

and flame structure. Preliminary experimental data are presented for the qualitative confirmation of model results.

2. THE MODEL

Consider a cloud of uniformly distributed coal particles of radius 'a' within a cylinder of radius 'R_c' (Fig. 1a). If this cloud is placed in a hot furnace, a thermal wave propagates from the ambient into the cloud (Fig. 1b). The bulk gas temperature increases, which, in turn, supplies heat to the particles. Thermal decomposition occurs, which releases the volatiles, when the temperature of the particles reaches the pyrolysis level. The volatiles diffuse into the bulk gas zone and establish a mixture of volatiles and oxygen in the bulk gas. Homogeneous ignition may occur if the cloud is dense and the gas phase temperature is high enough for the chemical reaction. However, a flammable mixture in the gas phase may not be formed if the cloud is dilute. The carbon in the coal may react with the oxygen near the particles and result in heterogeneous ignition. Thus, the ignition mode may be either homogeneous or heterogeneous depending upon the denseness of the cloud. The assumptions are:

(1) Cylindrical symmetry exists.

(2) ρD = constant

(3) The particles are point masses.

(4) The particles are fixed in space.

(5) The particle temperature is uniform.

(6) Pyrolysis occurs volumetrically with constant diameter while heterogeneous reactions occur at constant density and varying diameter.

(7) All gas phase chemical reactions for volatiles and CO occur by a single-step global reaction.

(8) The reactions in the present analysis are:

a.) heterogeneous reaction

$$C + 1/2O_2 \longrightarrow CO$$

b.) pyrolysis via competing reaction

$$\text{Coal} \begin{cases} \nearrow \alpha_I \text{ Volatiles-I} + (1-\alpha_I)C \\ \searrow \alpha_{II} \text{ Volatiles-II} + (1-\alpha_{II})C \end{cases}$$

where

$$\alpha_{II} \approx 2\alpha_I$$

c.) homogeneous (gas phase) reactions

$$CO + 1/2O_2 \rightarrow CO_2$$

$$\text{Volatiles (V)} + O_2 \rightarrow V \cdot O_2$$

3. CONSERVATION EQUATIONS

The conservation equations for a cylindrical cloud are:

3.1. Gas Phase Conservation Equations

3.1.1. Mass

The equation of continuity in cylindrical coordinates is given as

$$2\pi r\left(\frac{\partial \rho}{\partial t}\right) + \left(\frac{\partial \dot{m}}{\partial r}\right) = \dot{w}_m''' 2\pi r \tag{1}$$

where

$\dot{w}_m'''$ is the mass added to the gas phase by the particles per unit volume ($\dot{w}_m''' = n\dot{m}_p$, $r < R_c$; $\dot{w}_m''' = 0$, $r > R_c$).

$\dot{m}$ is mass flow rate.

$\dot{m}_p$ is particle burning rate.

3.1.2. Species

The species conservation in cylindrical coordinates is written as

$$2\pi r\left[\frac{\partial(\rho Y_k)}{\partial t}\right] + \frac{\partial(\dot{m}Y_k)}{\partial r} - \frac{\partial}{\partial r}\left[2\pi r \rho D\left(\frac{\partial Y_k}{\partial r}\right)\right] = \dot{w}_k''' 2\pi r \tag{2}$$

where

$\dot{w}'''_k$ is the mass production rate of species k per unit volume($\dot{w}'''_k = \dot{w}'''_{k,pp} + \dot{w}'''_{k,ch}$, $r<R_c$; $\dot{w}'''_k = \dot{w}'''_{k,ch}$, $r > R_c$).

$\dot{w}'''_{k,pp}$ is the species addition due to chemical reactions at the particle.

$\dot{w}'''_{k,ch}$ is the species addition due to gas phase chemical reaction.

3.1.3. Energy

The energy conservation in cylindrical coordinates is given as

$$2\pi r[\frac{\partial(\rho h_T)}{\partial t}] + \frac{\partial(\dot{m}h_T)}{\partial r} - \frac{\partial}{\partial r}[2\pi r\rho D(\frac{\partial h_T}{\partial r})] = \dot{w}'''_h 2\pi r \tag{3}$$

where

$\dot{w}'''_h$ is the enthalpy production rate per unit volume. ($\dot{w}'''_h = \dot{q}'''_{conv} + \dot{q}'''_{ch} + \dot{q}'''_m$, $r<R_c$; $\dot{w}'''_h = \dot{q}'''_{ch}$, $r>R_c$).

$\dot{q}'''_{conv}$ is the convective heat transfer between the gas phase and the particles.

$\dot{q}'''_{ch}$ is the enthalpy produced as a result of chemical reactions in the gas phase.

$\dot{q}'''_m$ is the enthalpy gained by the gas phase due to the addition of mass from the particles.

3.2. Solid Phase Equations

3.2.1. Particle mass (m_p)

Particle mass loss rate is expressed as

$$\frac{dm_p}{dt} = -\dot{m}_p \tag{4}$$

where dm_p/dt is the total rate of change of particle mass due to pyrolysis and heterogeneous reactions. The mass loss rate, $\dot{m}_p$, is the sum of the volatile liberation rate ($\dot{m}_V$) and carbon consumption rate ($\dot{m}_C$) due to heterogeneous reactions. This is expressed as

$$\dot{m}_p = \dot{m}_V + \dot{m}_C \tag{5}$$

The yield of volatiles is a function of temperature of particle and reacting rate. The higher the particle temperature and reacting rate, the higher the yield. A competing model explains the differing volatile yields. The competing reaction model assumes that the pyrolysis products consists of a lighter component (V_I, lower H/C ratio in volatiles) and a heavier component (V_{II}, higher H/C ratio in volatiles). The lighter component is released at low temperatures and the heavier component is the predominant pyrolysis product at high temperatures. According to the competing reaction model [5]

$$\dot{m}_V = \dot{m}_{V,I} + \dot{m}_{V,II} \tag{6}$$

where

$$\dot{m}_{V,i} = \alpha_i k_{V,i} m_{cu}, \quad i = I, II \tag{7}$$

$$k_{V,i} = B_{V,i} \exp(-E_{V,i}/(R_u T_p)) \tag{8}$$

A fraction of the coal decomposes as the volatiles are released. The rate of change of the uncomposed coal mass due to both reactions in the competing reaction model is

$$dm_{cu}/dt = -[(\dot{m}_{V,I}/\alpha_I) + (\dot{m}_{V,II}/\alpha_{II})] \tag{9}$$

where, at t=0, m_{cu} is the same as the initial particle mass ($m_{p,0}$).

The mass loss rate $\dot{m}_C$ due to heterogeneous char reactions is evaluated as follows. For the first order heterogeneous reaction ($C + 1/2O_2 \longrightarrow CO$) at constant density (zone II reaction)

$$\dot{m}_C = \rho_w k_C Y_{O_2,w} \pi d_p^2 \tag{10}$$

where

$$k_C = B_C \exp(-E_C/R_u T) \tag{11}$$

The oxygen mass fraction at the particle surface ($Y_{O2,w}$) is calculated in terms of the bulk

gas mass fraction (Y_{O2}) next to the particles by a mass balance that accounts for the blowing effects (Stefan flow) from the particle and chemical reactions at the surface. Eqs. (5)-(11) can evaluate $\dot{m}_p$ if T_p and d_p are known.

3.2.2. Particle Diameter (d_p)

The diameter of the particle shrinks since heterogeneous oxidation occurs at the particle surface with constant density. The relation between $\dot{m}_C$ and d_p for zone II reaction is

$$\frac{d(d_p)}{dt} = -\frac{2\dot{m}_C}{\pi \rho_p d_p^2} \tag{12}$$

3.2.3. Particle Density (ρ_p)

The particle density changes with time since pyrolysis occurs volumetrically at a constant particle size. The relation between $\dot{m}_V$ and ρ_p is

$$\frac{d(\rho_p)}{dt} = -\frac{6\dot{m}_V}{\pi d_p^3} \tag{13}$$

3.2.4. Particle Temperature (T_p)

The particle temperature is obtained from the energy balance around an individual particle in the cloud.

$$m_p c_p \left(\frac{d(T_p)}{dt}\right) = -(\dot{q}_{conv} + \dot{q}_{rad}) + \dot{q}_{ch,p} \tag{14}$$

where $\dot{q}_{ch,p}$ is the heat released (absorbed) due to heterogeneous reaction and pyrolysis.

$\dot{q}_{conv}$ is the convective heat transfer between the bulk gas and particle of size "d_p".

$\dot{q}_{rad}$ is radiative heat transfer between a particle of size "d_p" and ambience.

3.3. Boundary and Initial Conditions

at t = 0

gas phase: $Y_k = Y_{k,0}$, $T = T_{g,0}$ $r < R_c$

$Y_k = Y_\infty, \quad T = T_\infty, \quad r > R_c$

Solid Phase: $m_p = m_{p,0}, \quad d_p = d_{p,0}, \quad \rho_p = \rho_{p,0}, \quad T_p = T_{p,0}$

For $t > 0$

as $r \to \infty, \quad T = T_\infty, \quad Y_k = Y_{k,\infty}$

and at $r = 0 \quad dT/dr = dY_k/dr = \dot{m} = 0$

3.4. Non-Dimensional Form

Using the nondimensional form of time, radius, etc. (see nomenclature), one can normalize the gas phase conservation equations (1)-(3) as follows:

3.4.1. Mass

$$\frac{\partial \rho^*}{\partial \tau} - \xi^3\left(\frac{\partial \alpha}{\partial \xi}\right) = w_m \tag{15}$$

where w_m is the normalized mass source.

3.4.2. Species

$$\rho^* \frac{\partial Y_k}{\partial \tau} - \alpha \xi^3 \frac{\partial Y_k}{\partial \xi} - \xi^4\left(\frac{\partial^2 Y_k}{\partial \xi^2}\right) = w_k - w_m Y_k \tag{16}$$

where w_k is the normalized source for species.

3.4.3. Energy

$$\rho^* \frac{\partial h^*}{\partial \tau} - \alpha \xi^3\left(\frac{\partial h^*}{\partial \xi}\right) - \xi^4\left(\frac{\partial^2 h^*}{\partial \xi^2}\right) = w_h - w_m h^* \tag{17}$$

where w_h is the normalized source for enthalpy. Similarly, the solid phase equations and boundary conditions also can be normalized. Details are given elsewhere [6].

4. NUMERICAL PROCEDURE

The parabolic equations (15), (16), and (17) can be solved using an explicit upwind scheme. The source terms $\dot{w}_k'''$, $\dot{w}_m'''$, and $\dot{w}_h'''$ with $T_p = (T_p)_0$ were calculated with the given conditions at $t = 0$ for $(T)_0$, $(Y_k)_0$, $(m_p)_0$, $(T_p)_0$, $(\rho_p)_0$, and $(d_p)_0$. The properties at $t = \Delta t$, $2\Delta t$, $3\Delta t$, $\cdots$etc. were found using the source terms and the explicit method. Since the distance variable ξ is the reciprocal radius, the center of the cloud corresponds to $\xi \rightarrow \infty$. However, the maximum value of ξ used was 3 to reduce the computational time. Thus, the mass of the cloud within $r = R_c/3$ was neglected since the mass of the cloud within $r = R_c/3$ comprises only 11% of the initial cloud mass. Obtaining a smooth transition from ignition to combustion was difficult due to finite kinetics. A "source correction" method helped to overcome the difficulties of "stiff" equations [7].

The runs were made on a VAX 9000-210V computer and Figs. 2-7 shows the results. The CPU time for the ignition calculations is about 5 to 10 minutes, while CPU time for combustion calculations is above 20 minutes.

5. RESULTS

Ignition results will be presented first followed by combustion results and experimental data.

5.1. Ignition

Table 1 lists the base case data for both ignition and combustion. The ignition data is obtained with the cylindrical cloud model without dissociation. The results are obtained for ignition time versus coal number density. The coal number density is typical of number densities used in the experiments. The following parametric cases are conducted: (1) $T_\infty = 1000$ K, (2) $T_\infty = 1100$ K, (3) $T_\infty = 1250$ K, (4) $T_\infty = 1300$ K. Ignition occurs heterogeneously if particle temperature in the cloud is greater than the bulk gas temperature near the particles. Ignition

Association for Information and Image Management
1100 Wayne Avenue, Suite 1100
Silver Spring, Maryland 20910
301/587-8202

Centimeter

Inches

MANUFACTURED TO AIIM STANDARDS
BY APPLIED IMAGE, INC.

3 of 3

occurs homogeneously if there is a peak in gas temperature profile. Figure 2 plots the results for ignition time verse number density of particle in the cloud. Figure 2 shows that heterogeneous ignition for a dilute cloud occurs from an insufficient amount of volatiles. Ignition time increases weakly with particle number density in heterogeneous ignition regime due to an increasing heat sink effect. As the particle number density further increases, the volatile concentration increases to flammable level and, therefore, homogeneous ignition occurs. Homogeneous ignition time first decreases with an increase in denseness of the cloud due to increased volatile concentration. However, beyond an optimum denseness the ignition time increases again as the particle number density further increases. It is seen that a cloud that heterogeneously ignites at lower gas temperatures switches to homogeneous ignition at high gas temperatures. Such a trend also was observed for ignition of isolated coal particles. The experimental data confirms such a finding for an isolated particle [8]. Ruiz et al. [9] obtained experimental data on ignition time versus particle number density for a cylindrical stream of particles. Figure 3 presents a comparison of the data with the model predictions. Figure 3 shows that the ignition time at 1100 K qualitatively agrees with the experimental findings but differs quantitatively. Two possible reasons for the quantitative discrepancy are:

a) Gas temperatures in the experiment should be measured closer to the center since the wall temperature may be lower. The theoretical prediction used wall temperature.
b) The model assumes pure diffusional mixing (zero relative velocity between fuel stream and carrier air) while the fuel relative velocity in the experiment may be non-zero.

5.2. Combustion

Consider an initially cold cylindrical cloud of monosized coal particles ($n=7.3\times10^9$ particles/m^3, $d_p=64$ μm, $R_c=0.225$ cm, $T_{g,o}=T_{p,o}=300$ K) introduced into a hot quiescent oxidizing atmosphere ($T_\infty=1500$ K). The ignition is homogeneous and the ignition time is 67.3 ms. Figure 4 shows the development of the flame profiles at different time intervals after ignition has occurred. The curve for t=67 ms shows the temperature profile just before ignition. Upon reaching the pyrolysis temperature, the particles release volatiles that diffuse out of the

cloud into the surrounding high temperature environment. Once the volatile concentration is high enough, ignition occurs at a location outside the cloud at t=68 ms. Since the combustion rate is faster than the volatile production rate, the flame now propagates toward the cloud at t=71 ms. The particles near the cloud heat up rapidly once the flame moves to the cloud surface. The oxygen is now rapidly consumed at the cloud surface. Therefore, two flames (or two temperature peaks) are formed: (1) an "inner" flame that propagates into the premixed volatiles and oxygen in the cloud, and (2) the "outer" flame that propagates away from the cloud (t=71 and 71.5 ms). The inner flame, which moves into the premixed volatile-oxygen cloud, consumes the oxygen in the cloud. The propagation velocity is about 0.25 m/s. The outer diffusion flame moves toward the ambience. All the oxygen is consumed once the inner flame propagates to the center of the cloud. Thus, only a pure diffusion flame formes outside the cloud (t=73 ms).

Results for coal/air ratios of 0.5, 1 and 2 ($n=3.26\times10^9$, 6.52×10^9, and 1.3×10^{10} particles/m^3) obtain the effect of the cloud denseness on the combustion profile. Figure 5 shows the results for flame profile at the coal/air ratio of 0.5. The ignition time is 55.29 ms. However, the double flame does not appear for this dilute cloud because the coal mass density is low and the cloud does not release enough volatile to support the "inner flame" inside the cloud. Figure 6 shows the results at coal/air ratio of 1. The ignition time is 65.05 ms. Figure 6 clearly shows the double flame. The coal:air ratio in the fuel nozzle of a boiler burner is typically on the order of 0.5 to 1.0 and so a double flame may also exist in a boiler burner. The peak temperature of the outside flame is 3014 K while the inner flame is 2385 K. The peak temperature decreases to 2659 K when dissociation is included in the model. The high peak temperature is due to the high ambient temperature of 1500 K. At an ambient temperature of 1100 K, the peak temperature without dissociation is on the order of 2888 K for a coal: air ratio of 1. Figure 7 shows the results when the coal/air ratio is 2 at t= 89 ms. The ignition time for this case is 83.37 ms. The peak temperature of the outer flame is 2683 K and the inner flame is 1994 K.

6. EXPERIMENT

The analysis shows that a double flame is likely in ignited dense clouds. Experiments

verified the formation of a double flame.

The experimental facility centers around a flat flame burner. The burner used is a Holthius flat flame burner manufactured by McKenna Products (Fig. 8). The burner is of cylindrical construction with a 6 cm diameter flame area. A 6 cm diameter sintered stainless steel plug with cooling coils embedded in it stabilizes the flame. The flames are shielded from the entrainment effects by passing N_2 (inert) around the flame holder through a bronze porous plug of 6.6 cm diameter. This burner has a hollow stainless steel tube with a 2.03 mm internal diameter fixed at its center. This serves as a coal particle injector that provides a stream of particles. The burner is fixed onto a vertically traversing table that is on a mobile table. This arrangement enables portability of the entire setup. A Methane and air mixture is the flammable mixture for the flat flame. Adjusting the flows in the control panel controls the Air to Fuel ratio (A:F). Nitrogen gas flowing through the annular porous ring serves as the shield to minimize air entrainment into hot gas. The coal injector is connected to a Locally Fluidized Feeder (LFF) placed over a digital balance. The instantaneous reading with carrier air flow rate determines the A:F ratio of the stream. A water cooled particle collection system placed above the burner freezes the reactions of collected particles. The distance between the burner and the collection system determines the residence time. A Pt-Rh thermocouple measures the gas temperature while a Lancom exhaust gas analyzer measures the oxygen concentration. The measured air:fuel ratio and the stoichiometric calculation also verify the measured concentration.

A digital imaging system captures the coal stream combustion sequence. A 4MIP image processing software processes the acquired flame images. This software controls the camera operations and allows operators to assist in analyzing the flames in detail. The details of the flat flame burners and the imaging system are given by Gopalakrishnan [10].

The flame image shown in Fig. 9 is for 64 micron high volatile coal particles. The insert in Fig. 9 presents the arbitrary colors assigned to various pixel values. The red color is a highly luminous flame whose brightness (pixel value) is above 240 of 255. The change of color from green to yellow indicates the occurrence of ignition. Figure 9 clearly shows that the ignition starts at the periphery of the stream, which indicates homogeneous ignition as indicated in the theoretical analysis for a dense cloud. Since the stream of high volatile coal is dense, the flame begins to form outside the cloud because of volatiles, which can be conveniently termed as a

group flame. The divergence of the flame is partly due to both the entrainment effects of the surrounding air and increased volatile evolution from the stream and subsequent diffusion into surrounding hot gas. The flame splits into inner and outer flames with the "outer" flame propagating to ambience and the "inner" flame propagating towards the center of the stream. Further work is in progress.

7. SUMMARY

(1) A group combustion model is presented for the ignition and combustion of a cylindrical cloud of coal particles.

(2) Results reveal heterogeneous ignition for dilute clouds and homogeneous ignition for dense clouds.

(3) Heterogeneous ignition time increases weakly with particle number density. Homogeneous ignition occurs as the particle number density further increases. Ignition time decreases until a minimum is observed and then increases again as the particle number density is further increases.

(4) Results show the simultaneous existence of two flames: an inner flame propagating into premixed volatiles and oxygen and an outer diffusion flame. Inner flame occurs only for dense cloud.

(5) Preliminary data confirms the existence of double flame.

ACKNOWLEDGMENTS - This material was prepared with the support of the US DOE - Pittsburgh Grant No. DE -FG -90 PC90310 and the Center for Energy and Mineral Resources of the State of Texas. However, any findings, conclusions, or recommendations expressed herein are those of the authors and do not necessarily reflect the views of the DOE.

NOMENCLATURE

B	pre-exponential frequency factor, m/s
c	coal particle specific heat, kJ/kg K
D	diffusion coefficient, m^2 /s
d_p	particle diameter, m
E	activation energy, kJ/kmol
h_T	thermal enthalpy, kJ/kg
$h_{T,ref}$	reference enthalpy = C_pT_{ref}, kJ/kg
h^*	non-dimensional enthalpy = $h/h_{T,ref}$
k	specific reaction rate constant, m/s
$\dot{m}$	mass flow rate, kg/s
m_{cu}	undecomposed particle mass, kg
$\dot{m}_C$	heterogeneous mass burning rate, kg/s
m_p	particle mass
$\dot{m}_p$	particle mass loss rate, kg/s
$\dot{m}_{ref,g}$	reference mass flow rate = $4\pi\rho DR_{c,0}$, kg/s
$\dot{m}_{ref,p}$	reference particle mass loss rate = $m_{p,0}/t_{ref}$, kg/s
$\dot{m}_V$	mass loss rate due to pyrolysis, kg/s
n	particle number density, m^{-3}
P	pressure
$\dot{q}'''_{c\,onv}$	convective heat transfer between the gas phase and the particles, kJ/kg
$\dot{q}'''_{c\,h}$	enthalpy produced as a result of chemical reactions in the gas phase, kJ/kg
$\dot{q}'''_m$	enthalpy gained by the gas phase due to the addition of mass from the particles, kJ/kg
R_c	cloud radius of cylindrical cloud, m
R_u	universal gas constant, kJ/kmol K
r	radial distance from the cylindrical cloud center, m
T	temperature, K
T_{ref}	reference temperature = 300 K
t	time, s

t_{ref} reference time = $(\rho_{ref}R_C^2/\rho D)$

V volatiles

w_k non-dimensional source for species = $\dot{w}'''_k/\dot{m}'''_{ref,g}$

w_h non-dimensional source for enthalpy = $\dot{w}'''_h/\ \dot{m}'''_{ref,g}\ h_{T,ref}$

w_m non-dimensional volumetric mass source = $\dot{w}'''_m/\dot{m}'''_{ref,g}$

$\dot{w}'''_h$ volumetric gas phase enthalpy source, kw/m^3

$\dot{w}'''_k$ volumetric gas phase of species k, kg/m^3s

$\dot{w}'''_{k,ch}$ species addition due to gas phase chemical reaction, kg/m^3s

$\dot{w}'''_{k,pp}$ species addition due to chemical reactions at the particle, kg/m^3s

$\dot{w}'''_m$ volumetric mass source, kg/m^3s

Y species mass fraction

Greeks

α non-dimensional mass flow = $\dot{m}/\dot{m}_{ref}$

α_I,α_{II} Maximum volatile matter via pyrolysis routes I and II

ξ nor-dimensional inverse radius = $R_{c,0}/r$

ρ gas phase density, kg/m^3

ρ_{ref} reference density = P/R_uT_{ref}, kg/m^3

ρ^* non-dimensional density = ρ/ρ_{ref}

τ non-dimensional time = t/t_{ref}

Subscripts

C carbon, char

ch gas phase chemical reaction

ch,p particle chemical reaction

cu coal undecomposed

k species

I volatiles due to route I

II volatiles due to route II

O_2 Oxygen

ref	reference
T	thermal
V	volatiles
w	surface of the particle
0	at time t = 0
∞	infinite

Superscripts

$'''$	per unit volume
*	non-dimensional variable

REFERENCES

1. K. Annamalai and W. Ryan, Interactive Processes in Gasification and Combustion-II. Isolated Carbon, Coal and Porous Char Particles. *Prog. Energy Combust.* Sci., Vol. 19, pp. 383-446, 1993.
2. M. Labowsky, The Effects of Nearest Neighbor Interactions on the Evaporation Rate of Cloud Particles, *Chem. Eng. Sci.* 31, 803- 813, 1976.
3. K. Annamalai and S. Ramalingam, Group Combustion of Char Particles. *Combust. Flame*, Vol. 70, pp. 357-342, 1987.
4. K. Annamalai, S. Ramalingam, T. Dahdah, and D. Chi, Group Combustion of a Cylindrical Cloud of Char/Carbon Particles. *Journal of Heat Transfer*, Vol. 110, pp. 190-200, 1988.
5. S.K. Ubhayakar, D.B. Stickler, C.W. Von Rosenberg and R.E. Gannon, *Rapid Devolatization of Pulverized Coal in Hot Combustion Gases. 16th Symp. (int.) on Combustion*. pp.427-436, 1977.
6. X. Du, Transient Ignition and Combustion of Single Coal Particle and Coal Particle Streams, Ph.D Thesis, in preparation, Texas A&M University, College Station, Texas, 1994.
7. W. Ryan, Group Combustion of a Spherical Cloud of Coal Particles, Ph.D Thesis, Texas A&M University, College Station, Texas, 1992.
8. X. Du, Transient Ignition of Coal Particle, *Combst. Flame*, in press, 1994.
9. M. Ruiz, K. Annamalai and T. Dahdah, An Experimental Study on Group Ignition of Coal Particle Streams, *Heat and Mass Transfer in Fires and Combustion Systems*, W. L Grosshandler and H. G. Semerjian, eds., ASME HTD Vol. 148, pp. 19-26, 1990.
10. C.P. Gopalakrishnan, Digital Imaging of Coal Stream Combustion, M.S. Thesis, Texas A&M University, College Station, Texas, 1993.

Table 1 Base Case Data

Ambience:

Air, $T_\infty = 1500$ K, $Y_{O2} = 0.23$

Cloud:

$T_{g,c0} = 300$ K, $Y_{O2} = 0.23$, $R_c = 0.225$ cm, $d_p = 64$ μm

$\rho D = 5 \times 10^{-5}$ kg/ms, $C_p = 1.18$ kJ/kg K

Coal Composition:

C - 84.63, H - 5.47, N - 2.13, O - 7.77

Volatile Composition:

$V_I = CH_{2.64}N_{0.074}O_{0.24}$, $V_{II} = CHN_{0.28}O_{0.09}$

$HV_I = 3.95 \times 10^4$ kJ/kg, $HV_{II} = 3.72 \times 10^4$ kJ/kg

Kinetics:

Pyrolysis (Ubhayakar et al., 1977):

$\alpha_I = 0.4$, $\alpha_{II} = 0.8$, $B_I = 3.7 \times 10^5$ m/s, $B_{II} = 1.46 \times 10^{13}$ m/s

$E_1 = 7.37 \times 10^4$ kJ/K kmol, $E_2 = 25.1 \times 10^4$ kJ/K kmol

Heterogeneous Reactions (Smith, 1971):

$E_{C,1} = 6.64 \times 10^4$ kJ/K kmole, $B_{C,I} = 4.5 \times 10^3$ m/s

$n_{O2} = 1.0$

Volatiles and CO gas phase reactions (Howard et al., 1973):

$A = 5 \times 10^9$ m^3/kgs, $E = 1.26 \times 10^5$ kJ/k mole

$n_{O2} = 1.0$

LIST OF ILLUSTRATIONS

Fig. 1a Cylindrical model

Fig. 1b Temperature Profile

Fig.2 Ignition time versus coal number density (R_c=0.225 cm,d_p=64 μm, Y_{O2}=0.23, $T_{g,0}$=300 K, $T_{p,0}$=300 K)

Fig.3 Comparison between the predicted and measured ignition time (R_c=0.225 cm, T_∞= 1100 K,d_p=64 μm)

Fig.4 Flame profile at different time (R_c=0.225 cm, T_∞=1500, d_p=64 μm, Y_{O2}=0.23, $T_{g,0}$=300 K,$T_{p,0}$=300 K)

Fig.5 Effect of cloud denseness (coal/air=0.5, R_c=0.225 cm, T_∞=1500 K, d_p=64 μm, Y_{O2}=0.23)

Fig.6 Effect of cloud denseness (coal/air=1, R_c=0.225 cm, T_∞=1500 K, d_p=64 μm, Y_{O2}=0.23)

Fig.7 Effect of cloud denseness (coal/air=2, R_c=0.225 cm, T_∞=1500 K, d_p=64 μm, Y_{O2}=0.23)

Fig.8 Flat flame burner set up

Fig.9 Coal stream flame (reaction zone height 6 cm)(coal type-PSOC1336, d_p=64 μm, $Y_{O2,\infty}$=0.063, A:F=0.42, mass flow rate of coal-0.0718 g/sec)

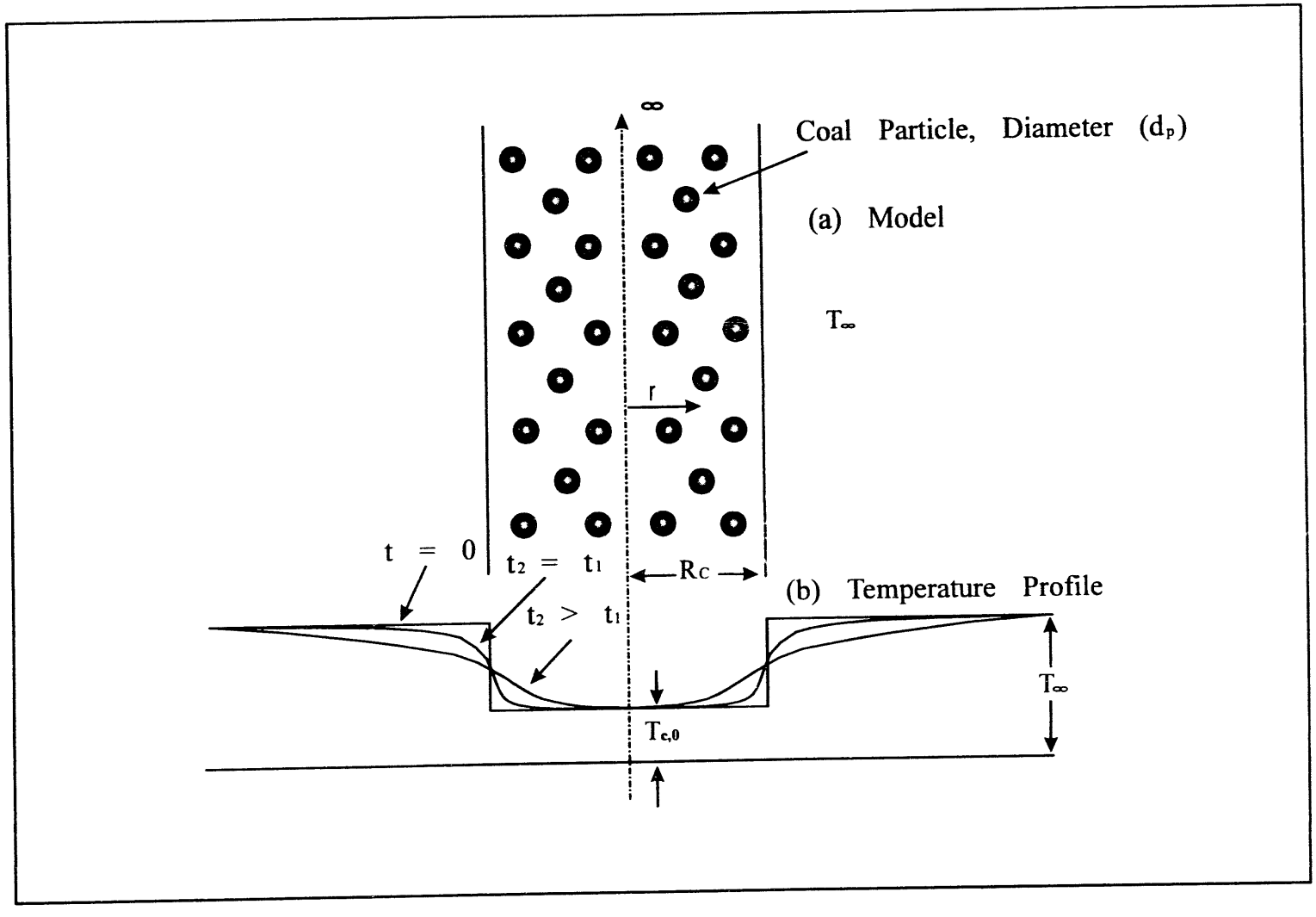

Fig. 1 (a) Cylindrical Model
(b) Temperature Profile

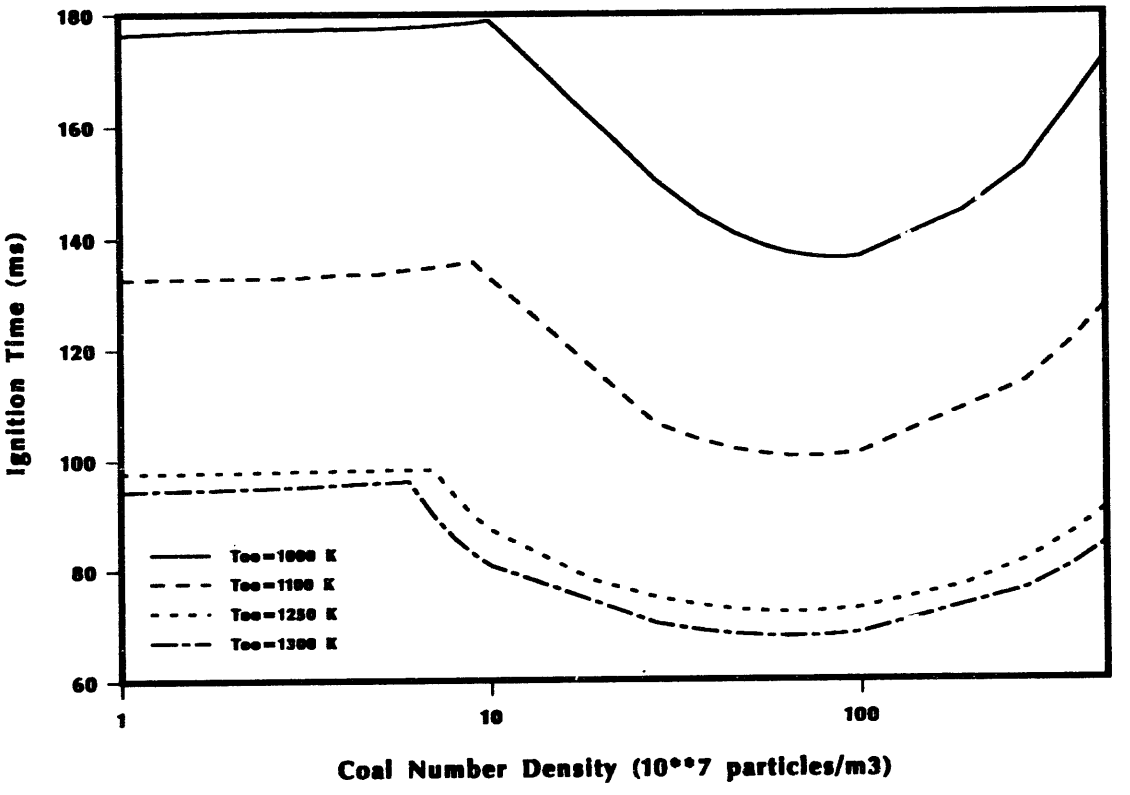

Fig.2 Ignition time versus coal number density

(R_c=0.225 cm,d_p=64 μm, Y_{O2}=0.23,$T_{g,0}$=300 K, $T_{p,0}$=300 K)

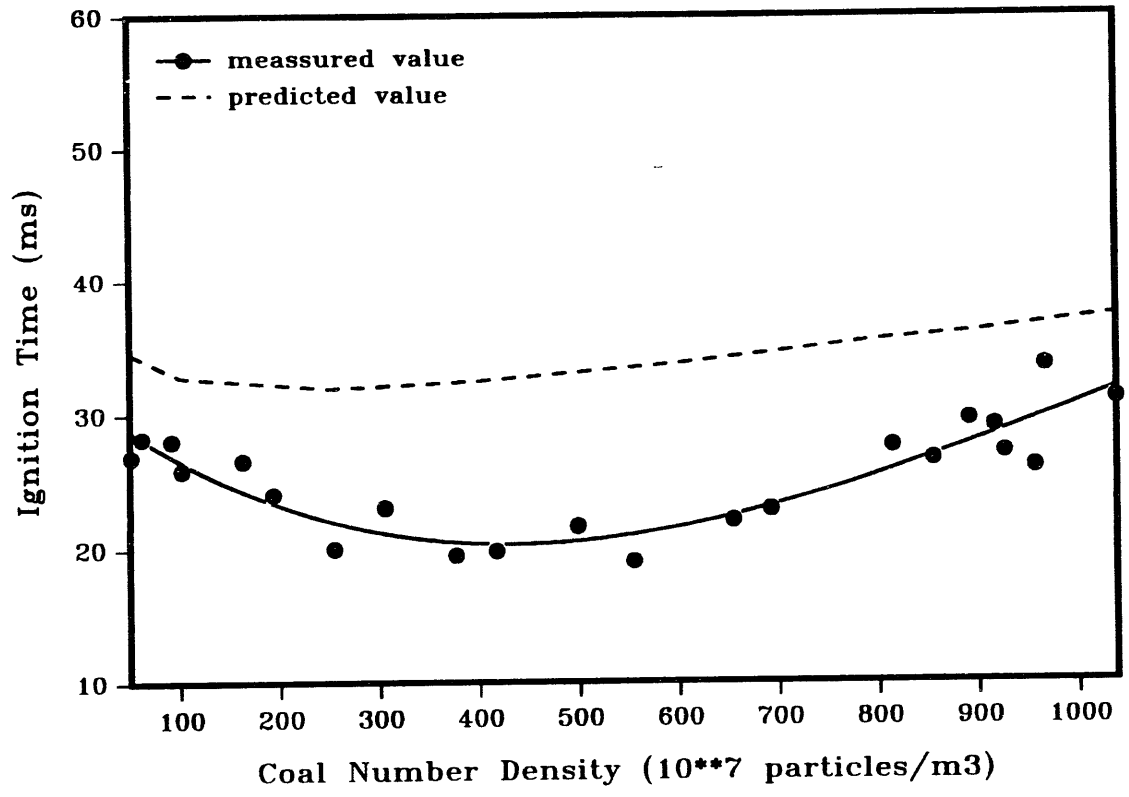

Fig.3 Comparison between the predicted and measured ignition time (R_c=0.225 cm,T_∞=1100 K,dp=64 μm)

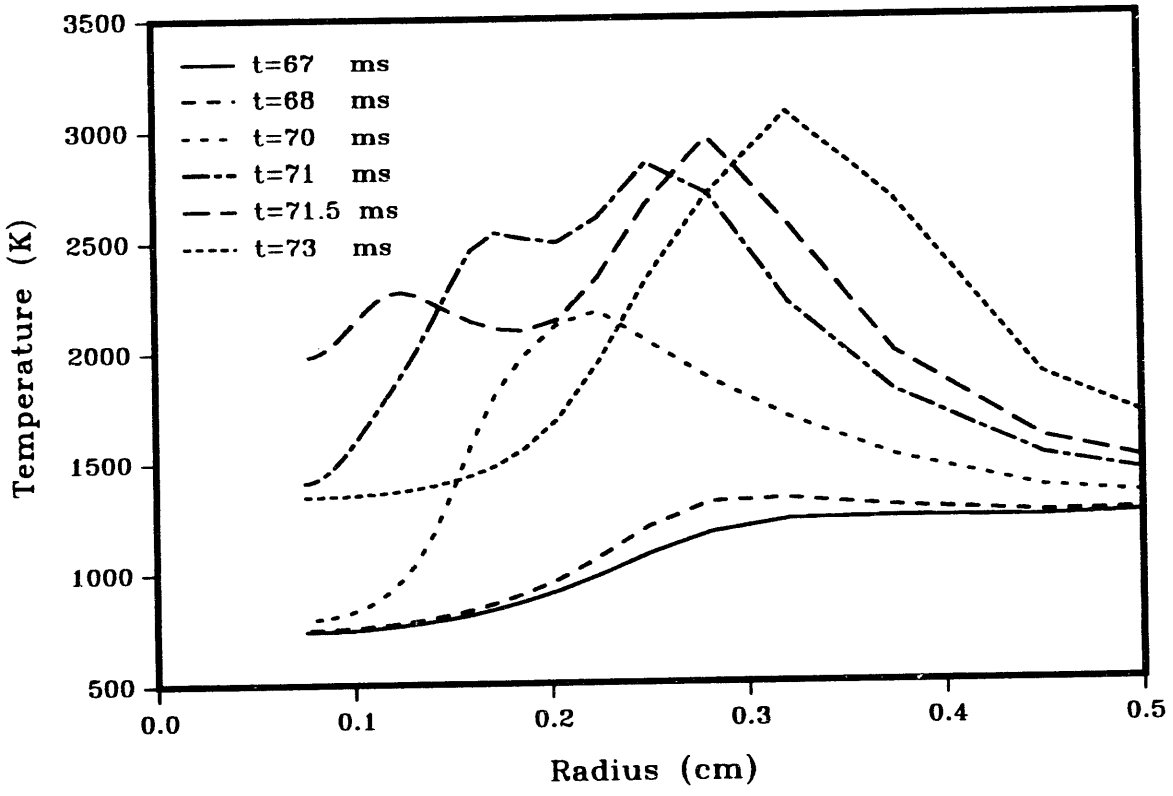

Fig.4 Flame profile at different time

(R_c=0.225 cm, T_∞=1500, d_p=64 μm, Y_{O2}=0.23, $T_{g,0}$=300 K, $T_{p,0}$=300 K)

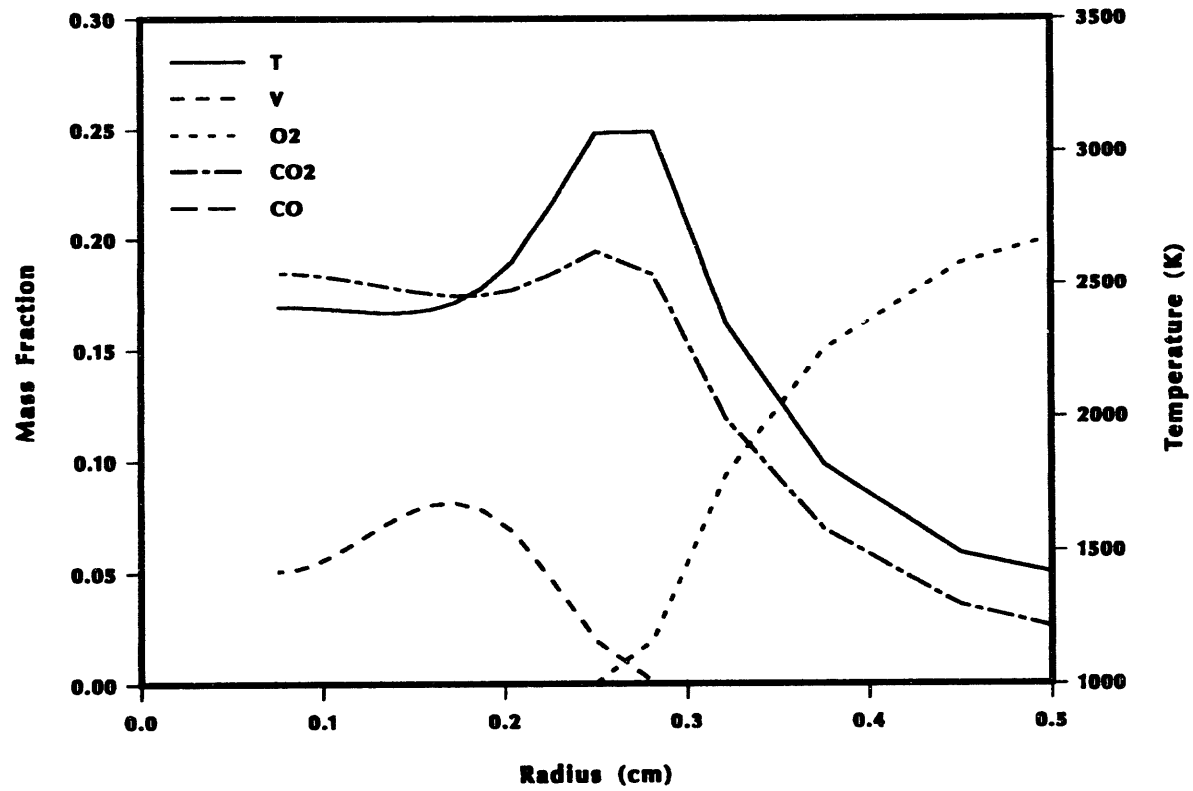

Fig.5 Effect of cloud denseness

(coal/air=0.5, R_c=0.225 cm, T_∞=1500 K, d_p=64 μm, Y_{O2}=0.23)

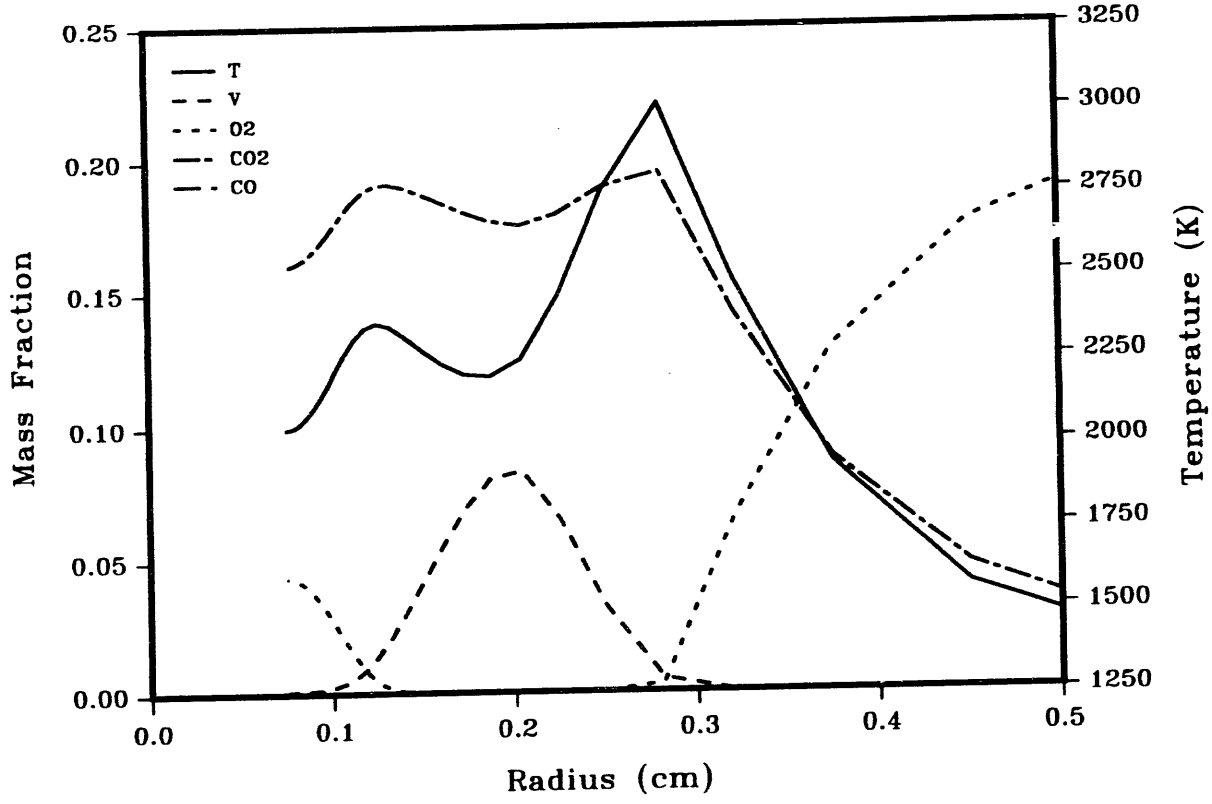

Fig.6 Effect of cloud denseness

(coal/air=1, R_c=0.225 cm, T_∞=1500 K, d_p=64 μm, Y_{O2}=0.23)

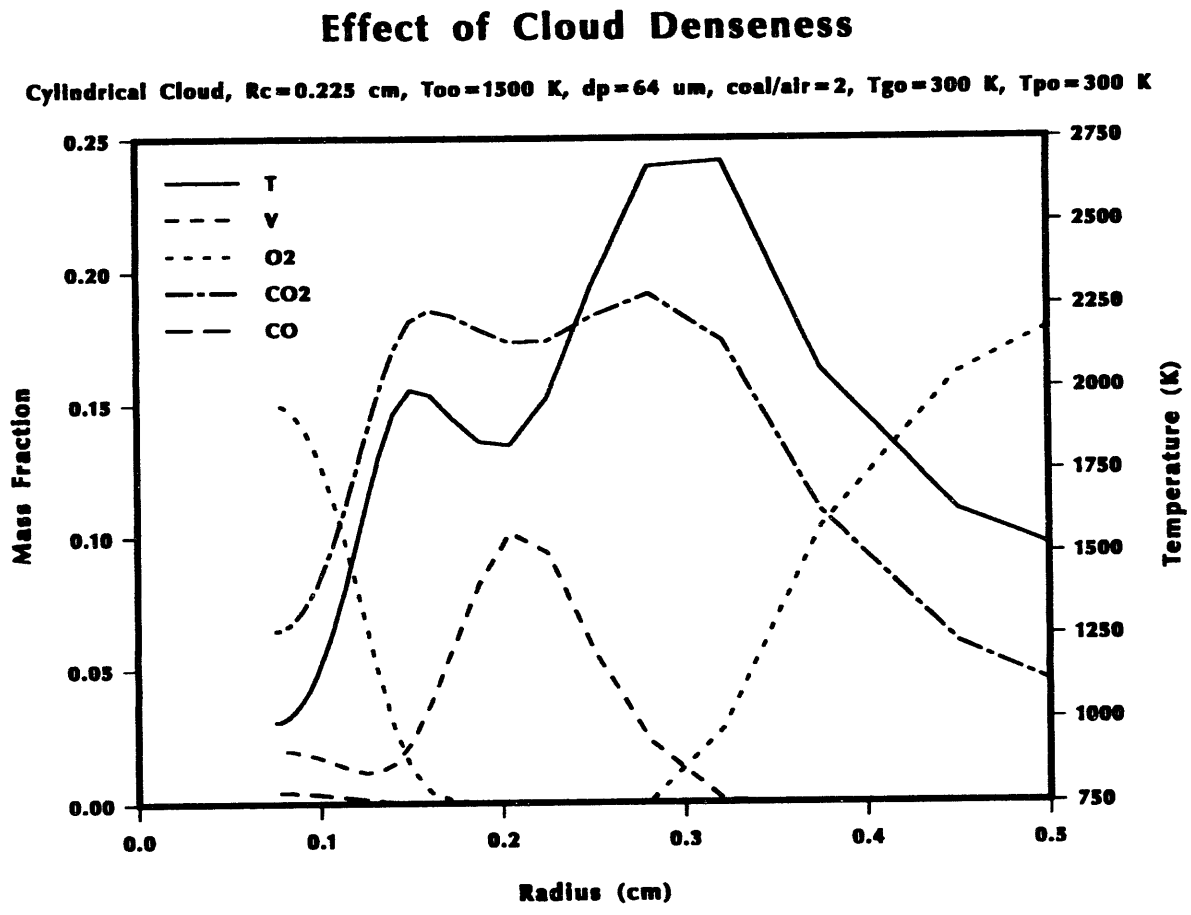

Fig.7 Effect of cloud denseness

(coal/air=2, R_c=0.225 cm, T_∞=1500 K, d_p=64 μm, Y_{O2}=0.23)

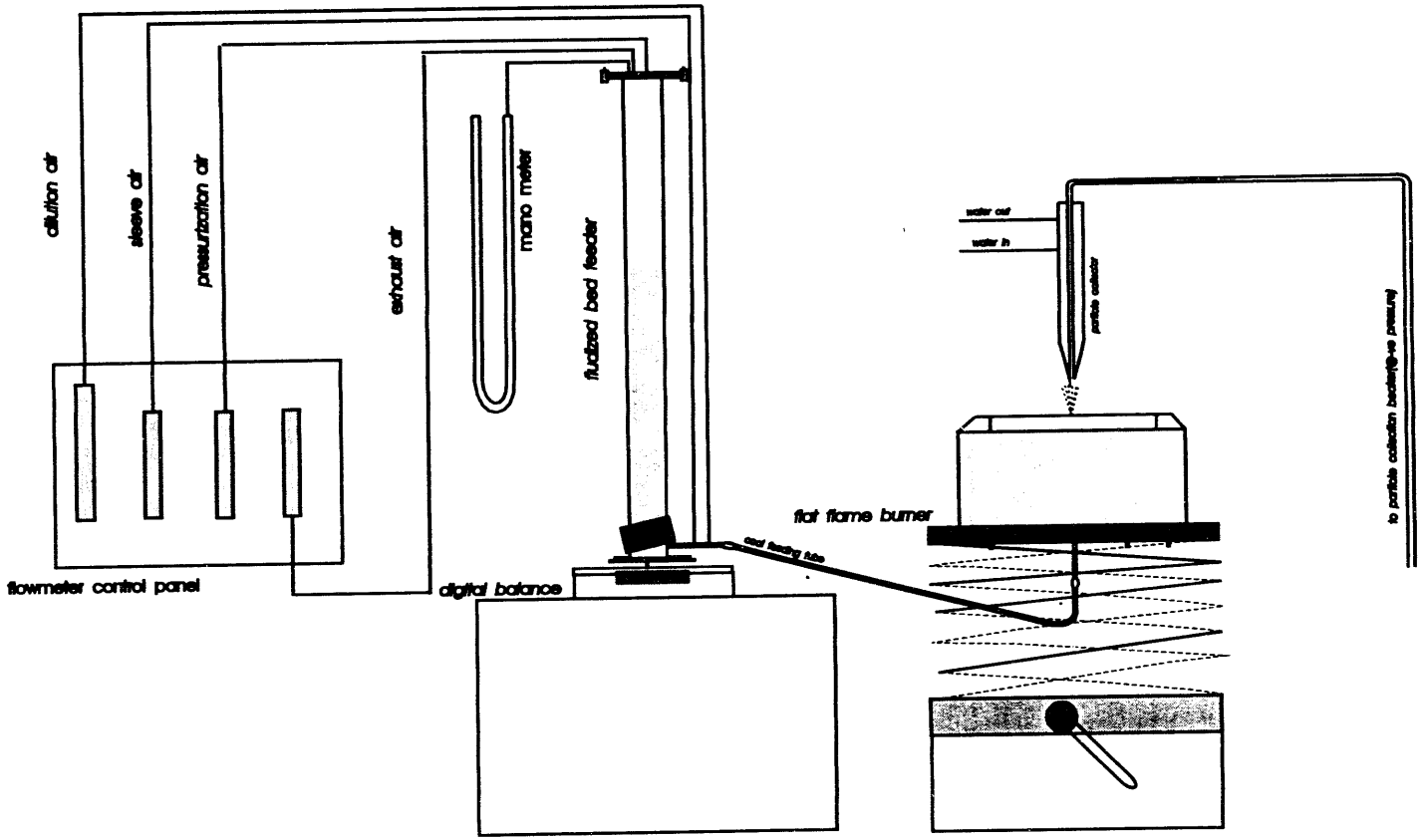

Fig.8 Flat Flame Burner Setup

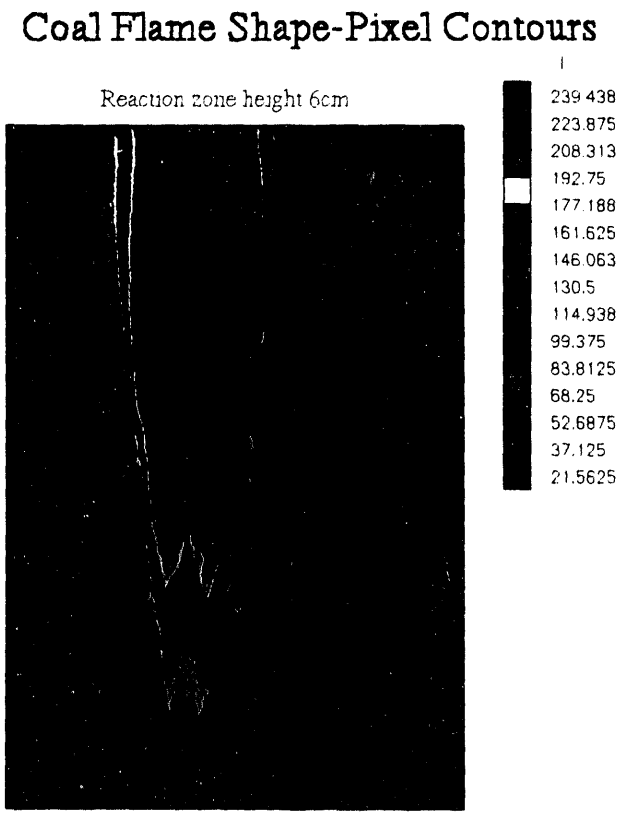

Fig. 9 Coal Stream Flame (Reaction Zone Height 6 cm) (Coal Type-PSOC1336, d_p = 64 μm, $Y_{O2,\infty}$ = 0.063, A:F = 0.42, mass flow rate = 0.0718 g/sec)

Appendix D

Group Ignition and Combustion Model with Cloud Expansion

Abstract

The group ignition and combustion model presented in Appendix C is extended to include cloud expansion due to heating, ignition and combustion. As a result of expansion, the gas and particles move in the cloud which increase the cloud radius. The heating of the cloud results in reduced ignition times since expansion results in increasing diluteness of cloud. Further the outer flame is at farther distance due to expansion effect. The peaks in temperatures are more pronounced.

1. INTRODUCTION

A model has been developed to simulate the group combustion of spherical and cylindrical clouds of pulverized coal particles. Results have been obtained for the ignition and combustion of such clouds. The assumption has been made in the previous model that particles are fixed in the space. However, this assumption needs to be relaxed and the movement of particles as result of gas movement should be accounted for. Thus, the assumption in the previous model has been extended to include the effect of cloud expansion. In the following report, the development of the non-dimensional governing partial differential equations is given to include the effect of cloud expansion.

The conservation equations for both gas and particles have been developed in Appendix A. The additional equations needed for cloud expansion and relevant numerical methods have been derived as following.

1. Single Particle Dynamics

Assuming that a particle with an initial velocity of v_p moves in a uniform flow field and in micro-gravity, the particle momentum equation in r direction is

$$\frac{\pi d_p^3}{6}\rho_p\frac{dv_p}{dt} = c_d\frac{\pi d_p^2}{4}\frac{\rho}{2}|v_g - v_p|(v_g - v_p) \qquad (1)$$

where

v_g is gas velocity,

v_p is particle velocity, and

c_d is drag coefficient.

The particle drag for different range of Reynolds number of relative motion can be given as:

Newton's formula

$$c_d = 0.44 \qquad (Re_p > 1000)$$

Wallis-Kliachko's formula

$$c_d = (1 + Re_p^{2/3}/6)24/Re_p \qquad (1 < Re_p < 1000)$$

Stokes' formula

$$c_d = 24/Re_p \qquad (Re < 1)$$

where

$$Re_p = |v_g - v_p| d_p/\nu$$

In case of higher particle temperature than gas temperature, the particle drag will be higher than that for isothermal case. In this case the gas viscosity in Re_p is determined by the so called 1/3 law, that is

$$\nu = \frac{1}{3}\nu_p + \frac{2}{3}\nu_g$$

where ν_p and ν_g are gas viscosity coefficients at temperature T_p and T_g respectively, and T_p and T_g are particle and gas temperature respectively. The blowing due to pyrolysis and heterogeneous reactions reduce the drag coefficient. The drag coefficient in the presence of mass transfer can be given as

$$c_d = c_{d0} F_B$$

where

F_B is the blowing correction factor due to the drag coefficient.

The blowing correction factor due to the drag coefficient is given as

$$F_B = \left[\frac{(\dot{m}_p/2\pi\rho D d_p)}{(\exp(\frac{\dot{m}_p}{2\pi\rho D d_p}) - 1)} \right]$$

Since $Re_p < 1$ in coal cloud expansion, the Stokes law for particle drag can be used. Substituting Stokes' formula for c_d into Eq. 4, we have

$$\frac{dv_p}{dt} = (v_g - v_p)/\tau \tag{2}$$

where

τ is relaxation time ($\tau = d_p^2 \rho_p/(18\mu)$).

Since time step is very small in the numerical solution of conservation equations, we can assume that $v_g(t)$ and τ are constant in each time step, but different at different time step. Integrating Eq. 2 with the initial condition of $v_p = v_p(t)$ at each time step gives

$$v_p(t+\Delta t) = v_g(t) - (v_g(t) - v_p(t))\exp(-\Delta t/\tau) \tag{3}$$

The integration of Eq. 2 yields the solution for particle trajectory.

$$x_p(t+\Delta t) = v_g(t)t - (v_g(t) - v_p(t))\tau(1 - \exp(-\Delta t/\tau)) \tag{4}$$

Similar equations can be found for non-Stokes particle drag and drag change by different gas and particle temperatures and devolatilization or heterogeneous reactions. Eqs. 2 and 3 point out that: the particle velocity approaches to the fluid velocity and the particle trajectory approaches to its asymptote $y = v_p\tau$. When $t = \tau$, $v_p = v_{p0}/e$. Hence the physical meaning of the relaxation time τ is the time needed for the reduction of particle-fluid velocity slip to 1/e times of its initial value. The smaller τ, the easier particle tracks the fluid.

2. Particle Number Density

Assuming spherical symmetry, the equation for number density of particles in spherical coordinates is given as

$$4\pi r^2\left(\frac{\partial n}{\partial t}\right) + \left(\frac{\partial \dot{N}}{\partial r}\right) = 0, \qquad r < R_c(t) \tag{5}$$

where

n is number density of particles,

$\dot{N}$ ($=4\pi r^2 n v_p$) is the particle flow rate at "r", and

v_p is particle velocity at "r".

As the combustion continues, the diameter of the particle $d_p(t)$ decreases with time. It is assumed that the cloud shrinks to new radius $R_C(t)$ wherever particle diameter $d_p(t)$ at the cloud periphery decreases to 1/10 of initial value.

3. Boundary and Initial Conditions

at t = 0

$$R_c = R_{c0}$$

gas phase: $Y_k = Y_{k,0}$, $T = T_{g,0}$ $r < R_c$

$Y_k = Y_\infty$, $T = T_\infty$, $r > R_c$

Solid Phase: $n = n_0$, $m_p = m_{p,0}$, $d_p = d_{p,0}$, $\rho_p = \rho_{p,0}$, $T_p = T_p$ $r < R_c$

$n = 0$ $m_p = 0$ $r > R_c$

For t > 0

as $r \rightarrow \infty$, $T = T_\infty$, $Y_k = Y_{k,\infty}$

and at r = 0 $dT/dr = dY_k/dr = dn/dr = \dot{N} = \dot{m} = 0$

4. Numerical Procedure

The parabolic equations (1), (2), (3) in appendix A and additional equations in appendix B can be solved using an explicit upwind scheme. A brief description of the numerical scheme used in the transient analysis is as follows:

a. Determine the source terms at t = 0:

With the given initial conditions at t = 0 for T_g, Y_k, m_p, T_p, ρ_p, and d_p, calculate the terms $\dot{w}_k'''$, $\dot{w}_m'''$, $\dot{w}_h'''$.

b. Determine the properties at t = Δt:

Gas Phase Properties (Y_k, T and ρ_k)

Using source terms in eqs (2) and (3) in appendix A and explicit method, determine Y_k and T_g at each location for the next time step. With the ideal gas law, find ρ = (P/RT) at t = Δt. Since ρ at Δt is different from ρ at t = 0, find $(\partial\rho/\partial t)$. Using the source term $\dot{w}_m'''$ and $(\partial\rho/\partial t)$, find $\dot{m}$ at t = Δt by the mass conservation Eq. 1 in appendix A.

Solid Phase Properties

With the gas mass flow rate $\dot{m}$ and gas density ρ, find gas velocity by $v_g = \dot{m}/(4\pi r^2\rho)$. With the gas velocity, determine particle velocity and particle trajectory by Eqs. 3 and 4 in appendix B. The new location of the cloud boundary can be determined by particle trajectory at cloud surface. With previous $\dot{N} = 4\pi r^2\rho v_p n$, find new distribution of number density of particles n(t)) at $t = \Delta t$ by particle number conservation Eq. 5 in appendix B. With the estimated T in zone II at $t = \Delta t$, determine the amount of heat transferred via convection to or from the particles within Δt. Determine the chemical heat liberated due to reactions at the coal particles ($\dot{q}_{ch,p}$) using Eq. 5 in appendix A. Then, using Eq. 14 in appendix A, find particle temperature $(T_p)_{t=\Delta t}$ with $\dot{m}_p = \dot{m}_{p,0}$. Determine the mass loss of the volatiles ($\dot{m}_V$) and the mass loss rate due to heterogeneous reactions ($\dot{m}_C$) within Δt using Eqs. 6 and 10 in appendix A and determine the particle diameter and density using Eqs. 12 and 13 in appendix A. Then, with $\dot{m}_p = \dot{m}_V + \dot{m}_C$, total mass loss rate are evaluated. Using the estimated total mass loss rate and Eq. 4 in appendix A, determine m_p at $t = \Delta t$.

Using particle trajectory at different locations at Δt, interpolate ρ_p, d_p and T_p for particles into shell positions.

c. Properties at $t = 2\,\Delta t$, $3\Delta t$ ... etc:

With knowledge of T_p at $t = \Delta t$, d_p at Δt, T at $t = \Delta t$, Y_k at $t = \Delta t$, $\dot{m}$ at $t = \Delta t$, etc, repeat step a and b for gas phase and solid phase properties.

5. Preliminary Results:

5.1. Velocity and Trajectory of Coal Particles at Cloud Boundary

Figure 1 shows that gas velocity and particle velocity at cloud boundary at different time. It can be seen that the gas phase obtains its velocity after the cold cloud has been suddenly put into the high temperature environment because of the change of the gas density due to the thermal effects. The gas velocity decreases with time due to the increase of gas temperature in the cold cloud. As the gas temperature in the cloud increases, the temperatures of particles also increase so that devolatization effect becomes dominant and the gas velocity slowly increases again with time. When the ignition approaches, the gas velocity increases fast as the more volatile releases.

The particles in the cloud obtain their velocities by the drag effects. Therefore, the

velocities of particles are dependent upon the gas velocity.

The cloud expansion is produced by the particle drag due to the thermal and devolatilization effects. The cloud radius has been increased to 1.5 times of its initial radius at the ignition time.

Figure 2 shows the particle velocity distribution in the cloud at different time. It can be seen that the particle velocity in the outer cloud is faster than that in the inner cloud. As time increases, the velocity distribution becomes flat.

5.2. Number of Density

Figure 3 shows the number of density distribution in the cloud. The particle number density in the outer cloud is much dilute than that in inner cloud since the particle velocity in the outer cloud is faster than that in the inner cloud. However, the number of density becomes roughly same in the cloud as time increases sincee the particle velocity distribution becomes flat. Because of the cloud expansion, the number of density at ignition time is much lower than that at initial time.

5.3. Double Flame

Figure 4 shows the flame structure when double flame occurs.

It is clear that double flame still exist even with cloud expansion. However, outer flame is shifted further away from the cloud.

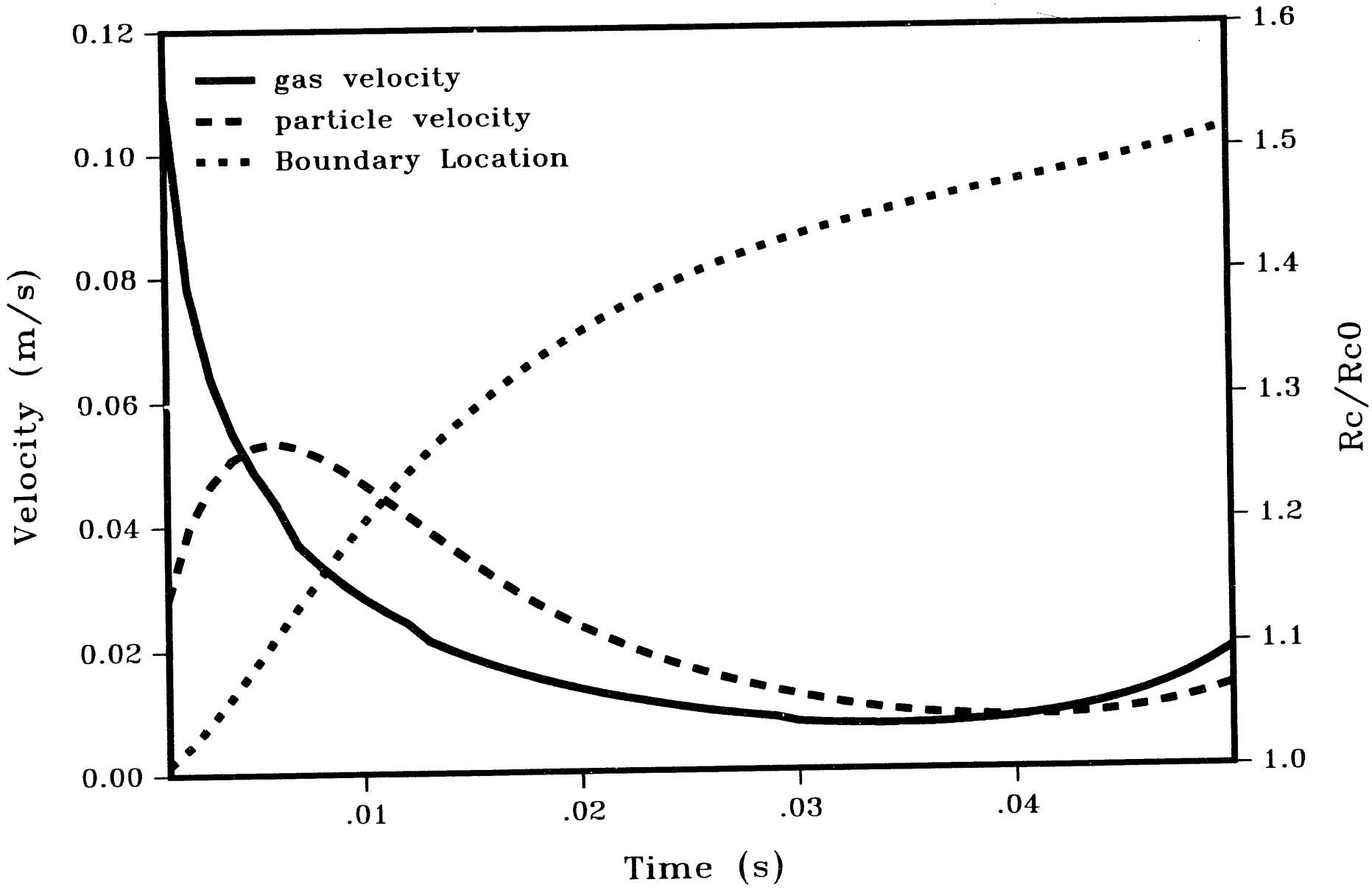

Fig. 1 Gas velocity and Particle velocity at cloud boundary and boundary movement (T_∞=1100 K, R_c=0.225 cm, d_p=64 μm, n=50.9 E+07 particles/m^3 , Ignition time=48.07 ms)

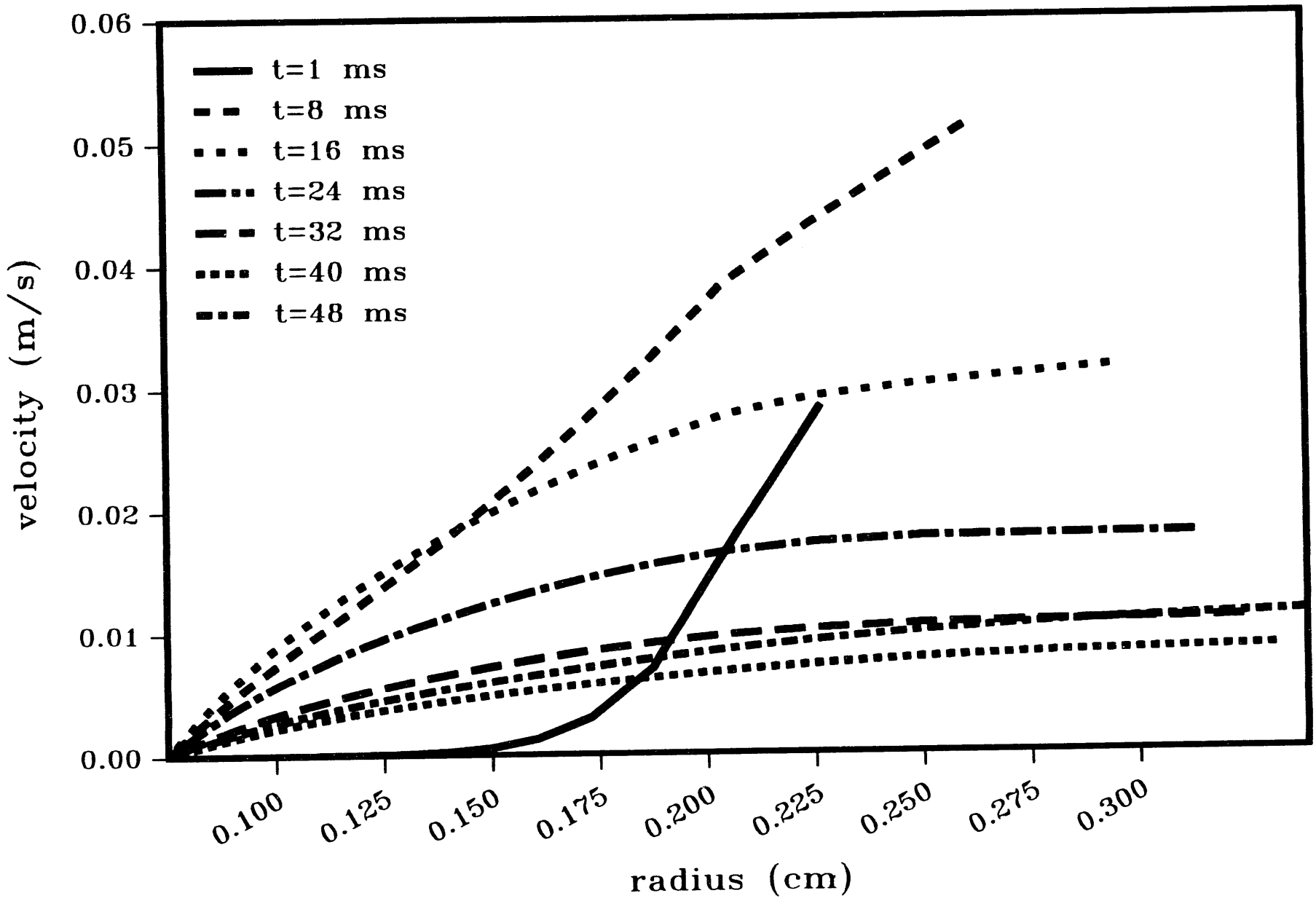

Fig. 2 Particle velocity distribution in different time (T_∞=1100 K, R_c=0.225 cm, d_p=64 μm, n=50.9 E+07 particles/m^3 , Ignition time=48.07 ms)

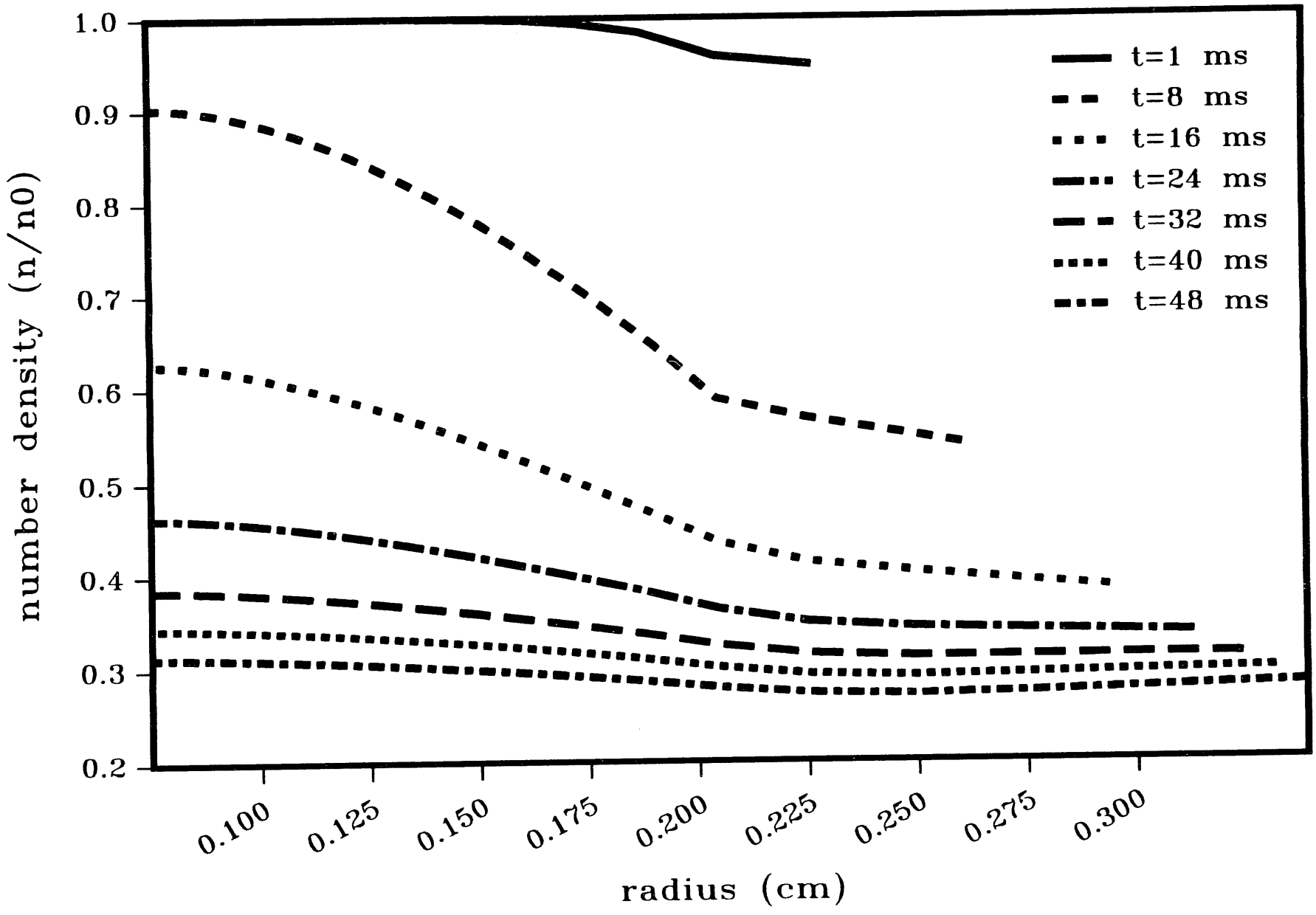

Fig. 3 Number density distribution with cloud radius
(T_∞=1100 K, R_c=0.225 cm, d_p=64 μm, n=50.9 E+07 particles/m^3 , Ignition time=48.07 ms)

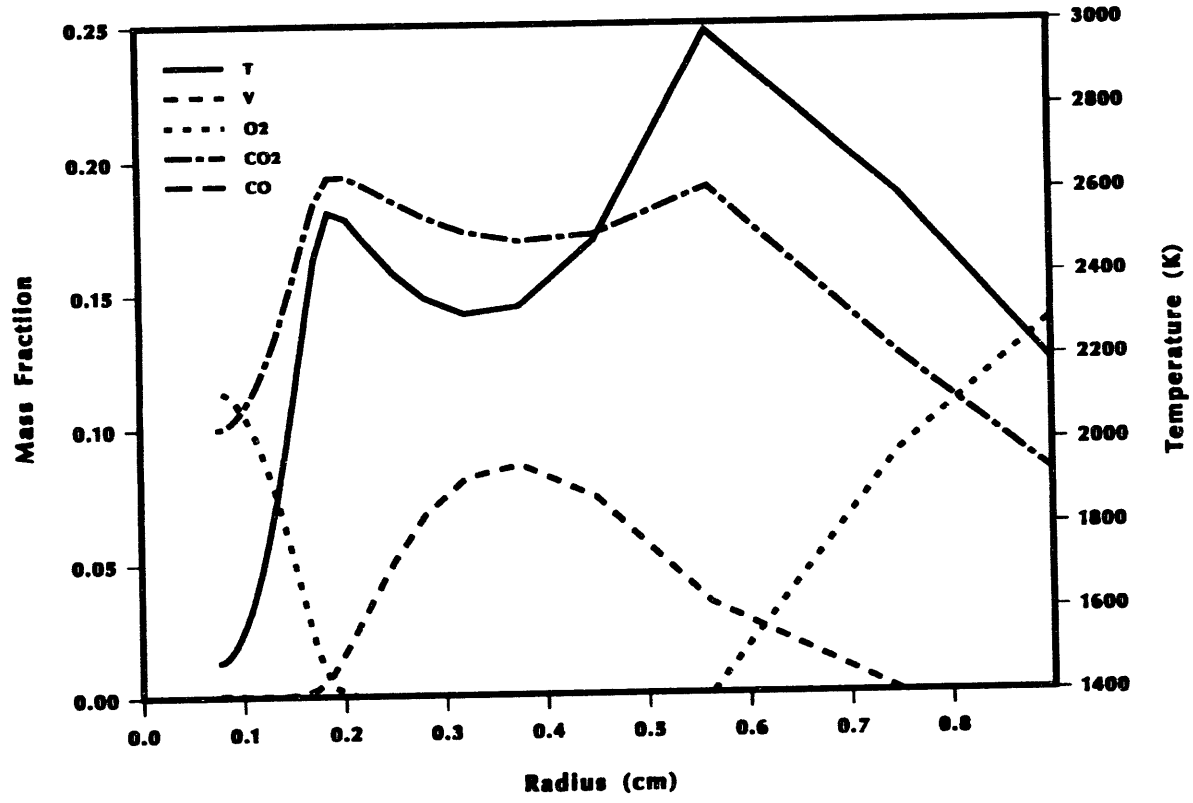

Fig. 4 Flame at t=53.9 ms (with cloud expansion)
(T_∞=1100 K, R_c=0.225 cm, d_p=64 μm, n=50.9 E+07 particles/m^3 , Ignition time=48.07 ms)

☆U.S. GOVERNMENT PRINTING OFFICE: 1994-550-168-00023

DATE
FILMED
11/14/94

END